

c2



# Lawrence Berkeley Laboratory

UNIVERSITY OF CALIFORNIA

RECEIVED

LAWRENCE  
BERKELEY LABORATORY

MAR 3 1989

LIBRARY AND  
DOCUMENTS SECTION

## Materials & Chemical Sciences Division

### Photodissociation of Cyclic Compounds in a Molecular Beam

X. Zhao  
(Ph.D. Thesis)

November 1988



Prepared for the U.S. Department of Energy under Contract Number DE-AC03-76SF00098.

LBL-26332  
c2

## **DISCLAIMER**

This document was prepared as an account of work sponsored by the United States Government. While this document is believed to contain correct information, neither the United States Government nor any agency thereof, nor the Regents of the University of California, nor any of their employees, makes any warranty, express or implied, or assumes any legal responsibility for the accuracy, completeness, or usefulness of any information, apparatus, product, or process disclosed, or represents that its use would not infringe privately owned rights. Reference herein to any specific commercial product, process, or service by its trade name, trademark, manufacturer, or otherwise, does not necessarily constitute or imply its endorsement, recommendation, or favoring by the United States Government or any agency thereof, or the Regents of the University of California. The views and opinions of authors expressed herein do not necessarily state or reflect those of the United States Government or any agency thereof or the Regents of the University of California.

**Photodissociation of Cyclic Compounds  
in a Molecular Beam**

Xinsheng Zhao  
(Ph.D. Thesis)

Department of Chemistry  
University of California  
and  
Materials and Chemical Sciences Division  
Lawrence Berkeley Laboratory  
1 Cyclotron Road  
Berkeley, California 94720

November 1988

**Photodissociation of Cyclic Compounds  
in a Molecular Beam**

Xinsheng Zhao

Abstract

A discussion on the dynamics and kinematics of photofragmentation-translational spectroscopy is presented, and the results are applied to experimental studies of four cyclic compounds: hexahydro-1,3,5-trinitro-1,3,5-triazine (RDX), s-tetrazine (ST), cyclohexene (CHN), and 1,4-cyclohexadiene (CHDN).

In infrared multiphoton dissociation (IRMPD) of RDX, the dominant primary channel is concerted triple fission to produce three  $\text{CH}_2\text{N}_2\text{O}_2$  fragments which subsequently undergo secondary dissociation. Concerted reactions predominate over simple bond rupture not only in the number of channels, but also in the amount of products.

Following  ${}^1\text{B}_{3u} + {}^1\text{A}_g$  ( $\text{S}_1 + \text{S}_0$ ) or  ${}^1\text{B}_{2u} + {}^1\text{A}_g$  (248 nm) excitation, ST reverts to the highly vibrationally excited ground electronic state through internal conversion (IC), and then decomposes into  $2\text{HCN} + \text{N}_2$  via concerted triple dissociation. The asymptotic angles between the  $\text{N}_2$  and HCN groups from the center-of-mass of ST are  $117.2^\circ$  and  $114.4^\circ$  for  $\text{S}_1 + \text{S}_0$  and 248 nm excitation respectively.

Comparing between IRMPD and 193 nm dissociation of CHN

and CHDN, the same reaction has similar translational energy distribution, indicating that IC occurs at 193 nm. The retro-Diels-Alder reaction is concerted up to an internal energy higher than 148 kcal/mol. C-H bond rupture and concerted H<sub>2</sub> elimination were observed from both CHN and CHDN. It is shown that the peak of the translational energy distribution of concerted dissociation for a moderate-sized hot molecule is mainly determined by the dynamics of the exit barrier release, and is not sensitive to either the amount of internal energy or the form of excitation.

### ACKNOWLEDGEMENTS

Graduate school is not easy, especially for me, a foreigner at an age too old to be a student. Thanks to so many people who have helped and encouraged me, I have survived.

I wish to thank Professor Lee and to express my respect to him. I feel grateful to Yuan, not only because of his support and advice in my research, but also because of his understanding of my goal, without which I would not be able to submit my thesis now. Everyone who has worked with Yuan Lee is impressed by his talent, his enthusiasm for working, and his deep commitment to science, and everyone has learnt a great deal from him.

I am indebted to Eric Hintsu, from whom I learnt how to run the rotating source machine. His support and help, his tolerance, and his warm-heartedness will be kept in my memory forever. Eric, among other people, made tremendous contribution to the work described in this thesis, and he has done a great job of putting up with my poor English. His help in shaping the language in this thesis and other papers is greatly appreciated.

I have had the pleasure of meeting Lisa Yeh. Being officemates, we have had conversations on lots of things and found agreement on most of them. Especially, we have a

common wish of equality, justice, and a better life for all human beings.

I am happy to have had the opportunity to work with Gilbert Nathanson. I am thankful to him for his patience when I asked him questions during my first year when I was just a stupid boy. Later, we together struggled to work out the computer program on secondary dissociation, part of which is contained in Chapters I, V and Appendices. I have benefitted greatly from him, and was filled with joy to work with him.

Besides the people mentioned above, a few other people have participated in or helped with the work described in this thesis: Alec Wodtke helped with the experiment presented in Chapter II, and I learnt skills necessary doing an experiment from him. I had a very pleasant time working with Dr. Walter Miller on the photodissociation of s-tetrazine. He is very kind and friendly, and it was he who synthesized s-tetrazine without which Chapter III would have to be erased. The heated discussion when Prof. Qihe Zhu was in the Lee group was beneficial to me, and it was exciting to assist Prof. Zhu on vibrationally resolved TOF spectra of  $\text{CH}_3\text{I}$  photodissociation. Finally, Dr. Atsushi Yokoyama joined the team for the work described in Chapter IV. Thanks to his analysis of another experiment, the photodissociation of benzene, I was able to focus on the primary processes in Chapter IV, without analyzing the dissociation

of benzene which is one of the products in the photolysis of the compounds studied. I am also thankful to Robert Continetti and Barbara Balko who kindly allowed us to use their machine and helped us to carry out  $H_2$  and H atom detection, which is included in Chapter IV.

Marion Helfand was always very generous whenever I borrowed some equipment from her, as was Robert Continetti. Pam Chu patiently answered for me every question about the computer and helped me to solve my computer problems. I am obliged to them. Thanks also to Gary Robinson and Anne-Marie Schmoltner; I have benefitted from my conversations and interactions with them. I appreciate Tzong-Tsong Miao, Arthur Suits, Jim Myers, and Mike Covinsky's kindness.

Special thanks go to Ann Weightman. She helped the Lee group run and kept us rolling smoothly through graduate school.

No words can express my gratitude to my family, to my friends in China, to my teachers in Peking University, especially Professors Yiliang Sun and Degang Han. Their love, their friendship, their expectations of me have been and still are some of the most important factors that support me both during the years at Berkeley and the years in the future.

Finally, various kinds of support from the staffs of the Department of Chemistry and of LBL are appreciated. The financial support for my first year of graduate study, which

came from the Department of Education of the People's Republic of China, is gratefully acknowledged. It was this support that made it possible for me to start a new life at UC Berkeley. This work was supported by the Office of Naval Research under Contract No. N00014-83-K-0069, and by the Director, office of Basic Energy Sciences, Chemical Sciences Division of the U.S. Department of Energy under Contract No. DE-AC03-76SF00098.

## CONTENTS

<b>Abstract</b> .....	1
<b>Acknowledgements</b> .....	i
<b>Chapter I Kinetics and kinematics of photochemistry</b>	
<b>via PTS technique</b> .....	1
I. INTRODUCTION.....	1
II. PRIMARY DISSOCIATION.....	3
A. Kinetics.....	3
B. Calculation of $\int_0^T N_R(v_R, w_R, \mathbf{x}, r_f, t) dt$ in (6)...	8
C. Integral over $\mathbf{x}$ in (6).....	10
D. Simplification of notation.....	10
E. Kinematics.....	14
III. SECONDARY DISSOCIATION.....	16
A. Secondary spontaneous dissociation.....	17
B. Secondary photon dissociation.....	26
IV. BRANCHING RATIO.....	33
V. SUMMARY.....	35
REFERENCES.....	37
FIGURE CAPTIONS.....	39
FIGURES.....	40
<b>Chapter II Infrared multiphoton dissociation of RDX</b>	
<b>in a molecular beam</b> .....	44

I.	INTRODUCTION.....	44
II.	EXPERIMENTAL.....	47
III.	RESULTS.....	49
IV.	ANALYSIS.....	51
V.	DISCUSSION.....	61
	A. Branching ratio.....	61
	B. Source of $\text{CH}_2\text{NNO}_2$ .....	63
	C. Importance of concerted reaction.....	67
VI.	SUMMARY.....	70
	REFERENCES.....	72
	TABLES.....	73
	FIGURE CAPTIONS.....	76
	FIGURES.....	77
 <b>Chapter III A concerted triple dissociation -</b>		
	<b>the photochemistry of s-tetrazine.....</b>	85
I.	INTRODUCTION.....	85
II.	EXPERIMENTAL.....	88
III.	RESULTS AND ANALYSIS.....	90
	A. General features.....	90
	B. Simple model for analysis of triple dissociation.....	92
	C. Analyzed results.....	99
IV.	DISCUSSION.....	103
	A. Triple dissociation vs. two-body sequential dissociation.....	103
	B. Dynamics of ST triple dissociation.....	106

V.	SUMMARY.....	110
	REFERENCES.....	112
	TABLES.....	115
	FIGURE CAPTIONS.....	117
	FIGURES.....	119
<b>Chapter IV Dissociation of cyclohexene and</b>		
<b>1,4-cyclohexadiene in a molecular beam... 128</b>		
I.	INTRODUCTION.....	128
II.	EXPERIMENTAL.....	132
III.	RESULTS AND ANALYSIS.....	134
	A. Photodissociation of CHN.....	134
	B. Photodissociation of 1,4-cyclohexadiene.....	138
IV.	DISCUSSION.....	141
	A. Features common to 193 nm photodissociation and IRMPD.....	141
	B. Dynamics of the retro-Diels-Alder reaction and H <sub>2</sub> elimination.....	142
	C. Difference in H atom elimination between CHN and CHDN.....	148
V.	SUMMARY.....	153
	REFERENCES.....	155
	FIGURE CAPTIONS.....	158
	FIGURES.....	162
<b>Chapter V Review of the approximations in</b>		
<b>Chapter I..... 179</b>		
	REFERENCES.....	184

**Appendix A Program CMLAB2.FOR..... 185**

**Appendix B Program CMLAB1.FOR..... 207**

CHAPTER I  
KINETICS AND KINEMATICS OF PHOTOCHEMISTRY  
VIA PTS TECHNIQUE

**I. Introduction**

Photodissociation is one of the most active areas of the modern physical chemistry. Among various experimental techniques, mass spectrometric detection of the time-of-flight (TOF) spectrum of photofragments in a molecular beam has proven to be one of the most powerful and universal tools.<sup>1</sup> This so-called photofragmentation-translational spectroscopy (PTS) has covered a variety of species, from simple diatomic to complicated polyatomic molecules. As the molecules become bigger and bigger, the involved chemical processes become more and more intricate. For example, secondary dissociation of the products are often observed among the dissociation channels.

The basic concepts and mathematical tools for data analysis in PTS for primary two-body dissociation were developed a long time ago. Since the beginning of PTS studies, it has been assumed that a product center-of-mass (c.m.) distribution in the translational degree of freedom,  $P(E_T, \hat{u})$ , can be decomposed into two independent distributions, an angular distribution,  $P_u(\hat{u})$ , and a translational energy distribution,  $P_E(E_T)$ . The analytical form of the

angular distribution was initially studied by Zare,<sup>2</sup> and was investigated from time to time.<sup>3-9</sup> Although the basic consideration by Zare<sup>2</sup> remains correct, it will be shown in Chapter III that the detailed interpretations given by previous workers need to be revised. One of the early discussions about obtaining  $P_E(E_T)$  from observed TOF spectra was given by Busch and Wilson.<sup>10</sup> Although there have been some analytical expressions for  $P_E(E_T)$  in the literature,<sup>11,12</sup> it is impossible to use one simple analytic function to describe  $P_E(E_T)$ 's, because  $P_E(E_T)$  strongly depends on the properties of individual systems. A routine procedure to obtain  $P_E(E_T)$  is, therefore, numerical fit of the experimental TOF spectra using trial  $P_E(E_T)$ . More detailed description for the formulas used in data analysis for two-body primary dissociation can be found in Lee and co-workers' papers.<sup>13,14</sup> For data analysis when secondary dissociation occurs, there also exist a few discussions.<sup>11,15</sup> The problem in the previous derivations on obtaining  $P_E(E_T)$ <sup>10-15</sup> is that, because only kinematics was discussed, the physical meanings of the quantities appearing in the formulas are not clear, and some of them are even misinterpreted. We have found that an approach beginning with the kinetics of the reaction describes secondary dissociation in the most natural and economic way.

In this chapter, we will discuss the kinetics as well as the kinematics of photodissociation in a PTS experiment

using model system. As a general discussion, the assumption of the separability of  $P(E_T, \hat{u})$  is not invoked, although we will use this assumption in specific calculations in following chapters. It is hoped that through the derivation of the final formulas used to fit observed TOF spectra, starting from general chemical and physical principles, we will conceptually establish a bridge between dynamical quantities and experimental observations. It is also hoped that, because the approximations used in the derivation will be explicitly pointed out, new directions and modifications for the programs in Appendices A and B will be straightforward.

Although a fully quantum mechanical description can be used as a starting point, the semi-classical description is much simpler and sufficient for our purposes. Here, primary dissociation is defined as the dissociation of the molecules in the initial molecular beam, and secondary dissociation is the subsequent dissociation of the products from primary dissociation. Primary dissociation must be photodissociation, while secondary dissociation can be either photodissociation or spontaneous dissociation.

## II. Primary dissociation

### A. Kinetics

For simplicity, only one-photon initiated two-body

dissociation is considered, although the generalization to resonant multiphoton absorption is straightforward. Three-body dissociation will be discussed in Chapter III.

Consider that molecule R in a molecular beam has  $N_p$  primary dissociation channels,



where  $n$  stands for the  $n$ th primary reaction channel. We assume that dissociation occurs directly from states which are populated by photon excitation, and that these states can be depopulated by both dissociation and intramolecular relaxation processes (including spontaneous photon emission).

A diagram of the system is shown in Fig. 1, where  $r_i$ ,  $r_f$  are full sets of quantum numbers for the internal degrees of freedom of initial state  $i$  and final state  $f$ , connected by photon excitation, of the reactant R respectively,  $r_j$  is that of the states into which  $f$  state can relax through intramolecular processes,  $a_n$  and  $b_n$  are the full sets of quantum numbers of internal degrees of freedom of products  $A_n$  and  $B_n$  respectively,  $k_n^d(r_f \rightarrow a_n, b_n)$  is the state-to-state unimolecular dissociation rate constant of the  $n$ th dissociation channel,  $k_{fj}$  is the first-order rate constant from state  $f$  to state  $j$ , and the photon excitation rate "constant" is

$$k_{if} = \sum_{\hat{\epsilon}} R_{if} |\langle i | \mu \cdot \hat{\epsilon} | f \rangle|^2 I(\mathbf{x}, t), \quad (2)$$

when the transition is electric dipole allowed, where  $R_{if}$  is a constant,  $\mu$  is the dipole moment operator, and  $\hat{\epsilon}$  and  $I(\mathbf{X},t)$  are unit direction vector of the electric field and intensity of the light, respectively. If the excitation is not an electric dipole transition, Eqn. (2) is replaced by some other proper expression. In the following discussion, an electric dipole allowed transition is assumed.

There are four general constraints on the system, namely, energy, momentum and angular momentum conservation, and symmetry restrictions. Since all these restrictions can be implied by the magnitude of the transition matrix elements  $k_{if}$ ,  $k_{fj}$  and  $k_n^d(r_f \rightarrow a_n, b_n)$ , these conservation laws will not be explicitly considered unless necessary.

In a typical PTS experiment, a pulsed laser crosses a molecular beam with a dimension of interaction region on the order of 1 mm. We introduce the effective reaction time,  $\tau$ , which is defined as the time when reactions are finished. The effective reaction time is determined by the pulse length of the laser and the lifetime of the energized molecule, and is usually shorter than the time resolution of TOF detection. During  $\tau$  the change of position of molecules in the beam is usually smaller than one tenth of the dimension of the interaction region. It is easy to verify that the momentum transfer of the photon to the molecule is negligible, if the wavelength of the light is in uv region or longer. In most cases the following approximations are

valid:

There is no momentum change of the molecule when it absorbs a photon. (A1)

Molecules do not change their positions during the effective reaction time  $\tau$ . (A2)

With the above approximations, the following differential equations to describe the kinetics of the system can be written,

$$\begin{aligned} \frac{dN_R(v_R, w_R, \mathbf{X}, r_f, t)}{dt} = & \\ & \sum_i k_{if} N_R(v_R, w_R, \mathbf{X}, r_i, t) - \sum_j k_{fj} N_R(v_R, w_R, \mathbf{X}, r_f, t) - \\ & \sum_n \sum_{a_n, b_n} k_n^d(r_f \rightarrow a_n, b_n) N_R(v_R, w_R, \mathbf{X}, r_f, t) , \end{aligned} \quad (3)$$

$$\begin{aligned} \frac{dN_{An}(v_{An}, w_{An}, \mathbf{X}, a_n, t)}{dt} = & \\ & \sum_{f, b_n} \int k_n^d(r_f \rightarrow a_n, b_n) N_R(v_R, w_R, \mathbf{X}, r_f, t) dv_R dw_R, \\ \{v_{An}, w_{An}\} & \end{aligned} \quad (4)$$

$$\begin{aligned} \frac{dN_{Bn}(v_{Bn}, w_{Bn}, \mathbf{X}, b_n, t)}{dt} = & \\ & \sum_{f, a_n} \int k_n^d(r_f \rightarrow a_n, b_n) N_R(v_R, w_R, \mathbf{X}, r_f, t) dv_R dw_R, \\ \{v_{Bn}, w_{Bn}\} & \end{aligned} \quad (5)$$

where  $N_Y(v_Y, w_Y, \mathbf{X}, y, t)$  is the density of species  $Y$  with respect to laboratory velocity  $v_Y$  and solid angle  $w_Y$ , and three dimensional spatial coordinate  $\mathbf{X}$ , in quantum state  $y$  at time  $t$ , and  $\{w, z, \dots\}$  stands for the summation and integration being constrained at values  $w, z, \dots$ .

In a PTS experiment, the product signal is resolved according to the arrival time,  $T$ , of the fragments in the detector, and the directly measured quantity is the number of signal counts for, say, product  $A_n$  per laser shot as a function of signal arrival time in the detector. Here, we use  $t$  as the time variable for reaction (in the interaction region) and  $T$  as the time variable for detection (in the detector region). The following approximations are usually good:

The effective reaction time  $\tau$  can be considered infinitely short with respect to the resolution of  $T$ .

(A3)

The size of the interaction region can be considered infinitely small compared to the resolution of  $T$ .<sup>16</sup> (A4)

Under (A3) and (A4), the TOF spectrum of species  $A_n$  is related to the quantity

$$N_{An}(v_{An}, w_{An}) dv_{An} dw_{An} = \sum_{f, a_n, b_n} \int k_n^d(r_f \rightarrow a_n, b_n) N_R(v_R, w_R, \mathbf{x}, r_f, t) dv_R dw_R dx dt, \quad \{v_{An}, dv_{An}, w_{An}, dw_{An}\} \quad (6)$$

where  $N_{An}(v_{An}, w_{An})$  is the laboratory velocity distribution of  $A_n$  produced by one laser pulse.

$$N_{An}^t = \int N_{An}(v_{An}, w_{An}) dv_{An} dw_{An} \quad (7)$$

is the total number of  $A_n$  produced from one laser pulse.

The analysis below is one approach towards solving Eqn. (6) which is a fundamental equation for data analysis.

B. Calculation of  $\int_0^{\tau} N_R(v_R, w_R, \mathbf{X}, r_f, t) dt$  in (6)

The integral of (3) with respect to  $t$  gives

$$\int \frac{dN_R(v_R, w_R, \mathbf{X}, r_f, t)}{dt} dt = \int \left[ \sum_i k_{if} N_R(v_R, w_R, \mathbf{X}, r_i, t) - \sum_j k_{fj} N_R(v_R, w_R, \mathbf{X}, r_f, t) \right] dt - \int \sum_n \sum_{a_n, b_n} k_n^d(r_f \rightarrow a_n, b_n) N_R(v_R, w_R, \mathbf{X}, r_f, t) dt, \quad (8)$$

where according to the definition of  $\tau$ , the upper limit of integration with respect to  $t$  can be expanded to  $\infty$ . The photon excited states  $r_f$  which can contribute to (6) are the states for which the population is 0 for both  $t=0$  and  $t \geq \tau$ , since reactions are complete after  $\tau$ . For these states the left side of (8) is 0, and (8) becomes

$$0 = \sum_i \int k_{if} N_R(v_R, w_R, \mathbf{X}, r_i, t) dt - \sum_j \int k_{fj} N_R(v_R, w_R, \mathbf{X}, r_f, t) dt - \sum_n \sum_{a_n, b_n} k_n^d(r_f \rightarrow a_n, b_n) \int N_R(v_R, w_R, \mathbf{X}, r_f, t) dt. \quad (9)$$

Using the rate "constant" expression (2), (9) can be rewritten as

$$\int N_R(v_R, w_R, \mathbf{X}, r_f, t) dt = \frac{\sum_{i, \hat{\epsilon}} R_{if} |\langle i | \mu \cdot \hat{\epsilon} | f \rangle|^2 \cdot \int I(\mathbf{X}, t) N_R(v_R, w_R, \mathbf{X}, r_i, t) dt}{\sum_j k_{fj} + \sum_n \sum_{a_n, b_n} k_n^d(r_f \rightarrow a_n, b_n)}. \quad (10)$$

For the molecules in  $r_i$ , the only important process is

photon excitation, therefore,

$$\frac{dN_R(v_R, w_R, \mathbf{X}, r_i, t)}{dt} = - \sum_{f', \epsilon} \hat{R}_{if'} |\langle i | \mu \cdot \hat{\epsilon} | f' \rangle|^2 I(\mathbf{X}, t) N_R(v_R, w_R, \mathbf{X}, r_i, t), \quad (11)$$

The density of starting molecules at time  $t$  during laser pulse is then

$$N_R(v_R, w_R, \mathbf{X}, r_i, t) = N_R^0(v_R, w_R, \mathbf{X}, r_i) e^{- \sum_{f', \epsilon} \hat{R}_{if'} |\langle i | \mu \cdot \hat{\epsilon} | f' \rangle|^2 \int_0^t I(\mathbf{X}, t') dt'}, \quad (12)$$

where  $N_R^0(v_R, w_R, \mathbf{X}, r_i)$  is the density of  $R$  in the molecular beam before irradiation.

Substituting (12) into (10), we get

$$\begin{aligned} & \int N_R(v_R, w_R, \mathbf{X}, r_f, t) dt = \\ & \sum_i \frac{\sum_{\epsilon} \hat{R}_{if} |\langle i | \mu \cdot \hat{\epsilon} | f \rangle|^2}{\sum_j k_{fj} + \sum_n \sum_{a_n, b_n} k_n^d(r_f \rightarrow a_n, b_n)} N_R^0(v_R, w_R, \mathbf{X}, r_i) \cdot \\ & \int_0^{\infty} I(\mathbf{X}, t) e^{- \sum_{f', \epsilon} \hat{R}_{if'} |\langle i | \mu \cdot \hat{\epsilon} | f' \rangle|^2 \int_0^t I(\mathbf{X}, t') dt'} dt \\ & = \sum_i \frac{\sum_{\epsilon} \hat{R}_{if} |\langle i | \mu \cdot \hat{\epsilon} | f \rangle|^2}{\sum_j k_{fj} + \sum_n \sum_{a_n, b_n} k_n^d(r_f \rightarrow a_n, b_n)} N_R^0(v_R, w_R, \mathbf{X}, r_i) \cdot \\ & \frac{1}{\sum_{f', \epsilon} \hat{R}_{if'} |\langle i | \mu \cdot \hat{\epsilon} | f' \rangle|^2} \\ & (1 - e^{- \sum_{f', \epsilon} \hat{R}_{if'} |\langle i | \mu \cdot \hat{\epsilon} | f' \rangle|^2 \int_0^{\infty} I(\mathbf{X}, t) dt}) \end{aligned} \quad (13)$$

### C. Integral over $\mathbf{X}$ in (6)

Clearly, if  $N_R^0(v_R, w_R, \mathbf{X}, r_i)$  and  $\int_0^\infty I(\mathbf{X}, t) dt$  are considered as non-constant functions of the position of the molecules  $\mathbf{X}$ , the integral will be very complicated. The following approximation is therefore introduced.<sup>16</sup>

$N_R^0(v_R, w_R, \mathbf{X}, r_i)$  and  $\int_0^\infty I(\mathbf{X}, t) dt$  are constants with respect to  $\mathbf{X}$  within the effective interaction volume  $V$ .

(A5)

With (A5), integration of (6) over  $\mathbf{X}$  simply gives a factor of the volume  $V$  of the interaction region. Thus, substituting (13) into (6), we get

$$\begin{aligned}
 & N_{A_n}(v_{A_n}, w_{A_n}) dv_{A_n} dw_{A_n} = \\
 & \int_{\{v_{A_n}, w_{A_n}, dv_{A_n}, dw_{A_n}\}} \int_V \sum_{i, f, a'_n, b'_n} \frac{\sum_{\epsilon} R_{if} |\langle i | \mu \cdot \hat{\epsilon} | f \rangle|^2 k_n^d(r_{f \rightarrow a'_n, b'_n})}{\sum_j k_{fj} + \sum_n \sum_{a'_n, b'_n} k_n^d(r_{f \rightarrow a'_n, b'_n})} \cdot \\
 & \frac{N_R^0(v_R, w_R, r_i)}{\sum_{f', \epsilon} \hat{R}_{if'} |\langle i | \mu \cdot \hat{\epsilon} | f' \rangle|^2} \cdot \\
 & (1 - e^{-\sum_{f', \epsilon} \hat{R}_{if'} |\langle i | \mu \cdot \hat{\epsilon} | f' \rangle|^2 \int_0^\infty I(t) dt}) dv_R dw_R. \quad (14)
 \end{aligned}$$

where  $a'_n$  and  $b'_n$  are another pair of running indices for the quantum states of  $A_n$  and  $B_n$ .

### D. Simplification of notation

To simplify the writing of (14), the following quan-

tities are defined.

$$I_0 = \int_0^{\infty} I(t) dt \quad (15)$$

is the photon fluence of the laser pulse.

$$F(I_0, r_i) = \frac{1}{\sum_{f', \hat{\epsilon}} \hat{R}_{if'} |\langle i | \mu \cdot \hat{\epsilon} | f' \rangle|^2} (1 - e^{-\sum_{f', \hat{\epsilon}} \hat{R}_{if'} |\langle i | \mu \cdot \hat{\epsilon} | f' \rangle|^2 I_0}) \quad (16)$$

is the laser power dependence factor of the products. In the low power limit  $F(I_0, r_i)$  is independent of  $r_i$ , since then using

$$e^{-x} \approx 1-x,$$

$$F(I_0, r_i) = I_0. \quad (17)$$

While in the high power limit, (16) approaches the upper limit

$$F(I_0, r_i) = \frac{1}{\sum_{f', \hat{\epsilon}} \hat{R}_{if'} |\langle i | \mu \cdot \hat{\epsilon} | f' \rangle|^2} \quad (18)$$

which is a function of  $r_i$  and is the basis for the so-called saturation effect.

The state-to-state quantities in (14) are not easy to be compared with PTS experiment. It is better to group the summation over  $r_{f'}$ ,  $a'_n$  and  $b'_n$  in (14) to terms that correspond with the c.m. translational energy  $E_{Tn}$  and solid angle  $\Omega_n$  of nth channel. I.e., we can define

$$f_n(E_{Tn}, \Omega_n, r_i) dE_{Tn} d\Omega_n = \int_V \sum_{f, a'_n, b'_n} \frac{\sum_i R_{if} |\langle i | \mu \cdot \hat{\epsilon} | f \rangle|^2 k_n^d(r_f \rightarrow a'_n, b'_n)}{\sum_j k_{fj} + \sum_n \sum_{a'_n, b'_n} k_n^d(r_f \rightarrow a'_n, b'_n)} \cdot \quad (19)$$

$$\{E_{Tn}, dE_{Tn}, \Omega_n, d\Omega_n\}$$

It should be emphasized that the grouping of the sum over  $f$ ,  $a'_n$  and  $b'_n$  with respect to  $u_{An}$  and  $\Omega_{An}$ , the velocity and solid angle of  $A_n$  in the c.m. frame of  $R$  respectively, is also valid, but then different forms of distribution for  $A_n$  and  $B_n$  have to be used, since they have different c.m. velocity, related to each other by momentum conservation. The advantage of (19) is that the distribution is the same for both fragments of the same reaction channel  $n$ . Using the above definitions, (14) becomes simpler:

$$N_{An}(v_{An}, w_{An}) dv_{An} dw_{An} = \int \sum_i F(I_0, r_i) f_n(E_{Tn}, \Omega_n, r_i) N_R^0(v_R, w_R, r_i) dv_R dw_R dE_{Tn} d\Omega_n \cdot \quad (20)$$

$$\{v_{An}, w_{An}, dv_{An}, dw_{An}\}$$

This expresses the product density as a convolution over the absorption and dissociation probabilities for each type of molecule in the interaction zone.

We now define the following function,

$$P_n(E_{Tn}, \Omega_n, r_i) = \frac{F(I_0, r_i) f_n(E_{Tn}, \Omega_n, r_i)}{C_n(r_i)}, \quad (21)$$

which is normalized with respect to  $E_{Tn}$  and  $\Omega_n$ , e.g.,

$$\int P_n(E_{Tn}, \Omega_n, r_i) dE_{Tn} d\Omega_n = 1, \quad (22)$$

where

$$C_n(r_i) = \int F(I_0, r_i) f_n(E_{Tn}, \Omega_n, r_i) dE_{Tn} d\Omega_n. \quad (23)$$

Using (21) and (23), (20) can be written as

$$N_{An}(v_{An}, w_{An}) dv_{An} dw_{An} = \int \sum_i C_n(r_i) P_n(E_{Tn}, \Omega_n, r_i) N_R^0(v_R, w_R, r_i) dv_R dw_R dE_{Tn} d\Omega_n \cdot \{v_{An}, w_{An}, dv_{An}, dw_{An}\} \quad (24)$$

$P_n(E_{Tn}, \Omega_n, r_i)$  is a product distribution from state  $r_i$  of the reactant. Our experiments yield results which are averaged over all molecular state and all molecules in the reaction zone. In order to obtain this ensemble probability, we need define a molecular beam population averaged probability, which is

$$P_n(E_{Tn}, \Omega_n) = \frac{\sum_i C_n(r_i) P_n(E_{Tn}, \Omega_n, r_i) N_R^0(v_R, w_R, r_i)}{\int \sum_i C_n(r_i) P_n(E_{Tn}, \Omega_n, r_i) N_R^0(v_R, w_R, r_i) dE_{Tn} d\Omega_n} \quad (25)$$

with

$$C_n^0 = \frac{\int \sum_i C_n(r_i) P_n(E_{Tn}, \Omega_n, r_i) N_R^0(v_R, w_R, r_i) dE_{Tn} d\Omega_n}{N_R^0(v_R, w_R)}, \quad (26)$$

where

$$N_R^0(v_R, w_R) = \sum_i N_R^0(v_R, w_R, r_i), \quad (27)$$

$$\int P_n(E_{Tn}, \Omega_n) dE_{Tn} d\Omega_n = 1. \quad (28)$$

Notice that both  $P_n(E_{Tn}, \Omega_n)$  and  $C_n^0$  are actually functions of

molecular beam population. We introduce the following approximation.

The internal state distribution of R is independent of  $v_R$  and  $w_R$  in a given molecular beam. (A6)

Using (A6), (24) becomes

$$N_{An}(v_{An}, w_{An}) dv_{An} dw_{An} = \int_{\{v_{An}, w_{An}, dv_{An}, dw_{An}\}} C_n^0 P_n(E_{Tn}, \Omega_n) N_R^0(v_R, w_R) dv_R dw_R dE_{Tn} d\Omega_n, \quad (29)$$

where  $P_n(E_{Tn}, \Omega_n)$  and  $C_n^0$  are constant with respect to  $v_R$  and  $w_R$ .  $P_n(E_{Tn}, \Omega_n)$  is the quantity that is typically determined in our experiments. It is a normalized probability, which when multiplied by  $C_n^0$  yields the absolute number of dissociation events.

### E. Kinematics

In a PTS experiment, product  $A_n$  with laboratory velocity  $v_{An}$  to  $v_{An} + dv_{An}$  at detector solid angle  $w_D$  is resolved according to arrival time  $T$  after passing through a flight length  $L$ . Therefore, the detected TOF signal,  $N_{An}^T(T, w_D)$ , should be given by

$$N_{An}^T(T, w_D) dT = \left[ \int_{\{w_D\}} N_{An}(v_{An}, w_{An}) \left| \frac{\delta v_{An}}{\delta T} \right| dw_{An} \right] dT, \quad (30)$$

where, from  $v_{An} = L/T$ ,

$$\left| \frac{\delta v_{An}}{\delta T} \right| = \frac{v_{An}}{T}. \quad (31)$$

To obtain the final formula, we need to transform variables in Eqn. (29) from the center of mass variables  $(E_{Tn}, \Omega_n)$  to the variables  $(v_{An}, w_{An})$  in the laboratory frame. Using

$$E_{Tn} = \frac{1}{2} \frac{M_R M_{An}}{M_{Bn}} u_{An}^2, \quad (32)$$

and

$$\frac{\partial(u_{An}, \Omega_n)}{\partial(v_{An}, w_{An})} = \frac{v_{An}^2}{u_{An}^2}, \quad (33)$$

where  $M_Y$  is the mass of species Y, and (33) is simply the Jacobian for coordinate transformation, the expression for the TOF spectrum of  $A_n$  is obtained,

$$N_{An}^T(T, w_D) = C_n^0 \frac{v_{An}^3}{T} \frac{M_R M_{An}}{M_{Bn}} \int \frac{P_n(E_{Tn}, \Omega_n)}{u_{An}} N_R^0(v_R, w_R) dv_R dw_R dw_{An} \quad (34)$$

Mass spectrometers do not detect the neutral  $A_n$  directly, but rather ions created by electron impact ionization. The efficiency of the Brink type ionizer, which is used by our PTS apparatus,<sup>1</sup> is dependent on the velocity of the molecules. We can write

$$N_{An}^{T+}(T) = \frac{\eta_{An}(v_{An})}{v_{An}} N_{An}^T(T), \quad (35)$$

where  $N_{An}^T(T)$  is the real TOF signal and  $N_{An}^{T+}(T)$  is the TOF signal of the ion counts, summed over all mass to charge ratios (m/e), produced by the ionizer. Although  $\eta_{An}(v_{An})$

may depend on internal energy of  $A_n$  and  $\propto v_{An}$  at the limit  $v_{An} \rightarrow 0$ , the following approximation can be made in vast range of velocity which is experimentally interested.

$$\eta_{An}(v_{An}) = \eta_{An}^0, \text{ a constant.} \quad (\text{A7})$$

Using approximation (A7), the calculated TOF spectrum, equivalent to Eqn. (5) in Ref. 13, is obtained,

$$N_{An}^{T+}(T, w_D) = C_n^0 \eta_{An}^0 \frac{v_{An}^2}{T} \frac{M_R M_{An}}{M_{Bn}} \int \frac{P_n(E_{Tn}, \Omega_n)}{u_{An}} N_R^0(v_R, w_R) dv_R dw_R dw_{An} \quad (36)$$

{T, w\_D}

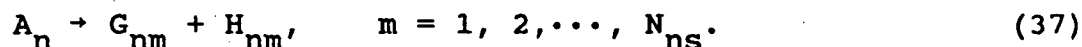
This final equation shows how the product c.m. distribution,  $P_n(E_{Tn}, \Omega_n)$ , determines the observed TOF spectrum.

### III. Secondary dissociation

Although discussions of secondary dissociation follow a similar route to the one described above, the validity of some of the approximations is now more questionable. However, in practice the situation is not very serious, since in most cases the measured TOF distributions of the secondary products are so broad and devoid of detail that the possible errors introduced by the approximations used above are still tolerable. In this section, all the assumptions and approximations made previously are used again. Of course, we should be prepared to remedy the situation if an inconsistency is observed.

### A. Secondary spontaneous dissociation

Consider dissociation events where a primary product  $A_n$  is energetic enough to fall apart. Let  $N_{ns}$  be number of secondary dissociation channels of  $A_n$ , where the reactions are represented by



A diagram of the system for spontaneous dissociation is drawn in Fig. 2, which should be considered as an expansion of Fig. 1, where  $g_{nm}$  and  $h_{nm}$  are the full sets of internal quantum numbers for  $G_{nm}$  and  $H_{nm}$  respectively, and  $k_{nm}^d(a_n \rightarrow g_{nm}, h_{nm})$  is the state-to-state unimolecular dissociation rate constant for the  $m$ th secondary channel of  $A_n$  following the  $n$ th primary channel. In secondary spontaneous dissociation, only the direct dissociation from states of  $A_n$  which are populated by primary dissociation are considered for simplicity. In this case the differential equations which are relevant to our interest are

$$\begin{aligned} \frac{dN_R(v_R, w_R, \mathbf{x}, r_f, t)}{dt} = & \sum_i k_{if} N_R(v_R, w_R, \mathbf{x}, r_i, t) - \sum_j k_{fj} N_R(v_R, w_R, \mathbf{x}, r_f, t) - \\ & \sum_n \sum_{a_n, b_n} k_n^d(r_f \rightarrow a_n, b_n) N_R(v_R, w_R, \mathbf{x}, r_f, t), \end{aligned} \quad (3)$$

$$\begin{aligned}
& \frac{dN_{A_n}(E_{Tn}, \Omega_n, \mathbf{x}, a_n, t)}{dt} = \\
& \int_{\{E_{Tn}, \Omega_n\}} \sum_{f, b_n} \int k_n^d(r_f \rightarrow a_n, b_n) N_R(v_R, w_R, \mathbf{x}, r_f, t) dv_R dw_R - \\
& \sum_m \sum_{g_{nm}, h_{nm}} k_{nm}^d(a_n \rightarrow g_{nm}, h_{nm}) N_{A_n}(E_{Tn}, \Omega_n, \mathbf{x}, a_n, t), \quad (38)
\end{aligned}$$

where variables  $(E_{Tn}, \Omega_n)$ , instead of  $(v_{A_n}, w_{A_n})$  or  $(u_{A_n}, \Omega_{A_n})$ , are used for the same reasons as before when deriving (19) in section II, and

$$\begin{aligned}
& \frac{dN_{G_{nm}}(v_{G_{nm}}, w_{G_{nm}}, \mathbf{x}, g_{nm}, t)}{dt} = \\
& \int_{\{v_{G_{nm}}, w_{G_{nm}}\}} \sum_{a_n, h_{nm}} \int k_{nm}^d(a_n \rightarrow g_{nm}, h_{nm}) N_{A_n}(E_{Tn}, \Omega_n, \mathbf{x}, a_n, t) dE_{Tn} d\Omega_n. \quad (39)
\end{aligned}$$

According to the model, the  $A_n$  that survive are those for which no dissociation occurs and  $k_{nm}^d(a_n \rightarrow g_{nm}, h_{nm}) = 0$ . Thus, the functional form of the TOF spectrum for stable  $A_n$  is exactly the same as that derived in section II, provided that the sum over  $a_n$  in (6) and the following related equations does not contain the states of  $A_n$  where  $A_n$  dissociate. To obtain the TOF spectrum of  $G_{nm}$ , the quantity

$$\begin{aligned}
& N_{G_{nm}}(v_{G_{nm}}, w_{G_{nm}}) dv_{G_{nm}} dw_{G_{nm}} = \\
& \int_{\{v_{G_{nm}}, w_{G_{nm}}\}} \sum_{a_n, g_{nm}, h_{nm}} \int k_{nm}^d(a_n \rightarrow g_{nm}, h_{nm}) N_{A_n}(E_{Tn}, \Omega_n, a_n, t) dE_{Tn} d\Omega_n dt \quad (40)
\end{aligned}$$

is needed, where the integral over  $\mathbf{x}$  has already been per-

formed. The procedure for evaluating Eqn. (40) is similar to the one used above.

For the state  $a_n$  which contributes to secondary dissociation, the integral of (38) is

$$\int_0^{\infty} \frac{dN_{An}(E_{Tn}, \Omega_n, a_n, t)}{dt} dt = 0$$

$$= \sum_{\substack{f, b_n \\ \{E_{Tn}, \Omega_n\}}} \int k_n^d(r_f \rightarrow a_n, b_n) N_R(v_R, w_R, r_f, t) dv_R dw_R dt -$$

$$\sum_m \sum_{g_{nm}, h_{nm}} k_{nm}^d(a_n \rightarrow g_{nm}, h_{nm}) \int N_{An}(E_{Tn}, \Omega_n, a_n, t) dt. \quad (41)$$

Rearranging (41), we have

$$\int N_{An}(E_{Tn}, \Omega_n, a_n, t) dt =$$

$$\frac{\sum_{\substack{f, b_n \\ \{E_{Tn}, \Omega_n\}}} \int k_n^d(r_f \rightarrow a_n, b_n) N_R(v_R, w_R, r_f, t) dv_R dw_R dt}{\sum_m \sum_{g_{nm}, h_{nm}} k_{nm}^d(a_n \rightarrow g_{nm}, h_{nm})}, \quad (42)$$

where, according to previous derivation of (13) and (16),

$$\int N_R(v_R, w_R, r_f, t) dt =$$

$$= \sum_i \frac{\sum_{\epsilon} R_{if} |\langle i | \mu \cdot \hat{\epsilon} | f \rangle|^2}{\sum_j k_{fj} + \sum_n \sum_{a_n, b_n} k_n^d(r_f \rightarrow a_n, b_n)} F(I_0, r_i) N_R^0(v_R, w_R, r_i). \quad (43)$$

Using (42) and (43), (40) becomes

$$N_{Gnm}(v_{Gnm}, w_{Gnm}) dv_{Gnm} dw_{Gnm} = v \int \sum_{a'_n, g'_{nm}, h'_{nm}} dE_{Tn} d\Omega_n dv_R dw_R \cdot \{v_{Gnm}, w_{Gnm}, dv_{Gnm}, dw_{Gnm}\}$$

$$\frac{\sum_m \sum_{g_{nm}, h_{nm}} k_{nm}^d(a'_n + g_{nm}, h_{nm})}{\sum_m \sum_{g_{nm}, h_{nm}} k_{nm}^d(a'_n + g_{nm}, h_{nm})} \sum_{\substack{i, f, b'_n \\ \{E_{Tn}, \Omega_n\}}} k_n^d(r_f \rightarrow a'_n, b'_n) \cdot$$

$$\frac{\sum_{i, f} R_{if} |\langle i | \mu \cdot \hat{\epsilon} | f \rangle|^2}{\sum_j k_{fj} + \sum_n \sum_{a_n, b_n} k_n^d(r_f \rightarrow a_n, b_n)} F(I_0, r_i) N_R^0(v_R, w_R, r_i). \quad (44)$$

Before further approximations are made, let us point out two amusing facts:

First, when  $m=1$  in (44) both the numerator and denominator contain the term

$$\sum_{g_{nm}, h_{nm}} k_{nm}^d(a'_n + g_{nm}, h_{nm}),$$

but they cannot be cancelled, because in the denominator the sum is over all  $\{g_{nm}, h_{nm}\}$  while the sum in the numerator is subject to the constraint  $\{v_{Gnm}, w_{Gnm}, dv_{Gnm}, dw_{Gnm}\}$ , i.e., for the latter the sum is a partial sum. This constraint is indicated by the symbol '. When (42) is integrated over all  $\{v_{Gnm}, w_{Gnm}\}$ , which is the total  $G_{nm}$  produced, then the two sums are indeed equal and cancelled, the result is just the same as the integral of (14) provided that the sum of  $a_n$  in (14) should be confined to those states where  $A_n$  dissociate, which is the total amount of  $A_n$  which undergo secondary dissociation. This equality is, of course, what is ex-

pected.

Second, part of Eqn. (44) looks very similar to Eqn. (14) except that sum over  $a'_n$  in (44) is coupled to secondary products. Eqn. (44) has the form

$$N_{Gnm}(v_{Gnm}, w_{Gnm}) dv_{Gnm} dw_{Gnm} = \sum_{Y_B} \{ f(Y_B) \sum_{Y_1} [f(Y_B, Y_1) \sum_{Y_2} f(Y_1, Y_2)] \}, \quad (45)$$

where  $Y_2$ ,  $Y_1$  and  $Y_B$  stand for the variables of secondary products, primary products and initial molecules respectively. To make this point clear, the following functions are defined. The first two functions describe  $f(y_1, y_2)$ ,

$$P_{nm}(E_{Tnm}, \Omega_{nm}, a_n) dE_{Tnm} d\Omega_{nm} = \sum_{\substack{g'_{nm}, h'_{nm} \\ \{E_{Tnm}, \Omega_{nm}, dE_{Tnm}, d\Omega_{nm}\}}} \frac{k_{nm}^d(a_n \rightarrow g'_{nm}, h'_{nm})}{\sum_m \sum_{g_{nm}, h_{nm}} k_{nm}^d(a_n \rightarrow g_{nm}, h_{nm})} \cdot \frac{1}{C_{nm}(a_n)}, \quad (46)$$

which is the analogy of (21) for secondary process, where  $E_{Tnm}$  and  $\Omega_{nm}$  are the translational energy and solid angle of the secondary reaction channel in the c.m. frame of  $A_n$ . The symbol ' is used for the indices over which the sum is only part of the ensemble, and

$$C_{nm}(a_n) = \frac{\sum_{g_{nm}, h_{nm}} k_{nm}^d(a_n \rightarrow g_{nm}, h_{nm})}{\sum_m \sum_{g_{nm}, h_{nm}} k_{nm}^d(a_n \rightarrow g_{nm}, h_{nm})}. \quad (47)$$

While (21) is not simply proportional to the unimolecular dissociation rate constant and is a combination of photon excitation, deactivation and dissociation, (46) does directly yield the relative secondary dissociation rate from

the state  $a_n$  of  $A_n$ , and  $C_{nm}(a_n)$  has the property

$$\sum_m C_{nm}(a_n) = 1. \quad (48)$$

The second two functions represent  $f(y_B, y_1)$ :

$$P_n(E_{Tn}, \Omega_n, r_i, a'_n) = VF(I_0, r_i) / C_n(r_i, a'_n) \cdot \left\{ \begin{array}{l} \sum_{f, b'_n} R_{if} |\langle i | \mu \cdot \hat{\epsilon} | f \rangle|^2 k_n^d(r_f \rightarrow a'_n, b'_n) \\ \epsilon \end{array} \right\} \frac{1}{\sum_j k_{fj} + \sum_n \sum_{a_n, b_n} k_n^d(r_f \rightarrow a_n, b_n)}, \quad (49)$$

where

$$\int P_n(E_{Tn}, \Omega_n, r_i, a'_n) dE_{Tn} d\Omega_n = 1, \quad (50)$$

and

$$C_n(r_i, a'_n) = v \int dE_{Tn} d\Omega_n \cdot F(I_0, r_i) \cdot \left\{ \begin{array}{l} \sum_{f, b'_n} R_{if} |\langle i | \mu \cdot \hat{\epsilon} | f \rangle|^2 k_n^d(r_f \rightarrow a'_n, b'_n) \\ \epsilon \end{array} \right\} \frac{1}{\sum_j k_{fj} + \sum_n \sum_{a_n, b_n} k_n^d(r_f \rightarrow a_n, b_n)} \quad (51)$$

Using above definitions and noticing that sum over  $a'_n$  must be grouped according to  $E_{Tn}$  and  $\Omega_n$ , (44) reads

$$N_{Gnm}(v_{Gnm}, w_{Gnm}) dv_{Gnm} dw_{Gnm} = \int \sum_i dE_{Tnm} d\Omega_{nm} dE_{Tn} d\Omega_n dv_R dw_R N_R^0(v_R, w_R, r_i) \cdot \left\{ v_{Gnm}, w_{Gnm}, dv_{Gnm}, dw_{Gnm} \right\} \sum_{a'_n} C_n(r_i, a'_n) C_{nm}(a'_n) P_n(E_{Tn}, \Omega_n, r_i, a'_n) P_{nm}(E_{Tnm}, \Omega_{nm}, a'_n). \quad (52)$$

We introduce a new approximation.

The secondary quantities in (52) can be replaced by the averaged quantity subject to constraint  $\{E_{Tn}, \Omega_n\}$ . (A8)

The averaged quantity is

$$C_{nm}(E_{Tn}, \Omega_n) P_{nm}(E_{Tn}, \Omega_n, E_{Tnm}, \Omega_{nm}) = \frac{(\sum_{a'_n} N(a'_n) C_{nm}(a'_n) P_{nm}(E_{Tnm}, \Omega_{nm}, a'_n))}{\sum_{a'_n} N(a'_n)}, \quad (53)$$

$$\{E_{Tn}, \Omega_n\} \quad \{E_{Tn}, \Omega_n\}$$

where  $N(a'_n)$  is the population of  $A_n$  in  $a'_n$ , and

$$\int P_{nm}(E_{Tn}, \Omega_n, E_{Tnm}, \Omega_{nm}) dE_{Tnm} d\Omega_{nm} = 1 \quad (54)$$

$$\sum_m C_{nm}(E_{Tn}, \Omega_n) = 1 \quad (55)$$

$C_{nm}(E_{Tn}, \Omega_n)$  is the percentage of dissociated  $A_n$  at  $E_{Tn}$  and  $\Omega_n$  through  $m$ th secondary channel among total dissociated  $A_n$  at  $E_{Tn}$  and  $\Omega_n$ , and  $P_{nm}(E_{Tn}, \Omega_n, E_{Tnm}, \Omega_{nm})$  is the secondary c.m. distribution of  $m$ th secondary channel at primary sample point  $E_{Tn}$  and  $\Omega_n$ .

Using (53), (52) can be written as

$$N_{Gnm}(v_{Gnm}, w_{Gnm}) dv_{Gnm} dw_{Gnm} = \int \sum_i dE_{Tnm} d\Omega_{nm} dE_{Tn} d\Omega_n dv_R dw_R N_R^0(v_R, w_R, r_i) \cdot \{v_{Gnm}, w_{Gnm}, dv_{Gnm}, dw_{Gnm}\} \sum_{a'_n} \{C_n(r_i, a'_n) P_n(E_{Tn}, \Omega_n, r_i, a'_n)\} \cdot \{E_{Tn}, \Omega_n\} C_{nm}(E_{Tn}, \Omega_n) P_{nm}(E_{Tn}, \Omega_n, E_{Tnm}, \Omega_{nm}) \quad (56)$$

where  $a'_n$  is used to emphasize that the sum is only for the states where  $A_n$  dissociate.

Using previous definitions in section II,

$$\sum_{\{E_{Tn}, \Omega_n\}} \{C_n(r_i, a'_n) P_n(E_{Tn}, \Omega_n, r_i, a'_n)\} = C_n(r_i) P_n(E_{Tn}, \Omega_n, r_i), \quad (57)$$

The expression on the right side of (57) is not exactly the same as that in (24), because  $\{a'_n\} \neq \{a_n\}$ , which means that generally the part of  $A_n$  which dissociate has different distribution from the other part which survive, or from that of the sum of the two together. Then the equivalent equation to (24) is obtained, that is,

$$\begin{aligned} N_{Gnm}(v_{Gnm}, w_{Gnm}) dv_{Gnm} dw_{Gnm} = \\ \int \sum_i dE_{Tnm} d\Omega_{nm} dE_{Tn} d\Omega_n dv_R dw_R N_R^0(v_R, w_R, r_i) \cdot \\ \{v_{Gnm}, w_{Gnm}, dv_{Gnm}, dw_{Gnm}\} \\ C_n(r_i) P_n(E_{Tn}, \Omega_n, r_i) C_{nm}(E_{Tn}, \Omega_n) P_{nm}(E_{Tn}, \Omega_n, E_{Tnm}, \Omega_{nm}). \end{aligned} \quad (58)$$

Using the definitions of Eqns. (25) and (26), Eqn. (58) becomes

$$\begin{aligned} N_{Gnm}(v_{Gnm}, w_{Gnm}) dv_{Gnm} dw_{Gnm} = \\ \int dE_{Tnm} d\Omega_{nm} dE_{Tn} d\Omega_n dv_R dw_R N_R^0(v_R, w_R) \cdot \\ \{v_{Gnm}, w_{Gnm}, dv_{Gnm}, dw_{Gnm}\} \\ C_n^0 P_n(E_{Tn}, \Omega_n) C_{nm}(E_{Tn}, \Omega_n) P_{nm}(E_{Tn}, \Omega_n, E_{Tnm}, \Omega_{nm}). \end{aligned} \quad (59)$$

The secondary dissociation properties  $C_{nm}(E_{Tn}, \Omega_n)$  and  $P_{nm}(E_{Tn}, \Omega_n, E_{Tnm}, \Omega_{nm})$  are functions of the primary process variables  $E_{Tn}$  and  $\Omega_n$ . However, when  $m = 1$ ,  $C_{nm}(E_{Tn}, \Omega_n) = 1$  according to (55), independent of  $E_{Tn}$  and  $\Omega_n$ .

Eqn. (59) is a good place to start to fit data, if we know how to handle  $C_{nm}(E_{Tn}, \Omega_n)$  and  $P_{nm}(E_{Tn}, \Omega_n, E_{Tnm}, \Omega_{nm})$ .<sup>17</sup> However, in the general cases, in order to make the calculation amenable, (A9) is introduced.

$C_{nm}(E_{Tn}, \Omega_n)$  and  $P_{nm}(E_{Tn}, \Omega_n, E_{Tnm}, \Omega_{nm})$  are constant with respect to  $E_{Tn}$  and  $\Omega_n$ . (A9)

(A9) simply means

$$C_{nm}(E_{Tn}, \Omega_n) = C_{nm}^0, \text{ a constant,} \quad (60a)$$

$$P_{nm}(E_{Tn}, \Omega_n, E_{Tnm}, \Omega_{nm}) = P_{nm}(E_{Tnm}, \Omega_{nm}). \quad (60b)$$

Using (60), (59) becomes

$$\begin{aligned} N_{Gnm}(v_{Gnm}, w_{Gnm}) dv_{Gnm} dw_{Gnm} = \\ \int \{ v_{Gnm}, w_{Gnm}, dv_{Gnm}, dw_{Gnm} \} dE_{Tnm} d\Omega_{nm} dE_{Tn} d\Omega_n dv_R dw_R N_R^0(v_R, w_R) \cdot \\ C_n^0 P_n(E_{Tn}, \Omega_n) C_{nm}^0 P_{nm}(E_{Tnm}, \Omega_{nm}). \end{aligned} \quad (61)$$

All further procedure would be similar to that in section II. Thus, only the final equation equivalent to (36) is presented:

$$\begin{aligned} N_{Gnm}^{T+}(T, w_D) = \\ C_{nm}^0 C_n^0 \eta_{Gnm}^0 \frac{v_{Gnm}^2}{T} \frac{M_R M_{An}}{M_{Bn}} \frac{M_{Gnm} M_{An}}{M_{Hnm}} \int du_{An} d\Omega_{An} dv_R dw_R dw_{Gnm} \cdot \\ P_n(E_{Tn}, \Omega_n) u_{An} \frac{P_{nm}(E_{Tnm}, \Omega_{nm})}{u_{Gnm}} N_R^0(v_R, w_R). \end{aligned} \quad (62)$$

where  $u_{Gnm}$  is the velocity of  $G_{nm}$  in the c.m. frame of  $A_n$ . Eqn. (62) is the final equation describing secondary

spontaneous dissociation, the one which can be readily used in practice.

### B. Secondary photo-dissociation

Consider further dissociation of  $A_n$  following (1), because and only because the products from (1) absorb second photon:

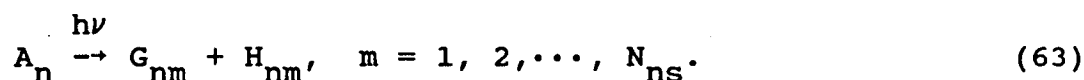


Fig. 3 shows the diagram for this case, where

$$k_{nn'} = A_{nn'} |\langle a_n | \mu_A \cdot \hat{\epsilon} | a_{n'} \rangle|^2 I(\mathbf{x}, t) \quad (64)$$

for an electric dipole allowed transition, where  $a_n$  and  $a_{n'}$  are full sets of quantum number of states of  $A_n$  before and after absorbing the second photon respectively. The other variables retain their meanings from the previous discussion. For simplicity, it is assumed that the only process occurring to  $A_n$  is the absorption of second photon and dissociation after photon absorption. Fig. 3 should be considered as an expansion of Fig. 1. In the case indicated by Figs. 1 and 3, the differential equations which are relevant to our interest are

$$\begin{aligned} \frac{dN_R(v_R, w_R, \mathbf{x}, r_f, t)}{dt} = & \\ & \sum_i k_{if} N_R(v_R, w_R, \mathbf{x}, r_i, t) - \sum_j k_{fj} N_R(v_R, w_R, \mathbf{x}, r_f, t) - \\ & \sum_n \sum_{a_n, b_n} k_n^d(r_f \rightarrow a_n, b_n) N_R(v_R, w_R, \mathbf{x}, r_f, t), \quad (3) \end{aligned}$$

$$\begin{aligned}
& \frac{dN_{An}(E_{Tn}, \Omega_n, \mathbf{x}, a_n, t)}{dt} = \\
& \sum_{\substack{f, b_n \\ \{E_{Tn}, \Omega_n\}}} \int k_n^d(r_f \rightarrow a_n, b_n) N_R(v_R, w_R, \mathbf{x}, r_f, t) dv_R dw_R - \\
& \sum_{a_n, \epsilon} \hat{A}_{nn}, |\langle a_n | \mu_A \cdot \hat{\epsilon} | a_n \rangle|^2 I(\mathbf{x}, t) N_{An}(E_{Tn}, \Omega_n, \mathbf{x}, a_n, t), \quad (65)
\end{aligned}$$

$$\begin{aligned}
& \frac{dN_{An}(E_{Tn}, \Omega_n, \mathbf{x}, a_n, t)}{dt} = \\
& \sum_{a_n, \epsilon} \hat{A}_{nn}, |\langle a_n | \mu_A \cdot \hat{\epsilon} | a_n \rangle|^2 I(\mathbf{x}, t) N_{An}(E_{Tn}, \Omega_n, \mathbf{x}, a_n, t) - \\
& \sum_m \sum_{g_{nm}, h_{nm}} k_{nm}^d(a_n, \rightarrow g_{nm}, h_{nm}) N_{An}(E_{Tn}, \Omega_n, \mathbf{x}, a_n, t), \quad (66)
\end{aligned}$$

and

$$\begin{aligned}
& \frac{dN_{Gnm}(v_{Gnm}, w_{Gnm}, \mathbf{x}, g_{nm}, t)}{dt} = \\
& \int_{\substack{a_n, h_{nm} \\ \{v_{Gnm}, w_{Gnm}\}}} \sum k_{nm}^d(a_n, \rightarrow g_{nm}, h_{nm}) N_{An}(E_{Tn}, \Omega_n, \mathbf{x}, a_n, t) dE_{Tn} d\Omega_n. \quad (67)
\end{aligned}$$

The quantity which is related to the TOF spectrum of  $G_{nm}$  is

$$\begin{aligned}
& N_{Gnm}(v_{Gnm}, w_{Gnm}) dv_{Gnm} dw_{Gnm} = \\
& v \int_{\substack{a_n, g_{nm}, h_{nm} \\ \{G_{nm}, w_{Gnm}, dv_{Gnm}, dw_{Gnm}\}}} \sum k_{nm}^d(a_n, \rightarrow g_{nm}, h_{nm}) N_{An}(E_{Tn}, \Omega_n, a_n, t) dE_{Tn} d\Omega_n dt. \quad (68)
\end{aligned}$$

The integrations of (65) and (66) give

$$\begin{aligned}
N_{An}(E_{Tn}, \Omega_n, a_n, t=\infty) = & \\
& \sum_{\substack{f, b_n \\ \{E_{Tn}, \Omega_n\}}} \int k_n^d(r_f \rightarrow a_n, b_n) N_R(v_R, w_R, r_f, t) dv_R dw_R dt - \\
& \sum_{a_n', \hat{\epsilon}} \hat{A}_{nn}, |\langle a_n | \mu_{\mathbf{A}} \cdot \hat{\epsilon} | a_n', \rangle|^2 \int I(t) N_{An}(E_{Tn}, \Omega_n, a_n, t) dt, \quad (69)
\end{aligned}$$

and

$$\begin{aligned}
0 = & \sum_{a_n', \hat{\epsilon}} \hat{A}_{nn}, |\langle a_n | \mu_{\mathbf{A}} \cdot \hat{\epsilon} | a_n', \rangle|^2 \int I(t) N_{An}(E_{Tn}, \Omega_n, a_n, t) dt - \\
& \sum_m \sum_{g_{nm}, h_{nm}} k_{nm}^d(a_n, \rightarrow g_{nm}, h_{nm}) \int N_{An}(E_{Tn}, \Omega_n, a_n', t) dt. \quad (70)
\end{aligned}$$

Therefore,

$$\begin{aligned}
& \int N_{An}(E_{Tn}, \Omega_n, a_n', t) dt \\
& = \frac{\sum_{a_n', \hat{\epsilon}} \hat{A}_{nn}, |\langle a_n | \mu_{\mathbf{A}} \cdot \hat{\epsilon} | a_n', \rangle|^2 \int I(t) N_{An}(E_{Tn}, \Omega_n, a_n, t) dt}{\sum_m \sum_{g_{nm}, h_{nm}} k_{nm}^d(a_n, \rightarrow g_{nm}, h_{nm})} \\
& = \sqrt{\frac{\sum_{\hat{\epsilon}} \hat{A}_{nn}, |\langle a_n | \mu_{\mathbf{A}} \cdot \hat{\epsilon} | a_n', \rangle|^2}{\sum_{a_n'} \sum_m \sum_{g_{nm}, h_{nm}} k_{nm}^d(a_n, \rightarrow g_{nm}, h_{nm}) \sum_{a_n', \hat{\epsilon}} \hat{A}_{nn}, |\langle a_n | \mu_{\mathbf{A}} \cdot \hat{\epsilon} | a_n', \rangle|^2}}{1}} \\
& \left( \sum_{\substack{f, b_n \\ \{E_{Tn}, \Omega_n\}}} \int k_n^d(r_f \rightarrow a_n, b_n) N_R(v_R, w_R, r_f, t) dv_R dw_R dt \right. \\
& \left. - N_{An}(E_{Tn}, \Omega_n, a_n, t=\infty) \right), \quad (71)
\end{aligned}$$

where  $a_n'$ , is another index for the states of  $A_n$  after photon absorption, and, according to (43),

$$\int N_R(v_R, w_R, r_f, t) dt =$$

$$= \sum_i \frac{\sum_{if} R_{if} |\langle i | \mu \cdot \hat{\epsilon} | f \rangle|^2}{\sum_j k_{fj} + \sum_n \sum_{a_n, b_n} k_n^d(r_f \rightarrow a_n, b_n)} F(I_0, r_i) N_R^0(v_R, w_R, r_i) .$$

(71) looks fairly complicated and generally is indeed difficult to be dealt with, because of  $N_{An}(E_{Tn}, \Omega_n, a_n, t=\infty)$ , which is no long zero. To obtain the exact solution, the coupled differential Eqns. (3) and (65) - (67) must be solved.

In the limit, that the secondary process is highly saturated,

$$N_{An}(E_{Tn}, \Omega_n, a_n, t=\infty) \approx 0 , \quad (72)$$

then (68) reduces to

$$N_{Gnm}(v_{Gnm}, w_{Gnm}) dv_{Gnm} dw_{Gnm} =$$

$$v \int \sum_i dE_{Tnm} d\Omega_{nm} dE_{Tn} d\Omega_n dv_R dw_R \cdot N_R^0(v_R, w_R, r_i) F(I_0, r_i) \cdot$$

$$\{ v_{Gnm}, w_{Gnm}, dv_{Gnm}, dw_{Gnm} \}$$

$$\sum_{\{E_{Tn}, \Omega_n\}} \left\{ \frac{\sum_{if} R_{if} |\langle i | \mu \cdot \hat{\epsilon} | f \rangle|^2}{\sum_j k_{fj} + \sum_n \sum_{a_n, b_n} k_n^d(r_f \rightarrow a_n, b_n)} \cdot \right.$$

$$\left. \sum_{a_n'} \left\{ \frac{\sum_{nm} k_{nm}^d(a_n \rightarrow g'_{nm}, h'_{nm})}{\sum_m g_{nm}, h_{nm}} \cdot \right. \right.$$

$$\left. \frac{\sum_{\epsilon} A_{nn}, |\langle a_n' | \mu_A \cdot \hat{\epsilon} | a_n \rangle|^2}{\sum_{a_n', \epsilon} A_{nn}, |\langle a_n' | \mu_A \cdot \hat{\epsilon} | a_n \rangle|^2} \right\} \right\} \quad (73)$$

where  $a'_n$  is another index for the states of  $A_n$  before photon absorption (distinguished from  $a_n$ , and  $a'_n$ , which are indices for states of  $A_n$  after photon absorption). Using (A8), Eqn. (73) becomes

$$\begin{aligned}
& N_{Gnm}(v_{Gnm}, w_{Gnm}) dv_{Gnm} dw_{Gnm} = \\
& v \int \sum_i dE_{Tnm} d\Omega_{nm} dE_{Tn} d\Omega_n dv_R dw_R \cdot N_R^0(v_R, w_R, r_i) F(I_0, r_i) \cdot \\
& \left\{ v_{Gnm}, w_{Gnm}, dv_{Gnm}, dw_{Gnm} \right\} \\
& \sum_{\epsilon} R_{if} |\langle i | \mu \cdot \hat{\epsilon} | f \rangle|^2 \\
& \left\{ \sum_{f, b'_n} k_{fn}^d(r_{f \rightarrow a'_n, b'_n}) \frac{\sum_{\epsilon} R_{if} |\langle i | \mu \cdot \hat{\epsilon} | f \rangle|^2}{\sum_j k_{fj} + \sum_n \sum_{a_n, b_n} k_{fn}^d(r_{f \rightarrow a_n, b_n})} \right\} \\
& \left\{ E_{Tn}, \Omega_n \right\} \\
& \sum_{\epsilon} k_{nm}^d(a_n, \rightarrow g'_{nm}, h'_{nm}) \\
& \left\{ N(a'_n) \sum_{a_n, m} \frac{g'_{nm}, h'_{nm}}{g_{nm}, h_{nm}} \frac{\sum_{\epsilon} k_{nm}^d(a_n, \rightarrow g'_{nm}, h'_{nm})}{\sum_{\epsilon} k_{nm}^d(a_n, \rightarrow g_{nm}, h_{nm})} \right\} \\
& \left\{ E_{Tn}, \Omega_n \right\} \\
& \left. \frac{\sum_{\epsilon} A_{nn}, |\langle a'_n | \mu_A \cdot \hat{\epsilon} | a_n, \rangle|^2}{\sum_{a'_n, \epsilon} A_{nn}, |\langle a'_n | \mu_A \cdot \hat{\epsilon} | a'_n, \rangle|^2} \right\} / \sum_{\left\{ E_{Tn}, \Omega_n \right\}} N(a'_n). \quad (74)
\end{aligned}$$

From (74) the same formulas as that of (61) and (62) can be obtained, where, however,  $C_{nm}^0$  and  $P_{nm}(E_{Tnm}, \Omega_{nm})$  will be defined correspondent to different dynamic quantities from that in spontaneous dissociation.

Finally, we turn back to the general case involving Eqns. (68) and (69). The physical meaning of (69) is clear: for a state  $a_n$  of  $A_n$  the left side is the number density of

$A_n$  which survive after laser pulse, while on the right side, the first term is the total number density of  $A_n$  converted from primary dissociation, and the second term is the number density of  $A_n$  which absorb second photon and dissociate. Therefore, if we define

$$N_{An}(E_{Tn}, \Omega_n, a_n, t=\infty) = \alpha \sum_{\substack{f, b \\ \{E_{Tn}, \Omega_n\}}} \int k_n^d(r_f \rightarrow a_n, b_n) N_R(v_R, w_R, r_f, t) dv_R dw_R dt, \quad (75)$$

it is reasonable to make the following approximation:

$$\alpha \text{ is only the function of } I_0 \text{ and } a_n. \quad (A10)$$

Using (A10), (75) becomes

$$N_{An}(E_{Tn}, \Omega_n, a_n, t=\infty) = \alpha(I_0, a_n) \sum_{\substack{f, b \\ \{E_{Tn}, \Omega_n\}}} \int k_n^d(r_f \rightarrow a_n, b_n) N_R(v_R, w_R, r_f, t) dv_R dw_R dt, \quad (76)$$

where  $0 \leq \alpha(I_0, a_n) \leq 1$ , with 0 and 1 respectively correspondent to the limits that the secondary photodissociation is totally saturated and the limit that there is no secondary photodissociation at all.  $\alpha(I_0, a_n)$ , therefore, contains information on the laser power dependence of the secondary photodissociation.

The general situation is obtained by multiplying by the additional factor  $(1 - \alpha(I_0, a_n))$ , for example, the equation equivalent to (74) is

$$\begin{aligned}
& N_{Gnm}(v_{Gnm}, w_{Gnm}) dv_{Gnm} dw_{Gnm} = \\
& v \int \sum_i dE_{Tnm} d\Omega_{nm} dE_{Tn} d\Omega_n dv_R dw_R \cdot N_R^0(v_R, w_R, r_i) G(I_0, r_i) \cdot \\
& \quad \{v_{Gnm}, w_{Gnm}, dv_{Gnm}, dw_{Gnm}\} \\
& \sum_{\left\{ \begin{array}{l} a'_n \\ E_{Tn}, \Omega_n \end{array} \right\}} \left( \frac{\sum_{f, b'_n} k_{fn}^d(r_f \rightarrow a'_n, b'_n)}{\sum_j k_{fj} + \sum_n \sum_{a_n, b_n} k_{fn}^d(r_f \rightarrow a_n, b_n)} \right) \cdot \\
& \quad \frac{\sum_{\epsilon} R_{if} |\langle i | \mu \cdot \hat{\epsilon} | f \rangle|^2}{\sum_{a'_n, m} \sum_{g_{nm}, h_{nm}} \frac{g'_{nm}, h'_{nm}}{k_{nm}^d(a_n \rightarrow g'_{nm}, h'_{nm})}} \cdot \\
& \quad \left. \frac{\sum_{\epsilon} A_{nn'} |\langle a'_n | \mu_A \cdot \hat{\epsilon} | a_n \rangle|^2}{\sum_{a'_n, \epsilon} A_{nn'} |\langle a'_n | \mu_A \cdot \hat{\epsilon} | a_n \rangle|^2} (1 - \alpha(I_0, a'_n)) \right) / \sum_{\left\{ \begin{array}{l} a'_n \\ E_{Tn}, \Omega_n \end{array} \right\}} N(a'_n).
\end{aligned}
\tag{77}$$

As results, Eqns. (61) and (62) can also be obtained for secondary photodissociation.

Here, an explanation of  $C_{nm}(E_{Tn}, \Omega_n)$  is in order. Unlike the cases of spontaneous and totally saturated photon dissociations when  $m = 1$ ,  $C_{nm}(E_{Tn}, \Omega_n)$  in a general photon dissociation is indeed a function of  $E_{Tn}$  and  $\Omega_n$  and does not satisfy Eqn. (55). For example, different  $E_{Tn}$  and  $\Omega_n$  correspond to different internal state distributions of  $A_n$ , and the absorption cross section for the second photon may now depend on the internal state and recoil angle of  $A_n$ .

#### IV. Branching Ratio

After the lengthy derivations presented above, it is easy to obtain branching ratios for different reaction channels. In Ref. 14, the definition of the branching ratio is not really clear. However, it is easy to be verified that the quantity derived in Ref. 14 is just the same quantity defined here for the case of primary dissociation.

Definition. The branching ratio of species 1 to 2 is the ratio of the total number of species 1 to 2 produced under the same experimental condition. The branching ratio of two reaction channels is the ratio of the relevant species, corrected by moles of reaction.

According to this definition, the branching ratio in general does not equal the ratio of dissociation rate constants, but in certain circumstances the two are equal to each other.

The total number of molecules produced during a primary dissociation is the integral of Eqn. (29) [see also Eqn. (7)],

$$\begin{aligned} N_{An}^t &= \int C_n^0 P_n(E_{Tn}, \Omega_n) N_R^0(v_R, w_R) dv_R dw_R dE_{Tn} d\Omega_n \\ &= C_n^0 N_0, \end{aligned} \quad (78)$$

where  $N_0$  is the spatial number density of R in the molecular beam.  $C_n^0$  can be obtained from the experimental total signal counts,  $N_{An, total}^{T+}(w_D)$ , and the calculation of the integral of (36) with respect to T,

$$C_n^0 = N_{An, total}^{T+}(w_D) / PINT_{An}(w_D). \quad (79)$$

$\text{PINT}_{\text{An}}(w_D)$  is defined as

$$\text{PINT}_{\text{An}}(w_D) = \eta_{\text{An}}^0 \int dT \frac{v_{\text{An}}^2}{T} \frac{M_{\text{R}} M_{\text{An}}}{M_{\text{Bn}}} \int \frac{P_{\text{n}}(E_{\text{Tn}}, \Omega_{\text{n}})}{u_{\text{An}}} N_{\text{R}}^0(v_{\text{R}}, w_{\text{R}}) dv_{\text{R}} dw_{\text{R}} dw_{\text{An}} \quad (80)$$

In Ref. 14, a detailed discussion on how to obtain  $N_{\text{An}, \text{total}}^{\text{T}+}(w_{\text{An}})$  and  $\eta_{\text{An}}^0$  is given.

The total number of molecules produced in a secondary dissociation is the integral of Eqn. (61), which is

$$\begin{aligned} N_{\text{Gnm}}^{\text{t}} &= \int dE_{\text{Tnm}} d\Omega_{\text{nm}} dE_{\text{Tn}} d\Omega_{\text{n}} dv_{\text{R}} dw_{\text{R}} N_{\text{R}}^0(v_{\text{R}}, w_{\text{R}}) \cdot \\ &\quad C_{\text{n}}^0 P_{\text{n}}(E_{\text{Tn}}, \Omega_{\text{n}}) C_{\text{nm}}^0 P_{\text{nm}}(E_{\text{Tnm}}, \Omega_{\text{nm}}) \\ &= C_{\text{n}}^0 C_{\text{nm}}^0 N_0, \end{aligned} \quad (81)$$

where, according to (62),

$$C_{\text{nm}}^0 C_{\text{n}}^0 = N_{\text{Gnm}, \text{total}}^{\text{T}+}(w_D) / \text{SINT}_{\text{Gnm}}(w_D), \quad (82)$$

where  $N_{\text{Gnm}, \text{total}}^{\text{T}+}(w_D)$  is an experimentally obtainable quantity and  $\text{SINT}_{\text{Gnm}}(w_D)$  is defined as

$$\begin{aligned} \text{SINT}_{\text{Gnm}}(w_D) &= \eta_{\text{Gnm}}^0 \int dT \left\{ \frac{v_{\text{Gnm}}^2}{T} \frac{M_{\text{R}} M_{\text{An}}}{M_{\text{Bn}}} \frac{M_{\text{Gnm}} M_{\text{An}}}{M_{\text{Hnm}}} \int du_{\text{An}} d\Omega_{\text{An}} dv_{\text{R}} dw_{\text{R}} dw_{\text{Gnm}} \cdot \right. \\ &\quad \left. P_{\text{n}}(E_{\text{Tn}}, \Omega_{\text{n}}) u_{\text{An}} \frac{P_{\text{nm}}(E_{\text{Tnm}}, \Omega_{\text{nm}})}{u_{\text{Gnm}}} N_{\text{R}}^0(v_{\text{R}}, w_{\text{R}}) \right\} \end{aligned} \quad (83)$$

It is emphasized that, in general, the  $C_{\text{n}}^0$ 's in (78) and (81) are not the same quantity for the reasons given in sections II and III.

Using Eqns. (78) - (83), the calculation of branching ratio between any pair of the products or of the reaction

channels using experimental data is straightforward. For example, the branching ratio of molecules X to Y is

$$R(X/Y) = N_X^t / N_Y^t . \quad (84)$$

It is easy to see that the laboratory angles for different species in the branching ratio calculation can be different.

## V. Summary

In this chapter we have discussed the general aspects of the PTS experiment and obtained equations necessary for data analysis, which are Eqns. (36), (62) and (84). The specific computer programs for data analysis based on these formulas are given in Appendix A, where more approximations are introduced<sup>17</sup> in order to perform a numerical calculation. Since the program itself shows where and what further approximations are made, we skip the discussion on the technique used in the program.<sup>18</sup> In following chapters, we will use the formulas derived in this chapter to analyze experimental results and check the validity of these approximations through the comparison between the experimental observation and the simulation. In Chapter V, we will come back to the approximations in this chapter, where we will give a physical interpretation and explain why these approximations are valid. We delay the discussion on the physical implications of the approximations introduced in this chapter to Chapter V, because after applying the

formulas developed in this chapter to data analysis, we will have examples to help us to understand the questions better.

**References**

- 1 A. M. Wodtke and Y. T. Lee, in Advances in Gas Phase Photochemistry and Kinetics, J. Baggott and M. Ashfold, Eds., Royal Society of Chemistry, London (1987).
- 2 R. N. Zare, Ph.D. Thesis, Harvard University, 1964; *Mol. Photochem.* **4**, 1 (1972).
- 3 R. Bersohn and S. H. Lin, *Adv. Chem. Phys.* **16**, 67 (1969).
- 4 C. Jonah, *J. Chem. Phys.* **55**, 1915 (1971).
- 5 G. E. Busch and K. R. Wilson, *J. Chem. Phys.* **56**, 3638 (1972).
- 6 S. C. Yang and R. Bersohn, *J. Chem. Phys.* **61**, 4400 (1974).
- 7 J. H. Ling and K. R. Wilson, *J. Chem. Phys.* **65**, 881 (1976).
- 8 a) Y. B. Band, K. F. Freed, and D. J. Kouri, *Chem. Phys. Lett.* **79**, 233, (1981); b) Y. B. Band and K. F. Freed, *Chem. Phys. Lett.* **79**, 238 (1981).
- 9 R. N. Dixon, *J. Chem. Phys.* **85**, 1866 (1986).
- 10 G. E. Busch and K. R. Wilson, *J. Chem. Phys.* **56**, 3626 (1972).
- 11 P. M. Kroger and S. J. Riley, *J. Chem. Phys.* **67**, 4483 (1977).
- 12 A. S. Sudbø, P. A. Schulz, E. R. Grant, Y. R. Shen, and Y. T. Lee, *J. Chem. Phys.* **70**, 912 (1979).

- 13 R. K. Sparks, K. Shobatake, L. R. Carlson, and Y. T. Lee, *J. Chem. Phys.* **75**, 3838 (1981).
- 14 D. Krajnovich, F. Huisken, Z. Zhang, Y. R. Shen, and Y. T. Lee, *J. Chem. Phys.* **77**, 5977 (1982).
- 15 a) A. M. Wodtke and Y. T. Lee, *J. Phys. Chem.* **89**, 4744 (1985); b) A. M. Wodtke, Ph.D. Thesis, University of California, Berkeley, 1986.
- 16 When this approximation needs to be improved, a convolution by finite interaction region should be introduced. But, this can be done at the end of the derivation, and the following discussion is not affected, provided that it is considered as one of individual segments of the volume of the interaction region on which convolution will be performed.
- 17 X. Zhao, G. M. Nathanson, and Y. T. Lee, to be published.
- 18 A necessary note. The definition of polarization angle used in the programs for a linearly polarized laser is shown in Fig. 4.

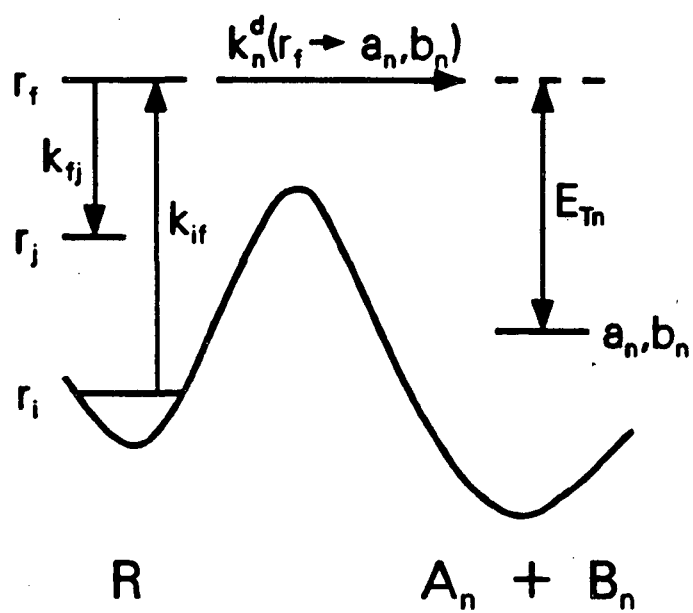
**Figure captions for Chapter I**

Fig. 1 Diagram of primary dissociation. Symbols are explained in the text.

Fig. 2 Diagram of secondary spontaneous dissociation. Symbols are explained in the text.

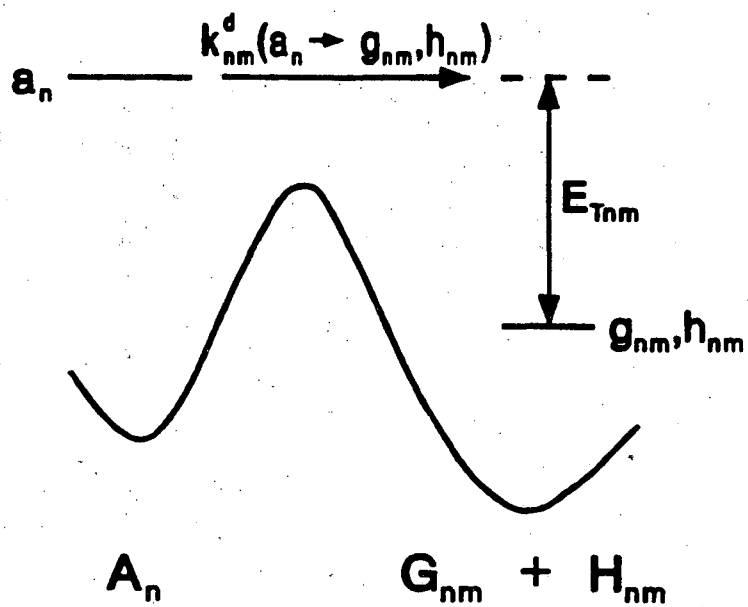
Fig. 3 Diagram of secondary photon dissociation. Symbols are explained in the text.

Fig. 4 Definition of laboratory angle and laser polarization angle used in programs in Appendices A and B.  $\hat{\epsilon}$  is the unit vector of electric field of the light.  $\theta$  is the laboratory angle of the molecular beam, and  $\gamma$  is the laser polarization angle.



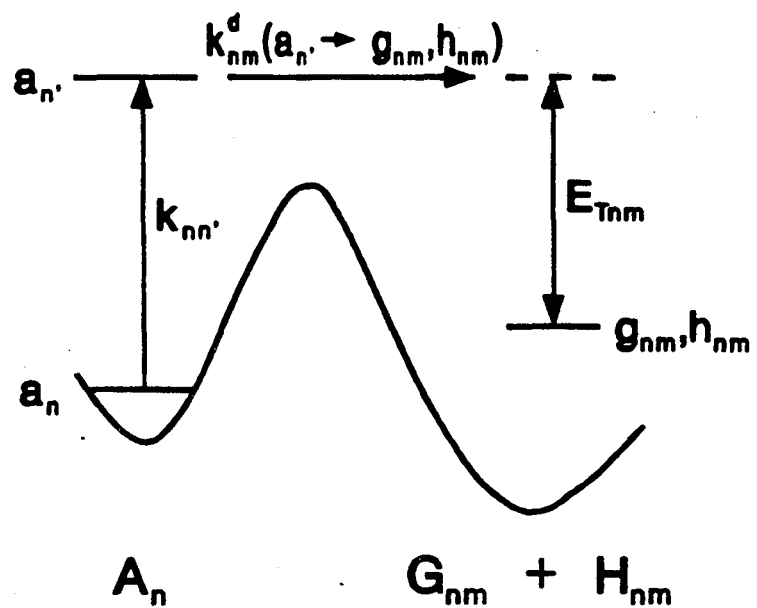
XBL 8811-3816

Fig. 1



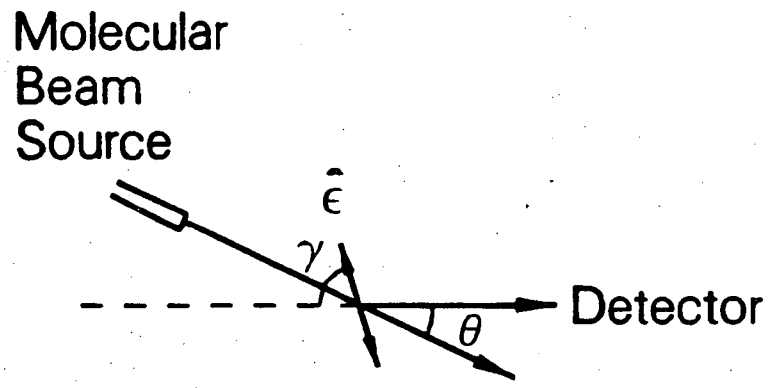
XBL 8811-3817

Fig. 2



XBL 8811-3818

Fig. 3



XBL 8811-3819

Fig. 4

**CHAPTER II**  
**INFRARED MULTIPHOTON DISSOCIATION OF RDX**  
**IN A MOLECULAR BEAM**

**I. Introduction**

Hexahydro-1,3,5-trinitro-1,3,5-triazine (RDX) is a relatively stable energetic compound which releases a large amount of energy in bulk decomposition. One of the interesting results from experimental studies of the thermal decomposition of RDX is that the observed products are almost exclusively simple molecules such as HCN, N<sub>2</sub>O, H<sub>2</sub>CO, H<sub>2</sub>O, NO<sub>2</sub>, NO, CO<sub>2</sub>, and CO. What the primary initiation and secondary decomposition processes are, which lead to the formation of a variety of simple stable molecules, and how the stored energy is released in decomposition have been two of the most important questions concerning the decomposition of RDX. Although RDX has been studied extensively for several decades both experimentally and theoretically,<sup>1-4</sup> the above questions are still unanswered.

It has been recognized that the decomposition of bulk RDX is a very complicated process involving both unimolecular and bimolecular reactions. It was commonly believed that the most probable initial decomposition step was simple bond rupture which eliminates NO<sub>2</sub> from RDX, since the weakest bond in RDX is the N-N bond. But this picture is

far from conclusive, and other possible mechanisms including unimolecular simple bond rupture or concerted dissociation as well as several bimolecular reactions between RDX molecules have been proposed. The crucial obstacle to the understanding of RDX decomposition has been the lack of an effective experimental tool to "follow" the primary and secondary elementary reactions directly.

Infrared multiphoton dissociation (IRMPD) of molecules in a molecular beam with measurements of product angular and velocity distributions has proven to be an ideal method to study unimolecular "thermal" decomposition of polyatomic molecules under isolated conditions.<sup>5-7</sup> It has been shown that for molecules which are moderate in size, the lifetime of the infrared-multiphoton-excited molecule is long enough to allow vibrational energy randomization before dissociation, and the same dissociation mechanism is observed for IRMPD as for thermal decomposition. The fact that we can "thermally heat" the isolated molecule in a molecular beam offers a greatly simplified environment for the investigation of unimolecular reactions without any complication from secondary bimolecular reactions of primary products. Measurements of angular and velocity distribution of fragments under collision-free conditions are not only important for the understanding of dissociation dynamics but also essential for the unambiguous identification of the primary products. Even if the products do not yield their

parent ions during the electron impact ionization, using the requirement of momentum conservation in the center-of-mass (c.m.) coordinate system to match the velocity distributions of various products, it is possible to determine the dissociation channels and their branching ratios as well as the product translational energy distribution,  $P_E(E_T)$ .

In a series of studies on the decomposition of ethers<sup>6</sup> and nitroalkanes,<sup>7</sup> it has been clearly shown that because of the different dissociation dynamics, concerted dissociation and simple bond rupture can be distinguished easily from the observed  $P_E(E_T)$ . In the case of simple bond rupture there is no appreciable exit barrier along the reaction coordinate so that the  $P_E(E_T)$  of the products is closely related to the energy distributed in the reaction coordinate. For molecules with many vibrational degrees of freedom which share internal energy statistically, only a small amount of translational energy is released with the peak of the  $P_E(E_T)$  almost at zero translational energy. In contrast, concerted dissociation has a substantial exit barrier, and upon overcoming this barrier the products have to carry away this potential energy. It is found<sup>7</sup> that the repulsion between products dominates the dissociation dynamics and about half of this exit barrier energy appears in translation. As a result, the average translational energy is usually substantially higher than that of a simple bond rupture and the peak of the  $P_E(E_T)$  is far away from zero translational

energy. Because of the complication caused by the excessive fragmentation of product molecules in the electron bombardment ionizer, the unique relation between dissociation dynamics and mechanism will be shown to play an important role in the elucidation of the dissociation mechanism of RDX.

In this chapter, results of experimental studies on the IRMPD of RDX in a molecular beam are presented. The reaction mechanism which best explains the experimental observations is proposed. It is found that the symmetrical fission of RDX into three  $\text{CH}_2\text{NNO}_2$  fragments is the dominant primary channel, and the subsequent concerted dissociations of  $\text{CH}_2\text{NNO}_2$  are found to be responsible for the production of such small molecules as HCN,  $\text{N}_2\text{O}$ ,  $\text{H}_2\text{CO}$ , and HONO. N-N bond rupture leading to the elimination of  $\text{NO}_2$  is also found to occur, but this is only a minor primary channel.

## II. Experimental

The experimental apparatus was basically the same as that described elsewhere.<sup>8</sup> Two modifications were made for this experiment. (1) The molecular beam source in Fig. 1 of Ref. 8 was replaced by a new oven composed of two parts, a reservoir which held RDX and a forward nozzle chamber on which there was a 1 mm diameter nozzle. The oven was sandwiched between two metal mounting plates which were welded to the back flange of the source chamber. Six pins

were used to kinematically mount the oven at the correct position, three above, spring loaded to apply pressure, and three below, engaged in T-shaped V grooves on the bottom of the oven to assure the positive alignment of the nozzle when the oven was heated. (2) A single skimmer, mounted on the wall of the source chamber, was located 2.5 cm from the nozzle and was heated to about 200 °C in order to prevent the condensation of RDX on the skimmer. This skimmer and the slit of the oven were used as the beam defining elements and the usual skimmer between the differential and main chambers was removed.

For producing the beam of RDX, the reservoir of the oven, in which RDX was loaded before the machine was evacuated, was heated to 130 °C at which the vapor pressure of RDX is estimated to be about 0.1 Torr, and the temperature of the nozzle was kept at 154 °C. He (99.995%) carrier gas at 50 Torr was led into the oven, then the mixture of He and RDX was expanded into the source chamber through the nozzle to produce an intense supersonic beam. The beam of RDX with a mean velocity of  $1.2 \times 10^5$  cm/s and a 13% FWHM velocity spread was then crossed with the beam of a pulsed CO<sub>2</sub> laser in the interaction region of the main chamber. RDX molecules in the beam were excited through IR multiphoton excitation (IRMPE) processes above the dissociation energy causing decomposition of the excited molecules. The dissociation fragments were detected by a mass spectrometer

at specified laboratory angles with respect to the direction of the molecular beam which is variable by rotating the entire molecular beam source chamber about the laser propagation axis. The time-resolved mass spectrometric signals, time-of-flight (TOF) spectra, triggered by laser pulse were recorded at all mass to charge ratios ( $m/e$ ) in which dissociation products were detectable for the analysis of product velocity distributions.

A Gentec DD-250 TEA  $\text{CO}_2$  laser was used as the IRMPE laser, and the P22 line of the  $00^1-10^0$  transition (at  $10.6 \mu\text{m}$ ) was chosen for excitation. The laser beam was focused to 1 mm diameter at the crossing point of the two beams. The temporal length of the laser pulse was around 600 ns, and two repetition rates of 30 and 100 Hz were used at various times. Laser fluences of 6 to  $20 \text{ J/cm}^2$  per pulse were used.

For a more detailed description of the machine and operating conditions as well as the technique of recording the TOF spectra, Refs. 7 and 8 are recommended. The RDX obtained from the Lawrence Livermore National Laboratory was used in this experiment without purification.

### III. Results

Prior to the photolysis experiment, the mass spectrum of RDX in the molecular beam was taken at various temperatures. Using a small (0.1 mm diameter) entrance slit on the

detector, the laboratory angle of the molecular beam was set to zero and the molecular beam was pointed straight into the detector, allowing the beam of RDX molecules to be detected directly using electron bombardment ionization followed by a quadrupole mass spectrometer. The temperature of the reservoir was maintained at 170 °C, and the temperature of the nozzle was varied from 170 °C upwards. Without the carrier gas, by using a spinning slotted disk to measure the TOF spectrum of the effusive beam at  $m/e = 30$  ( $\text{NO}^+$ ) it was found that the TOF distribution was exactly that expected from stable RDX at the nozzle temperature when the temperature was below 200 °C. When the temperature of the nozzle was raised above 200 °C a fast component from dissociation products appeared. The fast peak due to dissociation became substantial when the nozzle was heated to 220 °C. These observations imply that the rate of thermal decomposition of RDX is slow at temperature below 200 °C. The mass spectrum of RDX above  $m/e = 28$  contains all the masses reported by Farber and Srivastava,<sup>9</sup> with one significant difference. While Farber and Srivastava claimed that the RDX molecule does not appear in the gas phase, in this experiment not only parent ion with  $m/e = 222$  was detected but also, as mentioned above, below 200 °C the effusive beam from the oven consisted almost entirely of stable RDX molecules. The observed mass spectrum of RDX contains peaks of  $m/e = 222, 148, 132, 120, 102, 81-83, 74, 56, 46, 44, 42, 30, 26-28,$

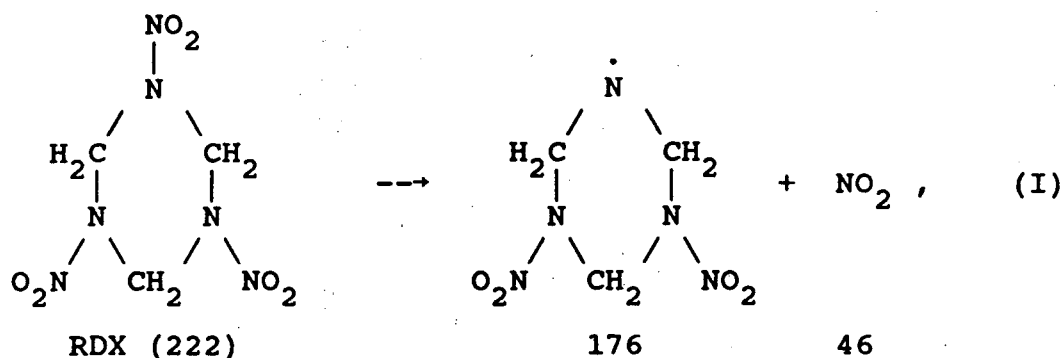
and 12-16, but not 175 nor 176.

Products from laser photolysis were detected and TOF spectra were obtained at  $m/e = 120, 119, 102, 80-82, 74, 56, 46, 44, 42, 26-30,$  and 12-17. Signals at  $m/e$  of 119, and both 82 and 80 were found to be the same as those at 120 and 81 respectively. Very weak signal at  $m/e = 83$  was observed, but it was too weak to be used for data analysis. A very careful scan between  $m/e = 120$  and 222 was performed, but no signal was detected within this range. For  $m/e = 120, 102, 81, 74$  and 30, TOF spectra at different laboratory angles were collected, while for other  $m/e$ 's only one laboratory angle was chosen. Figs. 1 and 2 show these TOF spectra with the fit using the mechanism presented in the next section. Most of these spectra were taken at a laser power of  $20 \text{ J/cm}^2$  and it was found that within the range of laser power of this experiment ( $6-20 \text{ J/cm}^2$ ) the shapes of the TOF spectra showed no significant differences.

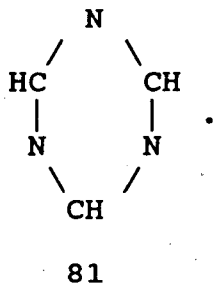
#### IV. Analysis

Using the computer program in Appendix A, which is based on the formulation developed in Chapter I, let us analyze the data, starting from the TOF spectrum of highest observed  $m/e$ .

Although  $m/e = 176$  was not detected (notice that even RDX itself gives no  $m/e = 176$  fragment in the mass spectrum) the existence of reaction (I),

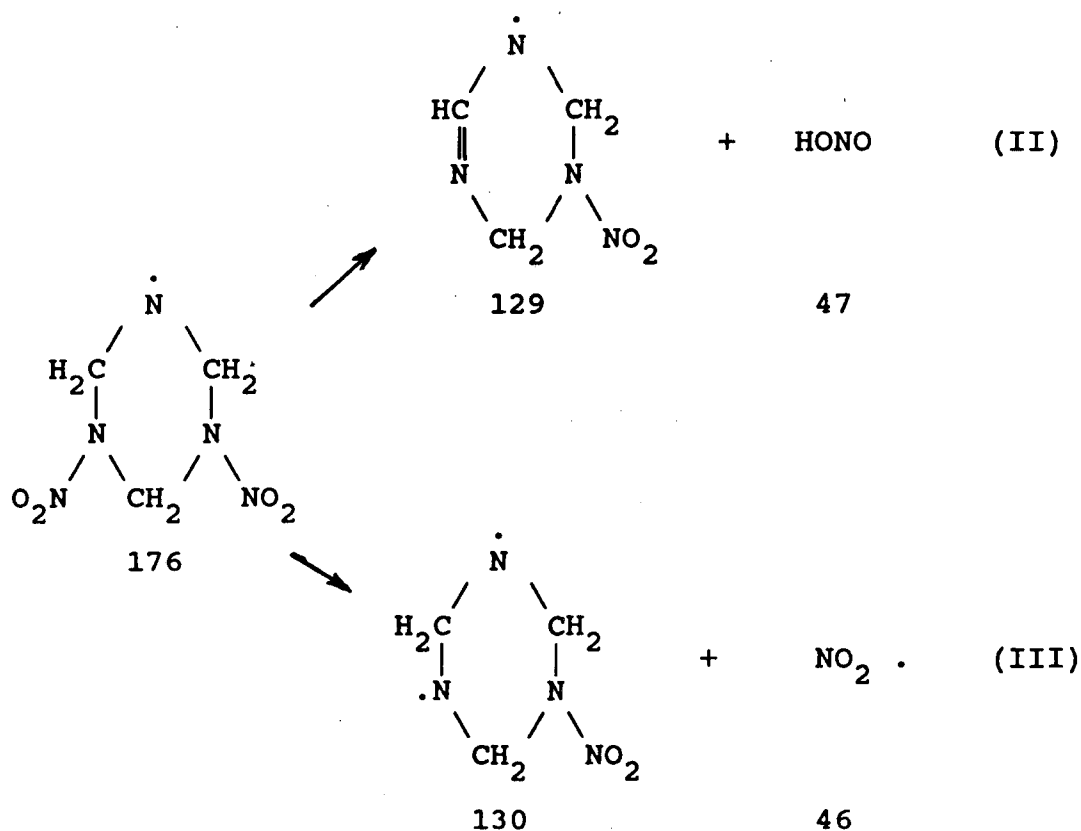


is evident. TOF spectra at  $m/e = 120$  and  $102$  have the same velocity distribution whose most probable velocity is almost the same as that of the molecular beam, showing that these fragments which have very small average c.m. recoil energies are produced from a simple bond rupture channel. The TOF spectra at  $m/e = 80-82$  also contain this component, implying that these ions are daughter ions of one primary product. A possible formula of  $120$  (hereafter the molecular weight in amu is used to represent the related species) is  $\text{CH}_2\text{N}_3\text{O}_4^+$ , and those of  $102$  are  $\text{C}_2\text{H}_4\text{N}_3\text{O}_2^+$  or  $\text{CH}_2\text{N}_4\text{O}_2^+$ , while the fragments around  $81$  must consist of the ring frame of RDX,



Therefore, the common parent product must be





It is also possible that 129, 130, and 175 undergo further dissociation by eliminating one or two  $\text{NO}_2$  or HONO molecules and contribute to the  $m/e = 81$  signal.

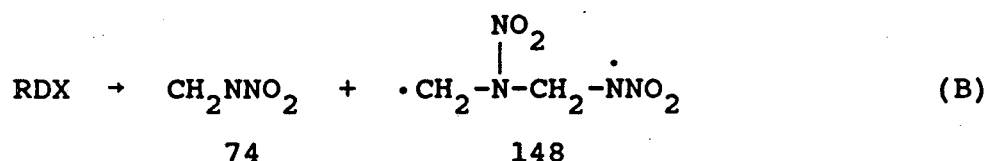
Because 175 has a similar ring structure as that of 176, it is expected that if reaction (A) took place, the faster  $m/e = 81$  component would have also appeared in the TOF spectra of  $m/e = 120$  or  $102$ , but it did not. The second product of reaction (A), HONO, does not yield parent ion ( $m/e = 47$ ). We have tried to match both the faster components of  $m/e = 81$  and  $17$  assuming they were from reaction (A), but the  $m/e = 17$  signal is too slow to match the fast component in the  $m/e = 81$  TOF spectrum by momentum conservation, showing that reaction (A) is not a major channel.

Since reaction (A) cannot be compatible with our experimental results, reaction (II) becomes the next likely candidate to explain the TOF spectra of both  $m/e = 81$  and 17. If the fast component in the  $m/e = 81$  TOF spectrum is from 129 produced from 176 product through reaction (II), by conservation of linear momentum in the dissociation of 176 we should be able to fit both the fast components in the TOF spectra of  $m/e = 81$  and 17 as a pair of products with mass numbers 129 and 47. In Figs. 1 and 2 both fast parts of the TOF spectra of  $m/e = 81$  and 17 shown as dash-dot curves are matched very well with each other assuming they are produced from the secondary dissociation of primary product 176 through reaction (II) using the  $P_E(E_T)$  presented in Fig. 4. The fact that the  $P_E(E_T)$  shown in Fig. 4 has a substantially higher average energy than that of reaction (I) and peaks away from zero implies that the products are from a concerted reaction, which is consistent with reaction (II). In order to perfectly fit the  $m/e = 81$  TOF spectrum another component with a velocity distribution between those of 176 and 129 is needed. The same problem occurs for fitting  $m/e = 56$  (with the possible formula  $C_2H_4N_2^+$ ) and especially 42 (with the possible formulas  $C_2H_4N^+$  or  $CH_2NN^+$ ). After reaction (III) is considered, all these problems disappear immediately. Fig. 5 shows the  $P_E(E_T)$  for reaction (III) which is again consistent with simple bond rupture.

We cannot absolutely rule out the possibility that the

m/e = 81 TOF spectrum could contain other products besides those from (I), (II), and (III), but since the data analysis assuming only reactions (I) - (III) gives satisfactory results we believe that other reaction channel whose products would appear at m/e = 81 are not significant.

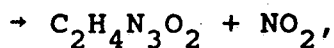
The m/e = 74 TOF spectra definitely differ from those with higher mass numbers. Farber and Srivastava suggested the following reaction channel:<sup>9</sup>



to explain the m/e = 74 peak they observed in their mass spectrometer, but in our experiment no trace of m/e = 148 was detected although the m/e = 148 peak is quite strong in the mass spectrum of RDX. Even if 148 was produced but was internally hot so that it would not survive in the ionizer, we should still be able to see the contribution of 148 at its fragment masses, especially at m/e = 74, which would show a slow peak obviously different from 74 itself in the TOF spectrum. If 148 from (B) underwent secondary dissociation as



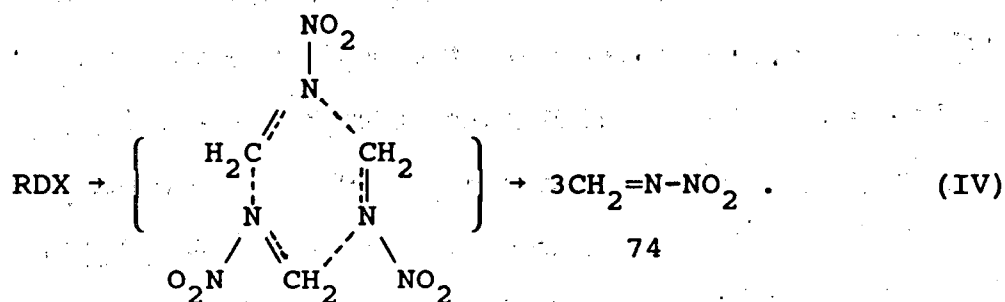
or



102

we should be able to detect these products at their charac-

teristic fragmentation pattern and velocity distributions, but no evidence was found. Because there is no trace of 148 or its fragments and the  $m/e = 74$  TOF is quite fast, which is inconsistent with a simple bond rupture reaction, the  $m/e = 74$  signal is most likely from concerted triple dissociation of reaction (IV), which has been suggested in the literature,<sup>1</sup> although it was thought not to be a major channel.



The  $P_E(E_T)$  for reaction (IV) is presented in Fig. (6). To fit the data it is assumed that the three product molecules have the same recoil velocity distribution in the c.m. coordinate system. More evidence to support mechanism (IV) will be given in the discussion section.

Using only reaction (I) - (IV) we cannot completely fit the TOF spectrum of  $m/e = 46$  ( $\text{NO}_2^+$ ), specifically the fast edge which cannot be attributed to any products from reactions (I) - (IV), indicating that there must be another dissociation channel which needs to be considered as will be shown later. Also, reactions (I) - (IV) cannot fit the fast part of the  $m/e = 44$  TOF spectrum which is most likely  $\text{N}_2\text{O}^+$  and must be explained by a secondary concerted dissociation

channel. To determine the partner of  $N_2O$ , we inspected the possibility of producing  $N_2O$  together with  $H_2CO$  from  $CH_2=N-NO_2$  through reaction (V).



$H_2CO$  can give signal at  $m/e = 30, 29$  and  $28$ , of which  $30$  and  $28$  may not be solely due to  $H_2CO$  whereas  $29$  can only be explained by the formation of  $HCO^+$  from  $H_2CO$ . It is found that based on reaction (V) the fast parts of the  $m/e = 44$  and  $29$  TOF spectra match each other well according to momentum conservation, indicating that reaction (V) is indeed responsible for the production of  $N_2O$  and  $H_2CO$ . The  $P_E(E_T)$  for reaction (V) used in the data analysis is shown in Fig. 7, the high average translational energy being consistent with that expected for a concerted reaction.

Like that of  $m/e = 17$  ( $OH^+$ ), the TOF spectrum of  $m/e = 26$  ( $CN^+$ ) strongly indicates another secondary concerted reaction channel. By studying the TOF spectra of  $m/e = 28, 27$  and  $26$ , we concluded that this concerted dissociation channel gives HCN as one of its products. Recalling the problem remaining in the fitting the fast component of the  $m/e = 46$  ( $NO_2^+$ ) TOF spectrum, we are led to assign this channel as



Reaction (VI) can match both the  $m/e = 26$  and the fast component in the  $m/e = 46$  TOF spectra well through momentum conservation, and Fig. 8 shows the  $P_E(E_T)$  for reaction (VI)

used to fit the TOF data.

The counterpart of HCN, which has a mass number of 47, in reaction (VI) is most likely to be HONO, but there are two observations which raise questions on this assignment. One is that Wodtke et al.<sup>7</sup> have shown that HONO produced from IRMPD of nitropropane does not give appreciable amounts of  $\text{NO}_2^+$  and this is also true for HONO from reaction (II) (this product is so fast that one cannot fit the fast component in the  $m/e = 46$  TOF spectrum by it), but the 47 in reaction (VI) contributes quite a bit of  $m/e = 46$ . Another is that when analyzing the  $m/e = 15$  TOF data, we found that none of the products from the channels considered could match the fastest component which arrived at the detector about the same time as the fast component at  $m/e = 46$ . If the 47 is assigned as  $\text{HNO}_2$ , a more unstable intermediate which can give  $m/e = 15$  ( $\text{HN}^+$ ) as well as  $m/e = 46$  ( $\text{NO}_2^+$ ) in the ionizer, both problems disappear. We cannot tell at this stage which isomer is more likely and it is possible that both species are produced.

When reactions (I) - (VI) are considered together with appropriate branching ratios, all of the observed TOF spectra can be fit well. In order to provide further verification of the assignment given above we have carried out a comparison of mass spectra of the products. In table I the relative yield of parent and daughter ions of some products measured in this experiment and those from the

literature are compared. Because the molecules produced in the decomposition of RDX are internally hot, it is not surprising that more smaller fragments are produced from the dissociation products than from the same molecules at room temperature. Comparison shows that the mass spectra of most of these species are in agreement with those in the literature. For  $N_2O$  the discrepancy seems large. This could be due to errors in fitting the data since  $N_2O$  is a small component, or it could be due to the really large difference in the cracking patterns between vibrationally hot  $N_2O$  and room temperature  $N_2O$  such that more  $m/e = 28$  ions are produced from  $N_2O$  in the decomposition of RDX.

Table II shows the results we have obtained for the laser power dependence of the signal counts. Because of the relative yield of products are nearly independent of laser power and the dependence of signal level on laser power is much less sensitive than one might expected, it is reasonable to assume that the primary dissociation processes are nearly saturated at  $20 \text{ J/cm}^2$  and that the secondary dissociation are mainly spontaneous dissociations rather than secondary photodissociations. More evidence for this will be presented later when RRKM dissociation rate constants are calculated.

## V. Discussion

Among many possible decomposition schemes tested to explain our experimental observations, the scheme of reactions (I) - (VI) gives the most satisfying results, but we cannot unambiguously conclude that they are the only reactions involved for the following reasons. First, there are too many components in most of the TOF spectra, the fit becomes more ambiguous for the minor components; second, the proposed reactions have many products with velocity distributions which are quite similar due to the symmetric structure of RDX and it is possible that some minor reaction channels have not been identified. Nevertheless, we believe that this scheme includes the most important unimolecular channels involved in RDX decomposition.

### A. Branching ratios

In the decomposition of RDX, competition between parallel dissociation channels was found to take place in both primary and secondary reactions. In spite of the fact that determining the relative yield and branching ratios involving minor component is quite difficult, it provides another way of checking the reliability of the dissociation mechanism.

Table III lists the calculated relative product yields for various products. The theoretical and mathematical details for the calculation have been given in Chapter I.<sup>10</sup>

As shown, among the primary channels the reaction rate of concerted reaction (IV) is about twice that for simple bond rupture (I), i.e., for each molecule of  $\text{NO}_2$  and 176 produced [from channel (I)], there are six  $\text{CH}_2=\text{N}-\text{NO}_2$  produced. The secondary dissociation branching ratios again show the domination of concerted channels, as can be seen when products from reactions (II) and (III) are compared. In the secondary dissociation of  $\text{CH}_2=\text{N}-\text{NO}_2$ , the channel producing HCN is found to be more important than the channel producing  $\text{H}_2\text{CO}$  and  $\text{N}_2\text{O}$ . It is also seen that most of the unstable products from the primary channels dissociate so that only a small percentage of them remain intact.

By adding up all the products which are initially formed as 176, including those which survive and those which undergo further dissociation, we have obtained a ratio of 0.90 for 176 to 46 from reaction (I), compared to the expected value of 1.00. The measured ratio of 129 to 47 from reaction (II) is 0.80. When similar comparisons are made on other channels, it is found that the agreement between measured and desired ratios of the products is not always as good as that shown above, although the uncertainty is relatively large. Nevertheless, the reasonably good agreement in the ratios of products for the important channels gives us confidence in our suggested mechanism.

### B. Source of $\text{CH}_2\text{NNO}_2$

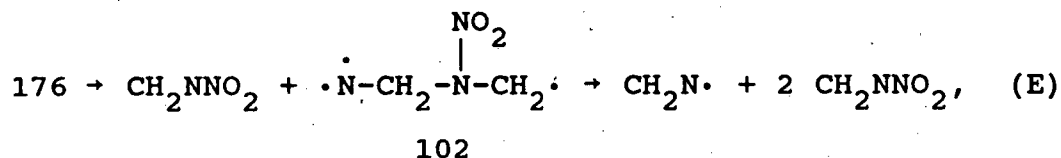
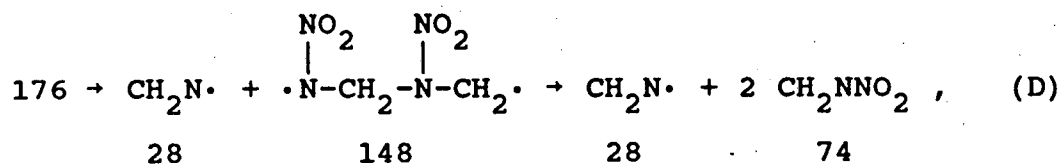
The species  $\text{CH}_2\text{NNO}_2$  (74) as an unstable intermediate in the decomposition of RDX has been recognized,<sup>1-3,9</sup> but there exists much speculation as to its origin. We have concluded that reaction (IV) is the main source of 74, because only this reaction can best explain our experimental observations, but according to theoretical calculations of Melius and Binkley<sup>3</sup> it is a very unlikely channel to compete with reaction (I).

Melius and Binkley<sup>3</sup> have estimated that the heat of formation of  $\text{CH}_2\text{NNO}_2$  is 33.6 kcal/mol, therefore the endothermicity of reaction (IV) would be about 80 kcal/mol. If the N-N bond energy in RDX is assumed to be 45 kcal/mol, then the excitation barrier for reaction (IV) would be at least 35 kcal/mol higher than for reaction (I). The question naturally arises: can the molecule be pumped by laser excitation to such high energy levels while reaction channel (I) is competing? To answer this question the unimolecular dissociation rate constants were calculated using RRKM theory. The calculations show that the RRKM rate constant for reaction channel (I) is only on the order of  $10^6 \text{ s}^{-1}$  even when the total energy in the molecule reaches 100 kcal/mol. Using a program developed by Schulz<sup>11</sup> one can calculate the total internal energy distribution of the molecules by IRMPE pumping, and using this information on the internal energy distribution one can then calculate

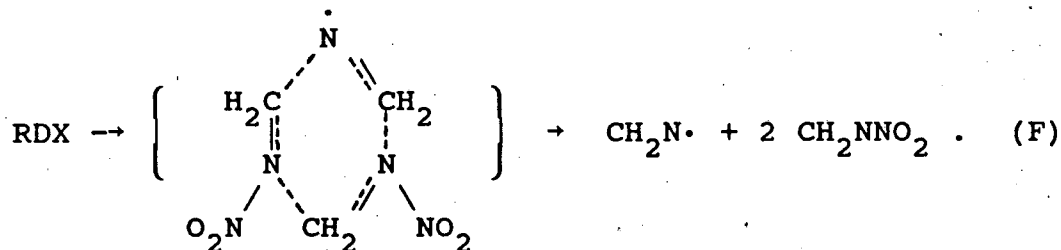
$P_E(E_T)$  for a simple bond rupture channel using RRKM theory. From a comparison between the calculated and observed  $P_E(E_T)$ 's, the average total internal energy can be derived.<sup>7</sup> The average total internal energy of the molecules after the laser pulse was calculated around 80 kcal/mol. These results imply that the dissociation of the molecule through reaction channel (I) in this environment will not limit the excitation of the molecule by CO<sub>2</sub> laser up-pumping (the laser pulse was shorter than 800 ns), and since the internal energy distribution of excited molecules is similar to that from thermal excitation, reaction (IV) is energetically accessible for a large fraction of the RDX in this experiment even though the endoergicity derived from the heat of formation of CH<sub>2</sub>NNO<sub>2</sub> given by Melius and Binkley seems unreasonably high. These results also means that most of the RDX dissociate after the laser pulse, and therefore it is almost certain that secondary dissociations are indeed spontaneous dissociations instead of secondary photodissociations during the laser pulse. The domination of reaction (IV) over (I) indicates that either the heat of formation of CH<sub>2</sub>NNO<sub>2</sub> estimated by Melius and Binkley is too high or the experimentally provided heat of formation of RDX is too low, or the pre-exponential factor of reaction (IV) is substantially higher than that of reaction (I).

Melius and Binkley suggested that one of the important reaction paths following reaction (I) may be that 176

undergoes a series of dissociation steps to give  $\text{CH}_2\text{N}$  and  $\text{CH}_2\text{NNO}_2$ . We have carefully studied this suggestion assuming the following mechanisms, which through various steps forms one  $\text{CH}_2\text{N}$  and two  $\text{CH}_2\text{NNO}_2$ .



and



Due to the similarity of the products, one cannot absolutely eliminate the possibility that those reactions occur in the experiment. However, we have observed no evidence for the existence of the intermediates in reactions (D) and (E), e.g.,  $m/e = 148$  or a faster second component in the  $m/e = 102$  TOF spectrum. In fact, reactions (D) and (E) are energetically unfavorable, because starting with about 80 kcal/mol of internal energy, formation of  $176 + \text{NO}_2$  has consumed about 45 kcal/mol, and there is simply not enough energy for the molecule to split further to form the more

unstable radical species. If reaction (D) is the main source of signal at  $m/e = 74$ ,  $\text{CH}_2\text{N}$  product would give a very fast component in the  $m/e = 28$  TOF spectrum by momentum conservation. If reaction (E) is the main source of signal at  $m/e = 74$ , we would likely see two components in the TOF spectrum of  $m/e = 74$ , because the two 74 species in reaction (E) would have different velocity distributions. All of the above expectation from reactions (D) and (E) were not observed from the experiment. To check reaction (F), more careful work is needed, since theoretically it is possible for reaction (F) to produce fast signal at  $m/e = 74$ , 28, 27, and 26, and there is a simultaneous three-body fission involved which makes analysis laborious. If reaction (F) was a main channel, we would expect that  $\text{CH}_2\text{N}$  would be responsible for the fast components in the TOF spectra of  $m/e = 28$ , 27, and 26. In order to fit the data, we have chosen several different effective masses to represent approximately two 74 fragments together, and found that the shape of the  $m/e = 74$  peak was too narrow to match that of  $m/e = 26$ . The shape of the fast edge of the  $m/e = 28$  TOF spectrum is different from that of  $m/e = 27$  and 26, which also indicates that those signals are not mainly from  $\text{CH}_2\text{N}$  and that reaction (F) is not important, if it occurs at all. We also checked the possibility of producing 74 from further dissociation of the product which appears as the fast component in the  $m/e = 81$  TOF spectrum, and found that we

could not fit the  $m/e = 74$  spectrum even by using an unrealistically narrow  $P_E(E_T)$ , ruling out the possibility of 74 being formed from larger products detected in this experiment. The most compelling evidence against reactions (D) - (F) is the branching ratio. If 74 was produced after reaction (I), we could at most obtain a ratio of 2:1 for  $\text{CH}_2\text{NNO}_2$  to  $\text{NO}_2$  from reaction (I), but in fact we obtained a ratio of 6, and the lowest bound of this value is still larger than 2 even considering the worst possible uncertainties. Also, the ratio of 176 to  $\text{NO}_2$  from (I) is 0.90, consistent with the picture that most of the 74 is not from further dissociation of 176.

### C. Importance of concerted reaction

The bulk thermal decomposition of RDX must contain both unimolecular and bimolecular processes. Since this experiment has eliminated the possibility of bimolecular reaction, the important unimolecular reactions involved are clearly revealed, even though it cannot answer all questions about the thermal decomposition of RDX. From the experimental results we have seen that unimolecular dissociation processes play important roles, especially in the initial steps. Comparing the product distribution observed in this experiment with that from thermal decomposition<sup>1</sup> we can say that unimolecular dissociation is the main avenue even for bulk RDX decomposition, because sequential unimolecular dissocia-

tion are responsible for the major products observed in the thermal decomposition.

There have been many reaction channels proposed for the thermal decomposition of RDX,<sup>1-4</sup> most of which are simple bond rupture or bimolecular processes. Our experiment has shown that through concerted unimolecular dissociation channels RDX goes to various final products similar to those of bulk dissociation in only two steps. For simple bond rupture, the potential energy surface of the molecules usually has a high activation energy with at most a small exit barrier. Most of the energy is either consumed to break the chemical bond or tied up in vibrational degrees of freedom, so that only a small amount of translational energy is released. In contrast, in concerted reactions the molecule usually has a strained configuration at the transition state, and after crossing this barrier to form products much of the extra potential energy of the transition state appears in the form of repulsion between the recoiling partners, i.e., in the form of translational energy.

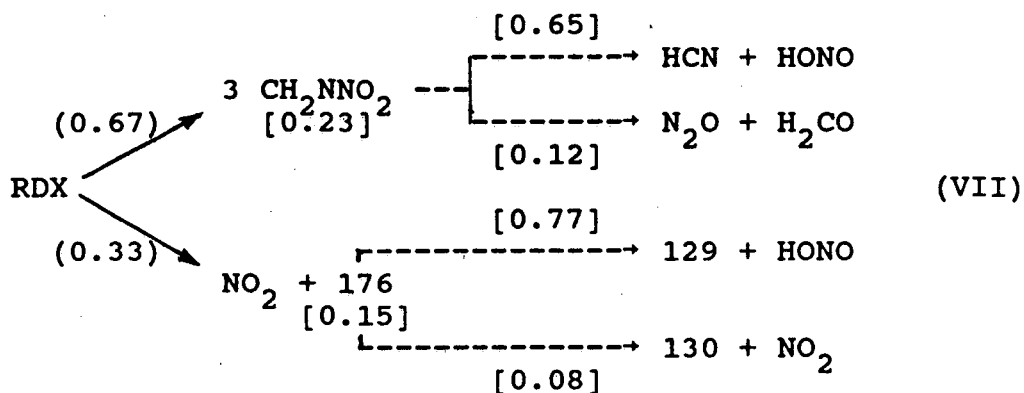
If the main reaction paths in the thermal decomposition of RDX were through bimolecular reactions, the bulk product distribution would be even more complicated than it is, because there are many possible ways for the unstable intermediates and radicals to combine with each other. It has been shown that at low temperatures the two most

probable products of thermal decomposition of RDX are  $N_2O$  and  $H_2CO$  (195 °C) which decrease as the temperature increases, while at high temperature (600 °C) HCN and NO become the two largest products,<sup>1</sup> consistent with the concerted reaction picture presented here. In this experiment among six observed reaction channels only two occur through simple bond rupture and, as seen above, their relative amounts are small. Concerted reaction is dominant not only in the number of channels but also in the amount of products formed.

Knowing the branching ratios we can answer another interesting question, i.e., how many molecules are produced and how much energy is released into translation per RDX molecule within this scheme. It is calculated that there are 4.5 molecules produced on average compared with bulk thermal decomposition where the average number of molecules produced is 7.<sup>12</sup> Obviously, in the case of thermal decomposition some of the products which are formed in IRMPD will undergo further reaction through either unimolecular or bimolecular paths and all of the unstable intermediates will be eventually converted into stable products.

In this experiment 26.4 kcal/(mol RDX) was released to translation in the c.m. frame of RDX. Although part of this energy is from the  $CO_2$  laser, it helps us to think about the case of thermal decomposition, where the activation of the molecules is by thermal energy, and after endothermic steps

further exothermic steps follow. Based on the thermochemical data given by Melius and Binkley<sup>3</sup> and the branching ratios obtained in this experiment, the endothermicity of reaction (VII),



is 32 kcal/(mol RDX) and the average internal energy of RDX is about 80 kcal/mol as shown before. Therefore, over half of the available energy appears in translation. The normalized branching ratio of the primary dissociation steps are shown in parentheses. For the secondary dissociations, the three numbers shown in brackets for each branch are the relative amount of those remaining as primary products and the two secondary reaction channels.

## VI. Summary

IRMPD in a molecular beam with its unique advantage has been successfully used to study unimolecular dissociation. This method is extended to even larger molecules and much more complicated processes than before, where its advantages become even more appreciable. We have shown that it is

possible to get enough RDX into the gas phase for molecular beam studies. We have also shown that RDX easily undergoes multi-step unimolecular dissociation. There are many channels competing with each other, with concerted dissociation as the dominant manner, allowing very simple products such as HCN, H<sub>2</sub>CO, and N<sub>2</sub>O observed in bulk thermal decomposition, to be produced in a few steps and a short time. A fair amount of translational energy release through concerted reaction has been observed, which is significant for an explanation of the nature of the energy release in RDX decomposition.

One of the most interesting results out of this study is the observation of the concerted triple dissociation channel. It is worthwhile paying more attention to this type of dissociation both experimentally and theoretically due to their importance in the dissociation of highly symmetric polyatomic molecules and their fascinating nature. In next chapter we will look into this subject in great detail on another molecule, s-tetrazine.

**References**

- 1 M. A. Schroeder has written a series of review articles, of which we quote most frequently M. A. Schroeder, Proceedings of the 18th JANNAF Combustion Meeting, Vol. II, 395 (1981).
- 2 J. J. Batten, Int. J. Chem. Kinet. **17**, 1085 (1985).
- 3 C. F. Melius and J. S. Binkley, submitted.
- 4 S. Bulusu, D. I. Weinstein, J. R. Autera, and R. W. Velicky, J. Phys. Chem. **90**, 4121 (1986).
- 5 D. krajnovich, F. Huisken, Z. Zhang, Y. R. Shen, and Y. T. Lee, J. Chem. Phys. **77**, 5977 (1982).
- 6 L. J. Butler, R. J. Buss, R. J. Brudzynski, and Y. T. Lee, J. Phys. Chem. **87**, 5106 (1983).
- 7 A. M. Wodtke, E. J. Hintsä, and Y. T. Lee, J. Phys. Chem. **90**, 3549 (1986).
- 8 A. M. Wodtke and Y. T. Lee, J. Phys. Chem. **89**, 4744 (1985).
- 9 M. Farber and R. D. Srivastava, Chem. Phys. Lett. **64**, 307 (1979).
- 10 The computing program is presented in Appendix A.
- 11 (a) E. R. Grant, P. A. Schulz, Aa. S. Sudbo, Y. R. Shen, and Y. T. Lee, Phys. Rev. Lett. **40**, 115 (1978);  
(b) P. A. Schulz, Ph.D. thesis, University of California, 1979.
- 12 J. J. Batten, Aust. J. Chem. **24**, 945 (1971).

**Table I**  
**Comparison of Mass Spectra<sup>a</sup>**

Species	m/e	Relative amount		Species	m/e	Relative amount	
		This work	Lit.			This work	Lit.
NO <sub>2</sub> (I)	46	335	370	NO <sub>2</sub> (II)	46	612	370
	30	1000	1000		30	1000	1000
	16	429	223		16	290	223
	14	117	96		14	80	96
N <sub>2</sub> O	44	131	1000	H <sub>2</sub> CO	30	174	600
	30	187	311		29	160	1000
	28	1000	108		28	1000	307
	16	27	50		16	55	18.8
	14	7	127		14	53	15.3
				13	82	8.2	
HCN	27	1000	1000	12	80	8.2	
	26	70	168				
	14	29	11				
	13	5	17				
	12	21	17				

<sup>a</sup> Literature values in this table are from Atlas of Mass Spectral Data, edited by E. Stenhagen, S. Abrahamsson, and F. W. McLafferty (Interscience, New York, 1969), Vol. I.

**Table II**  
**Experimental Laser Power Dependence of Signal Counts**  
**in Ions per Laser Shot**

m/e	Lab. angle (°)	Laser power in J/cm <sup>2</sup>		
		20	16	6
30	14	32.0		16.0
74	10	1.55		1.04
74	14	1.31		0.93
42	14	2.52		1.67
17	14	0.14	0.13	
102	10	1.24	1.07	

**Table III**  
**Relative Yield of Products<sup>a</sup>**

---

Primary					
Species	46(I)	176(I) <sup>b</sup>		74(IV) <sup>b</sup>	
Relative yield	1.0 <sup>c</sup>	0.90		6.1	
Secondary 1, from 74					
Species	27(VI)	47(VI)	44(V)	30(V)	74(IV) <sup>d</sup>
Relative yield	5.4	2.6	1.0 <sup>c</sup>	1.5	1.9
Secondary 2, from 176					
Species	129(II)	47(II)	130(III)	46(III)	176(I) <sup>d</sup>
Relative yield	9.6	12	1.0 <sup>c</sup>	4.3	1.9

---

a (I) - (VI) stand for the reaction channels in the text, and the number stands for the species of that molecular weight.

b Sum of those undergoing secondary dissociation and those which survive.

c Chosen as 1.0

d Only those which survive.

**Figure Captions for Chapter II**

Fig. 1 TOF spectra for the masses with  $m/e$  greater than 30.

The open circles are observed data, and the curves are calculated TOF spectra. The angle in each TOF spectrum is the laboratory angle at which the spectrum was taken.

Fig. 2 TOF spectra for the masses with  $m/e$  smaller than 30.

The open circles are observed data, and the curves are calculated TOF spectra. The angle in each TOF spectrum is the laboratory angle at which the spectrum was taken.

Fig. 3  $P_E(E_T)$  for reaction (I) used to fit experimental data in figs.1 and 2.

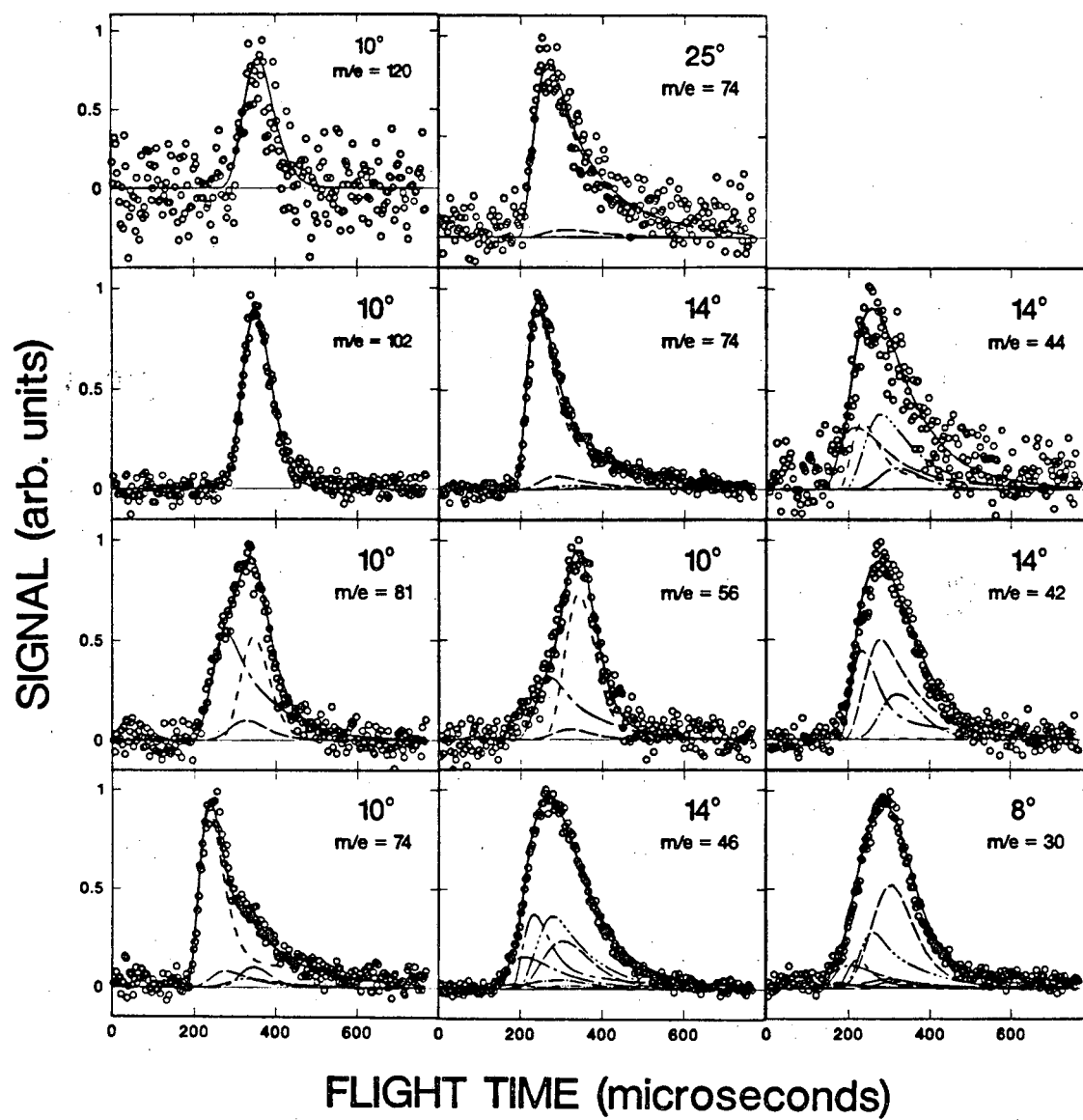
Fig. 4  $P_E(E_T)$  for reaction (II) used to fit experimental data in figs.1 and 2.

Fig. 5  $P_E(E_T)$  for reaction (III) used to fit experimental data in figs.1 and 2.

Fig. 6  $P_E(E_T)$  for reaction (IV) used to fit experimental data in figs.1 and 2.

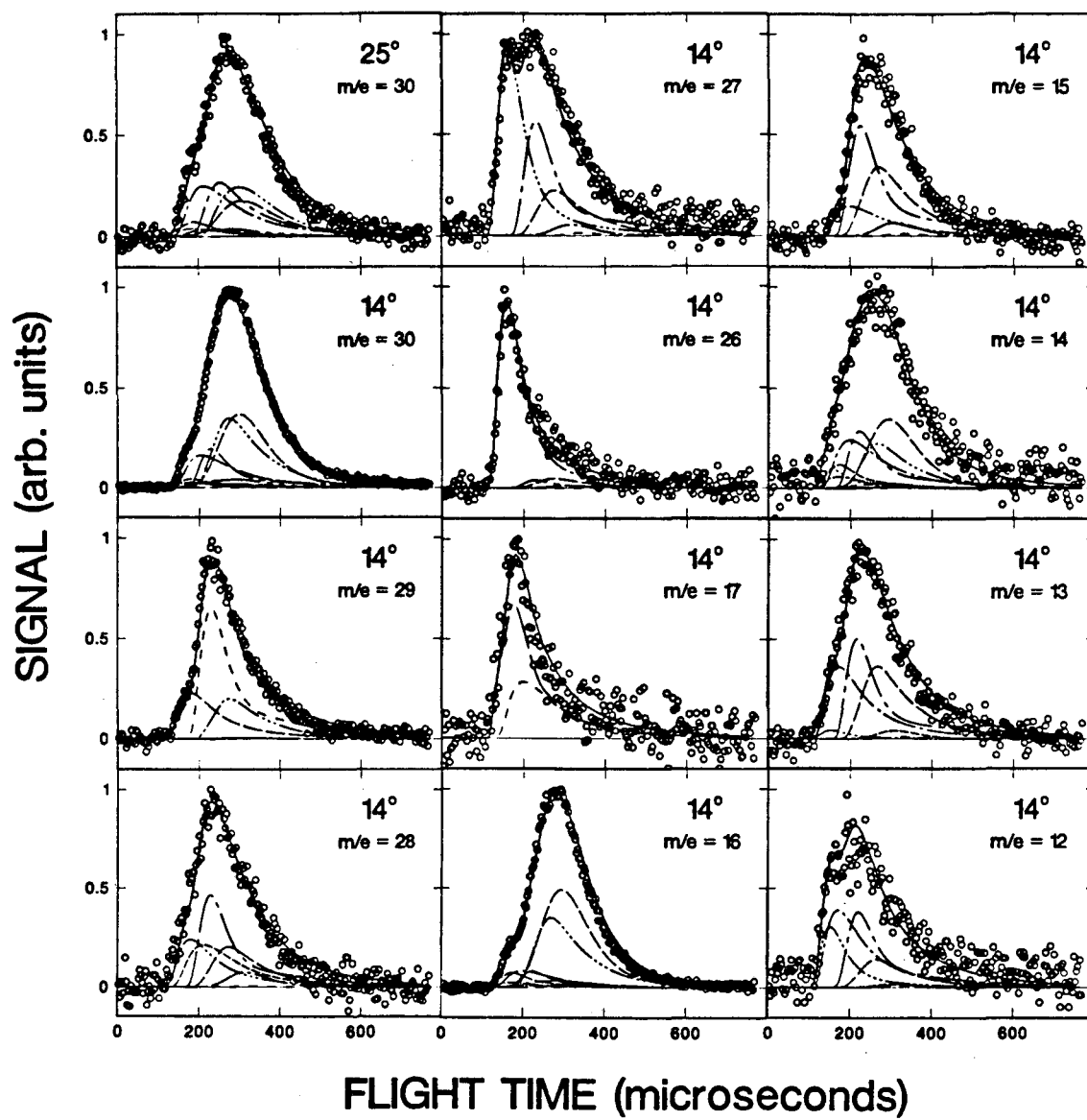
Fig. 7  $P_E(E_T)$  for reaction (V) used to fit experimental data in figs.1 and 2.

Fig. 8  $P_E(E_T)$  for reaction (VI) used to fit experimental data in figs.1 and 2.



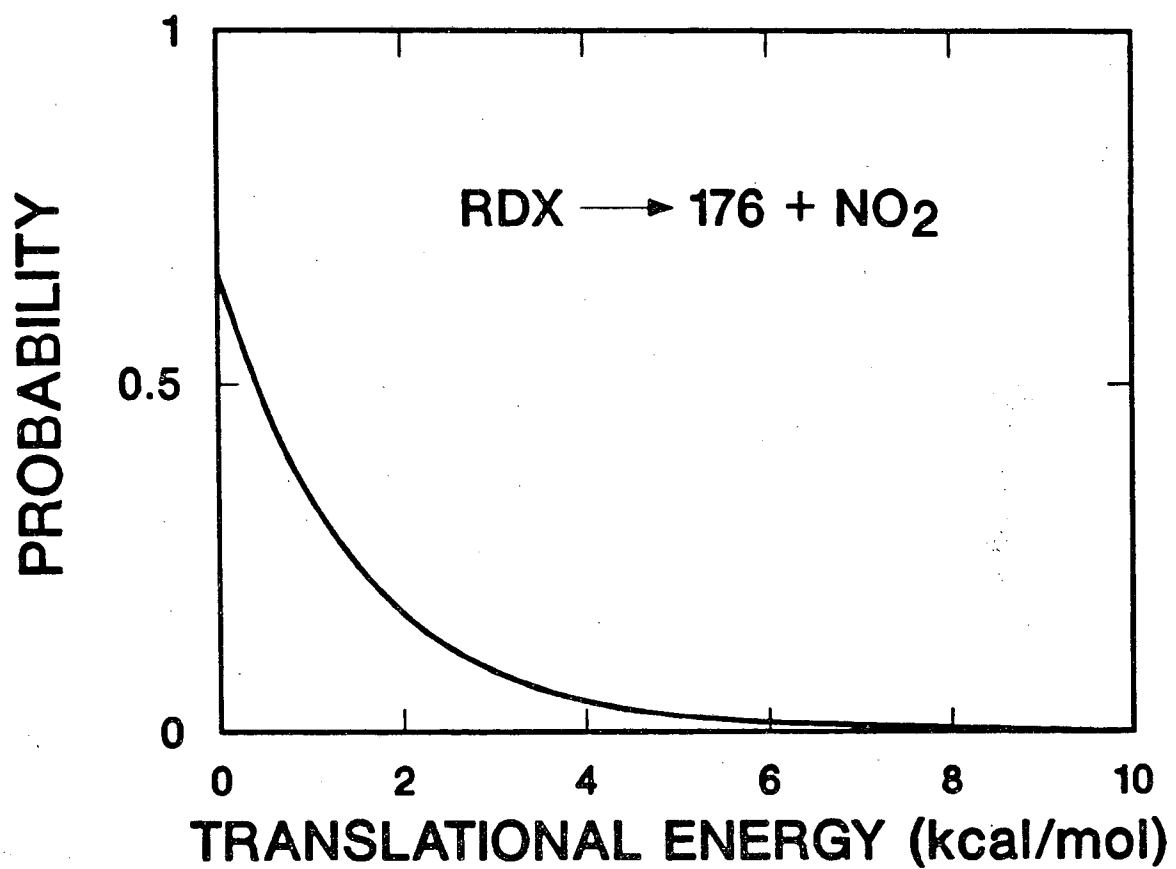
XBL 875-2319

Fig. 1



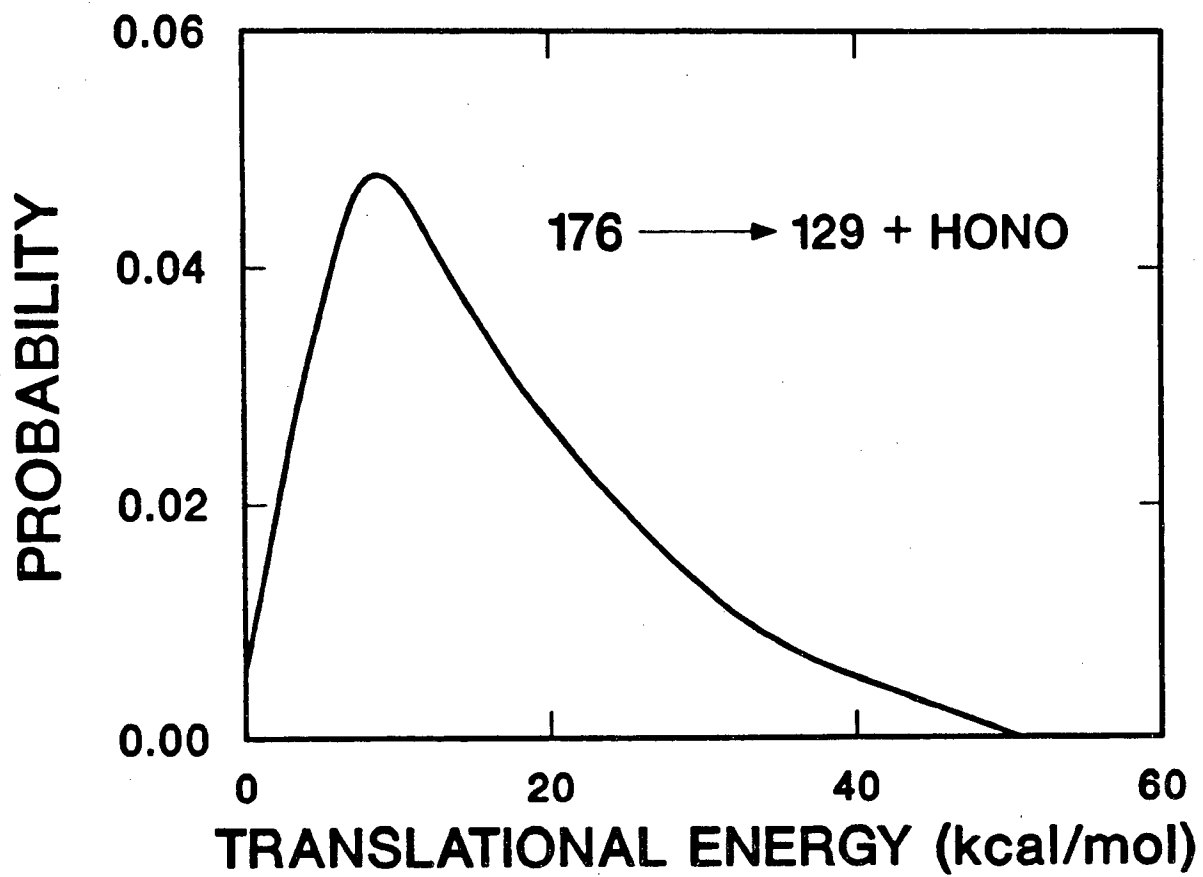
XBL 875-2318

Fig. 2



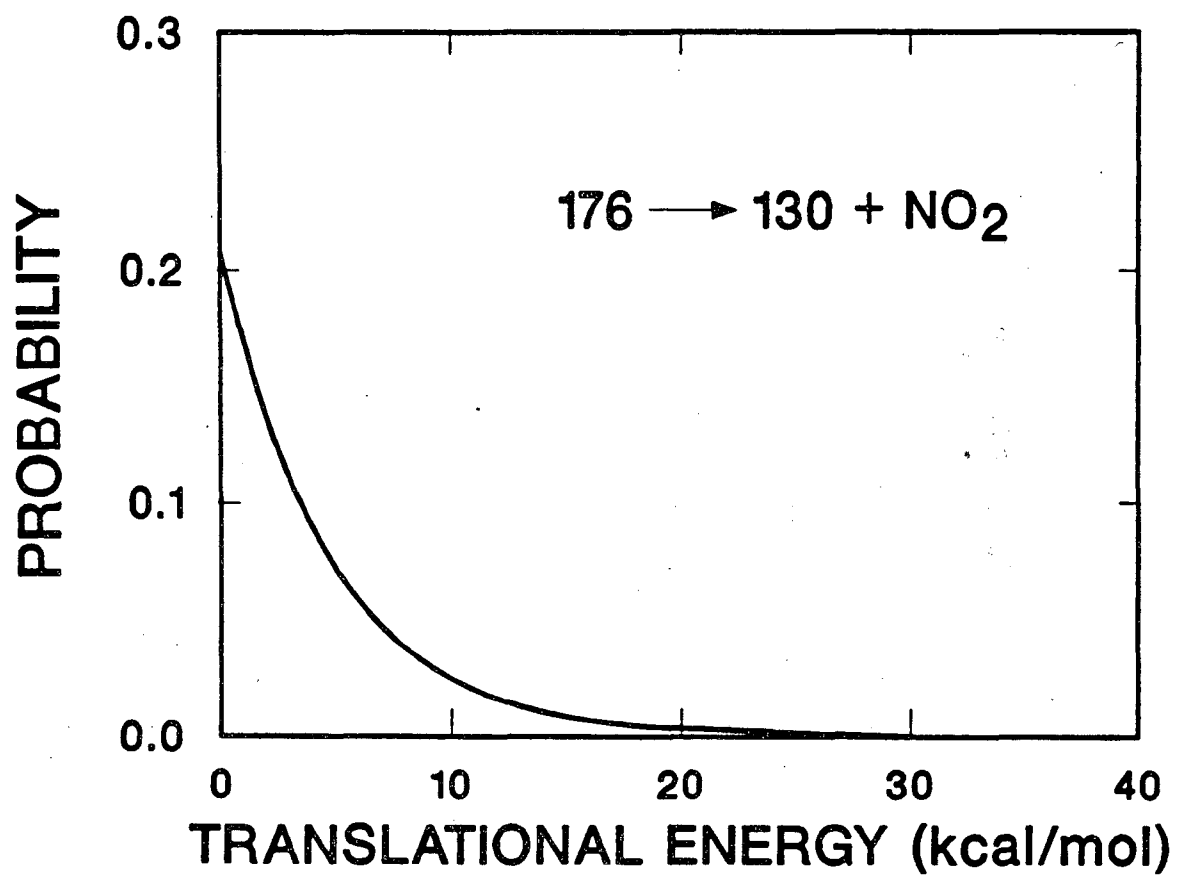
XBL 875-2325

Fig. 3



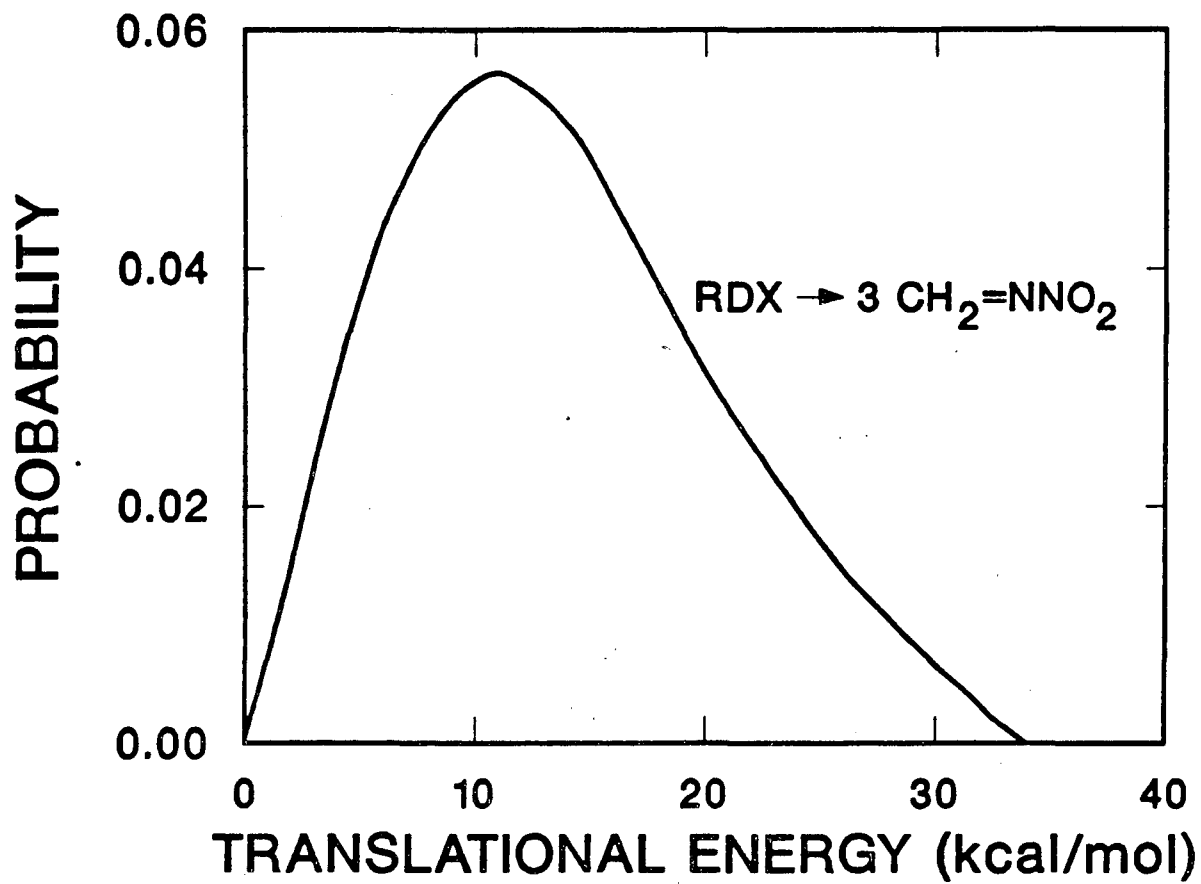
XBL 875-2323

Fig. 4



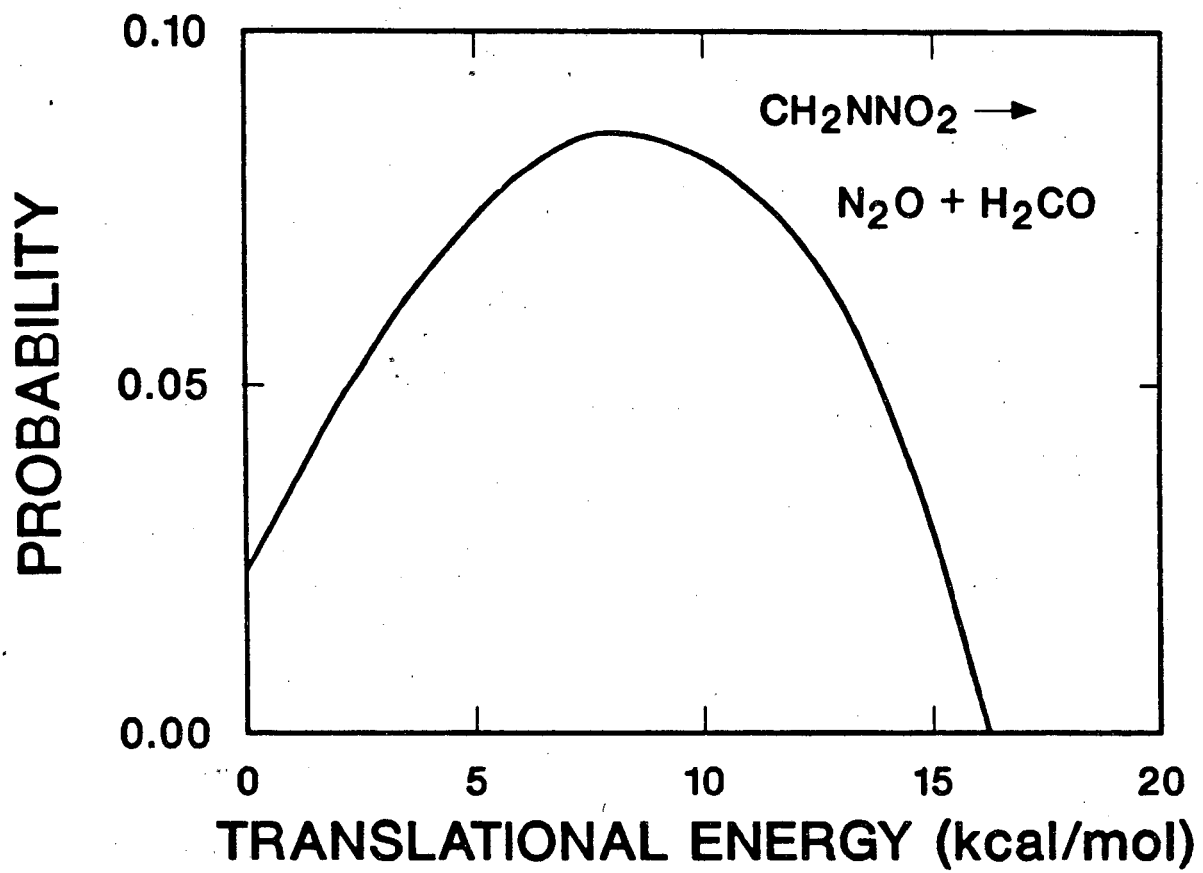
XBL 875-2324

Fig. 5



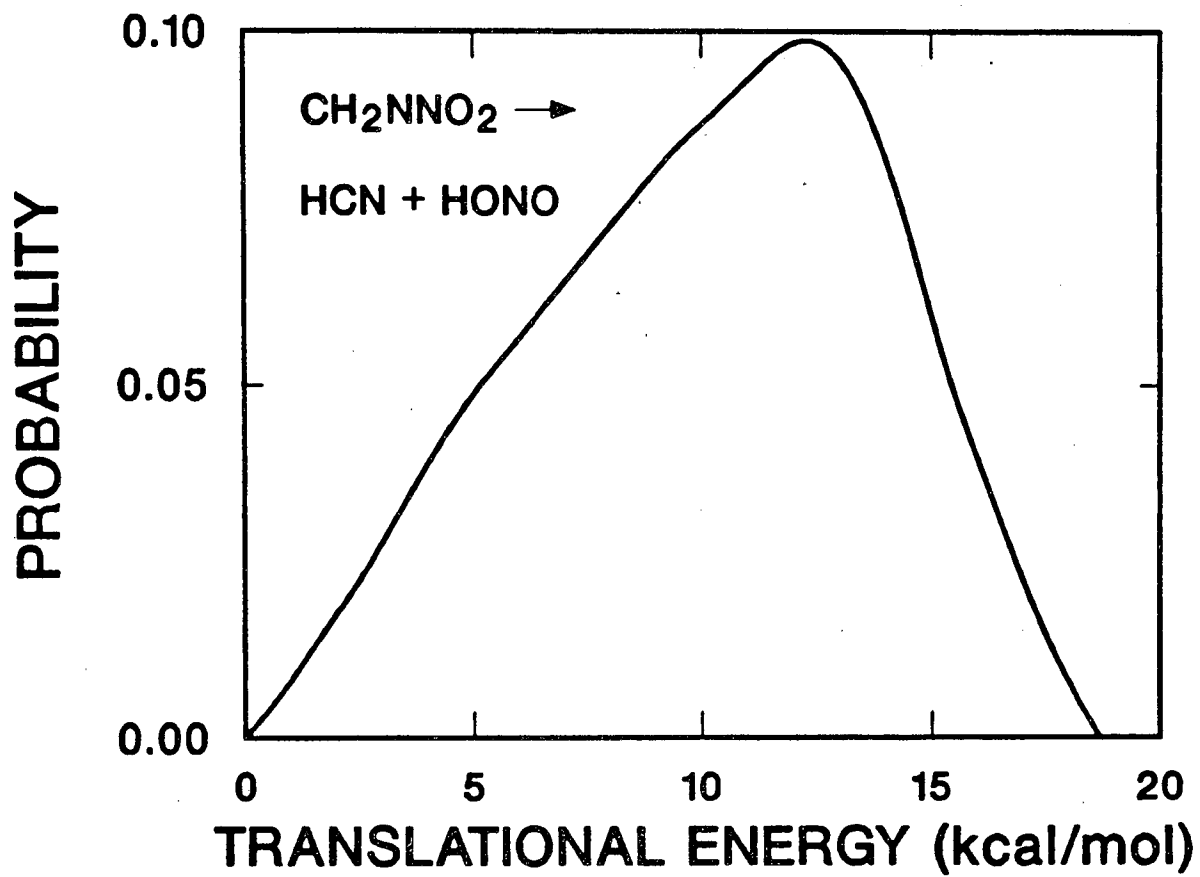
XBL 875-2320

Fig. 6



XBL 875-2321

Fig. 7



XBL 875-2322

Fig. 8

## CHAPTER III

A CONCERTED TRIPLE DISSOCIATION -  
THE PHOTOCHEMISTRY OF S-TETRAZINE

## I. Introduction

S-tetrazine (ST) is a member of the family of nitrogen containing compounds known as azines which are isoelectronic to each other and to benzene, and has long attracted attention from chemists due to its structure and properties. Since the pioneering work of Mason<sup>1</sup> and Spencer *et al.*,<sup>2</sup> this molecule has been intensively investigated and is now well understood spectroscopically in the neighborhood of the  $^1A_g(S_0)$ ,  $^1B_{3u}(S_1)$  and  $^3B_{3u}(T_1)$  states.<sup>3-9</sup>

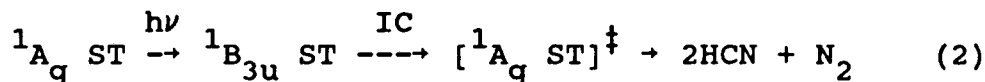
In contrast to the spectroscopy, a consensus has not been reached on the photochemistry of ST, as far as the dissociation mechanism is concerned.<sup>3</sup> Since an extensive review of the controversy over the suggested dissociation mechanism has been given in a recent publication by Scheiner and Schaefer (SS),<sup>3</sup> we will only emphasize a few important points.

While there is no doubt that the main outcome of  $S_1 \rightarrow S_0$  excitation is dissociation, and that the products are HCN and  $N_2$ , different experiments support different mechanisms for the reaction

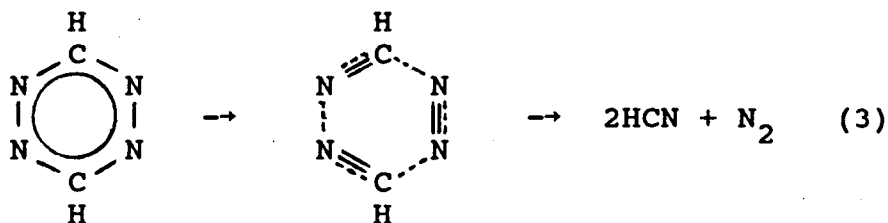


In the case of the  $S_1 \rightarrow S_0$  transition, the dissociation mechanisms can be classified into two categories.

Mechanism I: One photon absorption followed by internal conversion (IC) with dissociation occurring on the  $S_0$  potential energy surface (PES), i.e.,



Within this scheme, concerted triple dissociation



is the most plausible pathway.<sup>10,11</sup>

Mechanism II. Sequential two photon absorption followed by dissociation through an intermediate state other than the ground state:<sup>12,13</sup>

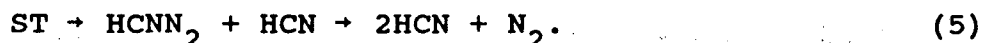


where  ${}^1X$  is the intermediate state.

The strongest support for mechanism I to date is the theoretical calculation by Scheiner, Scuseria, and Schaefer (SSS).<sup>10</sup> Using standard double  $\zeta$  and double  $\zeta$  plus polarization basis sets, they carried out self-consistent field and

configuration interaction calculations on ST. SSS were able to locate the transition state for triple dissociation on the  $S_0$  PES, which is energetically accessible by  ${}^1B_{3u} + {}^1A_g$  excitation and leads to ground electronic state products.  $SS^3$  also calculated the exothermicity of reaction (1). Fig. 1 presents an energy diagram according to the literature and the results of SS and SSS.

Support for mechanism II came from a molecular beam photofragmentation experiment by Glowacki and Riley (GR).<sup>14</sup> In their experiment a molecular beam of ST from an effusive source (at 50°C) was irradiated in a vacuum chamber by a pulsed Nd:Yag laser at either the second harmonic (532 nm) or the fourth harmonic (266 nm) frequency. The most interesting result that GR obtained is that the time-of-flight (TOF) spectra of HCN at both laser wavelengths were almost identical, with an obvious bimodal shape. The spectrum of HCN contains a very fast narrow peak and a broad slow tail, while the TOF spectra of  $N_2$  have only one component. Based on their analysis, GR argued for mechanism II with 532 nm excitation and assigned the intermediate state  ${}^1X$  in reaction (4) as a  ${}^1B_{2u}$  state, the same state reached by one photon excitation at 266 nm. GR argued further that the dissociation is a stepwise process:



Faced with the inconsistencies between theory and experiment, a new experiment with better characterized

experimental conditions has been carried out. As indicated by the title, our investigation has confirmed that s-tetrazine undergoes concerted triple dissociation, supporting the scheme of mechanism I. Furthermore, our results suggest that the photochemistry upon  ${}^1B_{2u} \leftarrow {}^1A_g$  excitation follows the same route as with the  ${}^1B_{3u} \leftarrow {}^1A_g$  transition.

It has been a challenge to analyze concerted triple dissociation product velocity and angular distributions obtained in molecular beam experiments.<sup>15-17</sup> Recently, a concerted triple dissociation similar to reaction (3) was observed<sup>17</sup> where the three fragments were identical, so that the inherent three-fold symmetry allowed analysis to be carried out simply and accurately. For the analysis of the results obtained in this experiment and other molecular beam experiments where triple dissociation is involved, a simple general and realistic model is developed.

## II. Experimental

The experimental apparatus has been described in detail elsewhere.<sup>18</sup> Briefly, a molecular beam and a laser beam were crossed at 90° in a vacuum chamber. Dissociation products passed through the aperture of the detector chamber at a variable angle with respect to the molecular beam. The neutral products were then ionized in an electron bombardment ionizer, mass selected by a quadrupole mass

filter, and detected with a Daly-type ion counter. A multi-channel scaler interfaced with an LSI-11 microcomputer recorded the arrival time of the signal relative to the laser pulse to obtain the TOF spectra. The distance between the interaction region and the ionizer is 36.7 cm. The angle between the molecular beam and the detector is variable between 0° and 90°, allowing us to detect even those products with very small center-of-mass (c.m.) translational energies. Installation of a liquid helium cooled cryopanel opposite the entrance slit to the detector not only greatly reduces the background, but, more importantly, prevents dissociation products which scatter in the opposite direction to the detector from bouncing back into the detector to create false signal. In order to reduce the velocity spread of the ST beam and the chances of forming ST dimer, ST was held at 20 °C, He was used as a carrier gas with a total pressure of about 100 Torr, and the nozzle temperature was kept at 78 °C. With the above conditions the average beam velocity was  $1.5 \times 10^5$  cm/sec with an 8% FWHM velocity spread.

For the excitation of the  ${}^1B_{3u} \rightarrow {}^1A_g$  transition, a Lambda Physik FL2002 dye laser was used with Coumarin 540A (Exciton), pumped by a Lambda Physik EMG 103 MSC excimer laser operated at 308 nm with a repetition rate of 100 Hz. The linewidth of the dye laser was about  $0.2 \text{ cm}^{-1}$ , and the laser was tuned to  $18128.0 \text{ cm}^{-1}$  for the 0-0 transition and

18830.9  $\text{cm}^{-1}$  for the  $6a_0^1$  transition.<sup>5</sup> A Glan-Taylor polarizer was used to obtain linearly polarized light in different directions. The laser beam was adjusted to a 1 mm diameter spot at the crossing point with the molecular beam.

To study the  ${}^1B_{2u} \rightarrow {}^1A_g$  transition, the same excimer laser was used with krypton fluoride at 248 nm, where the absorption of ST is almost at a maximum.<sup>2</sup> A MgF prism was used to separate the vertically and horizontally polarized laser beam, and the beam with the desired polarization was focused to 1 mm  $\times$  3 mm in the interaction region.

ST was synthesized according to the method given by Spencer *et al.*<sup>2</sup> The precursor, s-tetrazine dicarboxylic acid, was made in advance and ST was prepared fresh from the precursor immediately before each experiment.

### III. Results and analysis

#### A. General features

All the TOF spectra of mass-to-charge ratio ( $m/e$ ) = 27 ( $\text{HCN}^+$ ), two of which are shown in Fig. 2, and of  $m/e$  = 26 ( $\text{CN}^+$ ), which are identical to that of  $m/e$  = 27, consist of a single fast sharp peak. TOF spectra of  $m/e$  = 28 ( $\text{N}_2^+$ ) are also composed of only one peak, slightly broader and slower than that of the corresponding HCN, and two examples are also shown in Fig. 2. A search for fragments with  $m/e > 28$  was carried out, but no signal was detected. The single

fast peak in all the TOF spectra implies a one-step triple dissociation with large recoil velocity.

The TOF spectra due to excitation of two vibrational bands in the  ${}^1B_{3u} + {}^1A_g$  transition (hereafter 0-0 and  $6a_0^1$  are used to stand for the respective bands of the  ${}^1B_{3u} + {}^1A_g$  transition) look the same. The peak positions in the TOF spectra of the products from 248 nm excitation are similar to those from  $S_1 + S_0$  excitation, but the widths of the peaks are broader at 248 nm than that at  $S_1 + S_0$  excitation. The polarization angle of the laser affects neither the signal level nor the shape of the TOF spectra much for HCN at all laser frequencies, but it does strongly affect the  $N_2$  signal level at 248 nm.

At the normal output energy of the dye laser (about 10 mJ/pulse) the dissociation is highly saturated for both 0-0 and  $6a_0^1$ . In order to study the power dependence and to eliminate saturation effects, neutral density filters were placed in the path of the laser beam and the HCN fragment intensity was measured over a wide range of laser powers. The shape of the HCN TOF spectra was unchanged over the entire range. The dependence of the photolysis signal on the laser power for 0-0 plotted in Fig. 3 approaches linearity as the laser power approaches zero, providing unambiguous evidence that the dissociation of ST following  ${}^1B_{3u} + {}^1A_g$  excitation is a one photon event.

The laser power dependence at 248 nm showed similar

behavior, that is, saturation occurred at laser energies above 3 mJ/pulse, and the dependence approached linearity when the laser power was reduced below 3 mJ/pulse.

To prevent complications from saturation, the laser power was kept in the linear region when the laboratory angular dependence (varying the angle between the molecular beam and the detector) and laser polarization dependence (varying the angle between the electric vector of the laser and the detector) were measured for both 248 nm and  $S_1 \leftarrow S_0$  excitation.

#### B. Simple model for analysis of triple dissociation

It is well known that in a two-body dissociation process momentum and energy conservation uniquely determine the relationship between the two fragments. When three particles recoil from each other simultaneously, the situation becomes more complicated, because unless the three velocity vectors of the recoiling particles are measured simultaneously, it is difficult to get the translational energy distribution of the whole system from the measured individual velocity distributions of the fragments as can be done for two-body dissociation.

Consider a molecule simultaneously dissociating into particles 1, 2 and 3 with masses  $m_1$ ,  $m_2$  and  $m_3$  respectively. A diagram of the dissociation process in velocity space is shown in Fig. 4, where  $\hat{u}_1^0$ ,  $\hat{u}_2^0$  and  $\hat{u}_3^0$  are the direction

vectors of the asymptotic velocities of particles 1, 2 and 3 in a body-fixed c.m. frame respectively,  $\alpha$  and  $\beta$  are the angles between  $\hat{u}_1^0$  and  $\hat{u}_2^0$  and between  $\hat{u}_1^0$  and  $\hat{u}_3^0$  respectively, and  $\delta = \pi - \alpha$  and  $\gamma = \pi - \beta$ . At this geometry the c.m. translational energy is

$$E_T = 1/2 m_1 (u_1^0)^2 + 1/2 m_2 (u_2^0)^2 + 1/2 m_3 (u_3^0)^2, \quad (6)$$

and by momentum conservation,

$$\begin{aligned} m_2 u_2^0 \sin \delta &= m_3 u_3^0 \sin \gamma \\ m_1 u_1^0 &= m_2 u_2^0 \cos \delta + m_3 u_3^0 \cos \gamma, \end{aligned} \quad (7)$$

where  $u_1^0$ ,  $u_2^0$  and  $u_3^0$  are the magnitudes of the asymptotic velocities of the particles 1, 2 and 3 respectively.

If  $\gamma + \delta \neq 0$ , from (6) and (7) we have

$$E_T = \frac{m_1}{2} \left[ 1 + \frac{m_1}{\sin^2(\gamma + \delta)} \left( \frac{\sin^2 \delta}{m_3} + \frac{\sin^2 \gamma}{m_2} \right) \right] (u_1^0)^2. \quad (8)$$

When  $\gamma + \delta = 0$ , the relation between  $E_T$  and  $u_1^0$  becomes uncertain, but in the special situation when  $u_2^0 = u_3^0$ , the problem reduces to a two-body problem corresponding to the dissociation of the molecule into  $m_1$  and  $m_2 + m_3$ , and the following equation can be used,

$$E_T = \frac{m_1}{2} \frac{m_1 + m_2 + m_3}{m_2 + m_3} (u_1^0)^2, \quad \gamma + \delta = 0. \quad (9)$$

If the molecule dissociates through only one asymptotic geometry, namely one set of  $\alpha$  and  $\beta$ , the data analysis would be straightforward, using the method for two-body dissociation<sup>19</sup> with proper modification.

In a real system, although the angles  $\alpha$  and  $\beta$  in indi-

vidual dissociation events may vary, for a simultaneous triple dissociation the geometry must follow a certain distribution with respect to the two angles  $\alpha$  and  $\beta$  as well as  $E_T$ , say,  $F(\alpha, \beta; E_T)$ . Therefore one way to approach the problem of data analysis is to find  $F(\alpha, \beta; E_T)$  and to convolute the appropriate distribution.

In practice, however, there are some difficulties finding  $F(\alpha, \beta; E_T)$ : it does not treat the three particles equivalently. In the case where we do not know much about the structure and interaction potential of the transition state, we do not have any clue how  $F(\alpha, \beta; E_T)$  will look, and it is not known whether  $F(\alpha, \beta; E_T)$  is separable into  $F(\alpha, \beta; E_T) = f(\alpha, E_T)g(\beta, E_T)$ .

To avoid this problem we assume that at a fixed total internal energy there is a most probable dissociation geometry with reference angles  $\alpha_r$  and  $\beta_r$ . We also assume that the distribution of geometries does not depend on the translational energy and can be described by three factors which are functions of  $\theta$ ,  $\eta$  and  $\phi$  respectively, i.e.,

$$G(\theta, \eta, \phi) = G_1(\theta)G_2(\eta)G_3(\phi) , \quad (10)$$

where  $\theta$ ,  $\eta$  and  $\phi$  are the angles between a particular asymptotic geometry of  $m_1$ ,  $m_2$  and  $m_3$  and the most probable asymptotic geometry as shown in Fig. 4.

Since  $G(\theta, \eta, \phi)$  treats the three particles independently and consists of distributions about the most probable values, we assume that the  $G_i$ 's in equation (10) have the

same mathematical form, and that Gaussian functions can be used as an approximation,

$$G_i(x) = A_i e^{-1/2(x/\sigma_i)^2}; \quad i=1,2,3, \quad (11)$$

where  $A_i$  is a normalization factor and  $\sigma_i$  is a width parameter. Because it successfully fit the data, Eqn. (11) is the only functional form that we tried.

The angular distribution of the dissociation products for an electric dipole transition in a space-fixed c.m. coordinate frame has been expressed as<sup>20,21</sup>

$$P(\cos\Omega) = (1/4\pi)(1 + 2bP_2(\cos\Omega)) , \quad (12)$$

where  $\Omega$  is the polar angle of the direction of the fragments when the z axis is chosen along the electric field vector of the linearly polarized light,  $P_2(x)$  is the second Legendre polynomial, and b is defined by

$$b = b'P_2(\cos\tau) , \quad (13)$$

where  $\tau$  is the angle between the transition dipole and the recoil velocity in a body fixed c.m. coordinate system, and  $b'$  is a parameter which basically describes rotation and relaxation effects of the energized molecule. This interpretation has been rigorously verified for diatomic molecules.

For the triple dissociation of ST, let us consider that ST with a transition dipole along  $\hat{\mu}$  absorbs a photon with electric field along  $\hat{\epsilon}$ . The absorption probability is proportional to  $(\hat{\mu} \cdot \hat{\epsilon})^2$  in a classical picture, or in the conventional form

$$P_{\text{abs}}(\hat{\mu} \cdot \hat{\epsilon}) = (1/4\pi)(1+2P_2(\hat{\mu} \cdot \hat{\epsilon})), \quad (14)$$

where  $P_{\text{abs}}(\hat{\mu} \cdot \hat{\epsilon})$  is the angular distribution of absorption. After absorption the molecule can undergo a series of structural changes before it dissociates. We will assume that the lifetime of the molecule is long enough for the following discussion. Fig. 5 shows relevant relations, where  $T_0$  represents the direction from the c.m. of the molecule to the c.m. of the group of atoms which will be detected, at the moment of photon absorption, and  $T$  is the analogous direction at the transition state. Because the orientation of the molecules in space is isotropic, the initial directions of  $T_0$  which lead to the transition state along  $T$  are along circle 1 in Fig. 5. This means that the corresponding initial direction of the transition dipole  $\mu$  is along circle 2, with  $\theta_T$  the angle between  $\mu$  and  $T$ . The probability of a transition state along  $T$  is the average of equation (14) over circle 2, which is simply<sup>22</sup>

$$P_{\hat{T}}(\hat{T} \cdot \hat{\epsilon}) = (1/4\pi)(1+2P_2(\hat{\mu} \cdot \hat{T})P_2(\hat{T} \cdot \hat{\epsilon})). \quad (15)$$

If the asymptotic geometry is different from the transition state geometry, there is an angle between  $T$  and  $u^0$ , the asymptotic velocity of the detected fragment in the body-fixed c.m. coordinate system. This difference is the result of intramolecular relaxation and internal motion near the transition state. The probability of a fragment along  $u^0$  is (15) averaged over circle 3, which is

$$P_{\hat{u}^0}(\hat{u}^0 \cdot \hat{\epsilon}) = (1/4\pi)(1+2P_2(\hat{\mu} \cdot \hat{T})P_2(\hat{T} \cdot \hat{u}^0)P_2(\hat{u}^0 \cdot \hat{\epsilon})). \quad (16)$$

The physical basis of Eqn. (16) is that molecular rotation and internal motion of the molecule cause randomization of the direction of the tangential component of the fragment recoil velocity. This is an implicit effect which makes the average along circle 3 valid and is not directly reflected in the formula. In general, the magnitude of  $P_2(\hat{T} \cdot \hat{u}^0)$  is different for each individual fragment, and we call it the local anisotropy parameter. Then, as in previous papers<sup>20,21</sup> we introduce the parameter  $b_1$  to account for the smearing out effect of molecular rotation on the angular distribution of the photofragment in a space-fixed frame, which we call the direct effect of molecular rotation on the anisotropy. Mathematically,  $b_1$  is the result of the transformation of the c.m. coordinate system from the body-fixed frames to the space-fixed frame, summed over all possible relations between the different frames. Therefore, the photofragment c.m. angular distribution in the space-fixed frame is

$$P_{\hat{u}}(\hat{u} \cdot \hat{\epsilon}) = (1/4\pi) (1 + 2b_1 P_2(\hat{\mu} \cdot \hat{T}) P_2(\hat{T} \cdot \hat{u}^0) P_2(\hat{u} \cdot \hat{\epsilon})), \quad (17)$$

where  $\hat{u}$  is the unit vector of the asymptotic c.m. velocity of the fragment in the space-fixed frame. According to the above physical and mathematical explanations,  $b_1$  is the same for all the fragments, and we call  $b_1$  the global anisotropy parameter. It is emphasized that where the implicit effect of molecular rotation is important, Eqn. (17) reveals information about the geometry of the transition state. By

measuring the laboratory angular dependence and/or laser polarization dependence,  $\theta_T$  can be obtained within the above approximation.

Obviously, there is a distribution between  $u^0$  and  $T$ , and according to our approximation it is related to  $G(\theta, \eta, \phi)$  of Eqn. (10). Therefore, to get the overall probability of signal at direction  $\hat{u}$ , Eqn. (17) should be averaged over the distribution function (10). Since the further derivation to obtain the TOF distribution is similar to that for two-body dissociation which is presented elsewhere,<sup>19</sup> only the final formula is given,

$$N_{m_1, \text{lab}}^+(t, \omega_D) = C_{m_1}^+ \frac{v_1^2}{t} \int \lambda \frac{P_E(E_T)}{u_1} P_{\hat{u}}(\hat{u}_1 \cdot \hat{\epsilon}) \cdot N_B(V_B, \omega_B) G(\theta, \eta, \phi) dV_B d\omega_B d\theta d\eta d\phi d\omega_{m_1}, \quad (18)$$

where  $N_{m_1, \text{lab}}^+(t, \omega_D)$  is the calculated TOF spectrum of ion signal from  $m_1$ ,  $t$  is the arrival time,  $\omega_D$  is the detector solid angle,  $v_1$  and  $u_1$  are the laboratory and c.m. velocities of  $m_1$  respectively,  $C_{m_1}^+$  is a constant for each  $m/e$ ,  $P_E(E_T)$  is the product c.m. translational energy distribution,  $N_B(V_B, \omega_B)$  is the reactant laboratory velocity distribution as a function of the velocity  $V_B$  and solid angle  $\omega_B$  of the molecular beam,  $\omega_{m_1}$  is the laboratory solid angle of  $m_1$  in velocity space, and

$$\lambda = m_1 \left( 1 + \frac{m_1}{\sin^2(\delta + \gamma)} \left( \frac{\sin^2 \delta}{m_3} + \frac{\sin^2 \gamma}{m_2} \right) \right), \quad \delta + \gamma \neq 0;$$

$$= m_1 \frac{m_1 + m_2 + m_3}{m_2 + m_3}, \quad \delta + \gamma = 0. \quad (19)$$

### C. Analyzed results

#### a. $S_1 + S_0$ excitation

After the above discussion we can start to analyze the data using the triple dissociation mechanism. Since the  ${}^1B_{3u} + {}^1A_g$  transition dipole is perpendicular to the molecular plane, it must also be perpendicular to the recoil directions of all the fragments at the transition state, provided that the transition state is planar, as has been calculated by SSS.<sup>10</sup> As mentioned before, at the  $S_1 + S_0$  transition the dependence of the signal on the laser polarization angle is very weak, indicating that the lifetime of the energized molecule is much longer than its rotational period. From this fact we can immediately conclude that the absolute value of the global anisotropy parameter  $b_1$ , which is the same for both HCN and  $N_2$ , is very small, and the data is not sensitive to the geometry of the transition state. We did not collect any angular or polarization dependence data for  $N_2$ , because it would not provide any more information and the detection of  $N_2$  is much more difficult due to high detector background.

Testing different sets of parameters, we found that the peak positions in the TOF spectra are very sensitive to  $\alpha_r$  and  $\beta_r$ . Although the TOF spectra of  $N_2$  do not have good signal-to-noise, it was found that in order to fit all the

TOF spectra, the deviation in  $\alpha_r$  and  $\beta_r$  must be less than  $0.5^\circ$  from the best values. Setting all the  $\sigma_i$  to the same value, within the range  $0 \leq \sigma_i \leq 5.2^\circ$ , it was always possible to fit the data by adjusting the translational energy distribution,  $P_E(E_T)$ . But if the constraint of maximum translational energy ( $E_{\max}$ ) is imposed, both the  $P_E(E_T)$  and  $\sigma_i$  are uniquely determined within experimental error. For example, at a given  $E_{\max}$  the  $\sigma_i$  has uncertainty within  $\pm 0.2^\circ$ . The high sensitivity of the fit to  $\alpha_r$ ,  $\beta_r$  and  $\sigma_i$  provides a sensitive probe of the detailed dissociation dynamics.

The exothermicity of reaction (1) is not experimentally known, although there are some estimates and theoretical calculations.<sup>3,23</sup> The theoretical prediction given by SS<sup>3</sup> is 57.4 kcal/mol, which should be within a few kcal/mol of the true value. From this experiment an accurate value for the exothermicity of reaction (1) cannot be obtained due to the fact that  $E_{\max}$  and  $\sigma_i$  are correlated, but in order to fit the data the exothermicity of the reaction must range between 47.5 and 68.3 kcal/mol, which correspond to  $\sigma_i = 5.2^\circ$  and  $0^\circ$  respectively, if the  $E_{\max}$  corresponds to all the available energy in translation.

With the exothermicity given by SS, a set of parameters was obtained by fitting the experimental TOF spectra and is listed in Table 1. Examples of the fits of the individual TOF spectra are given in Fig. 2. The  $P_E(E_T)$  to fit the  $6a_0^1$

data is plotted as curve (a) in Fig. 6. Fig. 7 shows the laser polarization dependence of HCN at a laboratory angle of  $20^\circ$ . The  $b_1$  value obtained is in the range from 0 to 0.13. The near zero value of  $b_1$  is a reflection of the near isotropic dissociation.

The immediate conclusion from Fig. 6 is that most of the available energy is channeled into translation in the  ${}^1B_{3u} \leftarrow {}^1A_g$  transition. This is in good agreement with the observation by Coulter *et al.*<sup>24</sup> that the population of products excited in the stretching modes is low. The average translational energy from  $6a_0^1$  excitation is 82.2 kcal/mol, which is 73.9% of the total available energy of 111.2 kcal/mol, implying a very repulsive PES along the reaction coordinate after the transition state. Data from  $6a_0^1$  and 0-0 give the same information except that  $E_{\max}$  is adjusted correspondingly.

#### b. 248 nm excitation

At 248 nm, the transition is  ${}^1B_{2u} \leftarrow {}^1A_g$  and the transition dipole is along the y axis of the molecule (see Fig. 5 for the definition of the coordinates). The situation concerning anisotropy of different fragments is more interesting than in the case of the  $S_1 \leftarrow S_0$  transition, and we observed different polarization dependence for HCN and  $N_2$ , as shown in Table 2.

At 248 nm it was impossible to simultaneously fit the TOF spectra of HCN and  $N_2$  assuming the same  $\sigma_i$  for both the

fragments. Although the peaks in the TOF spectra do not change very much between 248 nm and  $S_1+S_0$  excitation, the  $\alpha_r$  and  $\beta_r$  derived from the data are noticeably different for the two wavelengths. The parameters which give the best fit are listed in Table 1 and examples of the fits to the individual spectra are shown in Fig. 2. The  $P_E(E_T)$  used to fit the data is presented as curve (b) in Fig. 6.

Comparing the two  $P_E(E_T)$ 's in Fig. 6, it can be seen that the energy distribution at 248 nm is much broader than that from  $S_1+S_0$  excitation. However, even though the photon energy at 248 nm is more than twice that of  $S_1+S_0$  excitation, the energies of the peaks of the  $P_E(E_T)$ 's are similar. The average translational energy release at 248 nm excitation is 96.2 kcal/mol or 55.8% of the available energy, 172.4 kcal/mol. The similarity of the peak translational energies at both 248 nm and  $S_1+S_0$  excitation is a very important phenomenon which will be discussed later.

Simulating the experimental results with the above model, we found that the fit to the individual TOF spectra does not depend strongly on information concerning the transition state, but because for 248 nm excitation the transition dipole is in the plane of the molecule and since the signal level strongly correlates with the laser polarization angle, the laser polarization dependence is very sensitive to the angle  $\theta_T$ . For  $N_2$  we set  $\theta_T$  to  $0^\circ$ , since if the change in geometry leading to the transition

state is defined within  $C_{2v}$  symmetry (correct according to SSS<sup>10</sup>), the  $N_2$  must remain aligned in the direction of  $\mu$  in the body-fixed c.m. frame. Therefore, from the fit to the  $N_2$  data,  $b_1 = 0.65 \pm 0.05$  in Eqn. (17) is obtained first, which we assume to be the same for HCN. Then we use this  $b_1$  to fit all the HCN data by adjusting  $\theta_T$  for HCN which is also the angle between the HCN and  $N_2$  groups at the transition state. By this procedure, a value of  $121.3 \pm 1^\circ$  for  $\theta_T$  is obtained. The laboratory angular distributions of HCN for both horizontally and vertically polarized light are plotted in Fig. 8. Similar to Fig. 7, the signal-to-noise ratio in Fig. 8 is not very satisfactory, since the laser power was set low to avoid saturation and the molecular beam density was rather low due to the low vapor pressure of ST. Long time averaging at one time is impossible due to the small amounts of ST obtained in each batch.

#### IV. Discussion

##### A. Triple dissociation vs. two-body sequential dissociation

Using our model, the experimental data are successfully interpreted by concerted triple dissociation (TD). However, we would like to determine the boundary between TD and two-body sequential dissociation (SD), since at the limit of an infinitesimal interval between the primary and secondary steps of SD, TD and SD both offer the same physical picture.

Attempts were made to fit the data as a process involving secondary dissociation,<sup>17,19</sup> although we did not find any signal for the intermediates of either reaction (5) or (20).



These attempts were all unsuccessful for a variety of reasons, such as the trial distributions being unphysical, the distributions which fit one fragment could not fit its counterpart, or the simulated laboratory angular distribution or polarization dependence did not agree with the experimental results. Our conclusion is that neither reaction (5) nor (20) is consistent with our observations.

In fact, reaction (5) can easily be rejected, because we would expect to see two different kinds of HCN fragments, but the results do not show this at all. Reaction (20) must be considered more carefully. In our experimental set up, if every dissociation event maintains  $C_{2v}$  symmetry, TD is equivalent to SD with the constraint that secondary dissociation occurs only in a direction perpendicular to the primary recoil velocity and the primary and secondary  $E_T$ 's are strongly correlated with each other.

Using mechanism (20), the TOF spectra of  $\text{N}_2$  were fit first to obtain a primary  $P_E(E_T)$  and an anisotropy parameter  $b_1$ . With those, the HCN TOF spectra were then fit by adjusting the secondary  $P_E(E_T)$  and c.m. angular distribution.

For 0-0 and  $6a_0^1$ , it was possible to fit all the data this way. In Fig. 9 the secondary c.m. angular distribution which fits the  $6a_0^1$  data is presented, where the distribution was made as broad as possible using the narrowest possible secondary  $P_E(E_T)$  for the purpose of the following argument. The secondary products are sharply distributed perpendicular to the primary velocity vector, implying that the secondary process in the SD scheme is strongly correlated to the primary process. If we assume that all the secondary recoil events occurred perpendicular to the primary recoil direction, and that the width of the secondary angular distribution in Fig. 9 was due only to the rotation of HCNCH, we can estimate the time,  $\Delta t$ , from the start of the primary recoil to the end of the secondary recoil, and estimate how far the fragments would fly away from each other during this time assuming that they had reached their asymptotic velocity.  $\Delta t$  is estimated to be 0.3 psec, with a displacement within a few angstroms. The values estimated above are rather crude, but in any event the time and distance are so short that it is inappropriate to consider the process separated in the sense of SD. Moreover, because the bond energy of any bond in ST is expected to be much higher than the  $6a_0^1$  photon energy of 53.8 kcal/mol, SD is energetically unlikely for  $S_1 \rightarrow S_0$  excitation.

For 248 nm excitation, the data cannot be fit using mechanism (20). We can fit the TOF spectrum of HCN at one

laboratory angle and one polarization angle by the same method as above, but it is impossible to simulate the TOF spectra at all angles using the same set of parameters. The calculated laboratory angular distribution and laser polarization dependence of the signal just did not agree with the experimental results, because of the observed anisotropy which is different from that for  $S_1+S_0$  excitation.

The above discussion implies that at long times SD is clearly distinguished from TD by the dissociation dynamics, but the boundary between TD and SD is not absolute and there is a transition region where both TD and SD features exist. We think that the criteria are how strongly correlated the distributions and variables are between the primary and secondary processes.

#### B. Dynamics of ST triple dissociation

According to SSS's orbital correlation diagram<sup>10</sup> neither  $^1B_{2u}$  nor  $^1B_{3u}$  correlate adiabatically with the product ground states if  $C_{2v}$  symmetry is maintained throughout dissociation. As shown in Fig. 1, the energy of the  $S_1+S_0$  transition is lower than the energy required to populate the lowest excited (singlet) states of the products, so that it is impossible to produce electronically excited product molecules. It has been reported<sup>25</sup> that the rate of relaxation from the  $S_1$  state is  $10^5$  times that from

the  $T_1$  state. Therefore, the path of dissociation after intersystem crossing is not important and the dissociation must occur on the  $S_0$  PES after IC. Experiments as well as theory show<sup>3,9,26</sup> that there is strong interaction between the  $S_0$  and  $S_1$  electronic states and that IC is the main deactivation pathway for  $S_1$ . Combined with the previous studies, our experiment provides convincing evidence for the mechanism described by equations (2) and (3).

We have found no other experimental studies of the photochemistry of  ${}^1B_{2u} + {}^1A_g$  except that of GR. The energy at 248 nm is high enough to allow one of the HCN molecules to be electronically excited. As shown in Fig. 6, the minimum translational energy released in 248 nm photolysis is 37.0 kcal/mol. Even if all the remaining energy went into electronic excitation, it would still be 13.6 kcal/mol less than that needed to reach the first excited singlet state of HCN. Therefore, it is almost certain that no electronically excited products are formed at 248 nm either. Since the  ${}^1B_{2u}$  state does not correlate with ground state products, it is unlikely that the dissociation is directly from  ${}^1B_{2u}$  reactant to products, even though calculations predict that there should be two imaginary vibrational modes on the  ${}^1B_{2u}$  PES within the constraint of  $D_{2h}$  symmetry.<sup>3</sup> As pointed out in many previous studies,<sup>17,27-29</sup> the translational energy release mainly correlates with the exit barrier along the reaction coordinate and is less influenced by the excess

energy when there is an appreciable exit barrier. If both dissociation processes occur on the  $S_0$  PES and the  $S_0$  lifetime is long enough to allow substantial intramolecular vibrational redistribution, the peak positions of the  $P_E(E_T)$ 's should be similar, because the fragments experience the same exit barrier. The excess energy is mainly distributed throughout all the internal modes (including the reaction coordinate). Thus, the most obvious difference between different internal energies for the same transition state is that the higher the energy the broader the distribution, while the change in the peak position will be much smaller than the change in the excess energy. Applying this idea to ST, it is obvious that the dissociation dynamics following the two electronic excitations are qualitatively very similar. Further evidence is that the angle between  $N_2$  and HCN at the transition state is  $121.3 \pm 1^\circ$  at 248 nm, which is fairly close to  $120.1^\circ$ , the value calculated from the transition state geometry provided by SSS.<sup>10</sup> Therefore, we suggest that the dissociation mechanism following  ${}^1B_{2u} \leftarrow {}^1A_g$  excitation is the same as that for  ${}^1B_{3u} \leftarrow {}^1A_g$  excitation, i.e., IC to ground state ST and triple dissociation to ground state products.

The parameter  $b_1$  gives an idea of how fast dissociation occurs with respect to the rotational period. For  $S_1 \leftarrow S_0$  excitation,  $b_1 \leq 0.13$  implies that dissociation is much slower than the rotational period of the parent molecule.

For 248 nm excitation,  $b_1 = 0.65$  indicates that the products still have a strong "memory" of the initial orientation, implying that the dissociation lifetime following  ${}^1B_{2u} + {}^1A_g$  excitation is comparable to or less than the rotational period. Assuming that RRKM theory<sup>30</sup> is applicable in predicting rate constants for triple dissociation, we can use a reasonable set of vibrational frequencies<sup>31</sup> and the potential barrier (shown in Fig. 1) given by SSS<sup>10</sup> to estimate the RRKM dissociation lifetime. Our calculation gives RRKM dissociation lifetimes for triple dissociation of 50 nsec and 0.2 psec for 0-0 and 248 nm excitation respectively. Although a lifetime of 0.2 psec is questionable because RRKM theory may not be valid on such a short timescale, the predicted lifetime for 0-0 transition is reasonable. The fluorescence lifetime from the  $S_1$  state has been measured to be on the order of 0.1 - 1 nsec.<sup>7</sup> Thus, the molecule has plenty of time to randomize its energy after IC in the case of  $S_1 + S_0$  excitation. At 248 nm, the value of  $b_1$  implies that IC rate is probably on the same order of magnitude as that of dissociation after IC.

It is instructive to compare the geometry change through the dissociation. The angles between the HCN and  $N_2$  groups for the most probable asymptotic geometries at 248 nm and  $S_1 + S_0$  excitation and the geometry of the transition state obtained in this experiment are  $114.4^\circ$ ,  $117.2^\circ$ , and  $121.3^\circ$  respectively. The asymptotic angles are smaller than

at the transition state, and the higher the available energy the smaller the angle, which implies that the repulsion between two HCN is stronger than that between HCN and  $N_2$  during the process of the molecule breaking the conjugated  $\pi$ - $\sigma$  bond system. Comparison of  $\sigma_i$  between the two laser wavelengths (in Table 1) indicates that at 248 nm, because of the higher available energy, the molecule can dissociate from configurations which deviate more from the lowest energy ST structure, and the dissociation becomes more asymmetric. These observations are consistent with our intuition and provide a vivid picture of the dynamics of ST triple dissociation.

## V. Summary

This experimental study has confirmed that the s-tetrazine photodissociation is a concerted triple dissociation. To analyze the experimental results, a simple model is proposed which has proven to be fruitful and sensitive to the experimental data. It is found that information on both the detailed dissociation dynamics and the transition state can be derived in certain systems using this model. An improved analysis of the physical significance of the anisotropy parameter is given, where the relation between the anisotropy parameter and the geometry of the transition state is explicitly constructed.

In this chapter we have assumed that the peak position

of the translational energy distribution of the same reaction channel is mainly determined by the exit barrier, if the reaction occurs on the ground electronic PES. This is essential for us to identify the mechanism of the dissociation of ST following 248 nm excitation. Although the validity of this assumption is physically understandable, we would like to find direct experimental evidences to support this important conclusion, because as will be seen in Chapter V this is also the bases for some approximations proposed in Chapter I. In next Chapter we will, among other things, discuss this problem.

**References**

1. S. F. Mason, J. Chem. Soc. (London) 1263, 1269 (1959).
2. G. H. Spencer Jr., P. C. Cross, and K. B. Wiberg, J. Chem. Phys. **35**, 1925, 1939 (1961).
3. A. C. Scheiner and H. F. Schaefer III, J. Chem. Phys. **87**, 3539 (1987), and references therein.
4. K. K. Innes, J. P. Byrne, and I. G. Ross, J. Mol. Spectrosc. **22**, 125 (1967), and references therein.
5. K. K. Innes, L. A. Franks, A. J. Merer, G. K. Vemulapalli, T. Cassen, and J. Lowry, J. Mol. Spectrosc. **66**, 465 (1977).
6. D. V. Brumbaugh and K. K. Innes, Chem. Phys. **59**, 413 (1981).
7. D. V. Brumbaugh, C. A. Haynam, and D. H. Levy, J. Mol. Spectrosc. **94**, 316 (1982).
8. K. B. Thakur, V. A. Job, and V. B. Kartha, J. Mol. Spectrosc., a) **107**, 373 (1984), b) **112**, 340 (1985).
9. A. Kiermeier, K. Dietrich, E. Riedle, and H. J. Neusser, J. Chem. Phys. **85**, 6983 (1986).
10. A. C. Scheiner, G. E. Scuseria, and H. F. Schaefer III, J. Am. Chem. Soc. **108**, 8160 (1986).
11. D. S. King, C. T. Denny, R. M. Hochstrasser, and A. B. Smith III, J. Am. Chem. Soc. **99**, 271 (1977).
12. D. M. Burland, F. Carmona, and J. Pacansky, Chem. Phys. Lett. **56**, 221 (1978).

13. M. Paczkowski, R. Pierce, A. B. Smith III, and R. M. Hochstrasser, *Chem. Phys. Lett.* **72**, 5 (1980).
14. J. H. Glowina and S. J. Riley, *Chem. Phys. Lett.* **71**, 429 (1980).
15. P. M. Kroger and S. J. Riley, *J. Chem. Phys.* **70**, 3863 (1979).
16. J. W. Hepburn, R. J. Buss, L. J. Butler, and Y. T. Lee, *J. Phys. Chem.* **87**, 3638 (1983).
17. Chapter II.
18. A. M. Wodtke and Y. T. Lee, *J. Phys. Chem.* **89**, 4744 (1985).
19. Chapter I.
20. R. N. Zare, *Mol. Photochem.* **4**, 1 (1972).
21. G. E. Busch and K. R. Wilson, *J. Chem. Phys.* **56**, 3638 (1972).
22. To obtain equations (15) and (16), the addition theorem of Legendre functions was used.
23. M. J. S. Dewar, *Pure Appl. Chem.* **44**, 767 (1975).
24. D. Coulter, D. Dows, H. Reisler, and C. Wittig, *Chem. Phys.* **32**, 429 (1978).
25. R. M. Hochstrasser and D. S. King, *J. Am. Chem. Soc.* **97**, 4760 (1975).
26. a) V. L. Windisch, A. B. Smith III, and R. M. Hochstrasser, *J. Phys. Chem.* **92**, 5366 (1988); b) K. K. Innes, *J. Chem. Phys.* **76**, 2100 (1982).
27. D. Krajnovich, F. Huisken, Z. Zhang, Y. R. Shen, and Y.

- T. Lee, J. Chem. Phys. **77**, 5977 (1982).
28. L. J. Butler, R. J. Buss, R. J. Brudzynski, and Y. T. Lee, J. Phys. Chem. **87**, 5106 (1983).
29. A. M. Wodtke, E. J. Hintsa, and Y. T. Lee, J. Phys. Chem. **90**, 3549 (1986).
30. P. J. Robinson and K. A. Holbrook, Unimolecular Reactions, Wiley, London (1972).
31. The calculated vibrational frequencies for the transition state were kindly provided by A. C. Scheiner. For consistency, the theoretically predicted vibrational frequencies for "stable" ST in ref. 3 were used in the RRKM calculation.

Table 1. Parameters derived from data analysis

	$\alpha_r(\text{HCN}, \text{HCN})$	$\alpha_r(\text{HCN}, \text{N}_2)$	$\sigma(\text{HCN})$	$\sigma(\text{N}_2)$
$S_1^+S_0$	125.7°	117.2°	4.4°	4.4°
248 nm	131.2°	114.4°	8.5°	9.0°
	$b_1$	$\theta_T(\text{HCN})$	$\theta_T(\text{N}_2)$	
$S_1^+S_0$	$\leq 0.13$	90°	90°	
248 nm	0.65	121.3°	0°	

Table 2. Laser polarization dependence  
for 248 nm excitation at 20°

Laser polarization	Signal Counts	
	HCN	N <sub>2</sub>
Vertical <sup>a</sup>	1.00	1.00
Horizontal	0.84	4.52

a Set to 1.00.

### Figure captions for Chapter III

Fig. 1 Energy diagram of ST photodissociation with energies in kcal/mol.

Fig. 2 TOF spectra at a laboratory angle of  $20^\circ$ . The scattered circles are the experimental data and the solid lines are the fits with the triple dissociation mechanism. The TOF spectra shown for  $6a_0^1$  ( ${}^1B_{3u} \leftarrow {}^1A_g$ ) excitation were taken using vertically polarized light, and for 248 nm excitation horizontally polarized light was used.

Fig. 3 Laser power dependence of the HCN signal for the 0-0 ( ${}^1B_{3u} \leftarrow {}^1A_g$ ) transition at  $20^\circ$  with the laser vertically polarized.

Fig. 4 Asymptotic geometry in velocity space for triple dissociation.  $\hat{u}_1^0$ ,  $\hat{u}_2^0$  and  $\hat{u}_3^0$  are the unit recoil velocity vectors in a particular dissociation event, while  $\hat{u}_1^r$ ,  $\hat{u}_2^r$  and  $\hat{u}_3^r$  are the reference velocity vector corresponding to the most probable dissociation geometry. The other variables are explained in the text.

Fig. 5 Diagram of the relations between fragments from photon absorption, through the transition state, to the asymptotic geometry. The direction of the transition dipole  $\mu$  in the figure corresponds to the

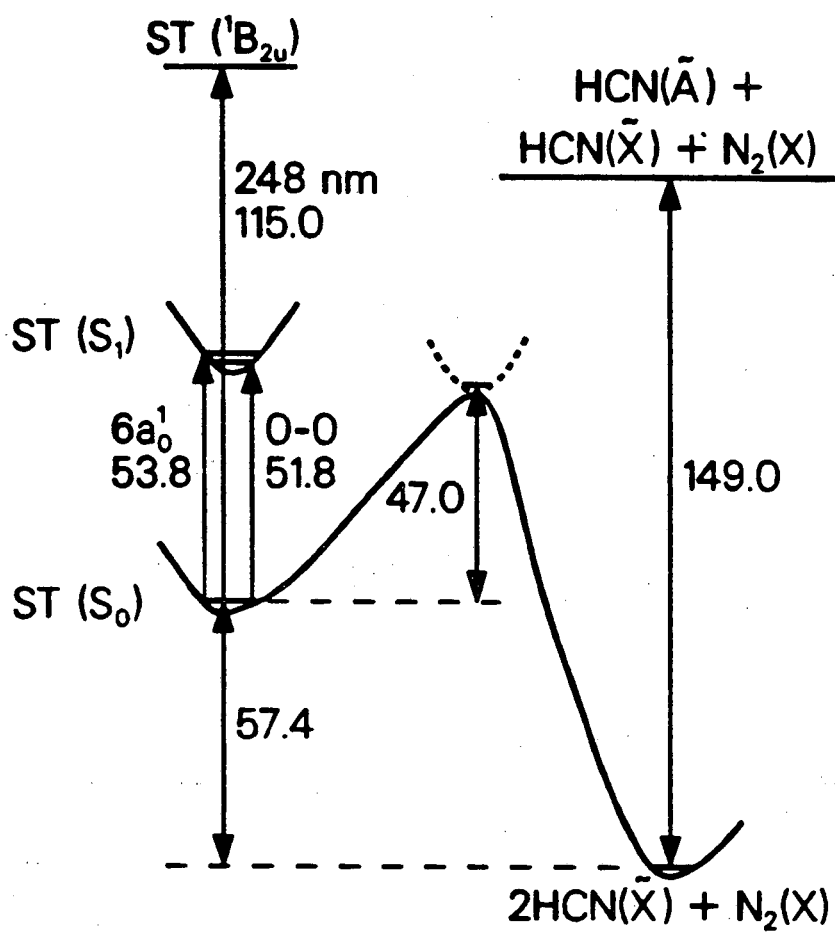
case of  ${}^1B_{2u} \leftarrow {}^1A_g$  UV excitation. All symbols are explained in the text.

Fig. 6 Triple dissociation  $P_E(E_T)$ 's used to fit the data. Curve (a) is for  $6a_0^1 ({}^1B_{3u} \leftarrow {}^1A_g)$  excitation, and curve (b) is for 248 nm excitation.

Fig. 7 Polarization dependence of HCN signal for the 0-0 ( ${}^1B_{3u} \leftarrow {}^1A_g$ ) transition at a laboratory angle of  $20^\circ$ . Points are experimental data and the line is the fit using  $b_1 = 0.13$  and other parameters in Table 1. If  $b_1 = 0$ , the fit would be a horizontal straight line.

Fig. 8 Laboratory angular distribution of HCN at 248 nm. Points are experimental data and the lines are the fits using the parameters in Table 1. V and H stand for vertically and horizontally polarized laser beams respectively. For an isotropic product distribution, the two lines would be identical.

Fig. 9 The secondary c.m. angular distribution of HCN used to fit the  $6a_0^1 ({}^1B_{3u} \leftarrow {}^1A_g)$  data by sequential reaction mechanism (20), where  $0^\circ$  corresponds to the direction of the primary recoil vector of  $H_2C_2N_2$ .



XBL 8811-3808

Fig. 1

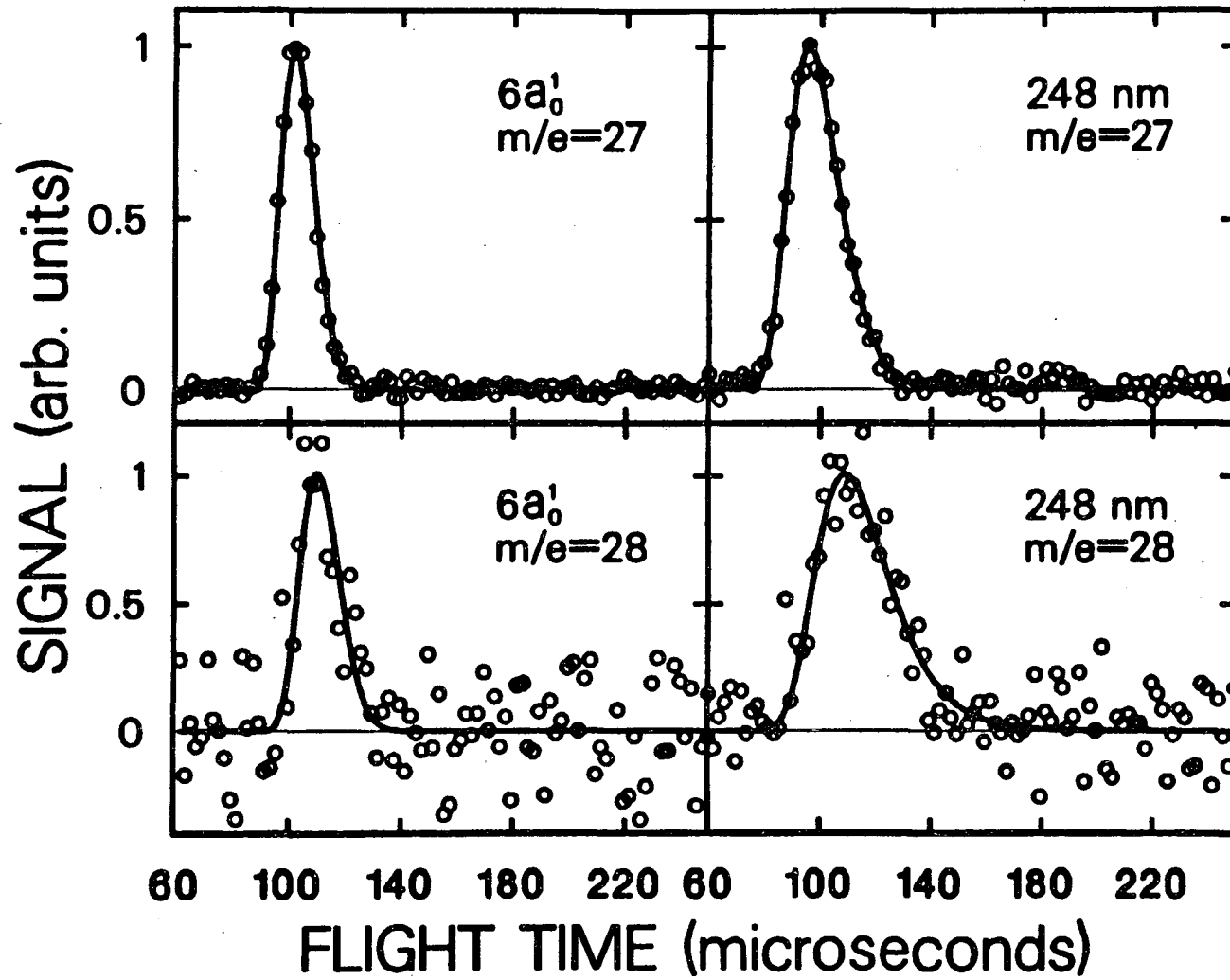
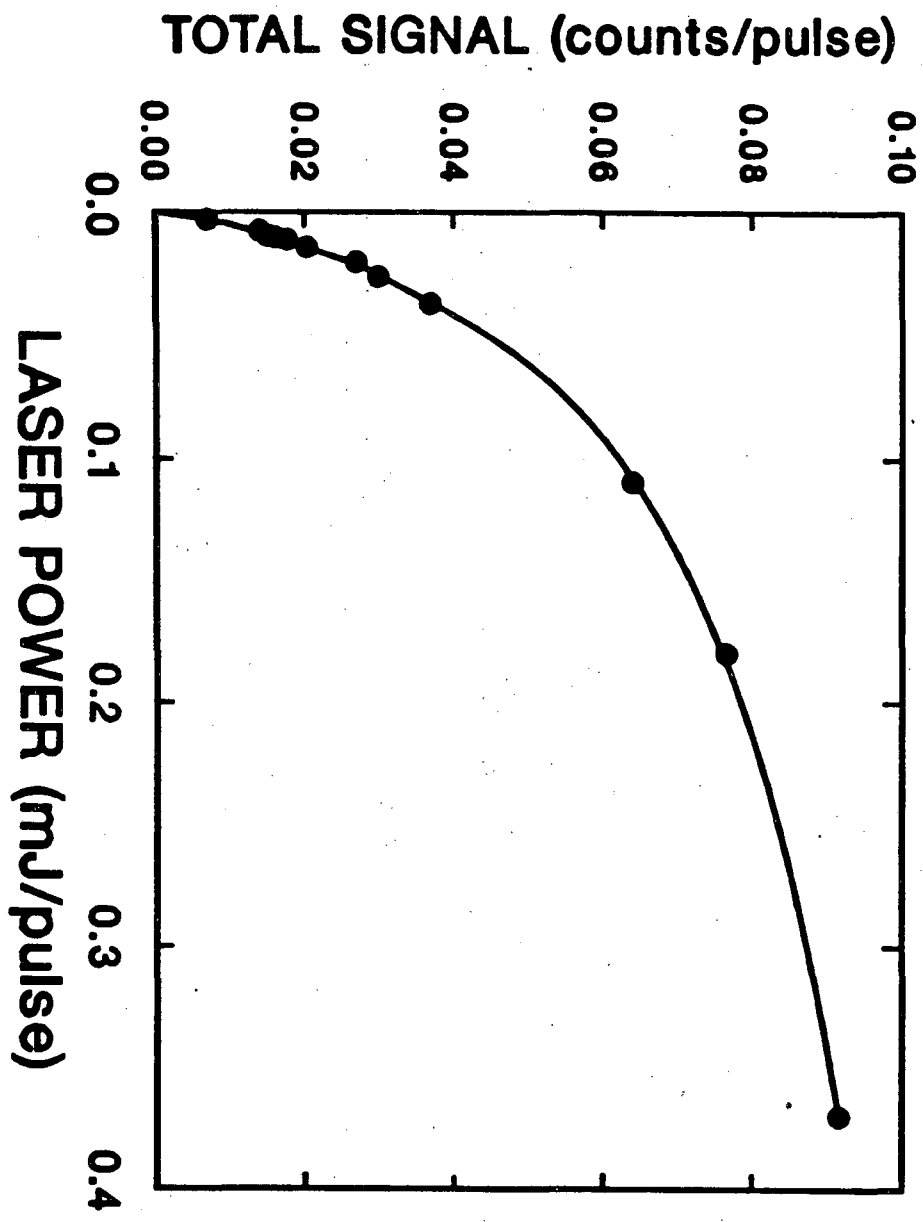
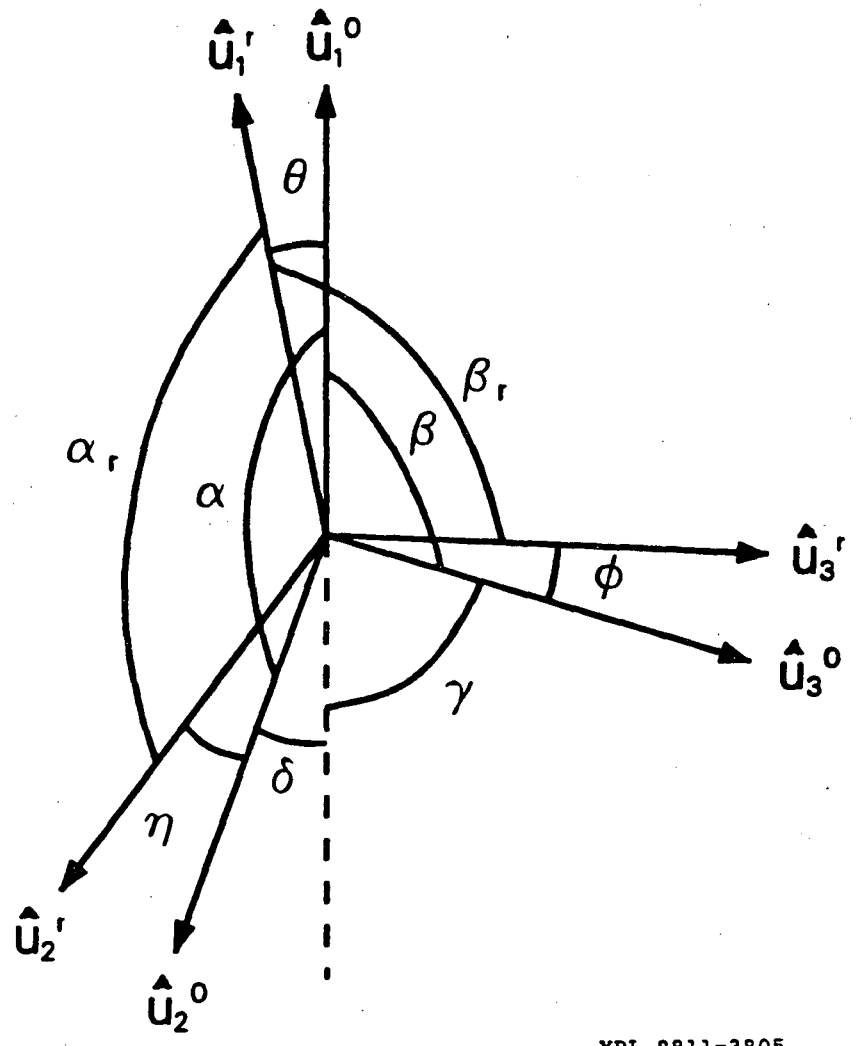


Fig. 2



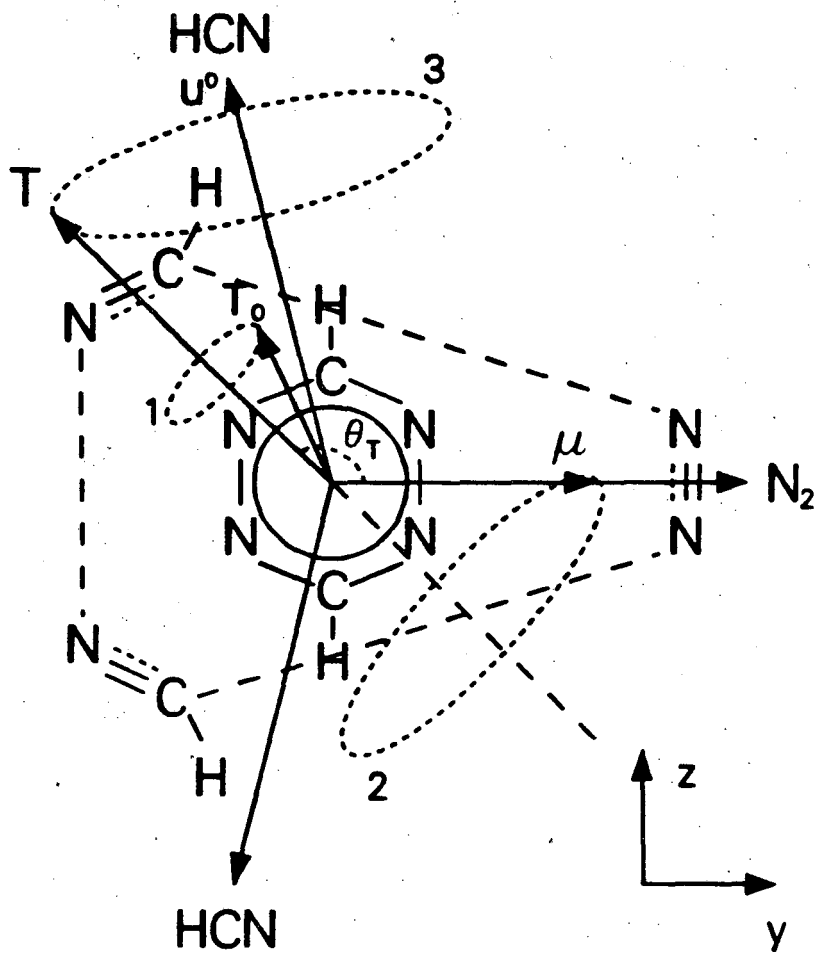
XBL 8811-3806

Fig. 3



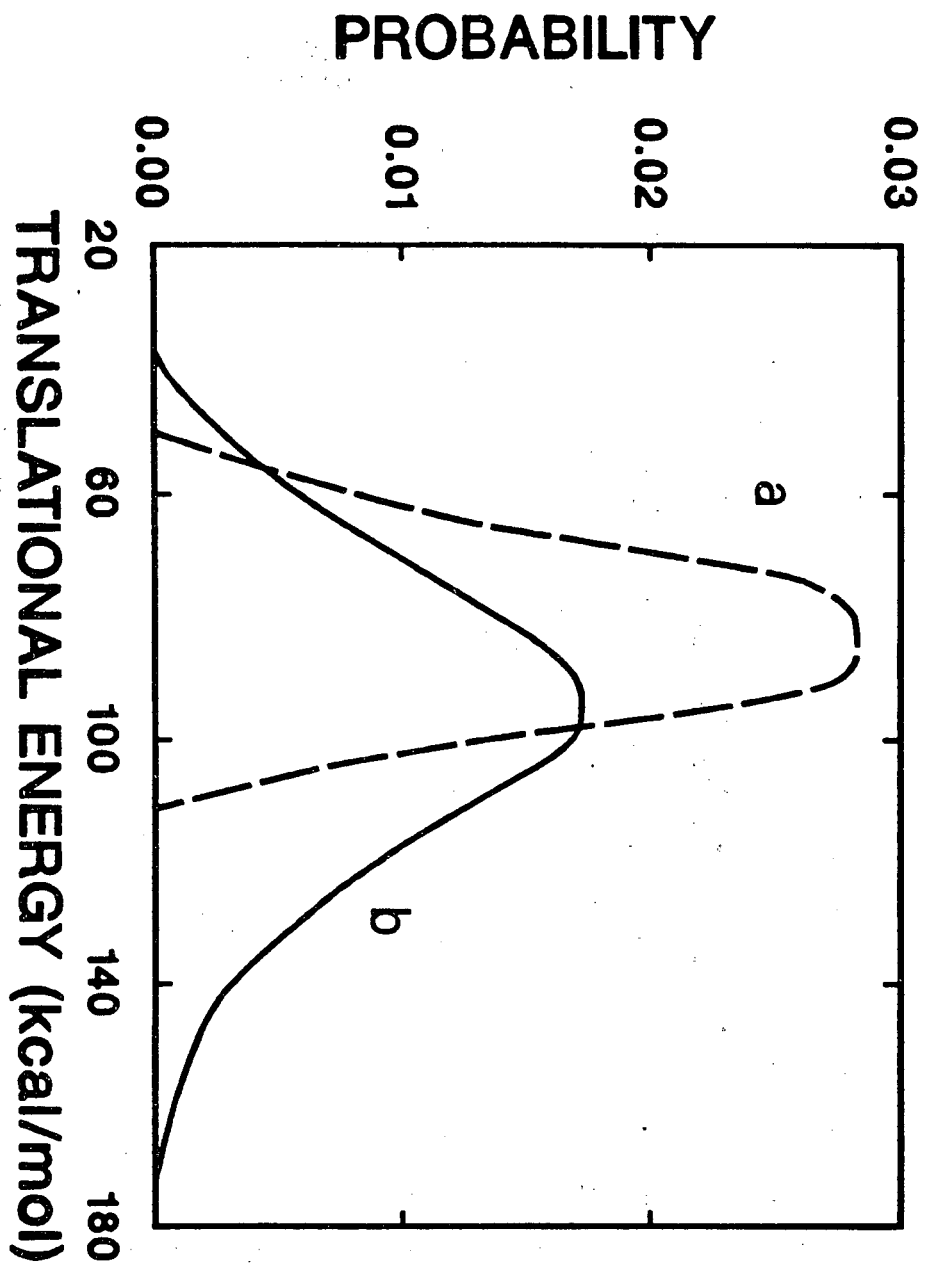
XBL 8811-3805

Fig. 4



XBL 8811-3804

Fig. 5



XBL 8811-3803

Fig. 6

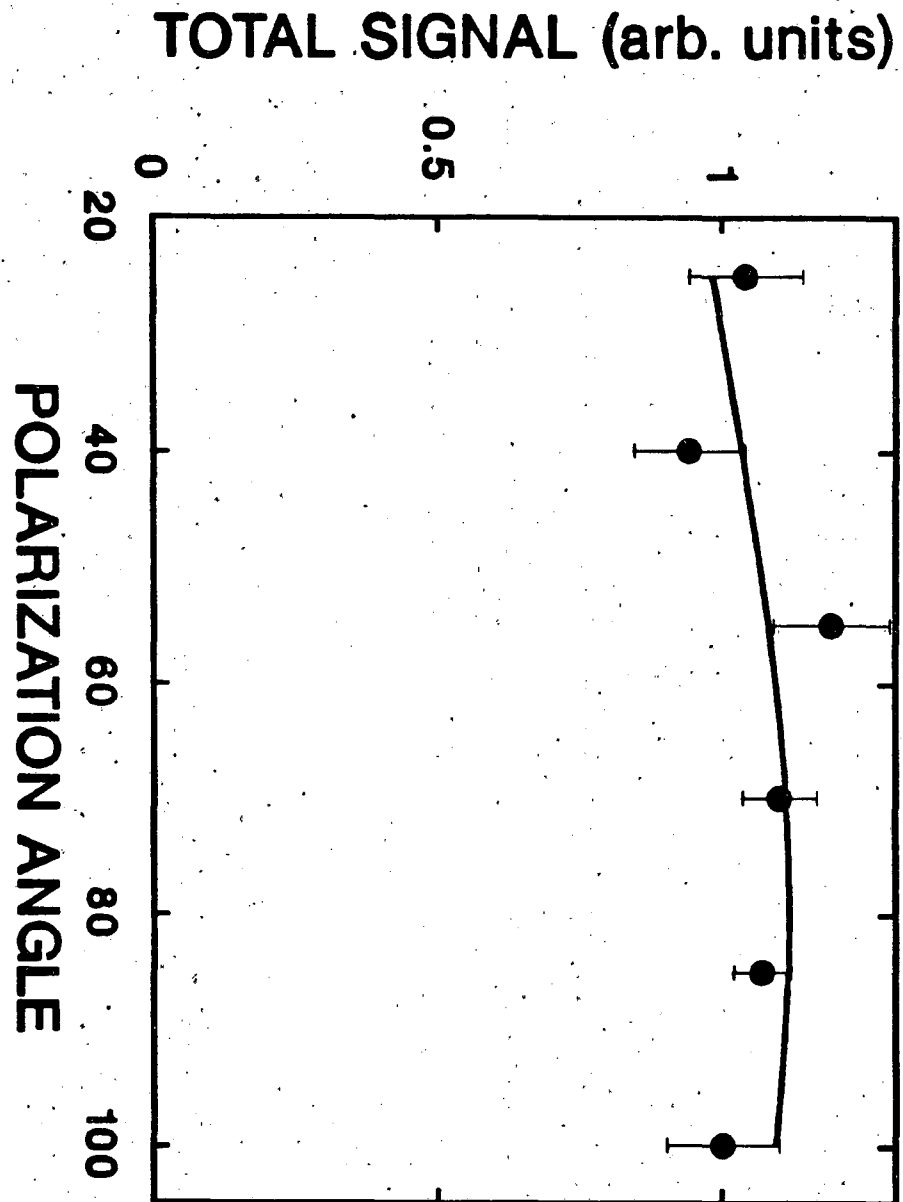


Fig. 7

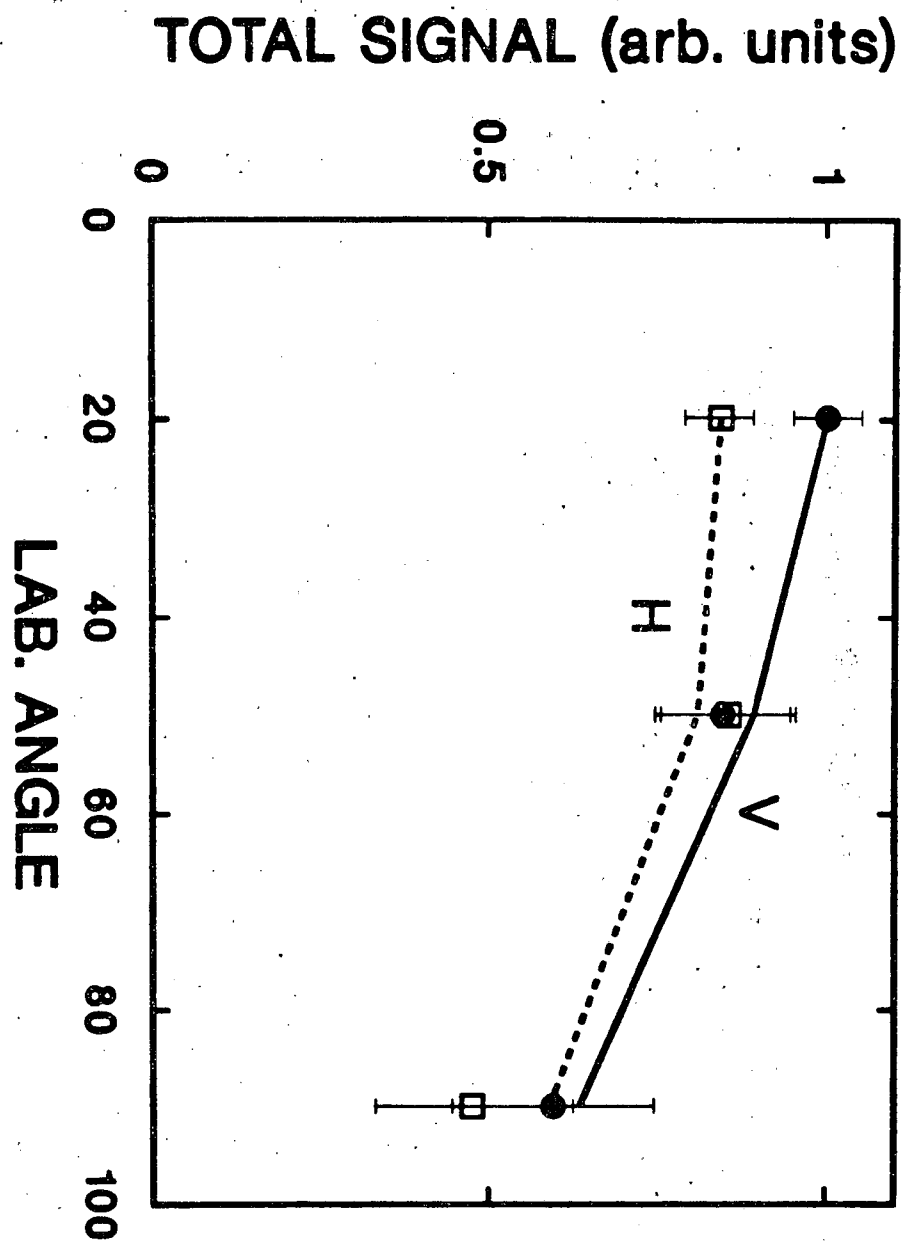
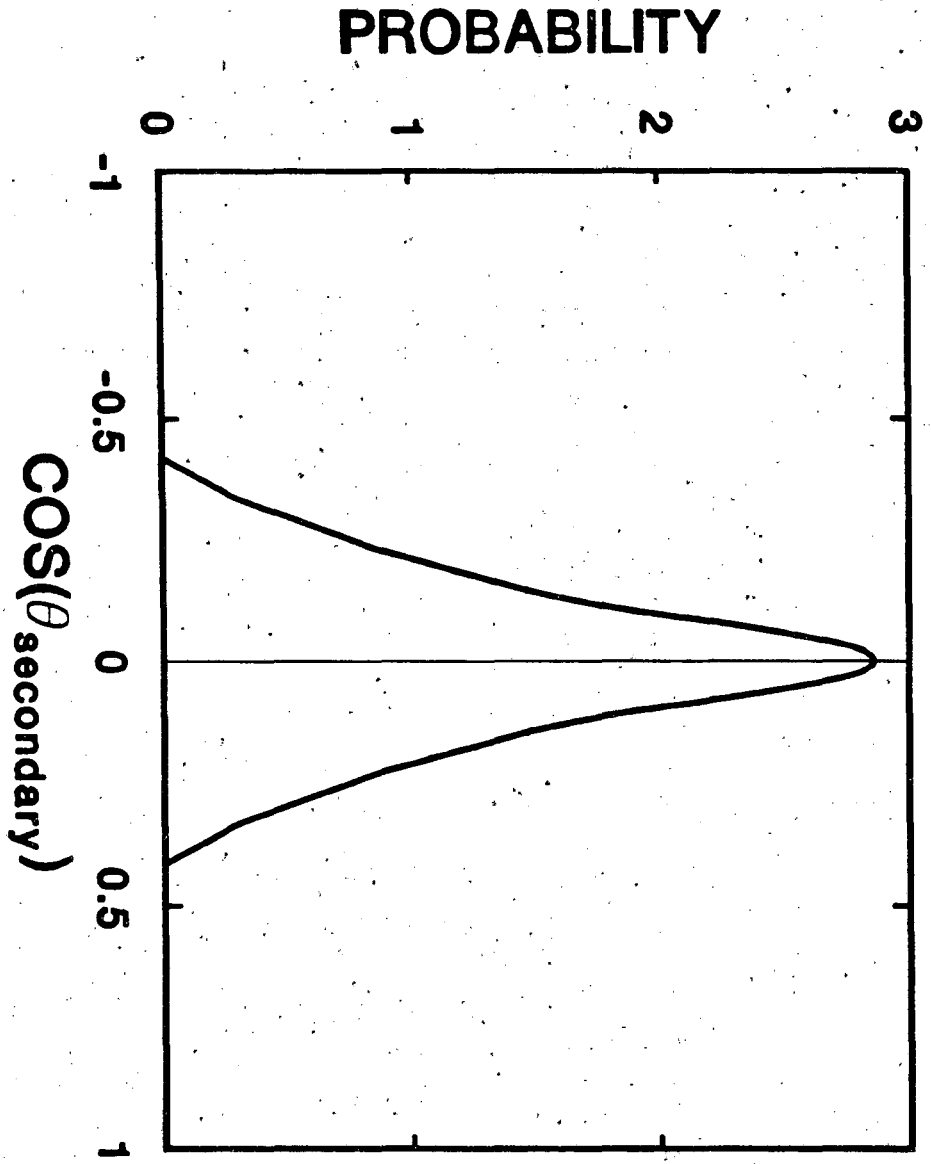


Fig. 8



XBL 8811-3800

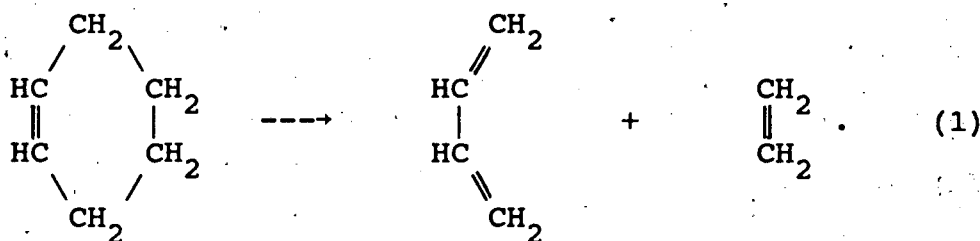
Fig. 9

## CHAPTER IV

DISSOCIATION OF CYCLOHEXENE AND  
1,4-CYCLOHEXADIENE IN A MOLECULAR BEAM

## I. Introduction

The dissociation of cyclohexene (CHN) is interesting because it can occur through the simplest retro-Diels-Alder reaction (1),



Although it is believed that the Diels-Alder reaction is concerted,<sup>1-7</sup> some calculations indicate that the process may not be totally symmetric and may have partial diradical character.<sup>3-7</sup> In fact, a true diradical mechanism is by no means energetically impossible.<sup>4,5</sup> Experimental results have implied a concerted mechanism for reaction (1).<sup>1</sup> Bulk studies of CHN dissociation showed that the retro-Diels-Alder reaction is the main channel in both thermal decomposition and infrared multiphoton dissociation (IRMPD).<sup>8-10</sup> However, there has been no direct experimental examination of the concerted nature of the retro-Diels-Alder reaction.

In a series of IRMPD studies carried out in this laboratory,<sup>11-14</sup> it was found that the vibrational energy

distributions in molecules prior to dissociation can be described by statistical theories. In addition, concerted dissociation forming stable products can be distinguished from simple bond rupture by the distinctly different product center-of-mass (c.m.) translational energy distributions,  $(P_E(E_T))$ .

In a concerted dissociation, the potential energy surface (PES) along the reaction coordinate has an appreciable exit barrier due to the strained conformation at the transition state and the closed-shell electronic structure of the products which repel each other as the dissociation proceeds beyond the transition state. As a result, the  $P_E(E_T)$  is determined by two factors, the potential energy release along the reaction coordinate into translation and the fraction of the excess energy shared by the reaction coordinate. The contribution to the translational energy from the latter factor is usually much smaller than that from the former for a moderate-sized molecule, because the exit barrier is often much higher than the average fraction of the excess energy available to each internal degree of freedom, and a large fraction of the potential energy of the exit barrier will appear as product translational energy.<sup>12-15</sup> Therefore, for molecular dissociation with an appreciable exit barrier, the  $P_E(E_T)$  is mainly determined by the dynamics of the exit barrier energy release, and the most probable translational energy is significantly greater

than what would be expected from the partitioning of the vibrational energy in the reaction coordinate at the transition state. In the case of simple bond rupture producing radical species, there is often no appreciable exit barrier along the reaction coordinate, and the main source of translational energy is the statistical distribution of the excess energy along the reaction coordinate. Because the reaction coordinate is only one of many vibrational degrees of freedom, statistical weighting favors the situation in which most of the energy is not stored in the reaction coordinate, and the  $P_E(E_T)$  will peak near zero translational energy. The above conclusion is also applicable to dissociation following electronic excitation where the reaction occurs on the ground electronic PES reached by internal conversion (IC).<sup>15</sup> This type of dissociation is also found to be adequately described by statistical theories, because the IC and intramolecular vibrational randomization rates are faster than the dissociation rate from the ground electronic state of the molecule.

There has been considerable interest in the relationship between the mechanism and dynamics of photodissociation and the form of excitation. Bond selective photodissociation has been observed in  $\text{CH}_2\text{BrI}$ , where the stronger C-Br bond, instead of the weaker C-I bond, is preferentially broken after absorption at 210 nm.<sup>16</sup> In general, for many polyatomic molecules, even when local excitation is pos-

sible, intramolecular processes are often fast enough to allow different reaction pathways to compete with each other, which complicates matters considerably.

This work is part of our effort to understand the photochemistry of cyclic compounds.<sup>13,15,17</sup> To investigate the questions addressed above, 193 nm photodissociation and IRMPD of CHN and 1,4-cyclohexadiene (CHDN) have been performed. The primary purpose of the IRMPD experiment is to serve as a reference for the results from 193 nm photodissociation. If the same dissociation channels are observed in both 193 nm dissociation and IRMPD, by comparing the observed  $P_E(E_T)$ 's we can determine whether dissociation at 193 nm occurs on the ground electronic PES following IC. This comparison will also provide a direct test of the hypothesis that the total energy and the form of excitation are less important in determining the  $P_E(E_T)$  than the role played by the exit barrier for concerted dissociation.<sup>15</sup>

The technique employed is photofragmentation-translational spectroscopy (PTS) in a molecular beam.<sup>18,19</sup> It was found that at 193 nm both CHN and CHDN produce benzene as one of the products, which itself undergoes very complicated secondary photodissociation reactions. Since an independent study of the photodissociation of benzene was also carried out and will be published in a forthcoming paper,<sup>17</sup> we will focus our attention on the primary dissociation processes. Energy diagrams of the dissociation channels of CHN and CHDN

are presented in Figs. 1 and 2.

## II. Experimental

The PTS technique has been described previously.<sup>18,19</sup> Briefly, a molecular beam and a laser beam were crossed at  $90^\circ$  in a vacuum chamber. Dissociation products entered a mass spectrometer detector at a variable angle with respect to the molecular beam. The products were ionized in an electron bombardment ionizer, mass selected by a quadrupole mass filter, and detected with a Daly-type ion counter. A multichannel scaler interfaced with an LSI-11 microcomputer recorded the arrival time of the signal relative to the laser pulse. From the observed time-of-flight (TOF) spectra, the  $P_E(E_T)$  and the product c.m. angular distribution,  $P_{\hat{u}}(\hat{u})$ , can be obtained. The basic principles involved in data analysis are presented elsewhere,<sup>20</sup> and a description of the data fitting procedure has been given by Wodkta and Lee.<sup>19</sup>

The experiments were carried out on two molecular beam apparatuses. TOF spectra with mass-to-charge ratio ( $m/e$ ) higher than 12 were taken on a rotating molecular beam apparatus (RMBA).<sup>19</sup> TOF spectra of  $m/e = 1$  and 2 were taken on a crossed molecular beam apparatus (CMBA) with a rotatable detector.<sup>21</sup>

On the RMBA, a continuous supersonic molecular beam was used. The distance between the interaction region and the

detector was 36.7 cm. CHN or CHDN was contained in a bubbler held at 0°C, where the vapor pressure for both CHN and CHDN is about 20 Torr. Argon carrier gas was bubbled through CHN or CHDN at a total pressure of 100 Torr. For CHDN, the nozzle was heated to 115°C and 245°C for 193 nm photodissociation and IRMPD respectively, and for CHN, 300°C and 560°C for 193 nm and IRMPD. Under the above experimental conditions the nominal molecular beam velocity was around 700 m/sec.

On the CMBA, a molecular beam produced by a piezoelectric pulsed valve<sup>22</sup> was skimmed and crossed with the laser beam at a distance of 3 cm from the nozzle. The distance between the interaction region and the detector was 39.2 cm. The direction of detection, the laser beam and the molecular beam were orthogonal. The pulsed beam source was kept at room temperature, and studies were done with both neat (10 and 15 Torr for CHDN and CHN respectively) and seeded (10% CHDN in neon with a total pressure of 100 Torr, and 10% CHN in argon with a total pressure of 200 Torr) beams. No significant differences in the TOF spectra were observed under these conditions, other than higher signal levels for the seeded beam, because the molecular beam velocity distribution is insignificant in the detection of very fast particles, such as the H or H<sub>2</sub> produced in 193 nm photodissociation.

A Lambda Physik excimer laser was used for 193 nm

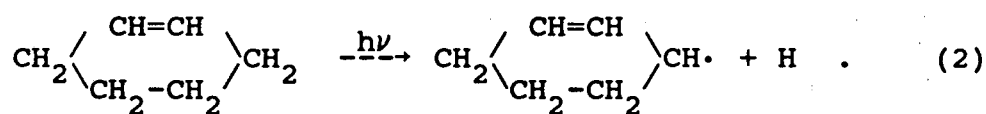
photodissociation, operating on the ArF transition and focused to  $1 \times 4 \text{ mm}^2$  in the interaction region. On both machines, the laser polarization dependence was studied using a rotatable pile-of-plates transmission polarizer, with 10 quartz plates set at Brewster's angle. In this way approximately 97% linearly polarized light was produced. For IRMPD, a Gentec TEA  $\text{CO}_2$  laser was focused to a 0.7 mm diameter spot and tuned to the P(16) line of the  $00^{\circ}1-10^{\circ}0$  transition for CHDN and to the P(28) line of the  $00^{\circ}1-02^{\circ}0$  transition for CHN. Both CHN (99.5%) and CHDN (99%) were obtained from Fluka and used without further purification.

### III. Results and analysis

#### A. Photodissociation of CHN

##### a. Photolysis at 193 nm

The TOF spectrum of the largest fragment is that of  $m/e = 81$ , shown in Fig. 3 a), which indicates the occurrence of reaction (2),



The H atom lost is most likely from an  $\alpha$  carbon (adjacent to the double bond). Fitting the experimental TOF spectrum, the  $P_E(E_T)$  for reaction (2) is obtained and presented as curve (a) in Fig. 4. This assignment is consistent with the  $m/e = 1$  TOF spectra, where, as shown in Fig. 5 b), the fast

edge of the  $m/e = 1$  TOF spectrum is fit well using the same  $P_E(E_T)$ . In Fig. 5 a), two TOF spectra of  $m/e = 1$  at different laser powers are plotted together to show that only the fast part of the  $m/e = 1$  TOF spectra is due to reaction (2), because the fast edge has a linear laser power dependence, while the slow components in the spectra have a stronger laser power dependence, indicating that they contain contributions from secondary and/or multiple photodissociation.

Curve (a) in Fig. 4 is truncated at about 18 kcal/mol, because information about translational energies lower than 18 kcal/mol for reaction (2) cannot be obtained from the fit. In fact, if reaction (2) releases less than 18 kcal/mol into translation, the product may have enough internal energy to undergo secondary spontaneous dissociation to produce cyclohexadiene and an H atom.

In Fig. 3 the TOF spectra of  $m/e = 78-80$  are also shown. At lighter and lighter masses, new fast components become more and more evident. Comparison of the  $m/e = 2$  TOF spectra at different laser powers in Fig. 5 c) indicates that there are two sequential dissociation channels producing  $H_2$ . The TOF spectra of  $m/e = 2$  and 78-80 suggest the occurrence of reactions (3) and (4),<sup>8</sup>



where cyclohexadiene<sup>‡</sup> in reaction (4) is a product of

reaction (3).

As shown in Figs. 3 b) - d) and 5 d), the observed TOF spectra of  $m/e = 2$  and 78-80 are fit well by reactions (2)-(4) using the  $P_E(E_T)$ 's plotted in Figs. 4, 6 and 7. The consistency of the fits of the  $m/e = 2$  and 78-80 data using reactions (2)-(4) does not rule out the possibility of other secondary photodissociation processes such as



where cyclohexadiene is from reaction (3), and



where the reactant is from reaction (2). In fact, we may have to consider reactions (5) and (6), among others, in order to fully explain the  $m/e = 1$  TOF spectra. However, the  $P_E(E_T)$  for reaction (3) can be obtained quite accurately from the  $m/e = 2$  TOF spectrum at low laser power and that of reaction (4) from the  $m/e = 2$  TOF spectrum at high power. The  $P_E(E_T)$ 's for reactions (2)-(4) can then be used to fit the TOF spectra of  $m/e = 78 - 80$ . Therefore, accurate information on secondary processes such as reactions (5) and (6) is not essential to our goal of elucidating the primary dissociation processes.

The  $m/e = 53$  TOF spectrum is presented in Fig. 8 a), where the signal due to daughter ions of heavier products from the previous dissociation channels are clearly separated by their (much slower) arrival times and are not seen

in this time frame. The peak shown is the result of the retro-Diels-Alder reaction (1) and is fit using the  $P_E(E_T)$  plotted as curve (a) in Fig. 9. This assignment is confirmed by the  $m/e = 28$  TOF spectrum, where the two peaks are due to the  $C_2H_4$  and  $C_4H_6$  from reaction (1) and are reproduced by the same  $P_E(E_T)$ , as the TOF spectrum in Fig. 8 b) illustrates.

For the retro-Diels-Alder reaction, if the c.m. angular distribution of the products is expressed as<sup>23</sup>

$$P_{\hat{u}}(\hat{u} \cdot \hat{\epsilon}) = (1/4\pi) (1 + \beta P_2(\hat{u} \cdot \hat{\epsilon})), \quad (7)$$

where  $\hat{u}$  is the unit vector of the fragment c.m. velocity,  $\hat{\epsilon}$  is the unit vector of the laser electric field,  $\beta$  is the conventionally defined anisotropy parameter,<sup>23</sup> and  $P_2(x)$  is the second Legendre polynomial, then  $\beta$  for reaction (1) is 0.21. The data and the fit of the polarization dependence of reaction (1) at  $m/e = 53$  is plotted in Fig. 10. For the other channels, observation of the polarization dependence was not successful. For the fragments with low c.m. velocities, the laboratory signal is not very sensitive to  $\beta$ . For H atoms at high laser power, most of the signal was not from primary processes, and the signal was nearly isotropic because of long lived intermediates. For H atoms at low laser power and  $H_2$ , the signal-to-noise level was too poor for a meaningful measurement of the polarization dependence.

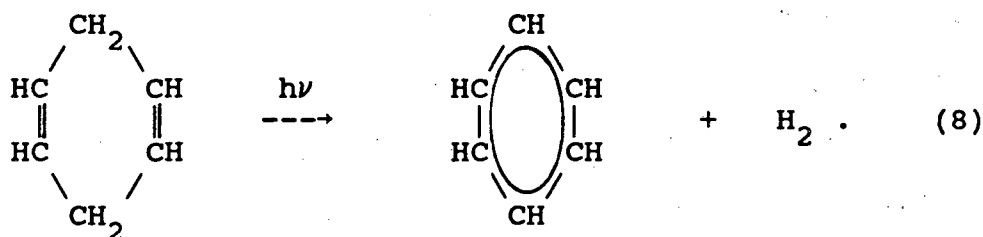
### b. IRMPD

Pure CHN in the gas phase was reported not to undergo IRMPD.<sup>9</sup> We initially found that no dissociation signal could be detected at low nozzle temperatures. Dissociation signal from the retro-Diels-Alder reaction (1) was finally observed by heating the nozzle to 560°C to increase the vibrational temperature of CHN. The observed TOF spectra, fit using the  $P_E(E_T)$  shown as curve (b) of Fig. 9, are presented in Fig. 11.

## B. Photodissociation of 1,4-cyclohexadiene

### a. Photolysis at 193 nm

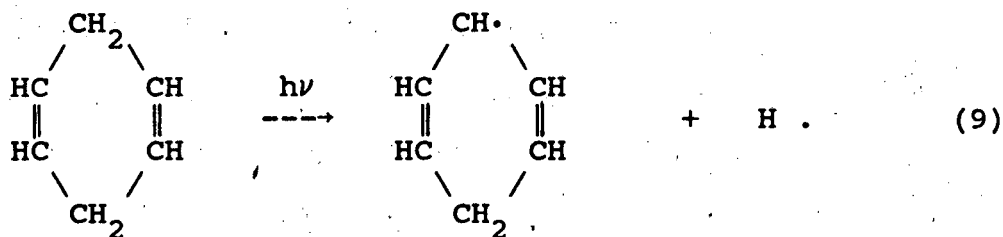
In the case of CHDN, the shape of the  $m/e = 2$  TOF spectra did not change when the laser power was varied, and the integrated signal as a function of laser power was linear, which indicates that the  $H_2$  signal, shown in Fig. 12 a), is from a primary dissociation channel presented as reaction (8).



This dissociation channel has been studied previously in the bulk.<sup>24-26</sup> The  $P_E(E_T)$  for reaction (8) obtained by fitting the  $m/e = 2$  TOF spectrum is shown as curve (b) in Fig. 7.

No signal from CHDN was observed at  $m/e = 79$ , which

might imply that the H elimination channel did not occur. However, an attempt to simultaneously fit the TOF spectra of  $m/e = 2$  and 78 with reaction (8) shows that the  $m/e = 2$  TOF spectrum is too narrow to account for all the signal at  $m/e = 78$ . In Fig. 12 b), two  $m/e = 1$  TOF spectra at different laser powers are shown. Similar to CHN dissociation, the fast component in the  $m/e = 1$  TOF spectra has a linear laser power dependence while the slow component does not. The above observations indicate the existence of reaction (9),



The  $P_E(E_T)$  for reaction (9), plotted as curve (b) in Fig. 4, is obtained by fitting the fast edge of the  $m/e = 1$  TOF spectrum and the slow part of the  $m/e = 78$  TOF spectrum simultaneously. Curve (b) of Fig. 4 terminates at 10 kcal/mol, because below about 10 kcal/mol information cannot be obtained from the fit. The fit to the  $m/e = 78$  TOF spectrum is shown in Fig. 13.

By more careful consideration, we realize that the components in the relevant TOF spectra attributed to reaction (9) are actually the result of both reaction (9) and an additional reaction, the spontaneous secondary dissociation of the cyclohexadienyl radical produced in reaction (9):



The heat of reaction for reaction (10) is 25 kcal/mol using the heat of formation of cyclohexadienyl radical provided by Ref. 32.<sup>34</sup> The exit barrier for reaction (10) is not known to us, but is likely no more than 10 kcal/mol. Fig. 2 and curve (b) of Fig. 4 imply that most of the cyclohexadienyl radical from reaction (9) has enough internal energy to undergo further spontaneous dissociation through reaction (10). This is the main reason that no signal at  $m/e = 79$  could be detected. Since the recoiling H atom is very light compared to benzene we expect that the TOF distribution of benzene from reaction (10) should be similar to that of cyclohexadienyl radical from reaction (9). Because of the same linear laser power dependence, the similarity in the kinematics, and the absence of any  $m/e = 79$  signal, we can not unambiguously separate the contributions to the TOF spectra from reactions (9) and (10). The  $P_E(E_T)$  presented as curve (b) in Fig. 4 is a convoluted result of contributions from both reactions (9) and (10). The true  $P_E(E_T)$  for both reactions (9) and (10) should be shifted to lower energy and narrower than curve (b) of Fig. 4.

Laser polarization studies did not provide reliable information for the same reasons as with CHN.

#### b. IRMPD

The IRMPD signal of CHDN was quite strong, and only reaction (8) was observed. The TOF spectra obtained at dif-

ferent laboratory angles are presented in Fig. 14 and are fit using the  $P_E(E_T)$  plotted as curve (c) in Fig. 7.

#### IV. Discussion

##### A. Features common to 193 nm photodissociation and IRMPD

Some dissociation channels show similar features for both 193 nm excitation and IRMPD. For CHN the common channel is the retro-Diels-Alder reaction, and for CHDN it is  $H_2$  elimination. Although the initial photon excitation mechanism is different, one being electronic and the other being vibrational excitation on the ground electronic PES, the dynamical features reflected in the  $P_E(E_T)$ 's are very similar for the same dissociation channel. The  $P_E(E_T)$ 's for the retro-Diels-Alder reaction plotted in Fig. 9 are almost identical. There is more difference among the  $P_E(E_T)$ 's for the various  $H_2$  elimination channels from cyclohexadiene shown in Fig. 7. At 193 nm, the maximum translational energy for reaction (4) is much higher than that for reaction (8), because in reaction (4) the product is the result of sequential two-photon dissociation with much more energy available, while in reaction (8) it is a one-photon process. The  $P_E(E_T)$  for reaction (8) from IRMPD is the narrowest in Fig. 7. Although there are clear differences in the maximum translational energy and the width of the  $P_E(E_T)$ 's, their peak positions are very similar. The

similarity of the  $P_E(E_T)$ 's obtained from 193 nm dissociation and IRMPD for the same reaction channels strongly suggests that following 193 nm excitation these reactions also proceed on the ground electronic PES, i.e., IC occurs prior to reactions (1) and (8) in 193 nm photolysis.

On the other hand, although H atom elimination was observed from both CHN and CHDN at 193 nm, the  $P_E(E_T)$ 's for these channels shown in Fig. 4 are strikingly different. The difference displayed by the  $P_E(E_T)$ 's strongly indicates different dissociation mechanisms between reactions (2) and (9). We will show later that for CHN the H atom is eliminated from an electronically excited state and there is competition between IC and direct dissociation, while for CHDN the H atom is eliminated from the ground electronic state as in the case of H atom elimination in the 193 nm photodissociation of benzene.<sup>17</sup>

#### B. Dynamics of the retro-Diels-Alder reaction and H<sub>2</sub> elimination

The  $P_E(E_T)$ 's for both reactions (1) and (8) peak substantially away from zero, which indicate the existence of an exit potential energy barrier. Based on previous studies mentioned in the introduction,<sup>11-15</sup> this observation is direct evidence of the concerted nature of both the retro-Diels-Alder reaction and reaction (8).

In the 193 nm photodissociation of CHN, the nozzle

temperature was 300°C. Since the stagnation pressure of the molecular beam was only 100 Torr and the expansion from a 0.13 mm diameter nozzle is not strong, so that vibrational relaxation should be far from complete. Therefore, the internal energy of the CHN after absorbing one 193 nm photon is more than 148 kcal/mol, much higher than the measured activation energy of reaction (1) (66.5 kcal/mol<sup>10</sup>) or the barrier for the retro-Diels-Alder diradical path.<sup>4,5</sup> IR multiphoton excitation of CHN leads to a broad internal energy distribution,<sup>11</sup> while at 193 nm the internal energy of all CHN molecules prior to dissociation is approximately the same. However, this experiment shows that the  $P_E(E_T)$  for the retro-Diels-Alder reaction at 193 nm is almost the same as that for IRMPD, implying that dissociation is still concerted at a high internal energy, and that the internal energy is not a dominant factor in the product translational energy distribution.

An interesting observation can be made by comparing the available energy shown in Fig. 1 and the  $P_E(E_T)$ 's in Fig. 9. The peak translational energy in IRMPD is 22.5 kcal/mol, 85% of the exit barrier of the retro-Diels-Alder reaction which is 26.4 kcal/mol. As mentioned in the introduction, the peak of the  $P_E(E_T)$  is mainly determined by the dynamics of the potential energy release as the products separate. The  $P_E(E_T)$ 's for reaction (1) indicate a very repulsive exit potential energy surface from the transition state to the

products and a dissociation process with a very small exit impact parameter and relatively rigid fragments, so that almost all of the exit potential energy is channeled into translation.

A simple calculation can quantitatively show the significance of the above statement. Let us assume that the peak energy in the  $P_E(E_T)$  in IRMPD is purely due to energy release along the exit barrier, the product molecules  $C_2H_4$  and  $C_4H_6$  are rigid, and the transition state is not coplanar but is symmetric with respect to the two breaking C-C bonds. Under the above approximations, the exit barrier energy roughly equals the observed 22.5 kcal/mol peak translational energy plus the rotational energy. From the maximum possible rotational energy set by the difference between the exit barrier and the peak translational energy we can calculate the value of the exit impact parameter, and therefore obtain information about the geometry of the transition state. The most important factor in the calculation is the angle between the two planes defined by the six carbon atoms at the transition state. If we take  $26.4 - 22.5 = 3.9$  kcal/mol as the rotational energy and use the bond lengths of  $C_4H_6$  at the transition state provided by Burke *et al.*,<sup>7a</sup> the corresponding impact parameter and the angle are calculated to be 0.40 Å and  $45^\circ$  respectively. According to the prediction of Burke *et al.*,<sup>7a</sup> the angle between the two planes is  $66^\circ$  with an exit impact parameter

of 0.52 Å. Although the rotational energy can be off by as much as a few kcal/mol in our simplified calculation due to our model and uncertainty in the potential barrier, a more realistic model taking into account excitation of vibrational degrees of freedom is likely to reduce the product rotational energy so that the exit impact parameter would be even smaller. Therefore, the theoretically predicted geometry is out of the range implied by our experiment. A new high-level theoretical investigation would be helpful in resolving this discrepancy.

Although the internal energy of CHN at 193 nm is high enough to break a C-C bond and lead to a sequential diradical path for the retro-Diels-Alder reaction, the dissociation dynamics observed in this experiment provide further evidence for the concerted mechanism. If the reaction occurred through a diradical path, the exit impact parameters would be on the order of 1 Å and the recoil would be from an asymmetric configuration, which would cause much rotational and vibrational excitation of the products. It is likely that less than half of the exit barrier energy would be channeled into translation at the peak translational energy. Therefore, the diradical mechanism is not consistent with the fact that the peak translational energy is 85-90% of the exit barrier.

Using the parameters provided by Kiefer and Shah<sup>10</sup> the RRKM<sup>27</sup> dissociation lifetimes of the retro-Diels-Alder

reaction (reciprocals of the RRKM unimolecular rate constants) at total energies of 148 kcal/mol and 158 kcal/mol are calculated to be 2.1 nsec and 0.93 nsec respectively. This is much longer than the timescale for IC, because IC was found to compete effectively with H atom elimination from a repulsive excited electronic PES.

For the 193 nm photodissociation of CHN, the dominant transition, assuming  $C_{2v}$  symmetry, is to a  ${}^1B_2$  state, and the transition dipole lies parallel to the y axis defined in Fig. 15. If the geometry of the transition state of the retro-Diels-Alder reaction is symmetric, the angle between the transition dipole and the recoil direction is  $90^\circ$ . According to the model given by Zhao et al.,<sup>15</sup> the conventional anisotropy parameter  $\beta$  in Eqn. (7) can be decomposed into,

$$\beta = 2b_1 P_2(\hat{\mu} \cdot \hat{T}) P_2(\hat{T} \cdot \hat{u}^0) , \quad (11)$$

where  $b_1$  is the global anisotropy parameter,  $\hat{\mu}$  is the unit vector of the transition dipole,  $\hat{T}$  is the unit vector from the c.m. of the molecule to the c.m. of the group of atoms at the transition state which will form the detected product, and  $\hat{u}^0$  is the unit vector of the asymptotic direction of the product in the body-fixed frame.  $b_1$  reflects the effect of molecular rotation on all the fragments,<sup>15</sup> and is related to the lifetime of the energized molecule. By using the observed  $\beta = -0.21$  for reaction (1) and assuming  $\hat{T} \cdot \hat{u}^0 = 1$ ,  $b_1 = 0.21$  is derived. In the triple

dissociation of s-tetrazine<sup>15</sup> the observed  $b_1 \leq 0.13$  and  $b_1 = 0.65$  at 552 nm and 248 nm correspond to calculated RRKM dissociation lifetimes of 50 nsec and about 1 psec respectively, while in this example  $b_1 = 0.21$  corresponds to an RRKM lifetime on the order of 1 nsec. These numbers provide some idea of the relationship between the observed  $b_1$  and the lifetime of an energized molecule in a PTS experiment for nonlinear polyatomic molecules.

Gas phase isotope labeling studies have established that most of the  $H_2$  produced in reaction (8) is from 3,6 elimination.<sup>26</sup> However, the same experiments indicated that there is isomerization between 1,3- and 1,4-cyclohexadiene in the energy range near 193 nm. Therefore, it is likely that the detected products in reaction (3) is a mixture of the two isomers. It is implied by the detected isotope labelled products that hot 1,3-cyclohexadiene can also produce benzene.<sup>26</sup> It is still unclear whether 1,3-cyclohexadiene can directly produce benzene through molecular  $H_2$  elimination at such a high energy. Symmetry arguments by Hoffmann<sup>28</sup> imply that it is difficult to obtain benzene from ground electronic state 1,3-cyclohexadiene through concerted elimination in thermal decomposition. Pyrolysis studies are consistent with this prediction,<sup>24,29</sup> and Benson and Shaw<sup>29</sup> estimated that the activation energy is larger than 53 kcal/mol, compared with 43.8 kcal/mol for reaction (8).<sup>25</sup> Since after 193 nm excitation the total energy in the

molecules is higher than 148 kcal/mol, it might be possible that 1,3-cyclohexadiene also produces  $H_2$  through four-center molecular elimination.

Reactions (3) and (8) have very similar  $P_E(E_T)$ 's. Reaction (3) has been previously observed in pyrolysis studies.<sup>8</sup> It was believed that the  $H_2$  was also produced by a 3,6 concerted elimination<sup>25</sup> with an activation energy of 71.2 kcal/mol.<sup>8</sup> The concerted nature of reaction (3) is shown by the  $P_E(E_T)$  in Fig. 6 which peaks at 20 kcal/mol. Considering the pyrolysis results and the similarity with reaction (8), there is little doubt that reaction (3) also occurs on the ground electronic PES.

### C. Difference in H atom elimination between CHN and CHDN

The H atom elimination channel (2) observed at 193 nm occurs on an excited repulsive electronic PES. As pointed out in the introduction, if simple bond rupture occurs on the ground electronic PES, we would expect the  $P_E(E_T)$  to peak near zero and have a low average translational energy. This has been confirmed not only in IRMPD<sup>11-14</sup> but also in H atom elimination from benzene at 193 nm.<sup>17</sup> The average translational energy released by reaction (2) is 36.3 kcal/mol and the peak is at about 36.5 kcal/mol, implying a repulsive PES along the reaction coordinate. This can be compared with the 37.8 kcal/mol translational energy release for C-H bond rupture in  $CH_3I$  at 193 nm.<sup>35</sup> To further

understand the mechanism of H atom elimination, a qualitative molecular orbital study of CHN is in order.

The bonds in CHN can be classified into two groups (see Fig. 15): an ethylene group which includes the  $\sigma$  and  $\pi$  bonds between  $C^1$  and  $C^2$ , the C-H  $\sigma$  bonds on  $C^1$  and  $C^2$ , and the  $C^1-C^6$  and  $C^2-C^3$   $\sigma$  bonds; and an alkyl group which contains the C-H  $\sigma$  bonds on  $C^3$  and  $C^6$ , and the  $C^3-C^4$  and  $C^5-C^6$   $\sigma$  bonds. The C-H bonds on  $C^4$  and  $C^5$  and the  $C^4-C^5$  bond are disregarded because they have negligible interaction with the  $\pi$  bond in the ethylene group as far as H atom elimination is concerned.

The lowest energy geometry of CHN is the half chair conformation<sup>36</sup> which has  $C_2$  symmetry. For our purpose, however, it is acceptable to assume that  $C^4$  and  $C^5$  are in the plane defined by the other four carbons, so that the molecule has  $C_{2v}$  symmetry. The reasons for this are: 1) we are investigating the most important interactions of the  $\pi$  bond with its neighbors, which become clear under  $C_{2v}$  symmetry; the difference between  $C_2$  and  $C_{2v}$  can be considered as a perturbation. 2) inter-conversion of the conformations of CHN at high internal energy makes the assumption of a planar molecule valid to some extent.

There have been systematic studies of the effect of alkyl substituents on the spectrum of ethylene,<sup>30,31</sup> but here we would like to ask the opposite question: what is the effect of ethylene on the alkyl group? On the left hand

side of Fig. 16 the orbitals of the ethylene group are listed in order of increasing energy, adapted to our symmetry notation from Merer and Mulliken.<sup>31</sup> The combined alkyl group orbitals in  $C_{2v}$  symmetry obtained by local-orbital mixing depicted in Fig. 17 are plotted on the right hand side of Fig. 16. The middle of Fig. 16 shows a qualitative ordering of the molecular orbitals after allowing the orbitals on the left and right to interact. As can be seen, the singlet state created by a one electron transition from the highest occupied orbital  $b_1$ , which has predominant  $\pi$ -ethylenic character, to the unoccupied orbital  $a_2$ , which has predominant  $\pi^*$ -ethylenic character, has  ${}^1B_2$  symmetry. This  ${}^1B_2$  state contains some character of the C-H  $\sigma^*$  orbital on  $C^3$  and  $C^6$ . None of the anti-bonding orbitals of the bonds which are in the plane of the molecule can mix with the  $\pi$  and  $\pi^*$  orbitals. This conclusion can be drawn in a more general way: because the  $\pi$  and  $\pi^*$  orbitals are anti-symmetric with respect to the mirror plane of the cyclic skeleton of the molecule, and any  $\sigma$  or  $\sigma^*$  orbital in the same plane is symmetric with respect to this mirror plane, it is impossible to get a combination of these  $\sigma$  and/or  $\sigma^*$  orbitals with the same symmetry as that of  $\pi$  or  $\pi^*$ , so that they cannot mix if only electronic interactions are considered. On the other hand, a proper combination of the  $\sigma$  or  $\sigma^*$  orbitals on the C-H bonds of  $C^3$  and  $C^6$ , which are out of that mirror plane, can have the same symmetry as the  $\pi$  or  $\pi^*$

orbitals, so that it is possible to mix the  $\pi$  or  $\pi^*$  orbitals with the  $\sigma$  or  $\sigma^*$  orbitals on those C-H bonds to form a mixed molecular orbital.

The initial 193 nm excitation of CHN is hard to attribute to a single state, because there are several absorption bands in the vicinity of 193 nm.<sup>30,31</sup> However, the dominant contribution to the 193 nm absorption is from the so-called V-N transition (predominantly a  $\pi^* + \pi$  transition)<sup>30,31</sup> whose absorption maximum is on the short wavelength side of 193 nm. This V state of CHN is just the  $^1B_2$  state discussed previously. As shown in Fig. 16 this V-N transition contains a  $\sigma^* + \sigma$  component of the C-H bond on the C<sup>3</sup> and C<sup>6</sup>. Now, the mechanism seems clear: It is very likely that the H atom elimination occurs on an excited electronic PES and the H atom eliminated is from an  $\alpha$  carbon. This is consistent with the observed large translational energy release.

The maximum translational energy from reaction (2) is  $61 \pm 3$  kcal/mol. The excited C-H stretch mode has negligible population in the molecular beam. For H elimination from the initially prepared repulsive state, we assume that the maximum translational energy observed corresponds to all the available energy being released into translation, which should be a good approximation for a very light atom recoiling from a very heavy particle. Using the above approximations, the maximum translational energy release of 61

$\pm 3$  kcal/mol yields a bond energy of  $87 \pm 3$  kcal/mol, consistent with what would be expected for a C-H bond on the  $\alpha$  carbon of a C=C bond.<sup>32</sup>

For C-H bond rupture in CHDN at 193 nm, the observed  $P_E(E_T)$  is very different from that of CHN, and it is very likely that this is not a direct dissociation. The initial state reached by 193 nm absorption is not clear.<sup>26,30,33</sup> Since the molecule is bent<sup>26</sup> and has two equivalent double bonds, if only symmetry arguments are used, mixing of the local orbitals would be possible among all of the bonds because of the loss of the mirror plane of the cyclic skeleton. Srinivasan *et al.*<sup>26</sup> have calculated that one of the two excited  $^1B_2$  states close to 6.44 eV (the photon energy at 193 nm) is mixed with the  $\sigma^*$  orbitals on the C<sup>3</sup> and C<sup>6</sup> C-H bonds. This was used to explain H atom migration in the molecule. The  $P_E(E_T)$  for reaction (9) is narrower and shifted to lower energy than curve (b) of Fig. 4 as previously discussed. This observation leads us to suggest that reaction (9) occurs on the ground electronic PES after IC and the H atom eliminated is from an  $\alpha$  carbon.

The C-H bond energy for CHDN cannot be obtained with confidence using the same method as for CHN, because if dissociation is not from an initially prepared repulsive state, the approximations used previously may not be valid.

## V. Summary

This study has provided the following information:

1) The retro-Diels-Alder reaction of cyclohexene is concerted up to a total energy higher than 148 kcal/mol.

2) H atom elimination observed in the 193 nm photodissociation of cyclohexene occurs on a repulsive excited electronic PES and is related to mixing with the C-H antibonding orbitals on the  $\alpha$  carbons. The bond energy for that C-H bond has been measured to be  $87 \pm 3$  kcal/mol.

3) Competition between dissociation from the excited electronic state and IC to the ground electronic state is observed in the photodissociation of cyclohexene at 193 nm.

4) A direct comparison between electronic and vibrational excitation has shown that the product translational energy distribution for the concerted dissociation of a moderate-sized molecule in the ground electronic state with an appreciable exit barrier is determined mainly by the dynamics of repulsive energy release of the exit barrier, while the total energy or the form of the initial excitation play less important roles.

In Chapters II, III and this chapter, the data analysis formulation developed in Chapter I has been applied to various processes. Although the power of the formulation is displayed by these chapters, the physical significance of the approximations used to derive the formulas was not examined carefully in Chapter I. With the examples presen-

ted in Chapters II, III, and IV, it is time to come to this question, to which Chapter V is devoted.

**References**

1. A. Wassermann, Diels-Alder Reactions, Elsevier Publishing Company, Amsterdam (1965).
2. R. B. Woodward and R. Hoffmann, The Conservation of Orbital Symmetry, VCH (1970).
3. J. W. McIver, Jr., *Acc. Chem. Res.* **7**, 72 (1974).
4. R. E. Townshend, G. Ramunni, G. Segal, W. J. Hehre, and L. Salem, *J. Am. Chem. Soc.* **98**, 2190 (1976).
5. M. J. S. Dewar, S. Olivella, and H. S. Rzepa, *J. Am. Chem. Soc.* **100**, 5650 (1978).
6. a) K. Jug, *Theor. Chim. Acta* **54**, 263 (1980). b) K. Jug and C. P. D. Dwivedi, *Theor. Chim. Acta*, **59**, 357 (1981).
7. a) L. A. Burke, G. Leroy, and M. Sana, *Theor. Chim. Acta*, **40**, 313 (1975). b) L. A. Burke, *Theor. Chim. Acta* **68**, 101 (1985).
8. S. R. Smith and A. S. Gordon, *J. Phys. Chem.* **65**, 1124 (1961).
9. D. Garcia and P. M. Keehn, *J. Am. Chem. Soc.* **100**, 6111 (1978).
10. J. H. Kiefer and J. N. Shah, *J. Phys. Chem.* **91**, 3024 (1987).
11. For a review of the early development of IRMPD, see, for example, P. A. Schulz, A. S. Sudbø, D. J. Krajnovich, H. S. Kwok, Y. R. Shen, and Y. T. Lee, *Ann. Rev. Phys. Chem.* **30**, 379 (1979).

12. a) A. M. Wodtke, E. J. Hintsä, and Y. T. Lee, *J. Phys. Chem.* **90**, 3549 (1986). b) E. J. Hintsä, A. M. Wodtke, and Y. T. Lee, *J. Phys. Chem.* **92**, 5379 (1988).
13. Chapter II.
14. L. J. Butler, R. J. Buss, R. J. Brudzynski, and Y. T. Lee, *J. Phys. Chem.* **87**, 5106 (1983).
15. Chapter III.
16. L. J. Butler, E. J. Hintsä, and Y. T. Lee, *J. Chem. Phys.* **84**, 4104 (1986).
17. A. Yokoyama, X. Zhao, E. J. Hintsä, R. E. Continetti, and Y. T. Lee, in preparation.
18. A. M. Wodtke and Y. T. Lee, in Advances in Gas Phase Photochemistry and Kinetics, J. Baggott and M. Ashfold, Eds., Royal Society of Chemistry, London (1987).
19. A. M. Wodtke and Y. T. Lee, *J. Phys. Chem.* **89**, 4744 (1985).
20. a) Chapter I. b) X. Zhao, G. M. Nathanson, and Y. T. Lee, to be published.
21. Y. T. Lee, J. D. McDonald, P. R. LeBreton, and D. R. Herschbach, *Rev. Sci. Instrum.* **40**, 1402 (1969).
22. T. Trickl, Private communication.
23. R. N. Zare, *Mol. Photochem.* **4**, 1 (1972).
24. R. J. Ellis and H. M. Frey, *J. Chem. Soc. (A)*, 553 (1966).
25. S. W. Benson and R. Shaw, *Trans. Faraday Soc.* **63**, 985 (1967).

26. R. Srinivasan, L. S. White, A. R. Rossi, and G. A. Epling, *J. Am. Chem. Soc.* **103**, 7299 (1981).
27. P. J. Robinson, K. A. Holbrook, Unimolecular Reactions, Wiley, London (1972).
28. R. Hoffmann, *Trans. N. Y. Acad. Sci.* **475** (1966).
29. S. W. Benson and R. Shaw, *J. Am. Chem. Soc.* **89**, 5351 (1967).
30. M. B. Robin, Higher Excited States of Polyatomic Molecules, Vol. II, Academic Press, New York (1975).
31. A. J. Merer and R. S. Mulliken, *Chem. Rev.* **69**, 639 (1969).
32. D. F. McMillen and D. M. Golden, *Ann. Rev. Phys. Chem.* **33**, 493 (1982).
33. R. P. Frueholz, W. M. Flicker, O. A. Mosher, and A. Kuppermann, *J. Chem. Phys.* **70**, 1986 (1979).
34. If we use the heat of formation of cyclohexadienyl radical provided by the CRC Handbook of Chemistry and Physics, the heat of reaction for reaction (10) is 10.5 kcal/mol. The value chosen in the text is for a conservative argument.
35. R. E. Continetti, B. A. Balko, and Y. T. Lee, *J. Chem. Phys.* **89**, 3383 (1988).
36. N. Neto, C. Di Lauro, E. Castellucci, and S. Califano, *Spectrochimica Acta*, **23A**, 1763 (1967).

**Figure captions for Chapter IV**

Fig. 1 Energy diagram of cyclohexene dissociation with energies in kcal/mol. The values for the transition states are the activation energies. See text for the source of the values.

Fig. 2 Energy diagram of 1,4-cyclohexadiene dissociation with energies in kcal/mol. The value for the transition state is the activation energy, taken from Ref. 25.

Fig. 3 TOF spectra from the 193 nm dissociation of CHN taken on the RMBA at 15°. Circles are the experimental data and lines are the fits. a) The line is the fit with reaction (2). b) and c) The slower component is from reaction (2), and the faster one from reaction (3). d) The slowest component is from reaction (2), the middle one is from reaction (3) and the fastest one from reaction (4).

Fig. 4  $P_E(E_T)$ 's for the H atom elimination channels. Curve (a) is for reaction (2) of CHN at 193 nm and curve (b) for reaction (9) of CHDN at 193 nm.

Fig. 5 TOF spectra from the 193 nm dissociation of CHN taken on the CMBA. a) Two sets of experimental TOF spectra of  $m/e = 1$  at different laser powers. Solid circles are the low power data, and the triangles are at high power. b) Fit of the fast edge of the  $m/e = 1$  spectrum using reaction (2). Circles are the exper-

imental data and the line is the contribution from reaction (2). c) Two experimental TOF spectra of  $m/e = 2$  at different laser powers. Solid circles are the low power data, and the triangles are at high power. d) Fit of the  $m/e = 2$  spectrum using reactions (3) and (4). The slower component is due to reaction (3) and the faster one is due to reaction (4). In a) and c) the two sets of experimental data have been normalized with respect to laser power, so that the TOF spectra would be identical if they were the results of one-photon processes with no saturation.

Fig. 6  $P_E(E_T)$  for reaction (3) used to fit the experimental TOF spectra.

Fig. 7  $P_E(E_T)$ 's for  $H_2$  elimination from cyclohexadiene used to fit the observed TOF spectra. Curve (a) is for reaction (4), the secondary photodissociation of cyclohexadiene from CHN at 193 nm. Curve (b) is for reaction (8) of CHDN at 193 nm. Curve (c) is for reaction (8) of CHDN following IRMPD.

Fig. 8 TOF spectra of CHN at 193 nm taken on the RMBA at  $20^\circ$ . The time window chosen shows only the retro-Diels-Alder reaction. Circles are the experimental data, and the lines are the fit using reaction (1). a) Signal due to the 1,3-butadiene fragment. b) The faster peak is from ethylene and the slower peak is from the daughter ions of 1,3-butadiene at mass 28.

Fig. 9  $P_E(E_T)$ 's for the retro-Diels-Alder reaction used to fit the experimental data. Curve (a) is for 193 nm dissociation and curve (b) is for IRMPD.

Fig. 10 Laser polarization dependence of the signal at  $m/e = 53$  for reaction (1) of CHN at 193 nm. Points are the experimental data and the line is the fit using  $\beta = -0.21$  and the  $P_E(E_T)$  plotted as curve (a) in Fig. 9.

Fig. 11 TOF spectra of the IRMPD of CHN taken on the RMBA at  $20^\circ$ . The signal is due to the retro-Diels-Alder reaction. Points are the experimental data and the lines are the fit. a) Signal from 1,3-butadiene. b) The faster peak is from ethylene and the slower one from 1,3-butadiene.

Fig. 12 TOF spectra of the 193 nm dissociation of CHDN taken on the CMBA. a)  $m/e = 2$  experimental results (points) and the fit using reaction (8). b)  $m/e = 1$  at different laser powers. Solid circles are at low laser power and the triangles are at high power. The plots are normalized to the laser power (see Fig. 5 caption). The line is the fit using reaction (9).

Fig. 13 The  $m/e = 78$  TOF spectrum of CHDN at 193 nm taken on the RMBA at  $15^\circ$ . The points are the experimental data. The lines are the simulation, with the slow component from reaction (9) and the faster component from reaction (8).

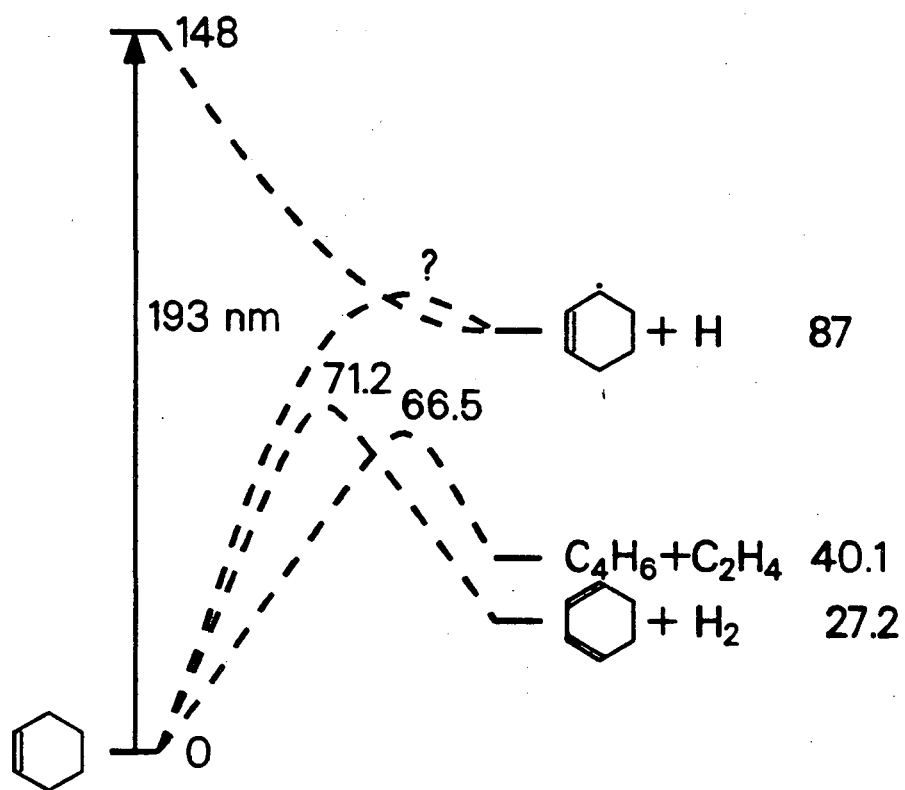
Fig. 14 The  $m/e = 52$  TOF spectra of IRMPD of CHDN taken on

the RMBA at different LAB angles. Circles are the data and the lines are the fits using reaction (8).

Fig. 15 The coordinate system for CHN. The molecule is assumed to be planar. See text for the details.

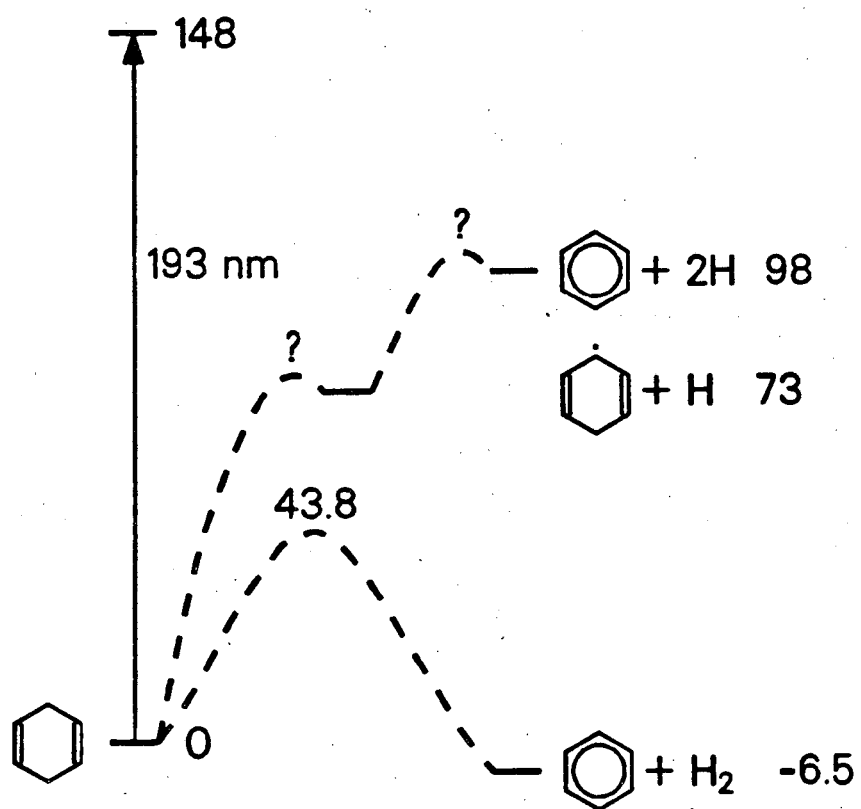
Fig. 16 A qualitative correlation diagram of the molecular orbitals with the local orbitals, showing that only the C-H bonds on C<sup>3</sup> and C<sup>6</sup>, which are out of the molecular plane, can interact with the  $\pi$  bond.

Fig. 17 Combination of the orbitals in the alkyl group under C<sub>2v</sub> symmetry to obtain the group orbitals used in Fig. 16. Notice that C-H bonds are out of the yz plane defined in Fig. 15.



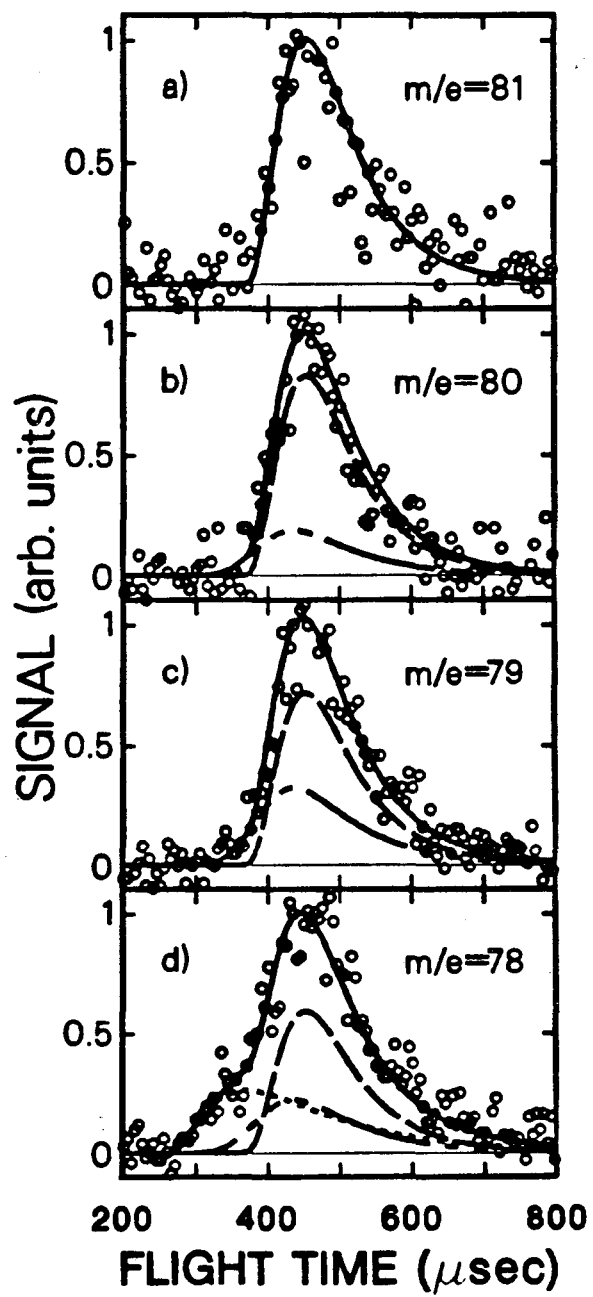
XBL 8810-3652

Fig. 1



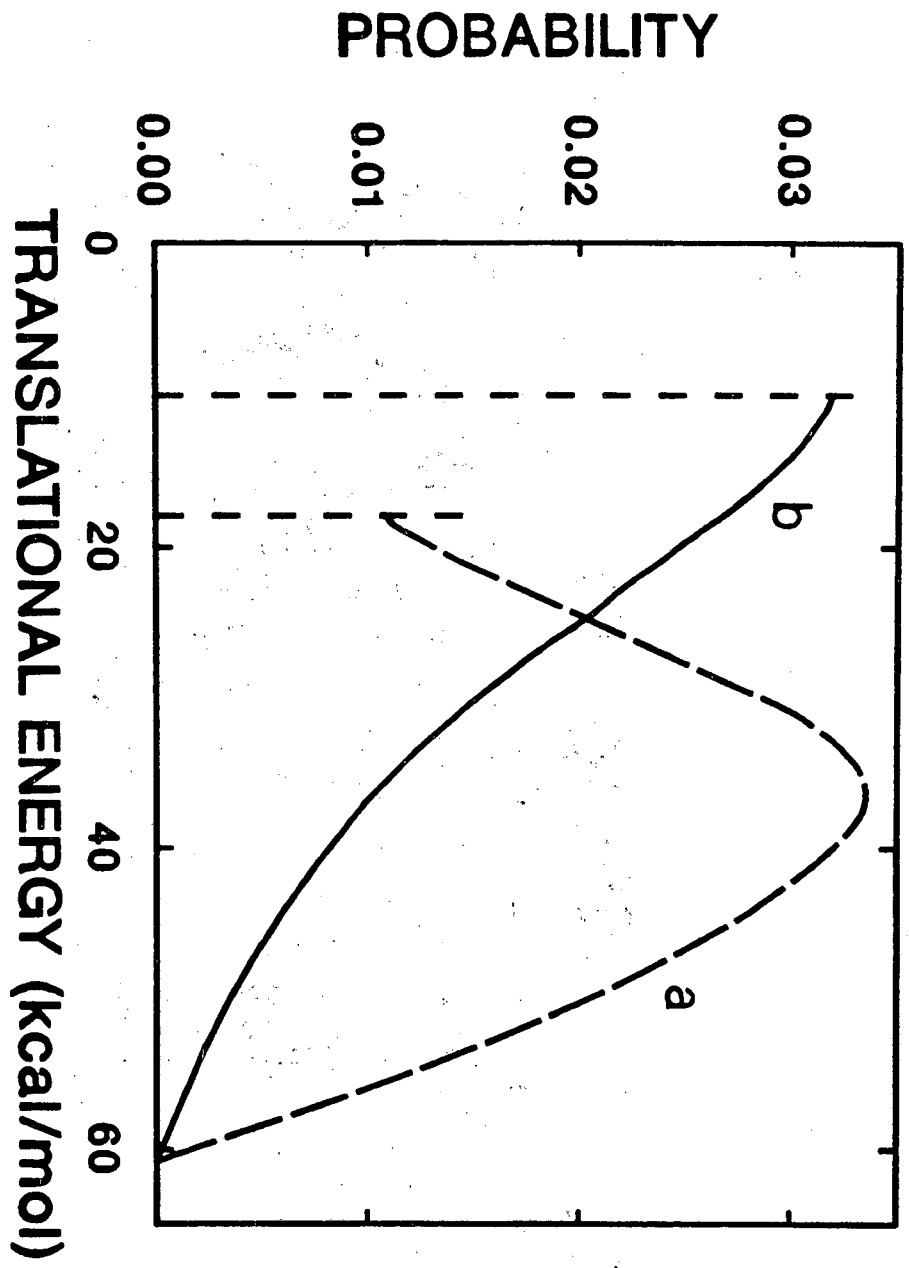
XBL 8810-3653

Fig. 2



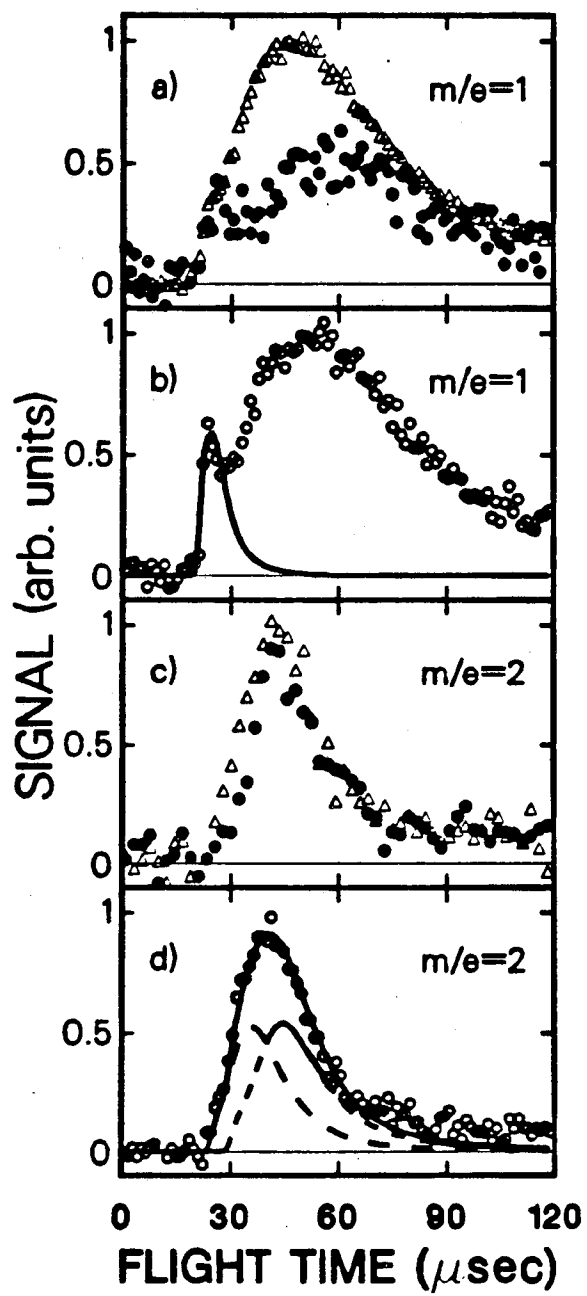
XBL 8810-3654

Fig. 3



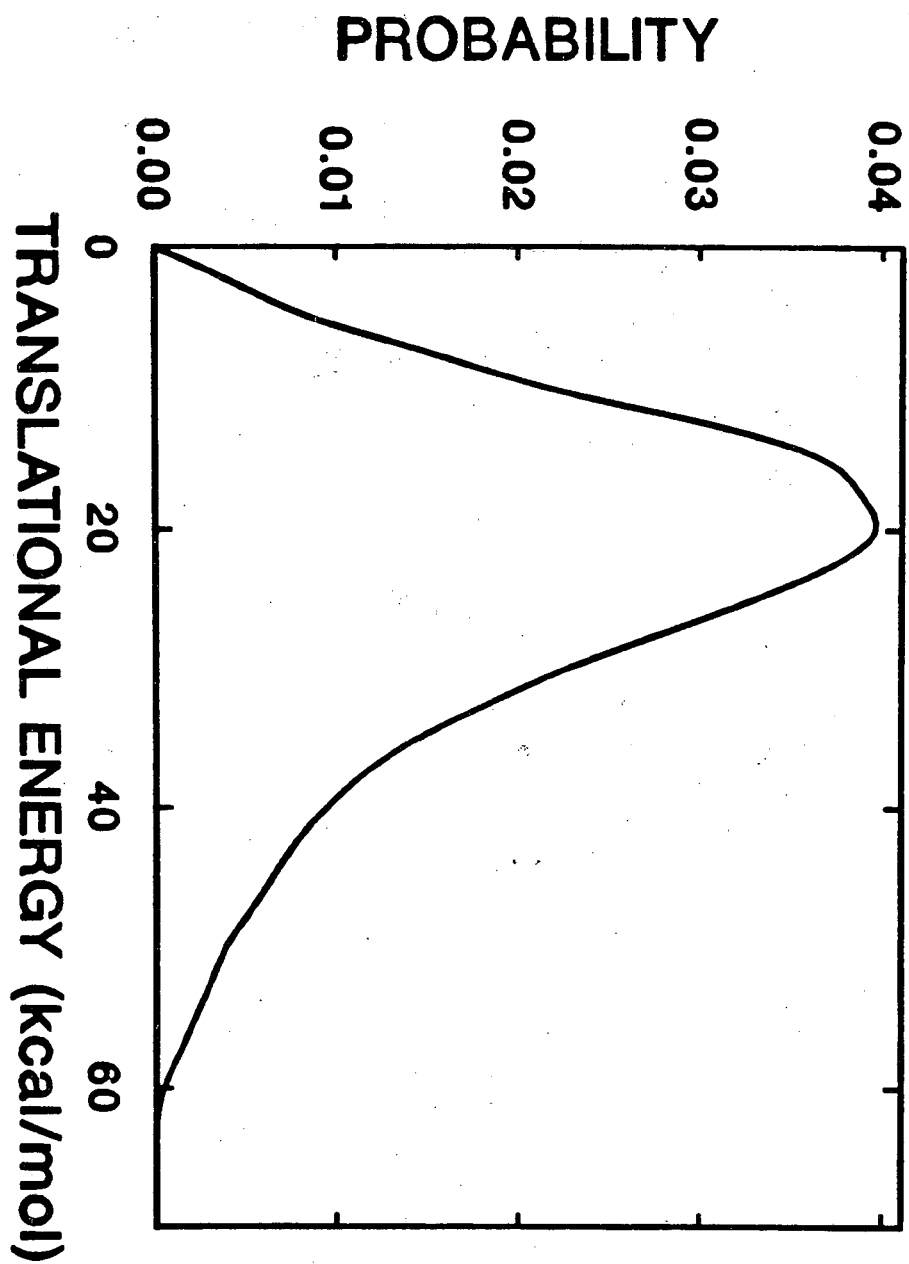
XBL 8810-3667

Fig. 4



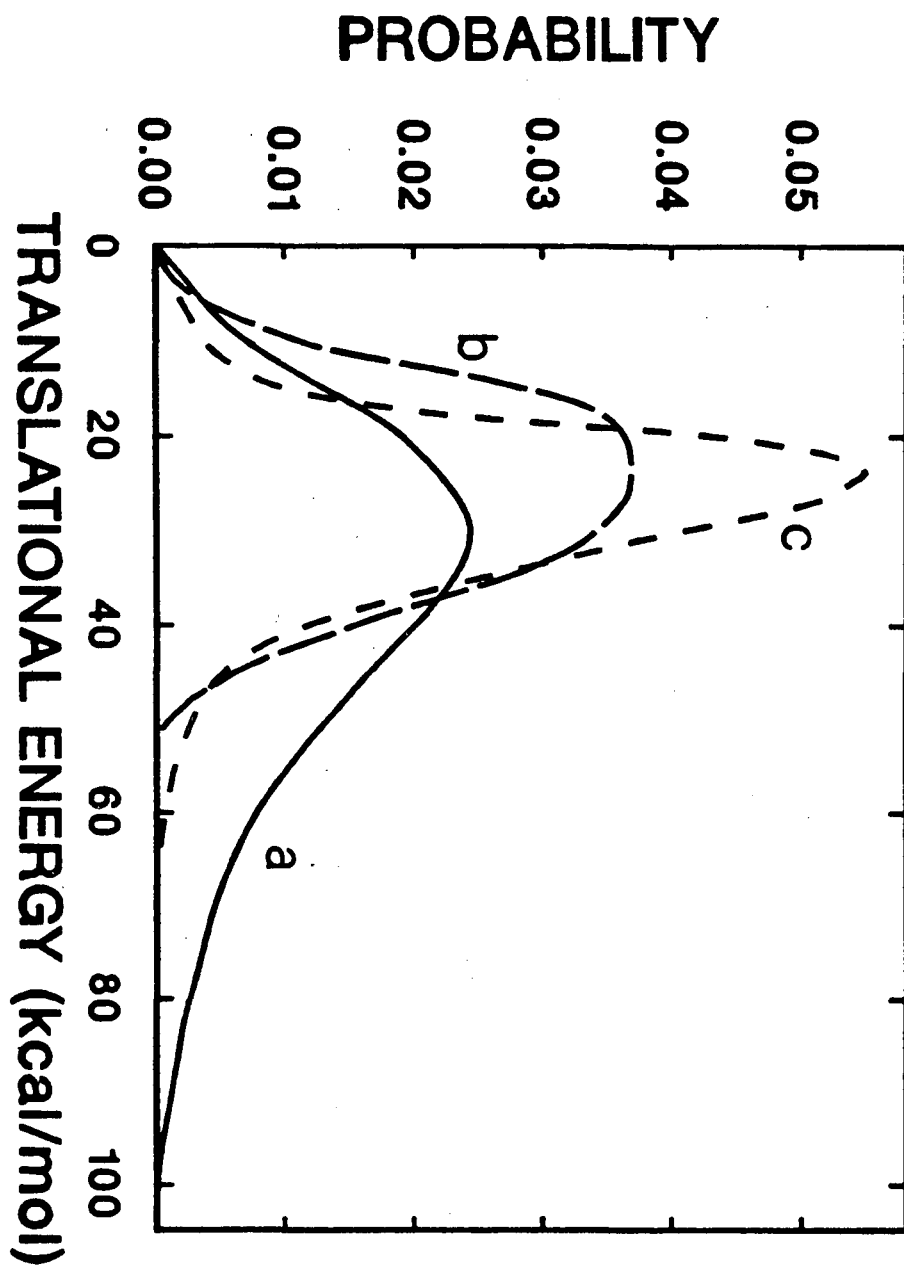
XBL 8810-3656

Fig. 5



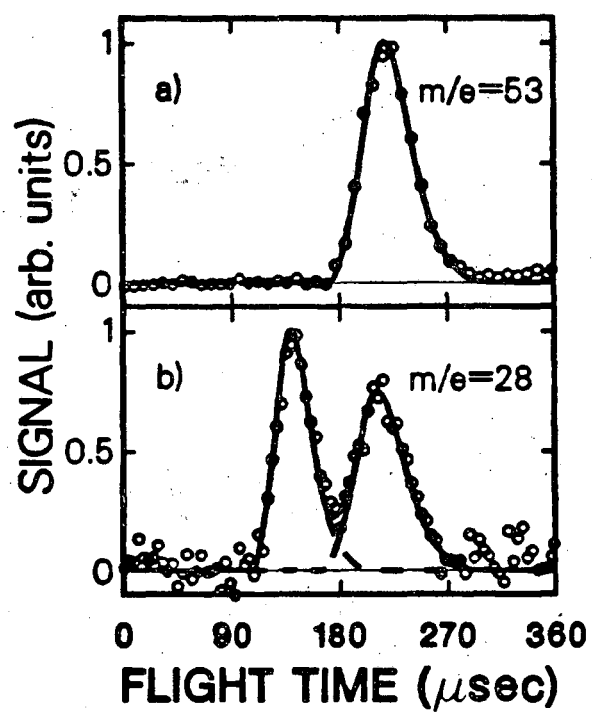
XBL 8810-3665

Fig. 6



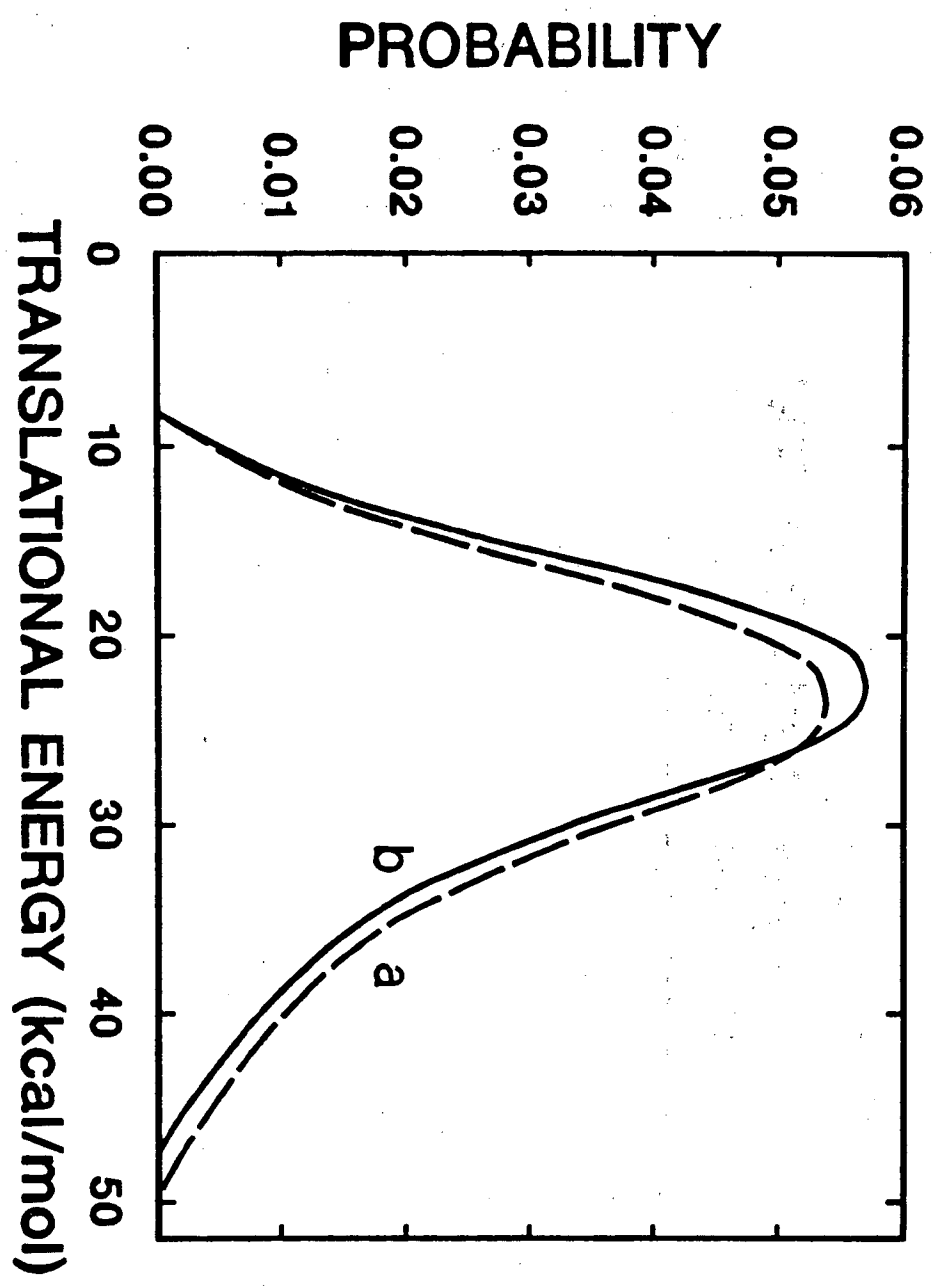
XBL 8810-3663

Fig. 7



XBL 8810-3658

Fig. 8



XBL 8810-3664

Fig. 9

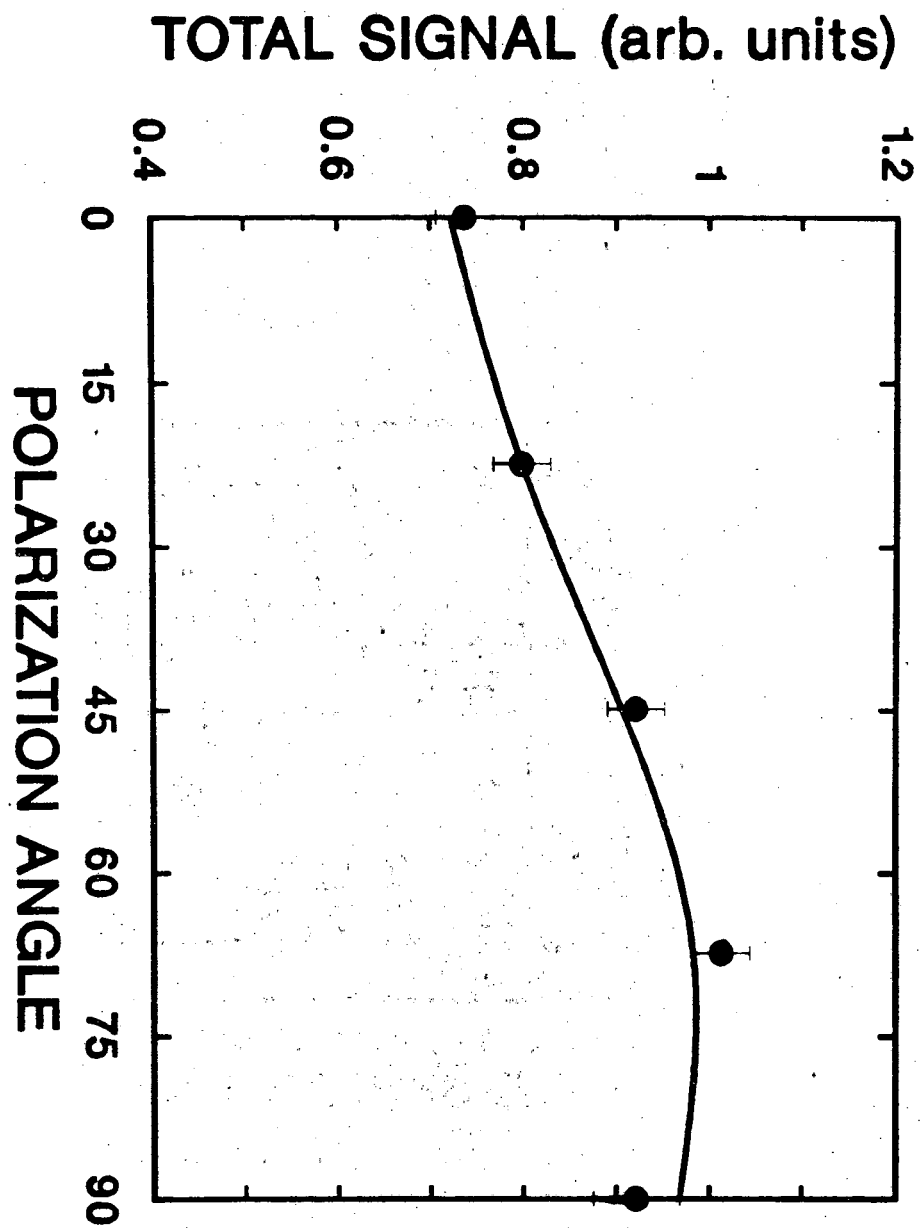
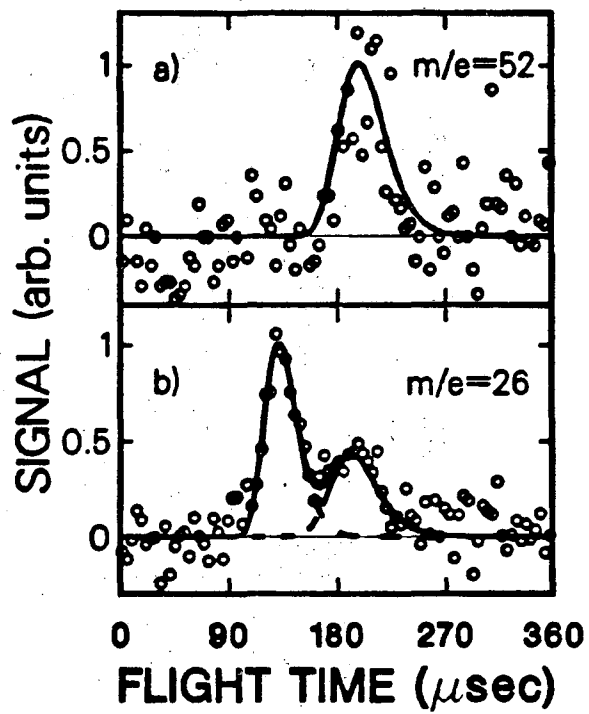
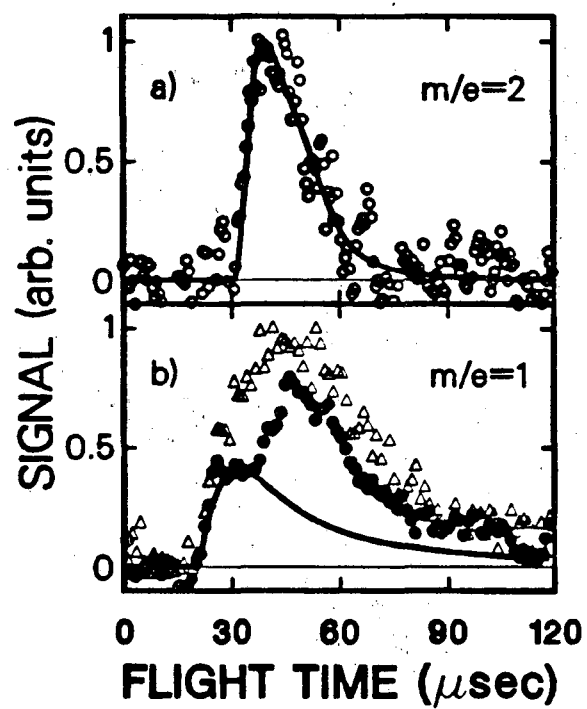


Fig. 10



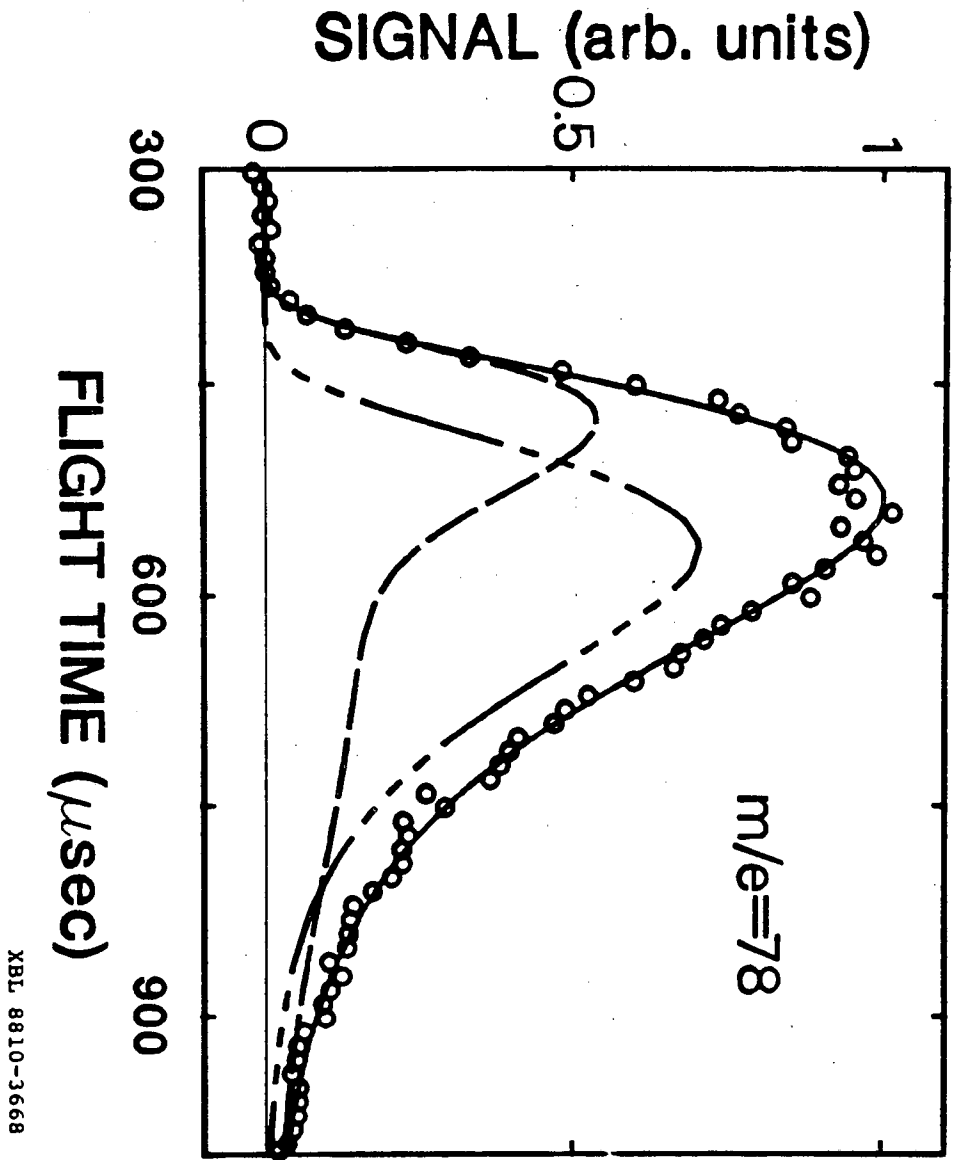
XBL 8810-3657

Fig. 11



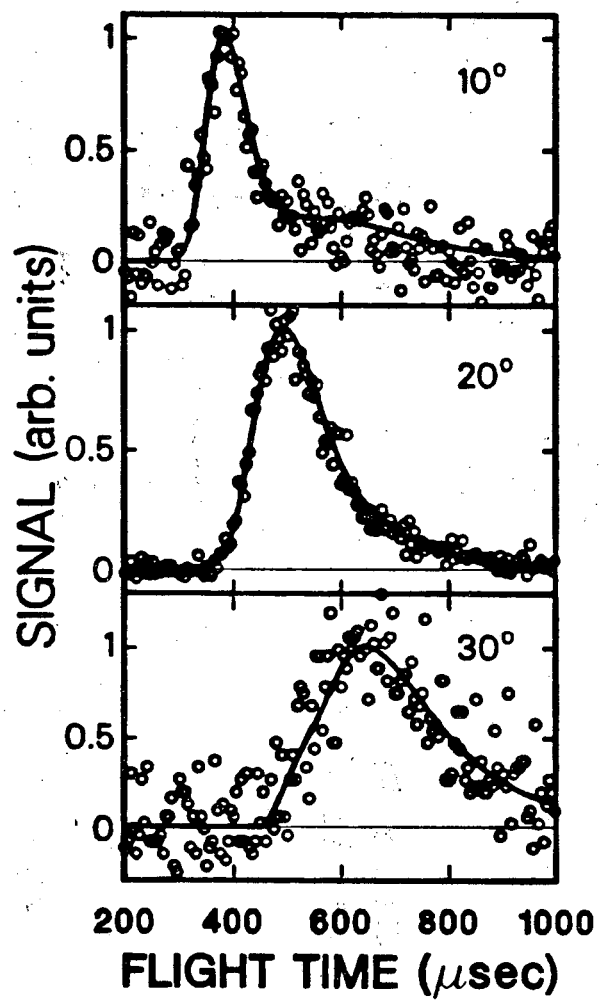
XBL 8810-3655

Fig. 12



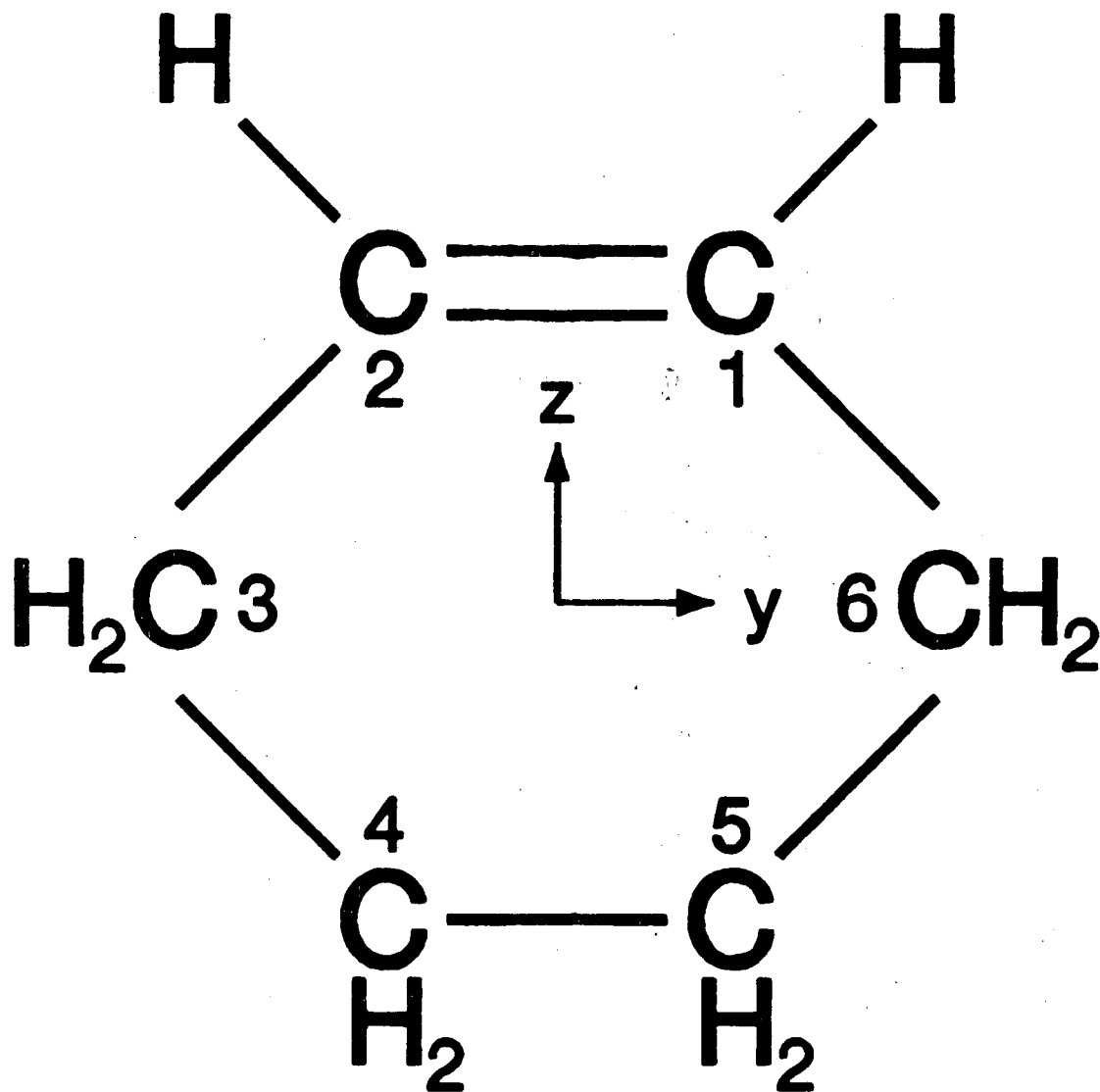
XBL 8810-3668

Fig. 13



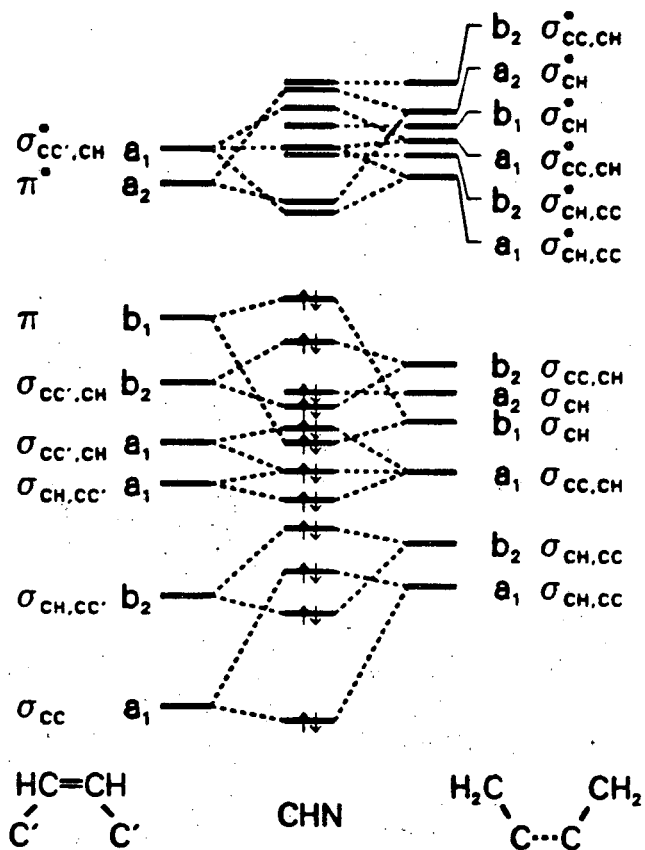
XBL 8810-3662

Fig. 14



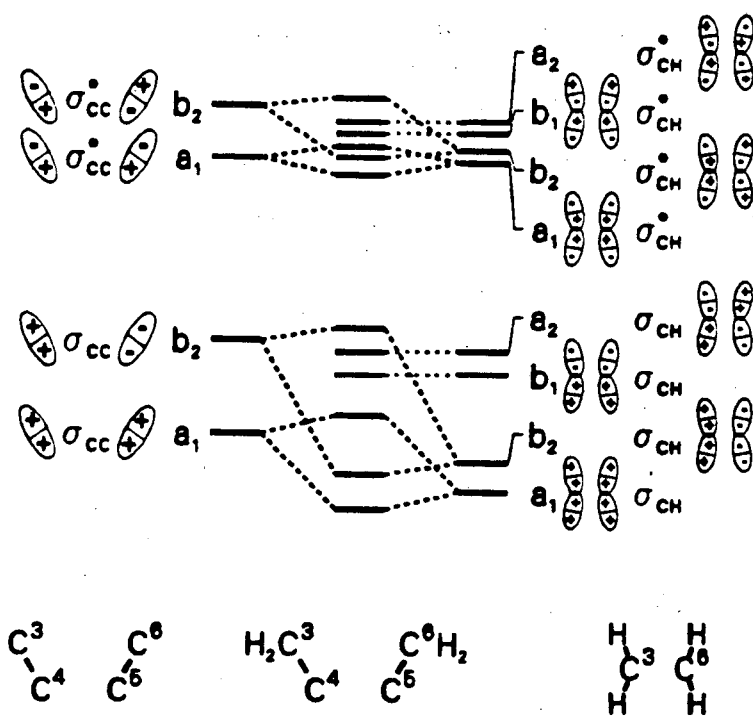
XBL 8810-3659

Fig. 15



XBL 8810-3660

Fig. 16



XBL 8810-3661

Fig. 17

**CHAPTER V**  
**REVIEW OF THE APPROXIMATIONS**  
**IN CHAPTER I**

In Chapter I, when the formulas for data analysis in a photofragmentation-translational spectroscopy experiment were derived, ten approximations were introduced. Among these approximations, some, such as those proposed when discussing primary dissociation, are expected to be valid in most cases for quite clear reasons, but the validity of some others, such as those proposed for secondary dissociation, is not clear. In Chapters II, III and IV, when the formulas were applied to real systems, we found that the fits were satisfactory, implying that all the approximations actually work quite well.

Now, we would like to reexamine these approximations, giving a physical explanation why these approximations work. We will only look through the approximations presented in Section III of Chapter I, although some approximations presented in Section II of Chapter I may also be questionable when they are applied to secondary dissociation process. In the following part,  $(A_n)$  is referred to the  $n$ th approximation and Eqn.  $(n)$  is referred to the Eqn.  $(n)$  in Chapter I.

One of the physical content of  $(A_8)$  is that primary and

secondary processes are separable and distinguishable, so that secondary process cannot affect the primary process. In Chapter III, we have discussed this aspect in quite a detail, and we pointed out there that this is actually the criterion to tell whether a dissociation is a secondary dissociation. If we use secondary dissociation picture to describe a primary triple dissociation, we will find that not only the primary process confines the secondary process, the secondary process confines the primary process as well. (A8) simply says that if a dissociation is truly secondary dissociation, the primary process must not be affected by the secondary process, instead the secondary process is affected by the primary process prior to it.

The second aspect of (A8) is that the secondary distribution is not state sensitive, rather it is energy sensitive. This approximation is exact at two limits. At the first limit, if the secondary dissociation is direct and is non-degenerate with respect to the primary translational energy, the sum in Eqn. (52) disappears. At the second limit, for spontaneous dissociation if the secondary dissociation rate constant is much smaller than the rate constant of intramolecular vibrational randomization, it can be shown that Eqn. (53) is exact.  $N(a'_n)/\sum N(a'_n)$  in this case are constants with respect to the time scale of dissociation due to the rapid intramolecular vibrational randomization. Therefore, both  $C_{nm}$  and  $P_{nm}$  are constants with respect to

time variable.

For spontaneous secondary dissociation, the statement of  $C_{nm} = \text{constant}$  in (A9) is exact if there is only one parallel secondary channel, since in this case  $C_{nm} = 1$ . When there are more than one parallel secondary channel, Eqn. (60a) is questionable, because  $C_{nm}(E_{Tn}, \Omega_n)$  is related to the ratio of rate constants of the parallel channels at certain  $E_{Tn}$  and  $\Omega_n$ , which is generally not constant with respect to  $E_{Tn}$  and  $\Omega_n$ . However, for spontaneous secondary dissociation  $C_{nm}$  in most cases is a slowly changing function of  $E_{Tn}$  and  $\Omega_n$ , and when necessary (A9) can be improved, for example, by using RRKM theory to determine  $C_{nm}$ . For secondary photodissociation, this problem is much more difficult to cope with from general principles. If the absorption cross section of the primary product at different primary velocities is not drastically different, Eqn. (60a) should hold approximately.

Eqn. (60b) is noticeably not accurate. For example, some secondary energies being sampled at certain primary translational energies cannot be reached at some other primary translational energies simply because of energy conservation. When we use Eqn. (60b), we obtain an averaged equivalent secondary distribution instead of the true secondary distribution which will be a function of the primary properties. The question raised immediately are, first, how powerful the formulas are in analyzing experi-

mental data since they are not exact, and second, how much useful information this averaged equivalent energy distribution can offer because true secondary distribution may be scattered broadly around this average distribution. Fortunately, answers to both questions are quite promising. As shown by Chapters II, III and IV the formulation developed in Chapter I is powerful in identifying some secondary dissociation channels and ruling out the possibility of some other channels, and quite detailed information can be obtained from the average secondary  $P_E(E_T)$  and  $P_u(\hat{u})$ . The reason for this is that nature happens to be the way it is.

As mentioned previously (in chapter II and IV) the  $P_E(E_T)$  of simple bond rupture of hot molecules can be described by statistical theory and is not a sensitive function of the internal energy for moderate-sized molecules such as those studied in this thesis. For concerted dissociation it has been shown in Chapter III and IV that the amount of internal energy and the form of excitation are less important factors to the  $P_E(E_T)$  than the dynamics of the exit barrier energy release. For dissociation occurring on repulsive potential energy surface, which in most case is direct dissociation from an excited electronic state, the correlation between  $P_E(E_T)$  and the internal energy of the molecule prior to absorption of photon is weak, so that the effect of difference of internal energy to the  $P_E(E_T)$  is also weak. Therefore, in almost all the cases, the secon-

dary  $P_E(E_T)$  is not a sensitive function of internal energy of the primary product so that Eqn. (60b) is not as bad as one might think. Eqn. (60b) can offer useful information even quantitatively, without detailed account of the difference of secondary  $P_E(E_T)$  with respect to primary variable, which is in general not a simple question.

(A10) is more like a notation rather than an approximation. But, (A10) is indeed an approximation, at least before we really obtain the exact solution. Although we know that  $\alpha$  in Eqn. (75) must be a function of laser power in some way, it may be a complicated integrated function of  $I(\mathbf{x},t)$ , the intensity of the laser beam, instead of a function of  $I_0$ , the photon fluence of the beam. However, since (A10) does not affect the final outcome of the derivation in Chapter I, we will not try to evaluate how good this approximation is, which is not important to the further effort to make secondary dissociation formulation work better, unless detailed laser power dependence is of quantitative interest.

As pointed in Chapter I, approximations in Chapter I, especially those for secondary dissociation should be used with caution. They should be and can be improved whenever inconsistency occurs.<sup>1</sup>

**References**

- 1 If a proper analytic form of secondary energy distribution can be found, it should be used to improve (A9). One example is to calculate secondary  $P_E(E_T)$  using RRKM theory for simple bond rupture of the hot molecule. A possible way to improve (A9) when numerical  $P_E(E_T)$  has to be used is to utilize the properties of the  $P_E(E_T)$  found in this thesis to properly scale the width and the peak of the  $P_E(E_T)$  with respect to different primary translational energy.

## Appendix A

## PROGRAM CMLAB2

```

C*****
c CMLAB2 is the modification of CMLAB to give extended functions for
c data analysis, such as anisotropy, smooth of experimental data
c for an arbitrary length of data points, branching ratio,
c lab. angular distribution and laser polarization dependence of
c total counts for individual components, and changable convolution
c over ionizer. The parallel program (but with less functions) of
c this one for triple dissociation is CMLAB1.
c
c A few approximations are introduced to get formulas used for this
c program. To understand the program, especially to be aware of the
c limit of formalism in this program, the thesis of Zhao Xinseng is
c recommended.
c
c Version May 1988, by Zhao, Xinseng
c-----
C CMLAB
C
C A PROGRAM TO HANDLE PHOTO DISSOCIATION
C INVOLVING BOTH PRIMARY AND SECONDARY PROCESSES IN AN
C ISOTROPIC CASE
C
C VERSION MAY 1986
C BY ZHAO, XINSHENG
C-----
C*****
C
C EXPLANATION SECTION
C
C THIS SECTION EXPLAINS THE INPUT DATA FILE
C
C UNITS USED IN THE PROGRAM ARE:
C-----
C MASS AMU
C ENERGY KCAL/MOL
C VELOCITY 10,000 CM/SEC
C TIME MICROSECOND
C DISTANCE CM
C ANGLE DEGREE
C-----
C
C LINE # VARIABLES DEFINITIONS
C ++++++ ++++++ ++++++
C
C 1 TITLE TITLE OF CALCULATION
c 1.1 konly whether do theoretical simulation
c =0, only work on raw data
c =1, work on theoretical simulation
c
c kscale how to scale the calculated results
c =0, scaled to calculated values among
c themselves
c =1, scaled to experimental data
c
c ktype type of simulation
c =0, fit individual TOF
c =1, lab. angular distribution
c =2, laser polarization dependence
c
c ntof # of sets exptl. TOF input, max. 3
c nthlab # of lab. angle of molecular beam
c nthpol # of polarization angle of laser
c kplot how to plot the data when ktype=1 or 2
c =0, min plot according to the available
c min, therefore plot is enlarged
c =1, min is taken to be 0
c | if konly=0.or.(ktype=0 and kscale=1) input 1.2 to 1.10

```

```

c | where i=1, ntof
c | 1.2 dtexpt(i) exptl. dwell time of MCS for ith TOF
c | 1.3 ltbexpt(i) first channel of ith exptl. TOF
c | to be analyzed
c | 1.4 lteexpt(i) last channel of ith exptl. TOF
c | to be analyzed
c | 1.4.1 nadd(i) whether different tof add together
c | =0, no addition
c | =-1, tof on which other tof's are added
c | =2, added to the tof with nadd=1
c | 1.4.2 radd(i) ratio to add ith tof to the tof with nadd=1
c | 1.5 lbgb(i) first channel used to subtract background
c | for ith exptl. TOF
c | 1.6 lbge(i) last channel used to subtract background
c | for ith exptl. TOF
c | 1.7 rtplot(i) scaling factor to plot ith TOF
c | 1.8 nsum(i) # of channels to sum over
c | 1.9 navrg(i) # of channels to average over, odd #
c | 1.10 offexpt(i) offset of time origin of ith TOF, which
c | is added to nominal time. It can be
c | adjusted arbitrarily according to your
c | purpose. But when konly=1 and ktype=0 and
c | kscale=1, the one for the ltof'th TOF
c | has to be the same as OFFSET of line 5 in
c | order to be compared with calculated TOF
c | if konly=1 input following parameters
c | 1.11 ltof which TOF is used to scale calcd. TOF
c | lthlab which lab. angle is used to calc. TOF or
c | laser polarization dependence
c | lthpol which laser polarization angle is used to
c | calc. TOF or lab. angular distribution
c | lscale which exptl point is used to scale calcd.
c | counts when ktype=1 or 2
c | rscale the scaling factor for comparing calcd.
c | to exptl results
c | 2 if kscale=0.or.ktype.ne.0 input
c | DWELL DWELL TIME OF MCS IN CALCULATION
c | NBCHAN FIRST CHANNEL IN TOF TO BE CALCULATED
c | NECHAN LAST CHANNEL IN TOF TO BE CALCULATED
c | 2.1 thlabv(i) lab. molecular beam angles, i=1, nthlab
c | 2.2 thpolv(i) laser polarization angles (angle between
c | the strongest direction of
c | electric field of the laser and the detector)
c | i=1, nthpol
c | 2.3 depola(i) ratio of intensities of the weakest to the
c | strongest directions of electric field
c | i=1, nthpol
c | for example =0, totally polarized laser
c | =-1, totally unpolarized
c | 2.4 if ktype not =0 and kscale=1 input
c | totexpt(i) exptl total counts, of angular distribution
c | when ktype=1 (then i=1, nthlab), or of laser
c | polarization dependence when ktype=2 (then
c | i=1, nthpol)
c | 3 TPNORM SCALING FACTOR FOR PRIMARY TOF
c | TSNORM SCALING FACTOR FOR SECONDARY TOF
c | SWITCH DETERMINATION WHETHER SECONDARY PROCESS
c | IS INCLUDED
c | =0 ONLY PRIMARY
c | =-1 PRIMARY AND SECONDARY
c | 4 ALPHA ALPHA FROM KELVIN PROGRAM
c | SPDRT SPEED RATIO FROM KELVIN PROGRAM
c | HTHBM HALF WIDTH OF DIVERGENT ANGLE OF SOURCE BEAM
c | NTHBM # OF DIVIDED SEGMENTS OF POLAR ANGLE OF BEAM
c | NVBM # OF DIVIDED SEGMENTS OF SOURCE BEAM VELOCITY
c | ODD #

```

```

C      5      DIMASS      DETECTED ION MASS/CHARGE RATIO
C      DIST      FLIGHT PATH LENGTH OF MAIN CHAMBER
C      DL      EFFECTIVE LENGTH OF IONIZER
C              in the case kion=0, dl=2*sigma
C      OFFSET      TIME DIFFERENCE BETWEEN TRIGGER AND LASER SHOT
C              THE DELAY OF TRIGGER IS A POSITIVE OFFSET
C      ALFA      ION FLIGHT CONSTANT
C      THD      WIDTH OF POLAR ANGLE OF DETECTOR APERTURE
C              WITH RESPECT TO THE CENTER OF REACTION
C              REGION
C      NTHD      # OF DIVIDED SEGMENTS OF POLAR ANGLE FOR
C              THE APERTURE OF DETECTOR
C      nion      # of points to convolute ionization
C              probability, odd #
C      kion      whether ionization efficiency is treated
C              normally as a gaussian distribution
C              =0, yes, gaussian
C              =1, no, special form
C      5.1 if kion=1, then input
C      pion(i)      probability of ionization, with the most
C              probable value in the middle, i=1,nion
C      6      VLMIN      MINIMUM LAB VELOCITY TO BE ANALYZED
C      VLINC      INCREMENT OF LAB VELOCITY
C      NVLAB      # OF SEGMENTS FOR LAB VELOCITY
C      7      NDIST      # OF INPUT PRIMARY P(E)
C      NPCHAN      # OF PRIMARY REACTION CHANNELS
C      8      NPE(I)      # OF POINTS IN EACH P(E), I=1,ndist
C      9      EMIN(I)      MINIMUM ENERGY IN EACH P(E)
C      10     EINC(I)      ENERGY INCREMENT IN EACH P(E)
C      11     M1(J)      DETECTED NEUTRAL MASS, J=1,npchan
C      12     M2(J)      THE COUNTERPART MASS OF M1(J)
C      13     NORD(J)     ORDER # OF P(E) WHICH THIS PRIMARY CHANNEL
C              USES WITH
C      14     PROB(J)     RELATIVE CONTRIBUTION OF EACH CHANNEL
C      14.1   thdipole(j) angle between transition dipole and
C              recoiling direction
C      14.2   betap(j)   anisotropy parameter for primary channel
C      15     NPDISP(J)  DETERMINATION IF THIS PRIMARY PROCESS
C              IS A COMPONENT OF TOF
C              =0 NO
C              =1 YES, IT IS A COMPONENT
C      16     PE(I,n)    INPUT P(E), I=1,npchan; n=1,npe(I)
C      THRU
C      N

```

```

C -----
C THE FOLLOWING INPUT IS ONLY NECESSARY IF SECONDARY DISSOCIATION IS
C CONSIDERED   input the followings when switch=1
C -----

```

```

C      N+1     NDSTS      # OF SECONDARY P(E)
C      NSCHAN   # OF SECONDARY REACTION CHANNELS
C      etotal   max. available energy
C      N+2     NPES(1)    # OF POINTS IN EACH SECONDARY P(E)
C              l=1, ndsts
C      N+3     EMINS(1)   MINIMUM ENERGY IN EACH SECONDARY P(E)
C      N+4     EINCS(1)   ENERGY INCREMENT IN EACH SECONDARY P(E)
C      N+5     M1S(K)     DETECTED NEUTRAL MASS OF SECONDARY PRODUCT
C              k=1, nschan
C      N+6     M2S(K)     THE COUNTERPART MASS OF M1S(K)
C      N+7     NSP(K)     ORDER NUMBER OF PRIMARY CHANNEL, TELLING
C              WHICH PRIMARY CHANNEL IS USED FOR THIS
C              SECONDARY PROCESS
C      N+8     NUP(K)     # OF VELOCITY INCREMENTS IN THE CALCULATING
C              PRIMARY PRODUCT DISTRIBUTION FOR
C              FURTHER CALC. ON SECONDARY PROCESS

```

```

C      N+9      NTHP(K)      # OF DIVIDED SEGMENTS OVER THE POLAR
C      N+10     NORDS(K)     ORDER # OF SECONDARY P(E) WHICH THIS
C      n+10.1   thdpls(k)   SECONDARY CHANNEL USES WITH
C      n+10.2   betas(k)    angle between transition dipole and
C      n+10.3   ndistri(k)  recoiling direction
C      anisotropy parameter for secondary channel
C      # of points for secondary C.M. angular
C      distribution, where z axis of the
C      secondary frame is chosen along recoiling
C      direction of ml, the primary fragment. The
C      points are equally divided according to cosine
C      of the polar angle and the limit is 1 to -1.
C      ndistri(k).gt.1
C      n+10.4   distr(k,m)  secondary angular distribution
C      k=1, nschan; m=1, ndistri(k)
C      note: this distribution is different from
C      the angular distribution due to
C      laser polarization dependence, where
C      it is assumed that the two effects
C      can be decoupled to two factors
C      N+11     PROBS(K)     RELATIVE CONTRIBUTION OF EACH SECONDARY CHANNEL
C      N+12     PES(1,n)   INPUT SECONDARY P(E), l=1, ndsts; n=1, npes(1)
C      THRU
C      M
C      M+1     NDPES(K)    DETERMINATION IF SAME PRIMARY P(E) IS USED
C      =0 YES
C      =1 NO, I HAVE TO INPUT NEW PRIMARY P(E) FOR
C      THE PURPOSE OF THIS SECONDARY PROCESS
C      M+2     PEAL(J,n)   WHEN NDPES(K)=1, INPUT ALTERNATIVE PRIMARY P(E)
C      THRU      WHICH HAS TO BE THE SAME FORMAT AS THE
C      I          SUBSTITUTED ONE
C      j=1, # of secondary channels whose ndpes=1
C      n=1, npe(nord(nsp(k))), where k is the oder
C      # of the secondary channel

```

\*\*\*\*\*

PREFACE  
BASIC INFORMATION ON THE SYSTEM

\*\*\*\*\*

When you create a parameter file according to previous section, notice whether the values in the file are within the limit of following relevant parameters. It will give you wrong fitting if any of the input parameters is beyond the limit. Change the following values if you need larger value of limitation to the input parameter.

```

c      PARAMETER(N1=1000)      ! N1 IS MAXIMUM NVLAB THE PROGRAM HANDLES
c      PARAMETER(N2=100)      ! N2 IS " NPE,NPES "
c      PARAMETER(N3=10)       ! N3 " NDIST,NDSTS "
c      PARAMETER(N4=5)        ! N4 " NTHD "
c      if you change n4, change n11 correspondingly
c      PARAMETER(N5=5)        ! N5 " NTHBM "
c      if you change n5, change n10 correspondingly
c      PARAMETER(N6=51)       ! N6 " NVBM "
c      PARAMETER(N7=2048)     ! N7 " # OF TOP CHANNELS TO BE READ
c      PARAMETER(N8=100)     ! N8 " NUP THE PROGRAM HANDLES
c      PARAMETER(N9=360)     ! N9 " NTHP "
c      PARAMETER(N10=13)     ! N10=3*N5-2
c      PARAMETER(N11=13)     ! N11=3*N4-2
c      parameter(n12=3)      ! n12 is maximum ntof the program handle
c      n12 is the only parameter which if you change you have to modify
c      the program correspondingly.
c      parameter(n13=10)     ! n13 " nthlab,nthpol "

```

```

parameter(n14=21)      ! n14  "      nion      "
parameter(n15=180)    ! n15  "      ndistri   "
REAL M1,M2,M1S,M2S
INTEGER SWITCH
CHARACTER*70 TITLE
DIMENSION VL(N1),VL2(N1)
DIMENSION NPE(N3),EMIN(N3),EINC(N3),M1(N3),M2(N3),NORD(N3),
*   PROB(N3),NPDISP(N3),PE(N3,N2)
*   DIMENSION NPES(N3),EMINS(N3),EINCS(N3),M1S(N3),M2S(N3),
*   NSP(N3),NUP(N3),NTHP(N3),NORDS(N3),PROBS(N3),
*   PES(N3,N2),PEAL(N3,N2),
*   NDPES(N3),CP(N3),CS(N3),UINC(N3)
DIMENSION EAV(N3),EAVS(N3),EAVAL(N3),NSAV(N3),TEMP(N3),
*   COUNTP(N3),COUNTS(N3),RCOUNTP(N3),RCOUNTS(N3),
*   dcthc(n3)
DIMENSION SPCALC(N3,N1),SSCALC(N3,N1),PSIGNAL(N3,N1),
*   SSIGNAL(N3,N1),PINT(N3),SINT(N3)
DIMENSION CTHD(N4),STHD(N4),SPHD(N4,N11),CPHD(N4,N11)
DIMENSION CTHBM(N5),STHBM(N5),PROBTHBM(N5),CPHBM(N5,N10),
*   SPHBM(N5,N10),COSA(N5,N10,N4,N11)
DIMENSION VBM(N6),VB2(N6),PROBVBM(N6),PROBM(N6,N5,N10)
DIMENSION RAWDATA(N7),TOFP(N7),TOFS(N7),
*   TOFCALC(N7),T(N7),AVPSIG(N3,N7),AVSSIG(N3,N7),
*   datas(n12,n7),datavrg(n12,n7)
DIMENSION USP(N3,N8),USP2(N3,N8),POFE1(N3,N8)
DIMENSION thsp(n3,n9),sthsp(n3,n9),CTHSP(N3,N9)
dimension dtexpt(n12),ltbexpt(n12),lteexpt(n12),lbgb(n12),
*   lbge(n12),nsum(n12),navrg(n12),rtplot(n12),
*   nctof(n12),tofbg(n12),tot(n12),offexpt(n12),
*   nadd(n12),radd(n12),npepoint(20)
*   dimension thlabv(n13),thpolv(n13),depola(n13),
*   totexpt(n13),anglall(n13)
*   dimension thdipole(n3),betap(n3),thdpls(n3),betas(n3),
*   ndistri(n3),distr(n3,n15),angles(n13,n3)
*   dimension pion(n14),cthsi(n3,n15),anglep(n13,n3),
*   dcths(n15)
DATA ECHANGE/4.184E10/      ! erg/kcal
p2(x)=0.5*(3.*x*x-1.)
-----
READ(5,5001)TITLE
read(5,*)konly,kyscale,ktype,ntof,nthlab,nthpol,kplot
if((kyscale.eq.0.or.ktype.ne.0).and.konly.ne.0)go to 6011
read(5,*)(dtexpt(i), i=1,ntof)
read(5,*)(ltbexpt(i), i=1,ntof)
read(5,*)(lteexpt(i), i=1,ntof)
read(5,*)(nadd(i),i=1,ntof)
read(5,*)(radd(i),i=1,ntof)
read(5,*)(lbgb(i), i=1,ntof)
read(5,*)(lbge(i), i=1,ntof)
read(5,*)(rtplot(i), i=1,ntof)
read(5,*)(nsum(i), i=1,ntof)
read(5,*)(navrg(i), i=1,ntof)
read(5,*)(offexpt(i),i=1,ntof)
do 6010 i=1,ntof
nctof(i)=max(lteexpt(i),lbge(i))
if(i.eq.1)then
6001 read(3,*,end=6001)(rawdata(nraw), nraw=1,n7)
continue
end if
if(i.eq.2)then
6002 read(4,*,end=6002)(rawdata(nraw), nraw=1,n7)
continue
end if
if(i.eq.3)then
6003 read(7,*,end=6003)(rawdata(nraw), nraw=1,n7)
continue

```

```

end if
dtexpt(i)=dtexpt(i)*nsum(i)
ltbexpt(i)=ltbexpt(i)/nsum(i)
lteexpt(i)=lteexpt(i)/nsum(i)
lbgb(i)=lbgb(i)/nsum(i)
lbge(i)=lbge(i)/nsum(i)
nctof(i)=nctof(i)/nsum(i)
if(ltbexpt(i).eq.0)ltbexpt(i)=1
if(lteexpt(i).eq.0)lteexpt(i)=1
if(lbgb(i).eq.0)lbgb(i)=1
if(lbge(i).eq.0)lbge(i)=1
if(nctof(i).eq.0)nctof(i)=1
do 6005 j=1,nctof(i)
jj=(j-1)*nsum(i)
datas(i,j)=0.
do 6004 k=1,nsum(i)
jj=jj+1
6004 datas(i,j)=datas(i,j)+rawdata(jj)
6005 continue
sum=0.
do 6006 j=lbgb(i),lbge(i)
6006 sum=sum+datas(i,j)
tofbg(i)=sum/(lbge(i)-lbgb(i)+1)
do 6007 j=1,nctof(i)
6007 datas(i,j)=datas(i,j)-tofbg(i)
jj=navrg(i)/2
do 6009 j=ltbexpt(i),lteexpt(i)
n=j-ltbexpt(i)+1
datavrg(i,n)=0.
do 6008 k=-jj,jj
kk=k+j
if(kk.lt.1)kk=1
if(kk.gt.nctof(i))kk=nctof(i)
6008 datavrg(i,n)=datavrg(i,n)+datas(i,kk)
6009 datavrg(i,n)=datavrg(i,n)/navrg(i)
nctof(i)=lteexpt(i)-ltbexpt(i)+1
tot(i)=0.
do 6010 j=1,nctof(i)
tot(i)=tot(i)+datavrg(i,j)
6010 datavrg(i,j)=datavrg(i,j)*rtplot(i)
lbase=1
do i=1,ntof
if(nadd(i).eq.1)lbase=i
end do
do 300 i=1,ntof
if(nadd(i).ne.2)go to 300
do 301 j=1,nctof(i)
if(j.gt.nctof(lbase))go to 301
datavrg(lbase,j)=datavrg(lbase,j)+datavrg(i,j)*radd(i)
301 continue
300 continue
6011 if(konly.eq.0)go to 7000
read(5,*)ltof,lthlab,lthpol,lscale,rscale
if(kscale.eq.1.and.ktype.eq.0)then
dwell=dtexpt(ltof)
nbchan=ltbexpt(ltof)
nechan=lteexpt(ltof)
else
READ(5,*)DWELL,NBCHAN,NECHAN
end if
read(5,*)(thlabv(i), i=1,nthlab)
read(5,*)(thpolv(i), i=1,nthpol)
read(5,*)(depola(i), i=1,nthpol)
if(ktype.eq.1)nangle=nthlab
if(ktype.eq.2)nangle=nthpol
if(ktype.ne.0.and.kscale.eq.1)then

```

```

read(5,*)(totexpt(i), i=1,nangle)
end if
READ(5,*)TPNORM,TSNORM,SWITCH
if(switch.eq.0)tsnorm=0.
ab=tpnorm+tsnorm
if(ab.ne.0.)then
a=tpnorm/ab
b=tsnorm/ab
end if

```

```

-----
C THIS SECTION READS THE INFORMATION ABOUT MOLECULAR BEAM
C AND DIVIDES THE BEAM PROFILE TO MANY SMALL SEGMENTS. VELOCITY
C DISTRIBUTION IS ASSUMED IN USUAL FUNCTION. DISTRIBUTION FUNCTION
C IS NORMALYZED.
C

```

```

3 READ(5,*)ALPHA,SPDRT,HTHBM,NTHBM,NVBM
SUM=0.
DCOSTHBM=(1.-COSD(HTHBM))/NTHBM
DO 3 I=1,NTHBM
CTHBM(I)=1.-(I-1)*DCOSTHBM
STHBM(I)=(1.-CTHBM(I)*CTHBM(I))**.5
PROBTHBM(I)=1.-FLOAT(I-1)/FLOAT(NTHBM)
SUM=SUM+PROBTHBM(I)
DO 4 I=1,NTHBM
4 PROBTHBM(I)=PROBTHBM(I)/SUM
VPK=(ALPHA*SPDRT/2)*(1.+SQRT(1.+4./SPDRT**2))
IF(NVBM.EQ.1)THEN
VBM(1)=VPK
VB2(1)=VPK*VPK
PROBVBM(1)=1
ELSE
SUM=0.
DELTA VBM=(ALPHA*2.5)/(NVBM/2)
VBMIN=VPK-(NVBM/2)*DELTA VBM
DO 5 I=1,NVBM
VBM(I)=VBMIN+(I-1)*DELTA VBM
if(vbm(i).lt.0.)vbm(i)=0.
PROBVBM(I)=VBM(I)**2*EXP(-(VBM(I)/ALPHA-SPDRT)**2)
5 SUM=SUM+PROBVBM(I)
DO 6 I=1,NVBM
VB2(I)=VBM(I)*VBM(I)
6 PROBVBM(I)=PROBVBM(I)/SUM
END IF
DO 7 J=1,NTHBM
KK=3*J-2
DPHI=6.283185/KK
DO 7 K=1,KK
CPHBM(J,K)=COS((K-1)*DPHI)
SPHBM(J,K)=SIN((K-1)*DPHI)
DO 7 I=1,NVBM
7 PROBM(I,J,K)=PROBVBM(I)*PROBTHBM(J)/KK

```

```

-----
C THIS SECTION READS THE INFORMATION ABOUT DETECTOR AND DIVIDES THE
C APERTURE OF DETECTOR TO SMALL SEGMENT SIMILAR AS BEAM IS DIVIDED
C

```

```

READ(5,*)DIMASS,DIST,DL,OFFSET,ALFA,THD,NTHD,nion,kion
if(kion.ne.0)go to 6012
pion(1)=1.
if(nion.eq.1)go to 6013
ii=nion/2
sum=1.
abc=2.5/ii
pion(ii+1)=1.
do 6014 i=1,ii
xyz=exp(-(abc*i)**2/2.)
pion(ii+i+1)=xyz

```

```

6014 pion(ii-i+1)=xyz
      sum=sum+2.*xyz
      do i=1,nion
        pion(i)=pion(i)/sum
      end do
      go to 6013
6012 read(5,*)(pion(i), i=1,nion)
      sum=0.
      do i=1,nion
        sum=sum+pion(i)
      end do
      do i=1,nion
        pion(i)=pion(i)/sum
      end do
6013 continue
      DCOSTHD=(1.-COSD(THD))/NTHD
      DO 8 I=1,NTHD
        CTHD(I)=1.-(I-1)*DCOSTHD
        STHD(I)=(1.-CTHD(I)*CTHD(I))**.5
        JJ=3*I-2
        DPFI=6.283185/JJ
        DO 8 J=1,JJ
          SPHD(I,J)=SIN((J-1)*DPFI)
          CPHD(I,J)=COS((J-1)*DPFI)
8
C
C THIS SECTION READS INFORMATION ON LAB VELOCITY USED IN SIMULATION
C
      READ(5,*)VLMIN,VLINC,NVLAB
      IF(VLMIN.EQ.0)VLMIN=0.5*VLINC
      DO I=1,NVLAB
        VL(I)=VLMIN+(I-1)*VLINC
        VL2(I)=VL(I)*VL(I)
      END DO
      ilabth=1
      ipolth=1
C
C *****
C
C          CHAPTER ONE
C          THE TREATMENT ON PRIMARY CONTRIBUTION
C *****
C
C § 1-1 INFORMATION ABOUT PRIMARY CHANNELS
C
      READ(5,*)NDIST,NPCHAN
      READ(5,*)(NPE(J),J=1,NDIST)
      READ(5,*)(EMIN(J),J=1,NDIST)
      READ(5,*)(EINC(J),J=1,NDIST)
      READ(5,*)(M1(J),J=1,NPCHAN)
      READ(5,*)(M2(J),J=1,NPCHAN)
      DO J=1,NPCHAN
        CP(J)=2.*M2(J)/(M1(J)+M2(J))/M1(J)*ECHANGE*1.E-8
      END DO
      READ(5,*)(NORD(J),J=1,NPCHAN)
      READ(5,*)(PROB(J),J=1,NPCHAN)
      read(5,*)(thdipole(j), j=1,npchan)
      read(5,*)(betap(j), j=1,npchan)
      do j=1,npchan
        betap(j)=2.*betap(j)*p2(cosd(thdipole(j)))
      end do
      READ(5,*)(NPDISP(J),J=1,NPCHAN)
      sum=0.
      do i=1,npchan
        if(npdisp(i).eq.0)prob(i)=0.
        sum=sum+prob(i)

```

```

end do
if(sum.ne.0.)then
do i=1,npchan
prob(i)=prob(i)/sum*a
end do
end if
C
C THIS SECTION READS PRIMARY P(E) AND NORMALIZES THEM
C
DO 10 J=1,NDIST
READ(5,*)(PE(J,I),I=1,NPE(J))
SUM=0.
EAV(J)=0.
DO I=2,NPE(J)
PEI=(PE(J,I)+PE(J,(I-1)))*.5
EAV(J)=(EMIN(J)+(I-1.5)*EINC(J))*PEI+EAV(J)
SUM=SUM+PEI
END DO
EAV(J)=EAV(J)/SUM
SUM=SUM*EINC(J)
DO I=1,NPE(J)
PE(J,I)=PE(J,I)/SUM
END DO
10 CONTINUE
C
C IF THERE ARE SECONDARY PROCESSES, INPUT INFORMATION ABOUT SECONDARY
C CALCULATION, WHICH GOES INTO CHAPTER TWO
C
IF(SWITCH.EQ.1)GO TO 100 ! LABLE 100 IS IN CHAPTER TWO
20 TYPE *,'INPUT SUCCESSFUL'
C
-----
C THIS SECTION CALCULATE COS(A), WHERE A IS THE ANGLE BETWEEN
C ONE OF THE BEAM VECTOR AND ONE OF THE DETECTOR VECTOR
C
thlab=thlabv(lthlab)
thpol=thpolv(lthpol)
depol=depola(lthpol)
30 if(ktype.eq.1)then
thlab=thlabv(ilabth)
end if
STHLAB=SIND(THLAB)
CTHLAB=COSD(THLAB)
DO 9 I=1,NTHBM
JJ=3*I-2
DO 9 J=1,JJ
DO 9 MTH=1,NTHD
JJJ=3*MTH-2
DO 9 MPH=1,JJJ
9 COSA(I,J,MTH,MPH)=STHBM(I)*CPHBM(I,J)*STHD(MTH)*CPHD(MTH,MPH)
* +STHBM(I)*SPHBM(I,J)*STHD(MTH)*SPHD(MTH,MPH)*CTHLAB
* -CTHBM(I)*STHD(MTH)*SPHD(MTH,MPH)*STHLAB
* +STHBM(I)*SPHBM(I,J)*CTHD(MTH)*STHLAB
* +CTHBM(I)*CTHD(MTH)*CTHLAB
25 if(ktype.eq.2)then
thpol=thpolv(ipolth)
depol=depola(ipolth)
end if
sthpol=sind(thpol)
cthpole=cosd(thpol)
depol1=1./(1.+depol)
depol2=depol/(1.+depol)
C
-----
C
C § 1-2 CALCULATION ON CONTRIBUTIION BY PRIMARY PROCESS

```

```

C
C-----
C
      DO 90 M=1,NPCHAN
C
C THIS DO LOOP 90 CALCULATES EVERY PRIMARY CHANNEL
C
      IF(NPDISP(M).EQ.0)GO TO 90
      N=NORD(M)
      pmass=(m1(m)+m2(m))*m1(m)/m2(m)
      EMAX=EMIN(N)+(NPE(N)-1)*EINC(N)
      DO 85 MV=1,NVLAB
C
C THIS DO LOOP 85 CALCULATES SIGNAL AT EVERY LAB VELOCITY SAMPLE POINT
C
      SPCALC(M,MV)=0.
      DO 80 MTH=1,NTHD
      MPHMAX=3*MTH-2
      DO 80 MPH=1,MPHMAX
C
C THESE DO LOOPS 80 AVERAGE OVER DETECTOR ANGLES
C
      DO 70 L=1,NVBM
      DO 70 I=1,NTHBM
      JJ=3*I-2
      DO 70 J=1,JJ
C
C THESE DO LOOPS 70 AVERAGE OVER BEAM DISTRIBUTION
C
      U2=abs(VB2(L)+VL2(MV)-2.*VBM(L)*VL(MV)*COSA(I,J,MTH,MPH))
      U=SQRT(U2)
      IF(U.EQ.0)GO TO 70
      E=U2/CP(M)
      IF(E.LT.EMIN(N).OR.E.GE.EMAX)GO TO 70
      x1=(vl(mv)*cthd(mth)-vbm(1)*(sphbm(i,j)*stbhm(i)*sthlab
      *      +ctbhm(i)*cthlab))/u
      if(abs(x1).gt.1.)x1=x1/abs(x1)
      x2=(vl(mv)*sphd(mth,mph)*sthd(mth)+vbm(1)*(ctbhm(i)*sthlab
      *      -sphbm(i,j)*stbhm(i)*cthlab))/u
      if(abs(x2).gt.1.)x2=x2/abs(x2)
      edotu1=x1*cthp1-x2*sthp1
      edotu2=x1*sthp1+x2*cthp1
      wth1=.5*(1.+betap(m)*p2(edotu1))
      wth2=.5*(1.+betap(m)*p2(edotu2))
      X=(E-EMIN(N))/EINC(N)
      INDEX=IFIX(X)+1
      POFE=PE(N,INDEX)+(X+1-INDEX)*(PE(N,(INDEX+1))
      *      -PE(N,INDEX))
      *
      SPCALC(M,MV)=SPCALC(M,MV)+PROBM(L,I,J)*POFE/U/MPHMAX*
      *      (depoll*wth1+depol2*wth2)
70    CONTINUE
80    CONTINUE
      SPCALC(M,MV)=SPCALC(M,MV)*VL2(MV)/NTHD*pmass
85    CONTINUE
90    CONTINUE
      IF(SWITCH.EQ.1)GO TO 200          ! LABLE 200 IS IN CHAPTER TWO
      GO TO 1000                        ! LABLE 1000 IS IN CHAPTER THREE
C*****
C
C          CHAPTER TWO
C          THE TREATMENT ON SECONDARY CONTRIBUTION
C*****
C
C § 2-1 INFORMATION ABOUT SECONDARY CALCULATION
C

```

```

100  READ(5,*)NDSTS,NSCHAN,etotal
      READ(5,*)(NPES(J),J=1,NDSTS)
      READ(5,*)(EMINS(J),J=1,NDSTS)
      READ(5,*)(EINCS(J),J=1,NDSTS)
      READ(5,*)(M1S(J),J=1,NSCHAN)
      READ(5,*)(M2S(J),J=1,NSCHAN)
      DO J=1,NSCHAN
        CS(J)=2*M2S(J)/(M1S(J)+M2S(J))/M1S(J)*ECHANGE*1.E-8
      END DO
      READ(5,*)(NSP(J),J=1,NSCHAN)
      READ(5,*)(NUP(J),J=1,NSCHAN)
C
C THIS SECTION DIVIDES THE POLAR ANGLE RANGE OF PRIMARY DISTRIBUTION
C IN C.M. OF BEAM
C
      READ(5,*)(NTHP(J),J=1,NSCHAN)
      DO 106 I=1,NSCHAN
        del=180./nthp(i)
        DO 106 J=1,NTHP(I)
          thsp(i,j)=(j-0.5)*del
          sthsp(i,j)=sind(thsp(i,j))
106   CTHSP(I,J)=cosd(thsp(i,j))
C
      READ(5,*)(NORDS(J),J=1,NSCHAN)
      read(5,*)(thdpls(j), j=1,nschan)
      read(5,*)(betas(j), j=1,nschan)
      do j=1,nschan
        betas(j)=2.*betas(j)*p2(cosd(thdpls(j)))
      end do
C
c this section reads the information on angular distribution of
c secondary dissociation due to geometry and impact parameter from
c primary product
C
      read(5,*)(ndistri(j), j=1,nschan)
      distrmax=0.
      do 125 i=1, nschan
        read(5,*)(distr(i,j), j=1,ndistri(i))
        sum=0.
        dcth(i)=2./(ndistri(i)-1)
        do 121 j=1, ndistri(i)
          cthsi(i,j)=1.-(j-1)*dcth(i)
121   if(j.gt.1)sum=sum+(distr(i,j)+distr(i,j-1))*0.5
        sum=sum*dcth(i)
        do 125 j=1,ndistri(i)
          distr(i,j)=distr(i,j)/sum
          distrmax=max(distrmax,distr(i,j))
          write(15,*)cthsi(i,j), distr(i,j)
125   continue
        distrmax=distrmax*1.1
        write(16,*)nschan
        write(16,*)(ndistri(j), j=1, nschan)
        write(16,*)'1. -1. 0.0',distrmax
C
      READ(5,*)(PROBS(J),J=1,NSCHAN)
      sum=0.
      do i=1,nschan
        sum=sum+probs(i)
      end do
      if(sum.ne.0.)then
        do i=1,nschan
          probs(i)=probs(i)/sum*b
        end do
      end if
C

```

C THIS SECTION READS SECONDARY P(E) AND NORMALIZES THEM  
C

```

DO 110 J=1,NDSTS
READ(5,*)(PES(J,K),K=1,NPES(J))
SUM=0.
EAVS(J)=0.
DO I=2,NPES(J)
PEI=(PES(J,I)+PES(J,(I-1)))*.5
EAVS(J)=(EMINS(J)+(I-1.5)*EINCS(J))*PEI+EAVS(J)
SUM=SUM+PEI
END DO
EAVS(J)=EAVS(J)/SUM
SUM=SUM*EINCS(J)
DO I=1,NPES(J)
PES(J,I)=PES(J,I)/SUM
END DO
110 CONTINUE

```

C THIS SECTION CHECKS IF ALTERNATED P(E) IS USED IN PRIMARY SIMULATION  
C WHICH IS FOR THE PURPOSE OF FURTHERE SECONDARY CALCULATION. IF YES,  
C READS ALTERNATIVE PRIMARY P(E) AND NORMALIZES THEM  
C

```

READ(5,*)(NDPES(J),J=1,NSCHAN)
DO 120 J=1,NSCHAN
IF(NDPES(J).EQ.0)GO TO 120
N=NORD(NSP(J))
READ(5,*)(PEAL(N,K),K=1,NPE(N))
SUM=0.
EVAL(N)=0.
DO I=2,NPE(N)
PEI=(PEAL(N,I)+PEAL(N,(I-1)))*.5
EVAL(N)=(EMIN(N)+(I-1.5)*EINC(N))*PEI+EVAL(N)
SUM=SUM+PEI
END DO
EVAL(N)=EVAL(N)/SUM
SUM=SUM*EINC(N)
DO I=1,NPE(N)
PEAL(N,I)=PEAL(N,I)/SUM
END DO
120 CONTINUE

```

C THIS SECTION FINDS OUT VELOCITY INCREMENTS IN CALCULATING PRIMARY PRODUCT  
C DISTRIBUTION AND ITS PROBABILITY  
C

```

DO 124 J=1,NSCHAN
N=NSP(J)
M=NORD(N)
UMIN=(CP(N)*EMIN(M))**.5
UMAX=((EMIN(M)+(NPE(M)-1)*EINC(M))*CP(N))**.5
UINC(J)=(UMAX-UMIN)/NUP(J)
DO 122 K=1,NUP(J)
USP(J,K)=UMIN+UINC(J)*(K-.5)
USP2(J,K)=USP(J,K)*USP(J,K)
E=USP2(J,K)/CP(N)
X=(E-EMIN(M))/EINC(M)
INDEX=IFIX(X)+1
IF(NDPES(J).EQ.0)THEN
POFE1(J,K)=PE(M,INDEX)+(X+1-INDEX)*(PE(M,
* (INDEX+1))-PE(M,INDEX))
ELSE
POFE1(J,K)=PEAL(M,INDEX)+(X+1-INDEX)*(PEAL(M,
* (INDEX+1))-PEAL(M,INDEX))
END IF
122 CONTINUE
124 CONTINUE
GO TO 20

```

! LABEL 20 IS IN CHAPTER ONE

```

-----
C
C   $ 2-2 CALCULATION ON SECONDARY CONTRIBUTION TO TOF
C
-----
C
C 200   DO 290 M=1, NSCHAN
C
C THIS DO LOOP 290 CALCULATES EVERY SECONDARY CHANNEL
C
      nn=nsp(m)
      N=NORDS(M)
      WMIN=(EMINS(N)*CS(M))**.5
      WMAX=((EMINS(N)+(NPES(N)-1)*EINCS(N))*CS(M))**.5
      smass=(m1(nn)+m2(nn))*m1(nn)/m2(nn)*
      *      (m1s(m)+m2s(m))*m1s(m)/m2s(m)
C
      DO 285 MV=1, NVLAB
C
C THIS DO LOOP 285 CALCULATES SIGNAL AT EVERY LAB VELOCITY SAMPLE POINT
C
      SSCALC(M, MV)=0.
      DO 280 MTH=1, NTHD
      MPHMAX=3*MTH-2
      DO 280 MPH=1, MPHMAX
C
C THESE DO LOOPS 280 AVERAGE OVER DETECTOR ANGLES
C
      DO 270 I=1, NTHBM
      JJ=3*I-2
      DO 270 J=1, JJ
      DO 270 L=1, NVBM
C
C THESE DO LOOPS 270 AVERAGE OVER BEAM DISTRIBUTION
C
      VREF2=VB2(L)+VL2(MV)-2.*VBM(L)*VL(MV)*COSA(I, J, MTH, MPH)
      vref2=abs(vref2)
      VREF=SQRT(VREF2)
      if(vref.eq.0.)go to 270
      DO 265 NUSP=1, NUP(M)
      epri=usp2(m, nusp)/cp(nn)
      e2max=etotal-epri
      e2li=emins(n)+(npes(n)-1)*eincs(n)
      if(e2max.ge.e2li)go to 245
      pe2=0.
      npe2=(e2max-emins(n))/eincs(n)+1
      if(npe2.lt.2)npe2=2
      do le2=2, npe2
      PEI=(PES(n, le2)+PES(n, (le2-1)))*.5
      pe2=pe2+PEI
      END DO
      if(pe2.ne.0)pe2=1./(pe2*EINCS(n))
      go to 246
245   pe2=1.
246   continue
      DO 265 NTHSP=1, NTHP(M)
C
C THESE DO LOOPS 265 CONSIDER ALL COMBINATIONS OF PRIMARY AND
C SECONDARY VELOCITIES WHICH CAN CONTRIBUTE TO SIGNAL AT A
C CERTAIN VLAB POINT
C
      W2=USP2(M, NUSP)+VREF2-2.*USP(M, NUSP)*VREF*CTHSP(M, NTHSP)
      w2=abs(w2)
      W=SQRT(W2)
      IF(W.LE.WMIN.OR.W.GE.WMAX)GO TO 265.
      E=W2/CS(M)

```

```

echeck=e+epri
if(echeck.gt.etotal)go to 265
cths=(vref2-w2-usp2(m,nusp))/(2.*w*usp(m,nusp))
x=(1.-cths)/dcths(m)
index=ifix(x)+1
if(index.ge.ndistri(m))go to 265
probths=distr(m,index)+(x+1-index)*(distr(m,index+1)
-distr(m,index))
*
X=(E-EMINS(N))/EINCS(N)
INDEX=IFIX(X)+1
POFE2=PES(N,INDEX)+(X+1-INDEK)*(PES(N,(INDEX+1))
-PES(N,INDEX))*pe2
*
x1=(vl(mv)*cthd(mth)-vbm(1)*(sphbm(i,j)*sthbm(i)*sthlab
+cthbm(i)*cthlab))/vref
*
if(abs(x1).gt.1.)x1=x1/abs(x1)
x2=(vl(mv)*sphd(mth,mph)*sthd(mth)+vbm(1)*(cthbm(i)*sthlab
-sphbm(i,j)*sthbm(i)*cthlab))/vref
*
if(abs(x2).gt.1.)x2=x2/abs(x2)
edotul=x1*cthpul-x2*sthpul
edotu2=x1*sthpul+x2*cthpul
p2edotul=p2(edotul)
p2edotu2=p2(edotu2)
wth1=.5*(1.+betap(nn)*p2edotul*p2(cthsp(m,nthsp)))
wth2=.5*(1.+betap(nn)*p2edotu2*p2(cthsp(m,nthsp)))
sths=sqrt(abs(1.-cths*cths))
csecond=cths*cthsp(m,nthsp)+sths*sthsp(m,nthsp)
if(abs(csecond).gt.1.)csecond=csecond/abs(csecond)
p2cs=p2(csecond)
wthsl=1.+betas(m)*p2edotul*p2cs
wthsl2=1.+betas(m)*p2edotu2*p2cs
SSCALC(M,MV)=SSCALC(M,MV)+PROBM(L,I,J)*POFE1(M,NUSP)
*
*POFE2/W/MPHMAX*USP(M,NUSP)*probths*
*
(depol1*wth1*wthsl+depol2*wth2*wthsl2)*
*
sthsp(m,nthsp)
265 CONTINUE
270 CONTINUE
280 CONTINUE
SSCALC(M,MV)=SSCALC(M,MV)*VL2(MV)*UINC(M)/NTHD/
*
NTHP(M)*7.5086e-3*smass
285 CONTINUE
290 CONTINUE
C
C*****
C
C CHAPTER THREE
C TOF COMPARED BETWEEN CALC.'S AND EXPT.'S
C*****
C
C $ 3-1 AVERAGE OVER IONIZER
C
1000 if(nion.eq.1)then
dlin=0
else
dlin=2.5*d1/(nion-1)
end if
jj=nion/2
DO 1011 M=1,NPCHAN
IF(NPDISP(M).EQ.0)GO TO 1011
DO 1010 I=1,NVLAB
ADD=0.
DO 1008 J=-jj,jj
VPRIME=VL(I)/(1+J*dlin/DIST)
IF(VPRIME.GE.VL(NVLAB).OR.VPRIME.LT.VLMIN)GO TO 1008
X=(VPRIME-VLMIN)/VLINC
IV=IFIX(X)+1

```

```

      ADD=ADD+pion(J+jj+1)*(SPCALC(M,IV)+(X+1-IV)*
      (SPCALC(M,(IV+1))-SPCALC(M,IV)))
*
1008 CONTINUE
1010 PSIGNAL(M,I)=ADD
1011 CONTINUE
      IF(SWITCH.EQ.0)GO TO 1021
      DO 1020 M=1,NSCHAN
      DO 1020 I=1,NVLAB
      ADD=0.
      DO 1018 J=-jj,jj
      VPRIME=VL(I)/(1+J*dlin/DIST)
      IF(VPRIME.GE.VL(NVLAB).OR.VPRIME.LT.VLMIN)GO TO 1018
      X=(VPRIME-VLMIN)/VLINC
      IV=IFIX(X)+1
      ADD=ADD+pion(J+jj+1)*(SSCALC(M,IV)+(X+1-IV)*
      (SSCALC(M,(IV+1))-SSCALC(M,IV)))
*
1018 CONTINUE
1020 SSIGNAL(M,I)=ADD
1021 continue
-----
C
C 3-2 PRESENT BOTH CALC. AND EXPT. TOP
C
-----
C THIS SECTION GETS REAL TOP IN LAB FRAME
C
1030 NCHAN=NECHAN-NBCHAN+1
      DO 1036 J=1,NCHAN
      T(J)=(J+NBCHAN-1.5)*DWELL+OFFSET-ALFA*SQRT(DIMASS)
      DO 1035 I=1,NPCHAN
      avpsig(i,j)=0.
      IF(NPDISP(I).EQ.0)GO TO 1035
      SIG=0.
      DO 1033 K=0,9
      VPRIME=DIST*100./((.1*K-.4)*DWELL+T(J))
      IF(VPRIME.LT.VLMIN.OR.VPRIME.GE.VL(NVLAB))GO TO 1033
      VX=(VPRIME-VLMIN)/VLINC
      INDEX=IFIX(VX)+1
      SIG=SIG+.1*(PSIGNAL(I,INDEX)+(VX+1-INDEX)*
      (PSIGNAL(I,(INDEX+1))-PSIGNAL(I,INDEX)))
*
1033 CONTINUE
      AVPSIG(I,J)=SIG/T(J)
1035 CONTINUE
1036 CONTINUE
      IF(SWITCH.EQ.0)GO TO 1046
      DO 1045 J=1,NCHAN
      DO 1045 I=1,NSCHAN
      SIG=0.
      DO 1043 K=0,9
      VPRIME=DIST*100./((.1*K-.4)*DWELL+T(J))
      IF(VPRIME.LT.VLMIN.OR.VPRIME.GE.VL(NVLAB))GO TO 1043
      VX=(VPRIME-VLMIN)/VLINC
      INDEX=IFIX(VX)+1
      SIG=SIG+.1*(SSIGNAL(I,INDEX)+(VX+1-INDEX)*
      (SSIGNAL(I,(INDEX+1))-SSIGNAL(I,INDEX)))
*
1043 CONTINUE
      AVSSIG(I,J)=SIG/T(J)
1045 CONTINUE
C
C THIS SECTION CALCULATES THE INTEGRAL INVOLVING P(E), WHICH IS
C USED TO CALCULATE BRANCHING RATIO
C
1046 checksig=0.
      DO 1048 I=1,NPCHAN
      PINT(I)=0.
      IF(NPDISP(I).EQ.0)GO TO 1048

```

```

DO 1047 J=1,nchan
1047 PINT(I)=PINT(I)+avpsig(i,j)*dwell
1048 checksig=checksig+pint(i)
IF(SWITCH.EQ.0)GO TO 1050
DO 1044 I=1,NSCHAN
SINT(I)=0.
DO 1049 J=1,nchan
1049 SINT(I)=SINT(I)+avssig(i,j)*dwell
1044 checksig=checksig+sint(i)

```

C

-----

C

```

1050 do 1051 j=1,nchan
TOFP(J)=0.
do 1051 i=1,npchan
1051 TOFP(J)=TOFP(J)+PROB(I)*AVPSIG(I,J)
if(switch.eq.0)go to 1053
do 1052 j=1,nchan
TOFS(J)=0.
do 1052 i=1,nschan
1052 TOFS(J)=TOFS(J)+PROBS(I)*AVSSIG(I,J)

```

C

C THIS SECTION FINDS OUT PEAK SIGNAL CHANNEL OF EXPTL. TOF

C

```

1053 if(kscale.eq.0.or.ktype.ne.0)go to 1057
PEAK=datavrg(ltof,1)
DO 1055 I=2,nchan
PEAK=max(datavrg(ltof,i),peak)
1055 CONTINUE

```

C

C THIS SECTION FINDS THE PEAK OF CALCULATED TOF AND SCALES IT WITH  
C RESPECT TO DATA TOF if scaling to expt. is desired

C

```

1057 if(checksig.eq.0.and.ktype.eq.0)then
type *,'calculated TOF is zero'
stop
end if
DO 1059 I=1,NCHAN
if(switch.eq.0)then
tofcalc(i)=tofp(i)
else
TOFCALC(I)=TOFP(I)+TOFS(I)
end if
1059 continue
peakcalc=tofcalc(1)
DO 1061 I=2,NCHAN
PEAKcalc=max(TOFCALC(I),peakcalc)
1061 CONTINUE
if(ktype.ne.0)ratio=1.
if(ktype.eq.0.and.kscale.eq.0)ratio=1000./peakcalc
if(ktype.eq.0.and.kscale.eq.1)RATIO=rscale*PEAK/peakCALC
DO I=1,NCHAN
TOFCALC(I)=TOFCALC(I)*RATIO
END DO
IF(SWITCH.EQ.0)THEN
DO 1067 J=1,NPCHAN
RATIO1=RATIO*PROB(J)
DO 1066 I=1,NCHAN
1066 AVPSIG(J,I)=AVPSIG(J,I)*RATIO1
1067 CONTINUE
ELSE
DO 1069 J=1,NPCHAN
RATIO1=RATIO*PROB(J)
DO 1068 I=1,NCHAN
1068 AVPSIG(J,I)=AVPSIG(J,I)*RATIO1
1069 CONTINUE

```

```

DO 1071 J=1,NSCHAN
RATIO2=RATIO*PROBS(J)
DO 1070 I=1,NCHAN
1070 AVSSIG(J,I)=AVSSIG(J,I)*RATIO2
1071 CONTINUE
END IF
countall=0.
label=1
if(ktype.eq.1)label=ilabth
if(ktype.eq.2)label=ipolth
DO 1073 i=1,NPCHAN
countp(i)=0.
DO 1072 j=1,NCHAN
1072 countp(I)=countp(i)+AVPSIG(i,j)
countall=countall+countp(i)
anglep(label,i)=countp(i)
1073 CONTINUE
if(switch.ne.0)then
DO 1075 i=1,NSCHAN
counts(i)=0.
DO 1074 j=1,NCHAN
1074 counts(I)=counts(i)+AVSSIG(i,j)
countall=countall+counts(i)
angles(label,i)=counts(i)
1075 CONTINUE
END IF
anglall(label)=countall
if(ktype.ne.1)go to 1077
ilabth=ilabth+1
if(ilabth.gt.nthlab)go to 3000
go to 30
1077 if(ktype.ne.2)go to 1078
ipolth=ipolth+1
if(ipolth.gt.nthpol)go to 3000
go to 25
1078 continue

```

```

-----
C
C   $ 3-3 DATA OUTPUT SECTION
C
C THIS SECTION CREATES AN OUTPUT RESULT FILE
C

```

```

WRITE(6,*)'
WRITE(6,*)'-----
WRITE(6,*)'
WRITE(6,5006)TITLE
WRITE(6,*)'
WRITE(6,*)'-----
WRITE(6,*)'
WRITE(6,5002)DIMASS,THLAB
WRITE(6,*)'
WRITE(6,*)'
WRITE(6,*)' AVERAGE TRANSLATIONAL ENERGY RELEASE'
WRITE(6,*)'
WRITE(6,*)' PRIMARY P(E)'
WRITE(6,5003)(I,I=1,NDIST)
WRITE(6,5004)(EAV(I),I=1,NDIST)
IF(SWITCH.EQ.0)GO TO 1091
WRITE(6,*)'
WRITE(6,*)' SECONDARY P(E)'
WRITE(6,5003)(I,I=1,NDSTS)
WRITE(6,5004)(EAVS(I),I=1,NDSTS)
ISAV=0
DO 1090 J=1,NSCHAN
IF(NDPES(J).EQ.0)GO TO 1090
ISAV=ISAV+1

```

```

NSAV(ISAV)=NORD(NSP(J))
TEMP(ISAV)=EVAL(NSAV(ISAV))
1090 CONTINUE
IF(ISAV.EQ.0)GO TO 1091
WRITE(6,*)' '
WRITE(6,*)' ALTERNATIVE PRIMARY P(E)'
WRITE(6,5003)(J,J=1,ISAV)
WRITE(6,5004)(TEMP(J),J=1,ISAV)
1091 CONTINUE
do j=1,npchan
RCOUNTP(J)=COUNTP(J)/COUNTALL
if(kscale.eq.0)countp(j)=10000.*rcountp(j)
END DO
IF(SWITCH.EQ.0)GO TO 1100
DO J=1,NSCHAN
RCOUNTS(J)=COUNTS(J)/COUNTALL
if(kscale.eq.0)counts(j)=10000.*rcounts(j)
END DO
1100 if(kscale.eq.0)countall=10000.
WRITE(6,*)' '
WRITE(6,*)' '
WRITE(6,*)' TOTAL DETECTED SIGNAL COUNTS'
WRITE(6,5007)IFIX(COUNTALL)
WRITE(6,*)' '
WRITE(6,*)' DETECTED PRIMARY SIGNAL COUNTS'
WRITE(6,5008)(J,J=1,NPCHAN)
WRITE(6,5009)(IFIX(COUNTP(J)),J=1,NPCHAN)
WRITE(6,5010)(RCOUNTP(J),J=1,NPCHAN)
IF(SWITCH.EQ.0)GO TO 1101
WRITE(6,*)' '
WRITE(6,*)' DETECTED SECONDARY SIGNAL COUNTS'
WRITE(6,5008)(J,J=1,NSCHAN)
WRITE(6,5009)(IFIX(COUNTS(J)),J=1,NSCHAN)
WRITE(6,5010)(RCOUNTS(J),J=1,NSCHAN)
1101 continue
WRITE(6,*)' '
WRITE(6,*)' '
WRITE(6,*)' INFORMATION FOR BRANCHING RATIO'
WRITE(6,*)' '
write(6,*)' PRIMARY CHANNELS'
WRITE(6,5008)(J,J=1,NPCHAN)
WRITE(6,5012)(PROB(J),J=1,NPCHAN)
WRITE(6,5014)(PINT(J),J=1,NPCHAN)
IF(SWITCH.NE.0)THEN
WRITE(6,*)' '
WRITE(6,*)' SECONDARY CHANNELS'
WRITE(6,5008)(J,J=1,NSCHAN)
WRITE(6,5012)(PROBS(J),J=1,NSCHAN)
WRITE(6,5014)(SINT(J),J=1,NSCHAN)
END IF

C
C THIS SECTION PREPARES FILES USED BY mongo TO PLOT
C CALCULATED TOF AS WELL AS DATA TOF
C
TION=ALFA*SQRT(DIMASS)
7000 if(konly.eq.1.and.kscale.eq.0)go to 1150
sigmin=datavrg(1,1)
sigmax=sigmin
tmin=(ltbexpt(1)-0.5)*dtexpt(1)+offexpt(1)
tmax=0
do 6020 i=1, ntof
do 6020 j=1,nctof(i)
ft=(j+ltbexpt(i)-1.5)*dtexpt(i)+offexpt(i)
tmin=min(ft,tmin)
tmax=max(ft,tmax)
sigmin=min(sigmin,datavrg(i,j))

```

```

        sigmax=max(sigmax,datavrg(i,j))
6020 write(8,*)ft,datavrg(i,j)
        if(konly.eq.0)go to 1500
1150 continue
        if(kscale.eq.0)then
            tmin=t(1)+tion
            tmax=tmin
            sigmin=tofcalc(1)
            sigmax=sigmin
        end if
        DO 1155 I=1,NCHAN
            FT=T(I)+TION
            tmin=min(tmin,ft)
            tmax=max(tmax,ft)
            sigmin=min(sigmin,tofcalc(i))
            sigmax=max(sigmax,tofcalc(i))
1155 WRITE(8,*)FT,TOFCALC(I)
C
        ntofch=0
        DO 1160 M=1,NPCHAN
            IF(NPDISP(M).EQ.0)GO TO 1160
            ntofch=ntofch+1
            DO 1158 I=1,NCHAN
                FT=T(I)+TION
1158 WRITE(8,*)FT,AVPSIG(M,I)
1160 CONTINUE
            IF(SWITCH.EQ.0)GO TO 1500
            DO 1170 M=1,NSCHAN
                ntofch=ntofch+1
                DO 1165 I=1,NCHAN
                    FT=T(I)+TION
1165 WRITE(8,*)FT,AVSSIG(M,I)
1170 CONTINUE
1500 sigmax=1.05*sigmax
            write(11,*)tmin,tmax,sigmin,sigmax,konly,kscale
            if(konly.eq.0.or.kscale.ne.0)write(11,*)ntof
            if(konly.eq.0.or.kscale.ne.0)write(11,*)nctof
            if(konly.ne.0)write(11,*)nchan,ntofch
            if(konly.eq.0)go to 7001
C
C THIS SECTION CREATES A FILE USED by mongo TO
C PLOT P(E)
C
        npech=ndist
        etmin=emin(1)
        etmax=(npe(1)-1)*einc(1)+emin(1)
        npepoint(1)=npe(1)
        do i=2,ndist
            if(emin(i).lt.etmin)etmin=emin(i)
            energy=(npe(i)-1)*einc(i)+emin(i)
            if(etmax.lt.energy)etmax=energy
            npepoint(i)=npe(i)
        end do
        pemax=0.
        DO 1520 M=1,NDIST
            DO 1510 I=1,NPE(M)
                ENERGY=(I-1)*EINC(M)+EMIN(M)
                if(pemax.lt.pe(m,i))pemax=pe(m,i)
1510 WRITE(9,*)ENERGY,PE(M,I)
1520 CONTINUE
            IF(SWITCH.EQ.0)GO TO 2000
            npech=npech+ndsts
            do i=1,ndsts
                if(emin(i).lt.etmin)etmin=emin(i)
                energy=(npe(i)-1)*eincs(i)+emin(i)
                if(etmax.lt.energy)etmax=energy

```

```

npepoint(i+ndist)=npes(i)
end do
DO 1530 M=1,NDSTS
DO 1525 I=1,NPES(M)
if(pemax.lt.pes(m,i))pemax=pes(m,i)
ENERGY=(I-1)*EINCS(M)+EMINS(M)
1525 WRITE(9,*)ENERGY,PES(M,I)
1530 CONTINUE
IF(ISAV.EQ.0)GO TO 2000
npech=npech+isav
do i=1,isav
npepoint(i+ndist+ndsts)=npe(i)
end do
DO 1550 M=1,ISAV
J=NSAV(M)
DO 1545 I=1,NPE(J)
ENERGY=(I-1)*EINC(J)+EMIN(J)
if(pemax.lt.peal(j,i))pemax=peal(j,i)
1545 WRITE(9,*)ENERGY,PEAL(J,I)
1550 CONTINUE
2000 write(12,*)npech
write(12,*)(npepoint(i),i=1,npech)
etmin=etmin*0.98
etmax=etmax*1.05
pemax=pemax*1.05
write(12,*)etmin,etmax,'0.0',pemax
STOP
-----
c this section for the output of laboratory angular
c distribution
c
3000 if(ktype.eq.2)then
do i=1,nangle
thlabv(i)=thpolv(i)
end do
end if
xyz=0.
do 1041 i=1,nangle
1041 xyz=max(xyz,anglall(i))
if(xyz.eq.0)then
type *,'Total counts are 0 at all angles'
stop
end if
xyz=1./xyz
if(kscale.eq.1)xyz=rscale*totexpt(lscale)/anglall(lscale)
do 3002 i=1,nangle
3002 anglall(i)=anglall(i)*xyz
if(kscale.eq.0)totexpt(i)=anglall(i)
sigmin=anglall(1)
sigmax=anglall(1)
do i=1,nangle
sigmax=max(sigmax,anglall(i),totexpt(i))
end do
do 3005 i=1,npchan
do 3004 j=1,nangle
anglep(j,i)=anglep(j,i)*xyz
3004 sigmin=min(sigmin,anglep(j,i))
3005 continue
if(switch.ne.0)then
do 3007 i=1,nschan
do 3007 j=1,nangle
angles(j,i)=angles(j,i)*xyz
3007 sigmin=min(sigmin,angles(j,i))
end if
sigmin=0.85*sigmin
sigmax=1.1*sigmax

```

```

if(kplot.eq.1)sigmin=0.
do i=1,nangle
write(10,*)thlabv(i),totexpt(i)
end do
do i=1,nangle
write(10,*)thlabv(i),anglall(i)
end do
krun=0
do 3010 j=1,npchan
if(npdisp(j).eq.0)go to 3010
krun=krun+1
do 3009 i=1,nangle
3009 write(10,*)thlabv(i),anglep(i,j)
3010 continue
if(switch.eq.1)then
do 3015 j=1,nschan
krun=krun+1
do 3014 i=1,nangle
3014 write(10,*)thlabv(i),angles(i,j)
3015 continue
end if
anglmin=thlabv(1)-0.1*abs(thlabv(1))
anglmax=thlabv(nangle)+0.1*abs(thlabv(nangle))
write(14,*)nangle,krun
write(14,*)anglmin,anglmax,sigmin,sigmax
WRITE(6,*)'
WRITE(6,*)'-----'
WRITE(6,*)'
WRITE(6,5006)TITLE
WRITE(6,*)'
WRITE(6,*)'-----'
WRITE(6,*)'
write(6,*)' Angular distribution of integrated counts'
write(6,5020)dimass
if(ktype.eq.1)then
write(6,5021)thpol
write(6,*)' Variable is lab. angle of the beam'
else
write(6,5022)thlab
write(6,*)' Variable is laser polarization angle'
end if
write(6,*)'
write(6,*)' angle(degree) counts(expt.) counts(calc.)'
do 3020 i=1,nangle
3020 write(6,5023)thlabv(i),totexpt(i),anglall(i)
write(6,*)'
write(6,*)' Integrated signal for primary channel'
write(6,*)' angle # of channel'
write(6,5024)(i, i=1,npchan)
do 3025 i=1,nangle
3025 write(6,5025)thlabv(i),(anglep(i,j), j=1,npchan)
if(switch.eq.1)then
write(6,*)'
write(6,*)' Integrated signal for secondary channel'
write(6,*)' angle # of channel'
write(6,5024)(i, i=1,nschan)
do 3026 i=1,nangle
3026 write(6,5025)thlabv(i),(angles(i,j), j=1,nschan)
end if
stop
c-----
7001 WRITE(6,*)'
WRITE(6,*)'-----'
WRITE(6,*)'
WRITE(6,5006)TITLE
WRITE(6,*)'

```

```

WRITE(6,*)'-----'
WRITE(6,*)'
do 7010 i=1,ntof
write(6,*)'
write(6,5027)i
write(6,5028)dtexpt(i)
write(6,5029)navrg(i)
write(6,5030)tofbg(i),dtexpt(i)
write(6,5031)tot(i)
7010 continue
stop
C-----
5001 FORMAT(A70)
5002 FORMAT(1X,'DETECTED MASS',F7.2,' AT ANGLE',
* F6.2,' DEGREE')
5003 FORMAT(1X,' # P(E) ',I10)
5004 FORMAT(1X,' <E> kcal/mol',10F7.2)
5006 FORMAT(1X,A70)
5007 FORMAT(1X,' ',I15)
5008 FORMAT(1X,' CHANNEL # ',7I10)
5009 FORMAT(1X,' COUNT # ',7I10)
5010 FORMAT(1X,' CONTRIBUTION',7F10.3)
5012 FORMAT(1X,' WEIGHTING ',7F10.3)
5014 FORMAT(1X,' INTEGRAL ',7E10:3)
5020 format(1x,' Detected mass (e/m) is',f7.2)
5021 format(1x,' Laser polarization angle is',f7.2,' degree')
5022 format(1x,' Lab. angle of beam is',f7.2,' degree')
5023 format(1x,3f15.3)
5024 format(1x,' ',7i10)
5025 format(1x,f7.2,7f10.3)
5027 format(1x,' The',i2,'th TOF spectrum')
5028 format(1x,' Dwell time is changed to',f6.2,' microsec.')
5029 format(1x,' Data are then smoothed by being averaged
* over',i3,' channels')
5030 format(1x,' Background:',f10.2,' every',f5.2,' microsec.')
5031 format(1x,' Total counts:',f15.2)
END
C-----
C END OF WHOLE PROGRAM
C*****

```

## Appendix B

## PROGRAM CMLAB1

```

-----
C
C
C   CMLAB1 is based on cmlab. The additional function this program
C   has is to handle primary triple dissociation and anisotropy.
C
C   If you do not care about calculation on branching ratio, you can
C   use it to fit both primary and secondary dissociations;
C   but if you do care, you have to modify the program, since this
C   version does not consider the question on branching ratio. If
C   only two body process is involved, CMLAB2 which, among other things,
C   has considered branching ratio calculation is the better version
C   for data analysis.
C
C   Version July 1987, by   Zhao, Xincheng
C
C*****
C   CMLAB
C
C   A PROGRAM TO HANDLE PHOTO DISSOCIATION
C   INVOLVING BOTH PRIMARY AND SECONDARY PROCESSES IN AN
C   ISOTROPIC CASE
C
C   VERSION   MAY   1986
C   BY   ZHAO, XINSHENG
C*****
C
C   EXPLANATION SECTION
C
C   THIS SECTION EXPLAINS THE INPUT DATA FILE
C
C   UNITS USED IN THE PROGRAM ARE:
C   -----
C           MASS           AMU
C           ENERGY        KCAL/MOL
C           VELOCITY        10,000 CM/SEC
C           TIME            MICROSECOND
C           DISTANCE        CM
C           ANGLE           DEGREE
C   -----
C
C   LINE #  VARIABLES      DEFINITIONS
C   ++++++  ++++++        ++++++
C
C   1      TITLE           TITLE OF CALCULATION
C   2      DWELL           DWELL TIME OF MCS
C           NBCHAN        FIRST CHANNEL IN TOF TO BE ANALYZED
C           NECHAN        LAST CHANNEL IN TOF TO BE ANALYZED
C           NACHAN        # OF CHANNELS USED TO FIND THE
C                           MAXIMUM VALUE OF TOF SPECTRUM
C           NBG1          FIRST CHANNEL USED IN BACKGROUND SUBTRACTION
C           NBG2          LAST CHANNEL USED IN BACKGROUND SUBTRACTION
C   3      TADJ           SCALING FACTOR TO ADJUST THE HEIGHT OF
C                           TOTAL CALCULATED TOF TO DATA TOF
C           TPNORM        SCALING FACTOR FOR PRIMARY TOF
C           TSNORM        SCALING FACTOR FOR SECONDARY TOF
C           SWITCH        DETERMINATION WHETHER SECONDARY PROCESS
C                           IS INCLUDED
C                           =0 ONLY PRIMARY
C                           =1 PRIMARY AND SECONDARY
C   3.1    labangle       determination whether the angular distribution
C                           is calculated
C                           =0, no
C                           =1, yes

```



```

c      n.7      ngamae      # of polarization angle of light
c      if ngamae=1, fit tof data
c      if ngamae.gt.1, calc polarization
c      dependence of total counts
c      if labangle=1, ngamae can only be 1
c      n.8      depolar(i)  ratio of intensity of weakest to strongest
c      direction of electric field, i=1,ngamae
c      example:
c      =0 totally polarized light
c      =1 totally unpolarized light
c      n.9      gammae(i)   angle between detector vector and strongest
c      direction of electric field
c      i=1,ngamae
c      n.10     betap(j)    anisotropy parameter for primary channel
c      n.11     thdple(j)   angle btween transition dipole and direction
c      of m1(j) at the moment of transition state
c      n.12     thgtou(j)   angle between above geometric direction
c      and the most probable leaving direction
c      of m1(j)
c      [if ngamae.ne.1 then
c      [ n.13     npexpt     if calcd. counts is scaled to expt. data
c      [         =0 no
c      [         =1 yes
c      [ n.14     input only if npexpt=1
c      [         indexpnorm  which expt. point is used to scale the
c      [         calcd. value
c      [         ctoep      scaling factor
c      [ n.15     input only if npexpt=1
c      [         totexpt(i)  expt. data, i=1,ngamae
c      [end if

```

-----  
C THE FOLLOWING INPUT IS ONLY NECESSARY IF SECONDARY DISSOCIATION IS  
C CONSIDERED  
C -----

```

C      N+1     NDSTS      # OF SECONDARY P(E)
C      NSCHAN  # OF SECONDARY REACTION CHANNELS
C      EPHOTON MAX AVAILABLE ENERGY
C      N+2     NPES(K)    # OF POINTS IN EACH SECONDARY P(E)
C      N+3     EMINS(K)   MINIMUM ENERGY IN EACH SECONDARY P(E)
C      N+4     EINCS(K)   ENERGY INCREMENT IN EACH SECONDARY P(E)
C      N+5     M1S(K)     DETECTED NEUTRAL MASS OF SECONDARY PRODUCT
C      N+6     M2S(K)     THE COUNTERPART MASS OF M1S(K)
C      N+7     NSP(K)     ORDER NUMBER OF PRIMARY CHANNEL, TELLING
C      WHICH PRIMARY CHANNEL IS USED FOR THIS
C      SECONDARY PROCESS
C      N+8     NUP(K)     # OF VELOCITY INCREMENTS IN THE CALCULATING
C      PRIMARY PRODUCT DISTRIBUTION FOR
C      FURTHER CALC. ON SECONDARY PROCESS
C      N+9     NTHP(K)    # OF DIVIDED SEGMENTS OVER THE POLAR
C      ANGLE OF PRIMARY PRODUCT DISTRIBUTION
C      N+10    NORDS(K)   ORDER # OF SECONDARY P(E) WHICH THIS
C      SECONDARY CHANNEL USES WITH
C      N+11    PROBS(K)   RELATIVE CONTRIBUTION OF EACH SECONDARY CHANNEL
C      N+12    PES(K,L)   INPUT SECONDARY P(E)
C      THRU
C      M
C      M+1     NDPES(K)   DETERMINATION IF SAME PRIMARY P(E) IS USED
C      =0 YES
C      =1 NO, I HAVE TO INPUT NEW PRIMARY P(E) FOR
C      THE PURPOSE OF THIS SECONDARY PROCESS
C      M+2     PEAL(J,I)  WHEN NDPES(K)=1, INPUT ALTERNATIVE PRIMARY P(E)
C      THRU      WHICH HAS TO BE THE SAME FORMAT AS THE
C      I         SUBSTITUTED ONE
C      i.1     ndistr(k) # of points for secondary c.m. angular
c      distribution where z axis of the secocondary

```

```

c
c
c          i.2      thsmin(k)      c.m. frame is chosen to be the direction of
c          i.3      thsmax(k)      m1, the primary fragment
c          i.4      distr(k,m)     min angle to be considered
c                                     max angle to be considered
c                                     input distribution where the variable is in
c                                     cos(ths), e.g. distr(k,m) will be normalized
c                                     with respect to cos(ths), m=1,ndistr(n)
c

```

```

C*****

```

```

C
C          PREFACE
C          BASIC INFORMATION ON THE SYSTEM
C

```

```

C*****

```

```

PARAMETER(N1=1000)      ! N1 IS MAXIMUM NVLAB THE PROGRAM HANDLES
PARAMETER(N2=100)       ! N2 IS " NPE,NPES "
PARAMETER(N3=3)         ! N3 " NDIST,NDSTS "
PARAMETER(N4=3)         ! N4 " NTHD "
PARAMETER(N5=3)         ! N5 " NTHBM "
PARAMETER(N6=15)        ! N6 " NVBM "
PARAMETER(N7=256)       ! N7 " # OF TOF CHANNELS TO BE READ
PARAMETER(N8=100)       ! N8 " NUP THE PROGRAM HANDLES
PARAMETER(N9=360)       ! N9 " NTHP "
PARAMETER(N10=7)        ! N10=3*N5-2
PARAMETER(N11=7)        ! N11=3*N4-2
PARAMETER(N12=11)       ! N12 MAX NGAUSS
PARAMETER(N13=10)       ! N13 MAX NANGLE
PARAMETER(N14=180)      ! N14 MAX NDISTR
REAL M1,M2,M1S,M2S,m3
INTEGER SWITCH
CHARACTER*70 TITLE
DIMENSION VL(N1),VL2(N1)
DIMENSION NPE(N3),EMIN(N3),EINC(N3),M1(N3),M2(N3),NORD(N3),
*   PROB(N3),NPDISP(N3),PE(N3,N2)
DIMENSION NPES(N3),EMINS(N3),EINCS(N3),M1S(N3),M2S(N3),
*   NSP(N3),NUP(N3),NTHP(N3),NORDS(N3),PROBS(N3),
*   PES(N3,N2),PEAL(N3,N2),
*   NDPES(N3),CS(N3),UINC(N3)
DIMENSION EAV(N3),EAVS(N3),EAVAL(N3),NSAV(N3),TEMP(N3),
*   COUNTP(N3),COUNTS(N3),RCOUNTP(N3),RCOUNTS(N3),
*   PWEIGHT(N3),SWEIGHT(N3)
DIMENSION SPCALC(N3,N1),SSCALC(N3,N1),PSIGNAL(N3,N1),
*   SSIGNAL(N3,N1),PINT(N3),SINT(N3)
DIMENSION CTHD(N4),STHD(N4),SPHD(N4,N11),CPHD(N4,N11)
DIMENSION CTHBM(N5),STHBM(N5),PROBTHBM(N5),CPHBM(N5,N10),
*   SPHBM(N5,N10),COSA(N5,N10,N4,N11)
DIMENSION VBM(N6),VB2(N6),PROBVBM(N6),PROBM(N6,N5,N10)
DIMENSION RAWDAT(N7),TOFSIG(N7),TOFP(N7),TOFS(N7),
*   TOFCALC(N7),T(N7),AVPSIG(N3,N7),AVSSIG(N3,N7)
DIMENSION USP(N3,N8),USP2(N3,N8),POFEL(N3,N8,N12,N12,N12)
DIMENSION CTHSP(N3,N9),npepoint(20)
DIMENSION GAUSS(11)
dimension thetalab(N13),totexpt(N13),totcalc(N13)
dimension probgama(n3,N12),factor(n3,N12,N12,N12),m3(n3),
*   alfa0(n3),beta0(n3),dalfa(n3),dbeta(n3),
*   domega(n3),theta1(n3),theta2(n3),theta3(n3),
*   alfainc(n3),betainc(n3),omegainc(n3),
*   ngauss(n3)
dimension betap(n3),thdple(n3),wth(n3,N12),thgtou(n3),
*   depolar(N13),gammae(N13)
dimension thsmin(n3),thsmax(n3),ndistr(n3),distr(n3,N14),
*   dcth(n3),cth(n3,N14)
DATA GAUSS/.0088,.027,.0648,.121,.1761,.1995,
*   .1761,.121,.0648,.027,.0088/
DATA ECHANGE/4.184E10/ ! erg/kcal
p2(x)=0.5*(3.*x*x-1.)

```

```

-----
C      READ(5,5001)TITLE
      READ(5,*)DWELL,NBCHAN,NECHAN,NACHAN,NBG1,NBG2
      READ(5,*)TADJ,TPNORM,TSNORM,SWITCH
      A=TPNORM/(TPNORM+TSNORM)
      B=TSNORM/(TPNORM+TSNORM)
C
C      this section reads the information on laboratory angular distribution
C
      read(5,*)labangle,nplot
      if(labangle.ne.1)go to 1
      read(5,*)nangle,nexpt
      read(5,*)(thetalab(i),i=1,nangle)
      if(nexpt.eq.1)then
      read(5,*)indexnorm,ctoe
      read(5,*)(totexpt(i),i=1,nangle)
      end if
      indexrun=1
-----
C      THIS SECTION READS THE INFORMATION ABOUT THE SOURCE BEAM,
C      AND DIVIDES THE BEAM PROFILE TO MANY SMALL SEGMENTS. VELOCITY
C      DISTRIBUTION IS ASSUMED IN USUAL FUNCTION. DISTRIBUTION FUNCTION
C      IS NORMALYZED.
C
1      READ(5,*)ALPHA,SPDRT,HTHBM,NTHBM,NVBM
      SUM=0.
      DCOSTHBM=(1.-COSD(HTHBM))/NTHBM
      DO 3 I=1,NTHBM
      CTHBM(I)=1.-(I-1)*DCOSTHBM
      STHBM(I)=(1.-CTHBM(I)*CTHBM(I))**.5
      PROBTHBM(I)=1.-FLOAT(I-1)/FLOAT(NTHBM)
3      SUM=SUM+PROBTHBM(I)
      DO 4 I=1,NTHBM
4      PROBTHBM(I)=PROBTHBM(I)/SUM
      VPK=(ALPHA*SPDRT/2)*(1.+SQRT(1.+4./SPDRT**2))
      IF(NVBM.EQ.1)THEN
      VBM(1)=VPK
      VB2(1)=VPK*VPK
      PROBVM(1)=1
      ELSE
      SUM=0.
      DELTAVBM=(ALPHA*2.5)/(NVBM/2)
      VBMIN=VPK-(NVBM/2)*DELTAVBM
      DO 5 I=1,NVBM
      VBM(I)=VBMIN+(I-1)*DELTAVBM
      PROBVM(I)=VBM(I)**2*EXP(-(VBM(I)/ALPHA-SPDRT)**2)
5      SUM=SUM+PROBVM(I)
      DO 6 I=1,NVBM
      VB2(I)=VBM(I)*VBM(I)
6      PROBVM(I)=PROBVM(I)/SUM
      END IF
      DO 7 J=1,NTHBM
      KK=3*J-2
      DPFI=6.283185/KK
      DO 7 K=1,KK
      CPHBM(J,K)=COS((K-1)*DPFI)
      SPHBM(J,K)=SIN((K-1)*DPFI)
      DO 7 I=1,NVBM
7      PROBM(I,J,K)=PROBVM(I)*PROBTHBM(J)/KK
-----
C      THIS SECTION READS THE INFORMATION ABOUT DETECTOR AND DIVIDES THE
C      APERTURE OF DETECTOR TO SMALL SEGMENT SIMILAR AS BEAM IS DIVIDED
C
      READ(5,*)DIMASS,THLAB,DIST,DL,OFFSET,ALFA,THD,NTHD
      DCOSTHD=(1.-COSD(THD))/NTHD
      DO 8 I=1,NTHD

```

```

      CTHD(I)=1.-(I-1)*DCOSTHD
      STHD(I)=(1.-CTHD(I)*CTHD(I))**.5
      JJ=3*I-2
      DPFI=6.283185/JJ
      DO 8 J=1,JJ
        SPHD(I,J)=SIN((J-1)*DPFI)
        CPHD(I,J)=COS((J-1)*DPFI)
      8
C
C THIS SECTION READS INFORMATION ON LAB VELOCITY USED IN SIMULATION
C
      READ(5,*)VLMIN,VLINC,NVLAB
      IF(VLMIN.EQ.0)VLMIN=0.5*VLINC
      DO I=1,NVLAB
        VL(I)=VLMIN+(I-1)*VLINC
        VL2(I)=VL(I)*VL(I)
      END DO
C
C*****
C
C          CHAPTER ONE
C          THE TREATMENT ON PRIMARY CONTRIBUTION
C*****
C
C § 1-1 INFORMATION ABOUT PRIMARY CHANNELS
C
      READ(5,*)NDIST,NPCHAN
      READ(5,*)(NPE(J),J=1,NDIST)
      READ(5,*)(EMIN(J),J=1,NDIST)
      READ(5,*)(EINC(J),J=1,NDIST)
      READ(5,*)(M1(J),J=1,NPCHAN)
      READ(5,*)(M2(J),J=1,NPCHAN)
      read(5,*)(m3(j),j=1,npchan)
      READ(5,*)(NORD(J),J=1,NPCHAN)
      READ(5,*)(PROB(J),J=1,NPCHAN)
      READ(5,*)(NPDISP(J),J=1,NPCHAN)
      SUM=0.
      DO J=1,NPCHAN
        IF(NPDISP(J).EQ.0)PROB(J)=0.
        SUM=SUM+PROB(J)
      END DO
      IF(SUM.NE.0.)THEN
        DO J=1,NPCHAN
          PROB(J)=PROB(J)/SUM
        END DO
      END IF
C
C THIS SECTION READS PRIMARY P(E) AND NORMALYZES THEM
C
      DO 10 J=1,NDIST
        READ(5,*)(PE(J,I),I=1,NPE(J))
        SUM=0.
        EAV(J)=0.
        DO I=2,NPE(J)
          PEI=(PE(J,I)+PE(J,(I-1)))*.5
          EAV(J)=(EMIN(J)+(I-1.5)*EINC(J))*PEI+EAV(J)
          SUM=SUM+PEI
        END DO
        EAV(J)=EAV(J)/SUM
        SUM=SUM*EINC(J)
        DO I=1,NPE(J)
          PE(J,I)=PE(J,I)/SUM
        END DO
      10 CONTINUE
C
C read the information about triple dissociation geometry

```

```

c
read(5,*)(alfa0(j),j=1,npchan)
read(5,*)(beta0(j),j=1,npchan)
read(5,*)(domega(j),j=1,npchan)
read(5,*)(dalfa(j),j=1,npchan)
read(5,*)(dbeta(j),j=1,npchan)
read(5,*)(ngauss(j),j=1,npchan)
do 15 i=1,npchan
  probgama(i,1)=1.
  if(ngauss(i).ne.1)then
    suml=1.
    ii=(ngauss(i)-1)/2
    probgama(i,ii+1)=1
    abc=2./ii
    do j=1,ii
      xyz=exp(-(abc*j)**2/2.)
      probgama(i,ii+j+1)=xyz
      probgama(i,ii-j+1)=xyz
      suml=suml+2.*xyz
    end do
    do j=1,ngauss(i)
      probgama(i,j)=probgama(i,j)/suml
    end do
    end if
    thetal(i)=0.
    theta2(i)=alfa0(i)
    theta3(i)=360.-beta0(i)
    if(ngauss(i).ne.1)then
      alfainc(i)=2.*dalfa(i)/ii
      betainc(i)=2.*dbeta(i)/ii
      omegainc(i)=2.*domega(i)/ii
      thetall=thetal(i)-2.*domega(i)
      theta2l=theta2(i)-2.*dalfa(i)
      theta3l=theta3(i)-2.*dbeta(i)
    else
      alfainc(i)=0.
      betainc(i)=0.
      omegainc(i)=0.
      thetall=thetal(i)
      theta2l=theta2(i)
      theta3l=theta3(i)
    end if
    do 15 k1=1,ngauss(i)
      omegal=thetall+(k1-1)*omegainc(i)
      do 15 k2=1,ngauss(i)
        alfa1=theta2l+(k2-1)*alfainc(i)
        alfav=alfa1-omegal
        deltav=180.-alfav
        do 15 k3=1,ngauss(i)
          beta1=theta3l+(k3-1)*betainc(i)
          betav=omegal-beta1+360.
          gamav=180.-betav
          gade=gamav+deltav
          if(gade.eq.0)go to 13
          if(gade.ge.180)go to 14
          if(deltav.le.0.and.gamav.gt.0)go to 14
          if(deltav.gt.0.and.gamav.le.0)go to 14
          factor(i,k1,k2,k3)=m1(i)/2.*(1+m1(i)/(sind(gade))**2
*          *((sind(deltav))**2/m3(i)+(sind(gamav))**2/
*          m2(i)))*1.e8/echange
          go to 15
13      factor(i,k1,k2,k3)=m1(i)/2.*(m1(i)+m2(i)+m3(i))/(m2(i)+
*          m3(i))*1.e8/echange
          go to 15
14      factor(i,k1,k2,k3)=0.
15      continue

```

```

C
C read the information about anisotropy
C
      read(5,*)ngamae
      read(5,*)(depolar(i),i=1,ngamae)
      read(5,*)(gammae(i),i=1,ngamae)
      if(labangle.eq.1)ngamae=1
      nerun=1
      read(5,*)(betap(j),j=1,npchan)
      read(5,*)(thdple(j),j=1,npchan)
      read(5,*)(thgtou(j),j=1,npchan)
      do 18 i=1,npchan
      ii=1
      if(ngauss(i).ne.1)ii=(ngauss(i)-1)/2
      do 18 k1=1,ngauss(ii)
      cdipo=cosd(thgtou(i)+(k1-ii-1)*omegainc(i))
18      wth(i,k1)=2.*betap(i)*p2(cdipo)*p2(cosd(thdple(i)))
      if(ngamae.eq.1)go to 19
      read(5,*)npexpt
      if(npexpt.eq.1)then
      read(5,*)indexpnorm,ctoep
      read(5,*)(totexpt(i),i=1,ngamae)
      end if
C
C IF THERE ARE SECONDARY PROCESSES, INPUT INFORMATION ABOUT SECONDARY
C CALCULATION, WHICH GOES INTO CHAPTER TWO
C
19      IF(SWITCH.EQ.1)GO TO 100          ! LABLE 100 IS IN CHAPTER TWO
20      TYPE *,'INPUT SUCCESSFUL'
C-----
C
C $ 1-2  CALCULATION ON CONTRIBUTION BY PRIMARY PROCESS
C-----
C THIS SECTION CALCULATE COS(A), WHERE A IS THE ANGLE BETWEEN
C ONE OF THE BEAM VECTOR AND ONE OF DETECTOR VECTOR
C
30      if(labangle.eq.1)thlab=thetalab(indexrun)
      STHLAB=SIND(THLAB)
      CTHLAB=COSD(THLAB)
      DO 9 I=1,NTHBM
      JJ=3*I-2
      DO 9 J=1,JJ
      DO 9 MTH=1,NTHD
      JJJ=3*MTH-2
      DO 9 MPH=1,JJJ
9      COSA(I,J,MTH,MPH)=STHBM(I)*CPHBM(I,J)*STHD(MTH)*CPHD(MTH,MPH)
      *      +STHBM(I)*SPHBM(I,J)*STHD(MTH)*SPHD(MTH,MPH)*CTHLAB
      *      -CTHBM(I)*STHD(MTH)*SPHD(MTH,MPH)*STHLAB
      *      +STHBM(I)*SPHBM(I,J)*CTHD(MTH)*STHLAB
      *      +CTHBM(I)*CTHD(MTH)*CTHLAB
25      gamae=gammae(nerun)
      depola=depolar(nerun)
      sgamae=sind(gamae)
      cgamae=cosd(gamae)
      depola1=1./(1.+depola)
      depola2=depola/(1.+depola)
C-----
      DO 90 M=1,NPCHAN
C
C THIS DO LOOP 90 CALCULATES EVERY PRIMARY CHANNEL
C
      IF(NPDISP(M).EQ.0)GO TO 90
      N=NORD(M)
      EMAX=EMIN(N)+(NPE(N)-1)*EINC(N)
      DO 85 MV=1,NVLAB

```

```

C
C THIS DO LOOP 85 CALCULATES SIGNAL AT EVERY LAB VELOCITY SAMPLE POINT
C
      SPCALC(M,MV)=0.
      DO 80 MTH=1,NTHD
      MPHMAX=3*MTH-2
      DO 80 MPH=1,MPHMAX
C
C THESE DO LOOPS 80 AVERAGE OVER DETECTOR ANGLES
C
      DO 70 L=1,NVBM
      DO 70 I=1,NTHBM
      JJ=3*I-2
      DO 70 J=1,JJ
C
C THESE DO LOOPS 70 AVERAGE OVER BEAM DISTRIBUTION
C
      U2=abs(VB2(L)+VL2(MV)-2.*VBM(L)*VL(MV)*COSA(I,J,MTH,MPH))
      U=SQRT(U2)
      IF(U.EQ.0)GO TO 70
      X1=(VL(MV)*CTHD(MTH)-VBM(L)*(SPHBM(I,J)*STHBM(I)*STHLAB
      *      +CTHBM(I)*CTHLAB))/U
      IF(ABS(X1).GT.1.)X1=X1/ABS(X1)
      X2=(VL(MV)*SPHD(MTH,MPH)*STHD(MTH)+VBM(L)*(CTHBM(I)*STHLAB
      *      -SPHBM(I,J)*STHBM(I)*CTHLAB))/U
      IF(ABS(X2).GT.1.)X1=X2/ABS(X2)
      EDOTU1=X1*CGAMAE-X2*SGAMAE
      EDOTU2=X1*SGAMAE+X2*CGAMAE
C
      DO 60 K1=1,NGAUSS(M)
      WTH1=1.+WTH(M,K1)*P2(EDOTU1)
      WTH2=1.+WTH(M,K1)*P2(EDOTU2)
      DO 60 K2=1,NGAUSS(M)
      DO 60 K3=1,NGAUSS(M)
C
C these do loops average over the angle change between the three fragments
C
      E=FACTOR(M,K1,K2,K3)*U2
      IF(E.LT.EMIN(N).OR.E.GE.EMAX)GO TO 60
      X=(E-EMIN(N))/EINC(N)
      INDEX=IFIX(X)+1
      POFE=PE(N,INDEX)+(X+1-INDEX)*(PE(N,(INDEX+1))
      *      -PE(N,INDEX))
      SPCALC(M,MV)=SPCALC(M,MV)+PROBM(L,I,J)*POFE/U/MPHMAX*
      *      PROBAMA(M,K1)*PROBAMA(M,K2)*PROBAMA(M,K3)*
      *      (DEPOLA1*WTH1+DEPOLA2*WTH2)*FACTOR(M,K1,K2,K3)
60      CONTINUE
70      CONTINUE
80      CONTINUE
      SPCALC(M,MV)=SPCALC(M,MV)*VL2(MV)/NTHD
85      CONTINUE
90      CONTINUE
      IF(SWITCH.EQ.1)GO TO 200
      GO TO 1000
      ! LABE 200 IS IN CHAPTER TWO
      ! LABE 1000 IS IN CHAPTER THREE
C*****
C
C          CHAPTER TWO
C          THE TREATMENT ON SECONDARY CONTRIBUTION
C*****
C
C § 2-1 INFORMATION ABOUT SECONDARY CALCULATION
C
100      READ(5,*)NDSTS,NSCHAN,EPHOTON
      READ(5,*)(NPES(J),J=1,NDSTS)

```

```

READ(5,*)(EMINS(J),J=1,NDSTS)
READ(5,*)(EINCS(J),J=1,NDSTS)
READ(5,*)(M1S(J),J=1,NSCHAN)
READ(5,*)(M2S(J),J=1,NSCHAN)
DO J=1,NSCHAN
  CS(J)=2*M2S(J)/(M1S(J)+M2S(J))/M1S(J)*ECHANGE*1.E-8
END DO
READ(5,*)(NSP(J),J=1,NSCHAN)
READ(5,*)(NUP(J),J=1,NSCHAN)
C
C THIS SECTION DIVIDES THE POLAR ANGLE RANGE OF PRIMARY DISTRIBUTION
C IN C.M. OF BEAM
C
  READ(5,*)(NTHP(J),J=1,NSCHAN)
  DO 106 I=1,NSCHAN
  DEL=2./NTHP(I)
  DO 106 J=1,NTHP(I)
106 CTHSP(I,J)=1.-(J-0.5)*DEL
C
  READ(5,*)(NORDS(J),J=1,NSCHAN)
  READ(5,*)(PROBS(J),J=1,NSCHAN)
  SUM=0.
  DO J=1,NSCHAN
  SUM=SUM+PROBS(J)
  END DO
  DO J=1,NSCHAN
  PROBS(J)=PROBS(J)/SUM
  END DO
C
C THIS SECTION READS SECONDARY P(E) AND NORMALYZES THEM
C
  DO 110 J=1,NDSTS
  READ(5,*)(PES(J,K),K=1,NPES(J))
  SUM=0.
  EAVS(J)=0.
  DO I=2,NPES(J)
  PEI=(PES(J,I)+PES(J,(I-1)))*.5
  EAVS(J)=(EMINS(J)+(I-1.5)*EINCS(J))*PEI+EAVS(J)
  SUM=SUM+PEI
  END DO
  EAVS(J)=EAVS(J)/SUM
  SUM=SUM*EINCS(J)
  DO I=1,NPES(J)
  PES(J,I)=PES(J,I)/SUM
  END DO
110 CONTINUE
C
C THIS SECTION CHECKS IF ALTERNATED P(E) IS USED IN PRIMARY SIMULATION
C WHICH IS FOR THE PURPOSE OF FURTHURE SECONDARY CALCULATION. IF YES,
C READS ALTERNATIVE PRIMARY P(E) AND NORMALYZES THEM
C
  READ(5,*)(NDPES(J),J=1,NSCHAN)
  DO 120 J=1,NSCHAN
  IF(NDPES(J).EQ.0)GO TO 120
  N=NORD(NSP(J))
  READ(5,*)(PEAL(N,K),K=1,NPE(N))
  SUM=0.
  EAVL(N)=0.
  DO I=2,NPE(N)
  PEI=(PEAL(N,I)+PEAL(N,(I-1)))*.5
  EAVL(N)=(EMIN(N)+(I-1.5)*EINC(N))*PEI+EAVL(N)
  SUM=SUM+PEI
  END DO
  EAVL(N)=EAVL(N)/SUM
  SUM=SUM*EINC(N)

```

```

DO I=1,NPE(N)
PEAL(N,I)=PEAL(N,I)/SUM
END DO
120 CONTINUE
C
C this section reads secondary angular distribution
C
read(5,*)(ndistr(j),j=1,nschan)
read(5,*)(thsmi(n,j),j=1,nschan)
read(5,*)(thsmx(j),j=1,nschan)
distrmax=0.
cthsmin=1.
cthsmax=-1.
do 125 i=1,nschan
read(5,*)(distr(i,j),j=1,ndistr(i))
sum=0.
emp1=cosd(thsmi(i))
emp2=cosd(thsmx(i))
cthsmin=min(cthsmin,emp2)
cthsmax=max(cthsmax,emp1)
dcths(i)=(emp1-emp2)/(ndistr(i)-1)
do 121 j=1,ndistr(i)
cthsi(i,j)=emp1-(j-1)*dcths(i)
121 IF(J.GT.1)sum=sum+(distr(i,j)+DISTR(I,J-1))*0.5
sum=sum*dcths(i)
do 125 j=1,ndistr(i)
distr(i,j)=distr(i,j)/sum
distrmax=max(distrmax,distr(i,j))
write(15,*)cthsi(i,j),distr(i,j)
125 continue
distrmax=distrmax*1.1
write(16,*)nschan
write(16,*)(ndistr(j),j=1,nschan)
write(16,*)cthsmax,cthsmin,' 0.0',distrmax
C
C THIS SECTION FINDS OUT VELOCITY INCREMENTS IN CALCULATING PRIMARY PRODUCT
C DISTRIBUTION AND ITS PROBABILITY
C
DO 124 J=1,NSCHAN
N=NSP(J)
M=NORD(N)
ii=ngauss(n)/2+1
umin=(emin(m)/factor(n,ii,ii,ii))**.5
eup=EMIN(M)+(NPE(M)-1)*EINC(M)
umax=(eup/factor(n,ii,ii,ii))**.5
do 123 k1=1,ngauss(n)
do 123 k2=1,ngauss(n)
do 123 k3=1,ngauss(n)
if(factor(n,k1,k2,k3).eq.0)go to 123
down=(emin(m)/factor(n,k1,k2,k3))**.5
up=(eup/factor(n,k1,k2,k3))**.5
umin=min(umin,down)
umax=max(umax,up)
123 CONTINUE
UINC(J)=(UMAX-UMIN)/NUP(J)
DO 122 K=1,NUP(J)
USP(J,K)=UMIN+UINC(J)*(K-.5)
USP2(J,K)=USP(J,K)*USP(J,K)
do 122 k1=1,ngauss(n)
do 122 k2=1,ngauss(n)
do 122 k3=1,ngauss(n)
E=USP2(J,K)*factor(n,k1,k2,k3)
IF(E.LT.EMIN(M).OR.E.GE.EUP)GO TO 126
X=(E-EMIN(M))/EINC(M)
INDEX=IFIX(X)+1
IF(NDPES(J).EQ.0)THEN

```

```

      POFEL(J,K,k1,k2,k3)=PE(M,INDEX)+(X+1-INDEX)*(PE(M,
*      (INDEX+1))-PE(M,INDEX))
      ELSE
      POFEL(J,K,k1,k2,k3)=PEAL(M,INDEX)+(X+1-INDEX)*
*      (PEAL(M,(INDEX+1))-PEAL(M,INDEX))
      END IF
      GO TO 122
126 POFEL(J,K,K1,K2,K3)=0.
122 CONTINUE
124 CONTINUE
      GO TO 20

```

! LABLE 20 IS IN CHAPTER ONE

```

C-----
C
C $ 2-2 CALCULATION ON SECONDARY CONTRIBUTION TO TOF
C
C 200 DO 290 M=1,NSCHAN
C
C THIS DO LOOP 290 CALCULATES EVERY SECONDARY CHANNEL
C
      nn=nsp(m)
      N=NORDS(M)
      WMIN=(EMINS(N)*CS(M))**.5
      WMAX=((EMINS(N)+(NPES(N)-1)*EINCS(N))*CS(M))**.5
      cthsmx=cosd(thsmn(m))
C
      DO 285 MV=1,NVLAB
C
C THIS DO LOOP 285 CALCULATES SIGNAL AT EVERY LAB VELOCITY SAMPLE POINT
C
      SSCALC(M,MV)=0.
      DO 280 MTH=1,NTHD
      MPHMAX=3*MTH-2
      DO 280 MPH=1,MPHMAX
C
C THESE DO LOOPS 280 AVERAGE OVER DETECTOR ANGLES
C
      DO 270 I=1,NTHBM
      JJ=3*I-2
      DO 270 J=1,JJ
      DO 270 L=1,NVBM
C
C THESE DO LOOPS 270 AVERAGE OVER BEAM DISTRIBUTION
C
      VREF2=VB2(L)+VL2(MV)-2.*VBM(L)*VL(MV)*COSA(I,J,MTH,MPH)
      vref2=abs(vref2)
      VREF=SQRT(VREF2)
      if(vref.eq.0)go to 270
      DO 265 NUSP=1,NUP(M)
      DO 265 NTHSP=1,NTHP(M)
C
C THESE DO LOOPS 265 CONSIDER ALL COMBINATIONS OF PRIMARY AND
C SECONDARY VELOCITIES WHICH CAN CONTRIBUTE TO SIGNAL AT A
C CERTAIN VLAB POINT
C
      W2=USP2(M,NUSP)+VREF2-2.*USP(M,NUSP)*VREF*CTHSP(M,NTHSP)
      w2=abs(w2)
      W=SQRT(W2)
      IF(W.LT.WMIN.OR.W.GE.WMAX)GO TO 265
      cths=(vref2-w2-usp2(m,nusp))/(2.*w*usp(m,nusp))
      if(cths.gt.cthsmx)go to 265
      x=(cthsmx-cths)/dcths(m)
      index=IFIX(x)+1
      if(index.GE.ndistr(m))GO TO 265
      probths=distr(m,index)+(x+1-index)*(distr(m,index+1)
*      -distr(m,index))
      E=W2/CS(M)

```

```

X=(E-EMINS(N))/EINCS(N)
INDEX=IFIX(X)+1
POFE2=PES(N,INDEX)+(X+1-INDEX)*(PES(N,(INDEX+1))
-PES(N,INDEX))
*
x1=(vl(mv)*cthd(mth)-vbm(1)*(sphbm(i,j)*sthbm(i)*sthlab
+cthbm(i)*cthlab))/vref
*
if(abs(x1).gt.1.)x1=x1/abs(x1)
x2=(vl(mv)*sphd(mth,mph)*sthd(mth)+vbm(1)*(cthbm(i)*sthlab
-sphbm(i,j)*sthbm(i)*cthlab))/vref
*
if(abs(x2).gt.1.)x2=x2/abs(x2)
edotu1=x1*cgamae-x2*sgamae
edotu2=x1*sgamae+x2*cgamae
temp1=p2(edotu1)*p2(cthsp(m,nthsp))
temp2=p2(edotu2)*p2(cthsp(m,nthsp))

c
do 260 k1=1,ngauss(nn)
wth1=1.+wth(NN,k1)*temp1
wth2=1.+wth(NN,k1)*temp2
do 260 k2=1,ngauss(nn)
do 260 k3=1,ngauss(nn)
ECHECK=E+USP2(M,NUSP)*FACTOR(NN,K1,K2,K3)
if(ephoton.lt.echeck)go to 260

c
c these do loops average over the angle change between the three primary
c fragments
c
SSCALC(M,MV)=SSCALC(M,MV)+PROBM(L,I,J)*POFE1(M,NUSP,
*
k1,k2,k3)*POFE2/W/MPHMAX*USP(M,NUSP)
*
*probgama(nn,k1)*probgama(nn,k2)*probgama(nn,k3)
*
*(depol1*wth1+depol2*wth2)*probths
*
*factor(m,k1,k2,k3)
260 continue
265 CONTINUE
270 CONTINUE
280 CONTINUE
SSCALC(M,MV)=SSCALC(M,MV)*VL2(MV)*UINC(M)/NTHD/
*
NTHP(M)
285 CONTINUE
290 CONTINUE
C*****
C
C CHAPTER THREE
C TOF COMPARED BETWEEN CALC.'S AND EXPT.'S
C*****
C
C § 3-1 AVERAGE OVER IONIZER
C
1000 DO 1011 M=1,NPCHAN
IF(NPDISP(M).EQ.0)GO TO 1011
DO 1010 I=1,NVLAB
ADD=0.
DO 1008 J=-5,5
VPRIME=VL(I)/(1+J*DL/DIST/4.)
IF(VPRIME.GE.VL(NVLAB).OR.VPRIME.LT.VLMIN)GO TO 1008
X=(VPRIME-VLMIN)/VLINC
IV=IFIX(X)+1
ADD=ADD+GAUSS(J+6)*(SPCALC(M,IV)+(X+1-IV)*
*
(SPCALC(M,(IV+1))-SPCALC(M,IV)))
1008 CONTINUE
1010 PSIGNAL(M,I)=ADD
1011 CONTINUE
IF(SWITCH.EQ.0)GO TO 1046
DO 1020 M=1,NSCHAN
DO 1020 I=1,NVLAB
ADD=0.

```

```

DO 1018 J=-5,5
VPRIME=VL(I)/(1+J*DL/DIST/4.)
IF(VPRIME.GE.VL(NVLAB).OR.VPRIME.LT.VLMIN)GO TO 1018
X=(VPRIME-VLMIN)/VLINC
IV=IFIX(X)+1
ADD=ADD+GAUSS(J+6)*(SSCALC(M,IV)+(X+1-IV)*
* (SSCALC(M,(IV+1))-SSCALC(M,IV)))
1018 CONTINUE
1020 SSIGNAL(M,I)=ADD
C
C THIS SECTION CALCULATES THE INTEGRAL INVOLVING P(E), WHICH IS
C USED TO CALCULATE BRANCHING RATIO
C
1046 DO 1048 I=1,NPCHAN
PINT(I)=0.
IF(NPDISP(I).EQ.0)GO TO 1048
DO 1047 J=1,NVLAB
1047 PINT(I)=PINT(I)+PSIGNAL(I,J)/VL(J)*VLINC
1048 CONTINUE
IF(SWITCH.EQ.0)GO TO 1030
DO 1049 I=1,NSCHAN
SINT(I)=0.
DO 1049 J=1,NVLAB
1049 SINT(I)=SINT(I)+SSIGNAL(I,J)/VL(J)*VLINC
C-----
C
C 3-2 PRESENT BOTH CALC. AND EXPT. TOF
C
C THIS SECTION GETS REAL TOF IN LAB FRAME
C
1030 NCHAN=NECHAN-NBCHAN+1
DO 1036 J=1,NCHAN
TOFP(J)=0.
T(J)=(J+NBCHAN-1)*DWELL+OFFSET-ALFA*SQRT(DIMASS)
DO 1035 I=1,NPCHAN
IF(NPDISP(I).EQ.0)GO TO 1035
SIG=0.
DO 1033 K=0,9
VPRIME=DIST*100./((.1*K-.4)*DWELL+T(J))
IF(VPRIME.LT.VLMIN.OR.VPRIME.GE.VL(NVLAB))GO TO 1033
VX=(VPRIME-VLMIN)/VLINC
INDEX=IFIX(VX)+1
SIG=SIG+.1*(PSIGNAL(I,INDEX)+(VX+1-INDEX)*
* (PSIGNAL(I,(INDEX+1))-PSIGNAL(I,INDEX)))
1033 CONTINUE
AVPSIG(I,J)=SIG/T(J)
TOFP(J)=TOFP(J)+PROB(I)*AVPSIG(I,J)
1035 CONTINUE
1036 CONTINUE
IF(SWITCH.EQ.0)GO TO 1050
DO 1045 J=1,NCHAN
TOFS(J)=0.
DO 1045 I=1,NSCHAN
SIG=0.
DO 1043 K=0,9
VPRIME=DIST*100./((.1*K-.4)*DWELL+T(J))
IF(VPRIME.LT.VLMIN.OR.VPRIME.GE.VL(NVLAB))GO TO 1043
VX=(VPRIME-VLMIN)/VLINC
INDEX=IFIX(VX)+1
SIG=SIG+.1*(SSIGNAL(I,INDEX)+(VX+1-INDEX)*
* (SSIGNAL(I,(INDEX+1))-SSIGNAL(I,INDEX)))
1043 CONTINUE
AVSSIG(I,J)=SIG/T(J)
TOFS(J)=TOFS(J)+PROBS(I)*AVSSIG(I,J)
1045 CONTINUE
C-----

```

C THIS SECTION READS TOF DATA AND SUBTRACTS BACKGROUND AND FINDS  
C OUT PEAK SIGNAL CHANNEL

```

C
1050 if(labangle.eq.1.or.ngamae.ne.1)go to 1057
      READ(7,*)(RAWDAT(I),I=1,N7)
      SUM=0.
      DO 1051 I=NBG1,NBG2
1051  SUM=SUM+RAWDAT(I)
      SUM=SUM/(NBG2-NBG1+1)
      DO 1052 I=1,NCHAN
1052  TOFSIG(I)=RAWDAT(NBCHAN+I-1)-SUM
      PEAK=TOFSIG(1)
      IPEAK=1
      DO 1055 I=2,NCHAN
      IF(TOFSIG(I).LE.PEAK)GO TO 1055
      PEAK=TOFSIG(I)
      IPEAK=I
1055  CONTINUE
      II=NACHAN/2
      SUM=0.
      DO 1056 I=0,(NACHAN-1)
1056  SUM=SUM+TOFSIG(IPEAK-II+I)
      AVPEAK=SUM/NACHAN

```

C THIS SECTION FINDS THE PEAK OF CALCULATED TOF AND SCALES IT WITH  
C RESPECT TO DATA TOF

```

C
1057 DO 1059 I=1,NCHAN
      IF(SWITCH.EQ.0) THEN
      TOFCALC(I)=TOFP(I)
      ELSE
      TOFCALC(I)=A*TOFP(I)+B*TOFS(I)
      END IF
1059 CONTINUE

```

C-----  
c this section calculates the total counts for laboratory angular  
c distribution

```

C
      if(labangle.eq.0.)go to 1060
      sum=0.
      do i=1,nchan
      sum=tofcalc(i)+sum
      end do
      totcalc(indexrun)=sum
      if(indexrun.eq.nangle)go to 3000
      indexrun=indexrun+1
      go to 30

```

C-----  
c this section calculates the total counts for polarization dependence

```

C
1060 if(ngamae.eq.1)go to 1062
      sum=0
      do i=1,nchan
      sum=tofcalc(i)+sum
      end do
      totcalc(nerun)=sum
      if(nerun.eq.ngamae)go to 3000
      nerun=nerun+1
      go to 25

```

C-----  
1062 PEAK=TOFCALC(1)  
IPEAK=1  
DO 1061 I=2,NCHAN  
IF(TOFCALC(I).LE.PEAK)GO TO 1061  
PEAK=TOFCALC(I)

```

1061 IPEAK=I
CONTINUE
SUM=0.
DO 1065 I=0,(NACHAN-1)
1065 SUM=SUM+TOFCALC(IPEAK-II+I)
AVCALC=SUM/NACHAN
RATIO=TADJ*AVPEAK/AVCALC
DO I=1,NCHAN
TOFCALC(I)=TOFCALC(I)*RATIO
END DO
IF(SWITCH.EQ.0)THEN
DO 1067 J=1,NPCHAN
IF(NPDISP(J).EQ.0)GO TO 1067
RATIO1=RATIO*PROB(J)
DO 1066 I=1,NCHAN
1066 AVPSIG(J,I)=AVPSIG(J,I)*RATIO1
1067 CONTINUE
ELSE
DO 1069 J=1,NPCHAN
IF(NPDISP(J).EQ.0)GO TO 1069
RATIO1=RATIO*PROB(J)*A
DO 1068 I=1,NCHAN
1068 AVPSIG(J,I)=AVPSIG(J,I)*RATIO1
1069 CONTINUE
DO 1071 J=1,NSCHAN
RATIO2=RATIO*PROBS(J)*B
DO 1070 I=1,NCHAN
1070 AVSSIG(J,I)=AVSSIG(J,I)*RATIO2
1071 CONTINUE
END IF

```

```

C -----
C
C   $ 3-3 DATA OUTPUT SECTION
C
C   THIS SECTION CREATES AN OUTPUT RESULT FILE
C

```

```

WRITE(6,*)'-----'
WRITE(6,*)'-----'
WRITE(6,*)'
WRITE(6,5006)TITLE
WRITE(6,*)'
WRITE(6,*)'-----'
WRITE(6,*)'
WRITE(6,5002)DIMASS,THLAB
WRITE(6,*)'
WRITE(6,*)'
WRITE(6,*)' AVERAGE TRANSLATIONAL ENERGY RELEASE'
WRITE(6,*)'
WRITE(6,*)' PRIMARY P(E)'
WRITE(6,5003)(I,I=1,NDIST)
WRITE(6,5004)(EAV(I),I=1,NDIST)
IF(SWITCH.EQ.0)GO TO 1091
WRITE(6,*)'
WRITE(6,*)' SECONDARY P(E)'
WRITE(6,5003)(I,I=1,NDSTS)
WRITE(6,5004)(EAVS(I),I=1,NDSTS)
ISAV=0
DO 1090 J=1,NSCHAN
IF(NDPES(J).EQ.0)GO TO 1090
ISAV=ISAV+1
NSAV(ISAV)=NORD(NSP(J))
TEMP(ISAV)=EAVAL(NSAV(ISAV))
1090 CONTINUE
IF(ISAV.EQ.0)GO TO 1091
WRITE(6,*)'
WRITE(6,*)' ALTERNATIVE PRIMARY P(E)'

```

```

WRITE(6,5003)(J,J=1,ISAV)
WRITE(6,5004)(TEMP(J),J=1,ISAV)
1091 COUNTALL=0.
DO 1092 N=1,NCHAN
1092 COUNTALL=COUNTALL+TOFCALC(N)
DO 1094 J=1,NPCHAN
COUNTP(J)=0.
IF(NPDISP(J).EQ.0)GO TO 1094
DO 1093 N=1,NCHAN
1093 COUNTP(J)=COUNTP(J)+AVPSIG(J,N)
1094 CONTINUE
DO J=1,NPCHAN
RCOUNTP(J)=COUNTP(J)/COUNTALL
END DO
IF(SWITCH.EQ.0)GO TO 1100
DO 1096 J=1,NSCHAN
COUNTS(J)=0.
DO 1095 N=1,NCHAN
1095 COUNTS(J)=COUNTS(J)+AVSSIG(J,N)
1096 CONTINUE
DO J=1,NSCHAN
RCOUNTS(J)=COUNTS(J)/COUNTALL
END DO
1100 WRITE(6,*)' '
WRITE(6,*)' '
WRITE(6,*)' TOTAL DETECTED SIGNAL COUNTS'
WRITE(6,5007)IFIX(COUNTALL)
WRITE(6,*)' '
WRITE(6,*)' DETECTED PRIMARY SIGNAL COUNTS'
WRITE(6,5008)(J,J=1,NPCHAN)
WRITE(6,5009)(IFIX(COUNTP(J)),J=1,NPCHAN)
WRITE(6,5010)(RCOUNTP(J),J=1,NPCHAN)
IF(SWITCH.EQ.0)GO TO 1101
WRITE(6,*)' '
WRITE(6,*)' DETECTED SECONDARY SIGNAL COUNTS'
WRITE(6,5008)(J,J=1,NSCHAN)
WRITE(6,5009)(IFIX(COUNTS(J)),J=1,NSCHAN)
WRITE(6,5010)(RCOUNTS(J),J=1,NSCHAN)
1101 DO I=1,NPCHAN
PWEIGHT(I)=0.
IF(PINT(I).NE.0)PWEIGHT(I)=1./PINT(I)
END DO
IF(SWITCH.EQ.0)GO TO 1120
DO I=1,NSCHAN
SWEIGHT(I)=0.
IF(SINT(I).NE.0)SWEIGHT(I)=1./SINT(I)
END DO
1120 WRITE(6,*)' '
WRITE(6,*)' '
WRITE(6,5015)A,B
WRITE(6,*)' '
WRITE(6,*)' PRIMARY WEIGHTING FACTOR'
WRITE(6,5008)(J,J=1,NPCHAN)
WRITE(6,5012)(PROB(J),J=1,NPCHAN)
WRITE(6,5014)(PWEIGHT(J),J=1,NPCHAN)
IF(SWITCH.NE.0)THEN
WRITE(6,*)' '
WRITE(6,*)' SECONDARY WEIGHT FACTOR'
WRITE(6,5008)(J,J=1,NSCHAN)
WRITE(6,5012)(PROBS(J),J=1,NSCHAN)
WRITE(6,5014)(SWEIGHT(J),J=1,NSCHAN)
END IF

```

```

C
C THIS SECTION PREPARES FILES USED BY THE mongo TO PLOT
C CALCULATED TOF AS WELL AS DATA TOF
C

```

```

TION=ALFA*SQRT(DIMASS)
sigmin=tofsig(1)
sigmax=tofsig(1)
DO 1150 I=1,NCHAN
FT=T(I)+TION
if(i.eq.1)timemin=ft
if(tofsig(i).gt.sigmax)sigmax=tofsig(i)
if(tofsig(i).lt.sigmin)sigmin=tofsig(i)
WRITE(8,*)FT,TOFSIG(I)
1150 CONTINUE
timemax=ft
sigmax=1.05*sigmax
C
DO 1155 I=1,NCHAN
FT=T(I)+TION
1155 WRITE(8,*)FT,TOFCALC(I)
C
ntofch=0
DO 1160 M=1,NPCHAN
IF(NPDISP(M).EQ.0)GO TO 1160
ntofch=ntofch+1
DO 1158 I=1,NCHAN
FT=T(I)+TION
1158 WRITE(8,*)FT,AVPSIG(M,I)
1160 CONTINUE
IF(SWITCH.EQ.0)GO TO 1500
DO 1170 M=1,NSCHAN
ntofch=ntofch+1
DO 1165 I=1,NCHAN
FT=T(I)+TION
1165 WRITE(8,*)FT,AVSSIG(M,I)
1170 CONTINUE
1500 write(11,*)nchan,ntofch
write(11,*)timemin,timemax,sigmin,sigmax
C
C THIS SECTION CREATES A FILE USED BY THE mongo TO
C PLOT P(E)
C
npech=ndist
etmin=emin(1)
etmax=(npe(1)-1)*einc(1)+emin(1)
npepoint(1)=npe(1)
do i=2,ndist
if(emin(i).lt.etmin)etmin=emin(i)
energy=(npe(i)-1)*einc(i)+emin(i)
if(etmax.lt.energy)etmax=energy
npepoint(i)=npe(i)
end do
pemax=0.
DO 1520 M=1,NDIST
DO 1510 I=1,NPE(M)
ENERGY=(I-1)*EINC(M)+EMIN(M)
if(pemax.lt.pe(m,i))pemax=pe(m,i)
1510 WRITE(9,*)ENERGY,PE(M,I)
1520 CONTINUE
IF(SWITCH.EQ.0)GO TO 2000
npech=npech+ndsts
do i=1,ndsts
if(emins(i).lt.etmin)etmin=emins(i)
energy=(npes(i)-1)*eincs(i)+emins(i)
if(etmax.lt.energy)etmax=energy
npepoint(i+ndist)=npes(i)
end do
DO 1530 M=1,NDSTS
DO 1525 I=1,NPES(M)
if(pemax.lt.pes(m,i))pemax=pes(m,i)

```

```

ENERGY=(I-1)*EINCS(M)+EMINS(M)
1525 WRITE(9,*)ENERGY,PES(M,I)
1530 CONTINUE
IF(ISAV.EQ.0)GO TO 2000
npech=npech+isav
do i=1,isav
npepoint(i+ndist+ndsts)=npe(i)
end do
DO 1550 M=1,ISAV
J=NSAV(M)
DO 1545 I=1,NPE(J)
ENERGY=(I-1)*EINC(J)+EMIN(J)
if(pemax.lt.peal(j,i))pemax=peal(j,i)
1545 WRITE(9,*)ENERGY,PEAL(J,I)
1550 CONTINUE
2000 write(12,*)npech
write(12,*)(npepoint(i),i=1,npech)
etmin=etmin*0.98
etmax=etmax*1.05
pemax=pemax*1.05
write(12,*)etmin,etmax,' 0.0',pemax
stop
-----
c this section for the output of laboratory angular distribution
c
3000 if(ngamae.ne.1)then
nnext=npnext
nangle=ngamae
do i=1,nangle
thetalab(i)=gammae(i)
end do
end if
xyz=totcalc(1)
do i=1,nangle
xyz=max(xyz,totcalc(i))
end do
if(xyz.eq.0)then
type *,'calculated total counts is 0'
stop
end if
xyz=1./xyz
if(nnext.ne.1)go to 3010
if(ngamae.ne.1)indexnorm=indexpnorm
if(ngamae.ne.1)ctoe=ctoe
xyz=totexpt(indexnorm)/totcalc(indexnorm)*ctoe
3010 do i=1,nangle
totcalc(i)=totcalc(i)*xyz
if(nnext.eq.0)totexpt(i)=totcalc(i)
end do
sigmin=totcalc(1)
sigmax=totcalc(1)
do i=1,nangle
sigmin=min(sigmin,totcalc(i),totexpt(i))
sigmax=max(sigmax,totcalc(i),totexpt(i))
end do
sigmin=0.8*sigmin
sigmax=1.1*sigmax
if(nplot.eq.1)sigmin=0.
do i=1,nangle
write(10,*)thetalab(i),totexpt(i)
end do
do i=1,nangle
write(10,*)thetalab(i),totcalc(i)
end do
anglemin=thetalab(1)-0.1*abs(thetalab(1))
anglemax=thetalab(nangle)+0.1*abs(thetalab(nangle))

```



LAWRENCE BERKELEY LABORATORY  
TECHNICAL INFORMATION DEPARTMENT  
1 CYCLOTRON ROAD  
BERKELEY, CALIFORNIA 94720